

Université de Montréal

**Development and Characterization of Polymeric Nanoparticles  
(NPs) made from Functionalized Poly (D,L- lactide) (PLA)**

**Polymers**

par

Sherief Essa

Faculté de Pharmacie

Thèse présentée à la Faculté des études supérieures  
en vue de l'obtention du grade de Philosophiae Doctor (Ph. D.)

en Sciences Pharmaceutiques

Option: Technologie Pharmaceutique

May 2011

© Sherief Essa, 2011

Université de Montréal  
Faculté des études supérieures

Cette thèse intitulée:

Development and Characterization of Polymeric Nanoparticles (NPs) made from  
Functionalized Poly (D,L-lactide) (PLA) Polymers

présentée par:

Sherief Essa

a été évaluée par un jury composé des personnes suivantes :

Dr. Suzanne Giasson, président-rapporteur

Dr. Patrice Hildgen, directeur de recherche

Dr. François-Xavier Lacasse, membre du jury

Dr. Pascal Janvier, examinateur externe

Dr. Daniel Lamontagne, représentant du doyen de la FES

## Résumé

Les nanoparticules polymériques biodégradable (NPs) sont apparues ces dernières années comme des systèmes prometteurs pour le ciblage et la libération contrôlée de médicaments. La première partie de cette étude visait à développer des NPs biodégradables préparées à partir de copolymères fonctionnalisés de l'acide lactique (poly (D,L)lactide ou PLA). Les polymères ont été étudiés comme systèmes de libération de médicaments dans le but d'améliorer les performances des NPs de PLA conventionnelles. L'effet de la fonctionnalisation du PLA par insertion de groupements chimiques dans la chaîne du polymère sur les propriétés physico-chimiques des NPs a été étudié. En outre, l'effet de l'architecture du polymère (mode d'organisation des chaînes de polymère dans le copolymère obtenu) sur divers aspects de l'administration de médicament a également été étudié. Pour atteindre ces objectifs, divers copolymères à base de PLA ont été synthétisés. Plus précisément il s'agit de 1) copolymères du poly (éthylène glycol) (PEG) greffés sur la chaîne de PLA à 2.5% et 7% mol. / mol. de monomères d'acide lactique (PEG2.5%-g-PLA et PEG7%-g-PLA, respectivement), 2) des groupements d'acide palmitique greffés sur le squelette de PLA à une densité de greffage de 2,5% (palmitique acid2.5%-g-PLA), 3) de copolymère « multibloc » de PLA et de PEG, (PLA-PEG-PLA)<sub>n</sub>. Dans la deuxième partie, l'effet des différentes densités de greffage sur les propriétés des NPs de PEG-g-PLA (propriétés physico-chimiques et biologiques) a été étudié pour déterminer la densité optimale de greffage PEG nécessaire pour développer la furtivité (« long circulating NPs »). Enfin, les copolymères de PLA fonctionnalisés avec du PEG ayant montré les résultats les plus satisfaisants en regard des divers aspects d'administration de médicaments, (tels que taille et de distribution de taille, charge de surface, chargement de drogue, libération contrôlée de médicaments) ont été sélectionnés pour l'encapsulation de l'itraconazole (ITZ). Le but est dans ce cas d'améliorer sa solubilité dans l'eau, sa biodisponibilité et donc son activité antifongique. Les NPs ont d'abord été préparées à partir de copolymères fonctionnalisés de PLA, puis ensuite analysés pour leurs paramètres physico-chimiques majeurs tels que l'efficacité d'encapsulation, la taille et distribution de taille, la charge de surface, les propriétés thermiques, la chimie de surface, le pourcentage de poly (alcool vinylique) (PVA) adsorbé à la surface, et le profil de libération de médicament. L'analyse de la chimie de surface par la spectroscopie de photoélectrons rayon X (XPS) et la microscopie à force

atomique (AFM) ont été utilisés pour étudier l'organisation des chaînes de copolymère dans la formulation des NPs. De manière générale, les copolymères de PLA fonctionnalisés avec le PEG ont montré une amélioration du comportement de libération de médicaments en termes de taille et distribution de taille étroite, d'amélioration de l'efficacité de chargement, de diminution de l'adsorption des protéines plasmatiques sur leurs surfaces, de diminution de l'internalisation par les cellules de type macrophages, et enfin une meilleure activité antifongique des NPs chargées avec ITZ. En ce qui concerne l'analyse de la chimie de surface, l'imagerie de phase en AFM et les résultats de l'XPS ont montré la possibilité de la présence de davantage de chaînes de PEG à la surface des NPs faites de PEG-g-PLA que de NPs faites à partir de (PLA-PEG-PLA)<sub>n</sub>. Nos résultats démontrent que les propriétés des NPs peuvent être modifiées à la fois par le choix approprié de la composition en polymère mais aussi par l'architecture de ceux-ci. Les résultats suggèrent également que les copolymères de PEG-g-PLA pourraient être utilisés efficacement pour préparer des transporteurs nanométriques améliorant les propriétés de certains médicaments, notamment la solubilité, la stabilité et la biodisponibilité.

**Mots-clés:** Acide poly(lactique), Architecture, PEG-PLA, Multi-bloc, Organisation de la chaîne, Spectroscopie de photoélectrons Rayon X (XPS), Microscopie à force atomique (AFM), Imagerie de phase, Faible solubilité.

## Abstract

Biodegradable polymeric nanoparticles (NPs) have emerged as promising drug delivery carriers for the controlled drug release and targeting. The first part of this study aimed to develop biodegradable NPs from functionalized copolymers of poly (D,L-Lactide) (PLA). Those copolymers were explored as drug delivery systems in attempt to improve the drug delivery performance of conventional PLA NPs. The effect of PLA functionalization (insertion of chemical substituents onto PLA backbone) on the physicochemical properties of the obtained NPs was investigated. Moreover, the effect of polymer architecture (mode of organization of polymer chains in the resultant copolymer) on various drug delivery aspects was also studied. To reach those goals, various PLA based copolymers namely poly(ethylene glycol) (PEG) grafted on PLA backbone at 2.5% & 7% mol/mol of lactic acid monomers (PEG2.5%-g-PLA and PEG7%-g-PLA, respectively), palmitic acid grafted on PLA backbone at 2.5% grafting density (palmitic acid2.5%-g-PLA), and multiblock copolymer of PLA and PEG, (PLA-PEG-PLA)<sub>n</sub> were synthesized. In the second part, the effect of different PEG grafting densities over PLA backbone on the properties of PEG-g-PLA NPs either physicochemical or biological properties was investigated to reveal the optimal PEG grafting density required to develop stealth particles (long circulating NPs). Finally, functionalized PEG/PLA copolymers that showed the most satisfactory results in terms of various drug delivery aspects, such as size and size distribution, surface charge, drug loading, and controlled drug release were selected for encapsulation of itraconazole (ITZ) to improve its aqueous solubility, bioavailability and hence its antifungal activity. NPs were first prepared from functionalized PLA copolymers then analyzed for their major physicochemical parameters such as encapsulation efficiency, size and size distribution, surface charge, thermal properties, surface chemistry, % poly(vinyl alcohol) (PVA) adsorbed at the surface of NPs, and drug release pattern. Surface chemistry analysis using x-ray photoelectron spectroscopy (XPS), and atomic force microscopy (AFM) phase imaging were used to study the chain organization behavior of each functionalized copolymer during NPs formulation. Generally speaking, functionalized PEG/PLA copolymers showed improved drug delivery behavior in terms of narrow size and size distribution, enhanced loading efficiency, less plasma protein adsorption onto their surfaces and less macrophage uptake, and finally better antifungal activity for ITZ loaded NPs. For the surface chemistry analysis, AFM phase imaging and XPS studies revealed the possibility of existence of more PEG chains at the surface of PEG-

g-PLA NPs than (PLA-PEG-PLA)<sub>n</sub> during NPs formation. Our results demonstrate that properties of PLA-based NPs can be tuned by proper selection of both polymer composition and polymer architecture. Results also suggest that PEG-g-PLA copolymers could be used efficiently as a nanocarrier to improve various drug properties e.g. solubility, stability, and bioavailability.

**Keywords:** Poly (D,L lactide), Architecture, PEG-PLA, Multiblock, Chain organization, X-ray photon spectroscopy (XPS), Atomic force microscopy (AFM) phase imaging, Poor solubility.

## Table of Contents

Résumé.....	I
Abstract.....	III
Table of Contents.....	V
List of tables.....	XIV
List of figures.....	XV
List of abbreviations.....	XX
Acknowledgements.....	XXIV
CHAPTER ONE.....	1
INTRODUCTION.....	1
Polymeric Nanoparticles (NPs) as Drug Delivery Systems.....	1
1.1. A Brief Overview of Nanotechnology.....	2
1.2. Nanotechnology and Drug Delivery.....	2
1.3. Design of Nanotechnology–Polymeric based Drug Delivery Systems.....	3
1.4. Review of Polymeric Nanoparticles as Delivery Systems.....	4
1.5. Factors affecting Performance of Polymeric Nanoparticles.....	5
1.6. Applications of Polymeric Nanoparticles.....	7
1.7. Preparation of Polymeric Nanoparticles.....	11
1.7.1. Classification of Copolymers used for Nanoparticles Formation.....	12
1.7.2. Polyesters .....	13
1.7.3. Poly(lactic acid) (PLA) .....	15
1.7.4. Functionalized Polyesters for Nanoparticles Preparation.....	16
1.7.5. Emulsification Solvent Evaporation.....	17
1.8. NPs Characterization.....	18
1.8.1. Size and Morphology.....	18
1.8.2. Surface Characteristics and Stability.....	20
1.8.3. Drug-Polymer Interactions.....	21

1.8.4. Drug Loading.....	22
1.8.5. Drug Release.....	23
1.9. Thesis rationale and research objectives.....	24
1.9.1. Rationale.....	24
1.9.2. Research objectives.....	26
1.10. References.....	29
CHAPTER TWO.....	48
RESEARCH PAPER.....	48
Effect of Aqueous Solubility of Grafted Moiety on The Physicochemical Properties of Poly(D,L-lactide) (PLA) based Nanoparticles <sup>1</sup> .....	48
2.1. Abstract.....	49
2.2. Keywords.....	50
2.3. Introduction .....	50
2.4. Materials and methods.....	52
2.4.1. Materials .....	52
2.4.2. Synthesis of Polymers.....	53
2.4.3. Preparation of nanoparticles (NPs) .....	54
2.4.4. Characterization of NPs.....	55
2.4.4.1. Particle size and zeta ( $\zeta$ ) potential measurements.....	55
2.4.4.2. Determination of residual PVA.....	55
2.4.4.3. NPs surface morphology and phase image analysis.....	56
2.4.4.4. Encapsulation efficiency (EE) .....	56
2.4.4.5. Differential Scanning Calorimetry (DSC) .....	57
2.4.4.6. XPS analysis.....	58

2.4.4.7. <sup>1</sup> H NMR spectroscopy.....	58
2.4.4.8. Erosion study.....	58
2.4.4.9. In vitro drug release study.....	59
2.5. Results and discussion: .....	59
2.5.1. Characterization of Polymers.....	59
2.5.2. Particle size and size distribution.....	60
2.5.3. Zeta (ζ) potential measurements.....	63
2.5.4. Residual PVA.....	63
2.5.5. Surface morphology and phase analysis.....	64
2.5.6. Encapsulation efficiency (EE) .....	66
2.5.7. DSC.....	67
2.5.8. XPS analysis.....	70
2.5.9. <sup>1</sup> H-NMR of NPs in D <sub>2</sub> O.....	75
2.5.10. Erosion study.....	78
2.5.11. In Vitro Drug Release. ....	79
2.6. Conclusion.....	82
2.7. Acknowledgment .....	83
2.8. References.....	84
CHAPTER THREE.....	88
RESEARCH PAPER.....	88

Effect of Polyethylene Glycol (PEG) Chain Organization on the Physicochemical Properties of Poly(D,L-lactide) (PLA) based Nanoparticles <sup>1</sup> .....	88
3.1. Abstract.....	89
3.2. Keywords.....	90
3.3. Introduction .....	90
3.4. Materials and methods.....	92
3.4.1. Materials .....	92
3.4.2. Synthesis of Polymers.....	92
3.4.3. Preparation of nanoparticles (NPs).....	93
3.4.4. Characterization of NPs.....	94
3.4.4.1. Particle size and size distribution.....	94
3.4.4.2. NPs surface morphology and phase image analysis.....	94
3.4.4.3. Zeta ( $\zeta$ ) potential measurements.....	95
3.4.4.4. Encapsulation efficiency (EE) .....	95
3.4.4.5. Determination of residual PVA.....	96
3.4.4.6. Differential Scanning Calorimetry (DSC) .....	97
3.4.4.7. XPS analysis.....	97
3.4.4.8. <sup>1</sup> H NMR spectroscopy.....	98
3.4.4.9. Erosion study.....	98
3.4.4.10. In vitro drug release study.....	98
3.5. Results and discussion.....	99

3.5.1. Characterization of Polymers.....	99
3.5.2. Particle size and size distribution.....	100
3.5.3. Surface morphology and phase analysis.....	103
3.5.4. Encapsulation efficiency (EE) .....	104
3.5.5. Zeta ( $\zeta$ ) potential measurements.....	105
3.5.6. Residual PVA.....	106
3.5.7. DSC.....	107
3.5.8. XPS analysis.....	112
3.5.9. $^1\text{H-NMR}$ of NPs in $\text{D}_2\text{O}$ .....	116
3.5.10. Erosion study.....	118
3.5.11. In Vitro Drug Release.....	119
3.6. Conclusion.....	124
3.7. Appendix A. Supplementary material.....	125
3.8. Acknowledgment .....	125
3.9. References.....	126
CHAPTER FOUR.....	132
RESEARCH PAPER.....	132
Characterization of Rhodamine Loaded PEG-g-PLA Nanoparticles (NPs): Effect of Poly(ethylene glycol) Grafting Density <sup>1</sup> .....	132
4.1. Abstract.....	133
4.2. Keywords.....	134

4.3. Introduction .....	134
4.4. Materials and methods.....	135
4.4.1. Materials .....	135
4.4.2. Synthesis of Polymers.....	136
4.4.3. Preparation of nanoparticles (NPs).....	137
4.4.4. Characterization of NPs.....	138
4.4.5. Encapsulation efficiency (EE) .....	139
4.4.6. In vitro drug release study.....	139
4.4.7. Evaluation of protein adsorption to NPs surface.....	140
4.4.8. Cell culture.....	140
4.4.8.1. Evaluation of cellular toxicity of PEG-g-PLA NPs.....	140
4.4.8.2. Cellular interaction with RAW 264.7: CLSM study.....	140
4.4.8.3. Cellular interaction with RAW 264.7: Fluorimetry analysis.....	141
4.4.9. Statistical analysis.....	141
4.5. Results and discussion.....	142
4.5.1. Characterization of Polymers.....	142
4.5.2. NPs characterization.....	143
4.5.3. Encapsulation efficiency (EE) .....	147
4.5.4. In Vitro Drug Release.....	149
4.5.5. Plasma protein adsorption.....	151
4.5.6. Cellular toxicity and uptake studies.....	153

4.6. Conclusions.....	154
4.7. Appendix A. Supplementary material.....	157
4.8. Acknowledgment.....	157
4.9. References.....	158
CHAPTER FIVE.....	164
RESEARCH PAPER.....	164
Improved Antifungal Activity of Itraconazole Loaded PEG/PLA Nanoparticles <sup>2</sup> .....	164
5.1. Abstract.....	165
5.2. Keywords.....	166
5.3. Introduction .....	166
5.4. Materials and methods.....	168
5.4.1. Materials .....	168
5.4.2. Synthesis of Polymers. ....	168
5.4.3. Preparation of nanoparticles (NPs) .....	169
5.4.4. Characterization of NPs.....	170
5.4.5. Loading efficiency (% LE) .....	171
5.4.6. Stability studies.....	171
5.4.7. Differential scanning calorimetry (DSC) .....	172
5.4.8. Powder X-ray diffractometry (PXRD) .....	172
5.4.9. Fourier transform infrared spectroscopy (FT-IR) study.....	172
5.4.10. In vitro drug release study.....	172

5.4.11. Hemolysis test.....	173
5.4.12. Fungal Growth Inhibition Studies.....	173
5.4.13. Strains and growth media.....	174
5.4.14. Petri Plate Culture.....	174
5.4.14.1. <i>C. albicans</i> .....	174
5.4.14.2. <i>A. fumigatus</i> .....	174
5.4.15. Statistical analysis.....	174
5.5. Results and discussion.....	175
5.5.1. Characterization of Polymers. ....	175
5.5.2. NPs characterization. ....	175
5.5.3. Stability studies.....	178
5.5.4. Differential scanning calorimetry (DSC) .....	180
5.5.5. Powder X-ray diffractometry (PXRD) .....	181
5.5.6. Fourier transform infrared spectroscopy (FT-IR) study.....	185
5.5.7. In Vitro Drug Release.....	185
5.5.8. Hemolysis analysis: .....	188
5.5.9. Fungal growth inhibition in Petri Plate Culture.....	189
5.6. Conclusions.....	192
5.7. Acknowledgment.....	193
5.8. References.....	194
CHAPTER SIX.....	199

GENERAL DISCUSSION.....	199
6.1. Synthesis and characterization of functionalized (PLA) polymers.....	201
6.2. Preparation and physicochemical characterization of NPs.....	203
6.3. <sup>1</sup> H-NMR and XPS analysis of NPs .....	206
6.4. In vitro release.....	207
6.5. Plasma protein adsorption.....	208
6.6. Cellular toxicity and uptake studies.....	209
6.7. Hemolysis analysis.....	210
6.8. Fungal growth inhibition in Petri Plate Culture.....	210
6.9. References.....	212
CHAPTER SEVEN.....	215
CONCLUSION AND PERSPECTIVES.....	215
7.1. Conclusion.....	216
7.2. Future work.....	217

## ist of tables

<b>Table 1.1.</b> Different applications of polymeric nanoparticles in pharmaceutical field.....	10
<b>Table 1.2.</b> Polymers and methods widely used in nanoparticle preparation.....	14
<b>Table 2.1.</b> Polymers characterization by <sup>1</sup> H NMR, DSC, and Gel Permeation Chromatography (GPC).....	61
<b>Table 2.2.</b> Characteristics of different NPs formulation.....	68
<b>Table 2.3.</b> Relative atomic percentages calculated from XPS Surface Analysis of pure materials used in NPs preparation.....	75
<b>Table 2.4.</b> Relative atomic percentages calculated from XPS Surface Analysis of synthesized polymers and formulated NPs using those polymers.....	76
<b>Table 3.1.</b> Polymers characterization by <sup>1</sup> H NMR, DSC, and Gel Permeation Chromatography (GPC).....	101
<b>Table 3.2.</b> Characteristics of different NPs formulation.....	108
<b>Table 3.3.</b> Relative atomic percentages calculated from XPS Surface Analysis of pure materials used in NPs formulation.....	113
<b>Table 3.4.</b> Relative atomic percentages calculated from XPS Surface Analysis of synthesized polymers and formulated NPs using those polymers.....	117
<b>Table 4.1.</b> Polymer characterization by <sup>1</sup> H NMR and Gel Permeation Chromatography (GPC).....	145
<b>Table 4.2.</b> Size distribution characteristics for different NPs after different stages of preparation.....	147
<b>Table 4.3.</b> Other physicochemical characteristics for different NPs formulation.....	148
<b>Table 5.1.</b> Characteristics of different NPs formulation.....	176
<b>Table 5.2.</b> Diameter of growth inhibition zone measured with <i>c. albicans</i> fungal strains.....	191

## List of figures

<b>Fig.1.1.</b> Schematics of polymeric nanoparticles. A. Matrix type nanosphere, drug molecules are uniformly dispersed in the polymer matrix. B. Core shell nanocapsules, drug molecules are presented in an oily or aqueous core covered with polymeric shell. C. matrix type nanosphere where drug crystals are embedded in a polymer matrix.....	5
<b>Fig.1.2.</b> Factors affecting the drug delivery performance of polymeric nanoparticles.....	7
<b>Fig.1.3.</b> Architectures of different copolymers used in the preparation of polymeric nanoparticles.....	13
<b>Fig. 1.4.</b> Chemical structure of poly(lactic acid).....	15
<b>Fig.1.5.</b> Schematic representation of the emulsification-evaporation technique.....	18
<b>Figure 2.1.</b> <sup>1</sup> H NMR spectra and chemical structures of PEG2.5%-g-PLA (1), and palmitic acid2.5%-g-PLA (2).....	62
<b>Figure 2.2.</b> Tapping mode AFM images of NPs, left panel shows topography (T) and right panel shows corresponding phase images (P); all images are acquired in air. Scan size [400 nm × 400 nm]; PLA (a), PEG2.5%-g-PLA (b), palmitic acid2.5%-g-PLA (c).....	69
<b>Figure 2.3.a.</b> DSC curves of ibuprofen, physical mixture of PEG2.5%-g-PLA with ibuprofen, PEG2.5%-g-PLA polymer, and ibuprofen loaded NPs. Inset inside the figure shows clear thermograms for both physical mixtures and NPs, Ibuprofen melting peak is encircled.....	71
<b>Figure 2.3.b.</b> DSC curves of ibuprofen, physical mixture of palmitic acid2.5%-g-PLA with ibuprofen, palmitic acid2.5%-g-PLA polymer, and ibuprofen loaded NPs. Inset inside the figure shows clear thermograms for both pure polymer and NPs. Ibuprofen melting peak is encircled.....	72
<b>Figure 2.4.</b> <sup>1</sup> H-NMR of blank NPs of PLA (1), palmitic acid2.5%g-PLA (2), and PEG2.5%g-PLA (3) in D <sub>2</sub> O. PEG peaks at 3.6 ppm are encircled.....	77
<b>Figure 2.5.</b> Schematic representation of polymer chain organization inside the NPs: PLA (a), Palmitic acid2.5%-g-PLA (b), PEG2.5%-g-PLA (c).....	78

- Figure 2.6.** Erosion of different ibuprofen loaded NPs in phosphate buffer saline (PBS, pH 7.4) at 37 °C..... 80
- Figure 2.7.** Effect of PLA grafting on the in vitro release behavior of ibuprofen loaded NPs; values are represented as mean  $\pm$ S.D. of three independent experiments..... 82
- Figure 3.1.** <sup>1</sup>H NMR spectra and chemical structures of PEG7%-g-PLA, and multiblock copolymer, (PLA-PEG-PLA)<sub>n</sub>..... 102
- Figure 3.2.** Tapping mode AFM images of NPs, left panel shows topography (T) and right panel shows corresponding phase images (P); all images are acquired in air. PLA (a) [Scan size: 1  $\mu$ m $\times$ 1  $\mu$ m], PEG7%-g-PLA (b) [Scan size: 2  $\mu$ m $\times$ 2  $\mu$ m], and (PLA-PEG-PLA)<sub>n</sub> (c) [Scan size: 750 nm $\times$ 750 nm]..... 109
- Figure 3.3.a.** DSC curves of ibuprofen, physical mixture of PEG7%-g-PLA with ibuprofen, PEG7%-g-PLA polymer, and ibuprofen loaded NPs. Inset inside the figure shows clear thermogram for NPs..... 111
- Figure 3.3.b.** DSC curves of ibuprofen, physical mixture of (PLA-PEG-PLA)<sub>n</sub> with ibuprofen, (PLA-PEG-PLA)<sub>n</sub> polymer, and ibuprofen loaded NPs. Inset inside the figure shows clear thermograms for both physical mixtures and NPs..... 112
- Figure 3.4.** <sup>1</sup>H-NMR of blank NPs of PLA (1), PEG7%-g-PLA (2), and (PLA-PEG-PLA)<sub>n</sub> (3) in D<sub>2</sub>O. PEG peaks at 3.6 ppm are encircled..... 118
- Figure 3.5.** Erosion of different ibuprofen loaded NPs in phosphate buffer saline (PBS, pH 7.4) at 37 °C..... 120
- Figure 3.6.** Effect of PEG chain organization on the in vitro release behavior of ibuprofen loaded NPs; values are represented as mean  $\pm$ S.D. of three independent experiments..... 121
- Figure 3.7.** Schematic representation of polymer chain organization inside the NPs: PLA (a), PEG7%-g-PLA (b), and multiblock copolymers (PLA-PEG-PLA)<sub>n</sub> (c)..... 124
- Figure 3.S (supporting information):** XRD spectra of ibuprofen, physical mixture of PEG7%-g-PLA with ibuprofen, PEG7%-g-PLA polymer, and ibuprofen loaded NPs..... 131

- Figure 4.1.**  $^1\text{H}$  NMR spectra and chemical structure of PEG-g-PLA copolymers of different PEG grafting densities over PLA backbone..... 144
- Figure 4.2.** AFM images of PEG7%-g-PLA NPs encapsulating rhodamine B (RHO), before (a) and after (b) lyophilization; surface morphology (left, S) and phase image (right, P)..... 149
- Figure 4.3.** In vitro release behavior of RHO from different PEG-g-PLA NPs in comparison to PLA NPs and RHO solution; values are represented as mean  $\pm$ S.D. of three independent experiments..... 150
- Figure 4.4.** a): DLS size distribution data (nm) of different NPs upon incubation at 37 °C for 24 h with 5% FBS. b): DLS size data (nm) of NPs upon incubation at 37 °C for 24 h with 2% BSA..... 152
- Figure 4.5.** Cytotoxicity of pegylated NPs of different PEG grafting densities over PLA backbone (1, 7, and 20% mol/mol) in RAW 264.7 cells by MTT assay..... 154
- Figure 4.6.** Fluorescence images (right panels) and their corresponding phase contrast images (left panels) of RAW 264.7 cells after incubation with a) RHO, b) RHO loaded PLA NPs, c) RHO loaded PEG1%-g-PLA NPs, d) RHO loaded PEG7%-g-PLA NPs, and d) RHO loaded PEG20%-g-PLA NPs. red images show RHO. Scale bar=50  $\mu\text{m}$ ..... 156
- Figure 4.7.** RAW 264.7 cellular uptake of RHO encapsulated NPs made from PEG-g-PLA copolymer of different PEG grafting densities in comparison to PLA NPs. RAW 264.7 cells were incubated with NPs at 37°C for 24 h..... 157
- Figure 4.S1.** a): Polydispersity index values of different NPs upon incubation at 37 °C for 24 h with 5% FBS. b): Polydispersity index values of NPs upon incubation at 37 °C for 24 h with 2% BSA..... 163
- Figure 5.1.** AFM image of lyophilized ITZ loaded PEG7%-g-PLA NPs..... 177
- Figure 5.2.** The stability index of ITZ-NPs in the particle size shown as diameter [D] (a), polydispersity index [PDI] (b), and loading efficiency [% LE] (c) during storage for 30 days [d] at room temperature. Data are expressed as the mean $\pm$ S.D. (n = 3)..... 179, 180

**Figure 5.3a.** DSC curves of ITZ, physical mixture of (PLA-PEG-PLA)<sub>n</sub> with ITZ, (PLA-PEG-PLA)<sub>n</sub> copolymer, and ITZ loaded (PLA-PEG-PLA)<sub>n</sub> NPs.....181

**Figure 5.3b.** DSC curves of ITZ, physical mixture of PEG7%-g-PLA with ITZ, PEG7%-g-PLA copolymer, and ITZ loaded PEG7%-g-PLA NPs.....182

**Figure 5.4a.** XRD spectra of ITZ, physical mixture of (PLA-PEG-PLA)<sub>n</sub> with ITZ, (PLA-PEG-PLA)<sub>n</sub> copolymer, and ITZ loaded (PLA-PEG-PLA)<sub>n</sub> NPs.....183

**Figure 5.4b.** XRD spectra of ITZ, physical mixture of PEG7%-g-PLA with ITZ, PEG7%-g-PLA copolymer, and ITZ loaded PEG7%-g-PLA NPs.....184

**Figure 5.5a.** FT-IR spectra of ITZ, physical mixture of (PLA-PEG-PLA)<sub>n</sub> with ITZ, (PLA-PEG-PLA)<sub>n</sub> copolymer, and ITZ loaded (PLA-PEG-PLA)<sub>n</sub> NPs [ITZ main characteristic peaks are marked with arrows].....186

**Figure 5.5b.** FT-IR spectra of ITZ, physical mixture of PEG7%-g-PLA with ITZ, PEG7%-g-PLA copolymer, and ITZ loaded PEG7%-g-PLA NPs [ITZ main characteristic peaks are marked with arrows].....187

**Figure 5.6.** In vitro release behavior of ITZ from PEG/PLA NPs either from PEG7%-g-PLA or (PLA-PEG-PLA)<sub>n</sub> in comparison to PLA NPs and ITZ solution; values are represented as mean ±S.D. of three independent experiments.....188

**Figure 5.7.** Erythrocyte lysis caused by ITZ loaded PEG/PLA NPs preparations compared to free ITZ and ITZ-PLA NPs. Values are expressed as mean of % lysis of three separate experiments ±S.D.....189

**Figure 5.8a.** Plates inoculated with *C. albicans* fungal cells and incubated at 30 °C, treated with 12.5 μl of (a) ITZ-Water, (b) ITZ-DMSO, (c) ITZ-PLA NPs, (d) ITZ-PEG7%-g-PLA NPs, and (e) ITZ-(PLA-PEG-PLA)<sub>n</sub> NPs. Lower plates (a-e) represent control experiments corresponding to each upper plate either using only the solvent in case of ITZ-Water, and ITZ-DMSO or only blank NPs ( no ITZ) in case of NPs formulations.....191

**Figure 5.8b.** Plates inoculated with *A. fumigatus* fungal cells and incubated at 30 °C, treated with (a) ITZ-Water, (b) ITZ-DMSO, (c) ITZ-PLA NPs, (d) ITZ-PEG7%-g-PLA NPs, and (e) ITZ-

(PLA-PEG-PLA)<sub>n</sub> NPs. Lower plates (a-e) represent control experiments corresponding to each upper plate either using only the solvent in case of ITZ-Water, and ITZ-DMSO or only blank NPs ( no ITZ) in case of NPs formulations.....192

**List of abbreviations**

AFM	Atomic Force microscope
ANOVA	Analysis of variance
BSA	Bovine serum albumin
°C	Degree Celsius
CDCl <sub>3</sub>	Deuteriated chloroform
DCM	Dichloromethane
DLS	Dynamic light scattering
DL	Drug loading
DMEM	Dulbecco's modified eagl's medium
DMSO	Dimethyl sulfoxide
D <sub>2</sub> O	Deuterium oxide
DSC	Differential scanning calorimetry
EPR	Enhanced permeability and retention
FBS	Fetal bovine serum
FTIR	Fourier transform infrared spectroscopy
GPC	Gel permeation chromatography
h	Hour
HCl	Hydrochloric acid
<sup>1</sup> H NMR	Proton nuclear magnetic resonance
HPLC	High performance liquid chromatography
ITZ	Itraconazole

IV	Intravenous
kDa	Kilo Dalton
LE	Loading efficiency
$M_n$	Number average molecular weight
$M_w$	Weight average molecular weight
MPS	Mononuclear phagocytic system
MTT	3-(4,5-dimethylthiazol-2-yl)-2,5-diphenyltetrazolium bromide
MWCO	Molecular weight cut off
$M_w$	Molecular weight
NPs	Nanoparticles
NaCl	Sodium chloride
NaOH	Sodium hydroxide
O/W	oil in water
PBS	Phosphate buffered saline
PCL	Poly( $\epsilon$ -caprolactone)
PDI	Polydispersity index
PEG	Poly(ethylene glycol)
PCS	Photon correlation spectroscopy
PEG-g-PLA	Poly(ethylene glycol)-grafted-poly(D,L-lactide)
PEG2.5%-g-PLA	Poly(ethylene glycol)2.5%-grafted-poly(D,L-lactide)
PEG7%-g-PLA	Poly(ethylene glycol)7%-grafted-poly(D,L-lactide)

PEG20%-g-PLA	Poly(ethylene glycol)20%-grafted-poly(D,L-lactide)
(PLA-PEG-PLA) <sub>n</sub>	(poly(D,L-lactide)-block- poly(ethylene glycol) block-poly(D,L-lactide)) <sub>n</sub>
PLA	Poly(lactic acid)
PGA	Poly(glycolic acid)
PLGA	Poly(lactic- <i>co</i> -glycolic acid)
PVA	Polyvinyl alcohol
PXRD	Powder x-ray diffraction pattern
$d_h$	Hydrodynamic diameter
RHO	Rhodamine
RPMI	Royal Park Memorial Institute (culture medium)
SD	Standard deviation
SEM	Scanning electron microscopy
$T_g$	Glass transition temperature
TEM	Transmission electron microscopy
TM-AFM	Tapping mode atomic force microscope
UV	Ultraviolet
wt	Weight
$\lambda_{\max}$	Wavelength of maximum absorbance
$\lambda_{\text{ex}}$	Excitation wavelength
$\lambda_{\text{em}}$	Emission wavelength
XPS	X-ray photoelectron spectroscopy

*To my mother, my kids, my wife and the souls of  
of Egyptian Revolution martyrs.*

## **Acknowledgements**

This work was carried out at the Division of Pharmaceutics, Faculty of Pharmacy, University of Montreal. I wish to express my gratitude to my supervisor, Dr. Patrice Hildgen for his continuous support and guidance into the world of science. I would also like to thank him for always being available and willing to help me in the challenges of this work. During my studies, he has given me the freedom and reliable basis necessary to advance this project and to develop as an independent researcher. Also, I really value his deep involvement and valuable criticism throughout the course of my doctoral studies without which it would have been difficult to finish this thesis.

I am sincerely grateful to all my co-authors, Jean Michel Rabanel, Fatiha Louhichi, and Dr. Martine Raymond, for their remarkable contribution to this work. Special thanks are due to Jean Michel Rabanel for his technical assistance, valuable discussion and suggestions during my study. I would like to express my warmest thanks to all my lab colleagues for discussions, friendship and for creating a pleasant atmosphere during these years. I also express my gratitude for Dr. Grégoire Leclair, evaluator of my progress reports for his valuable time and thoughtful discussion. I also acknowledge Mme. Suzie Poulin, research associate, Ecole polytechnique, Montreal University for her unlimited help and patience in interpretation of XPS data.

Finally, I would like to express my gratitude to my mother, my wife, and my little kids for their endless support and love. It is their sacrifice and understanding that allowed me to work hard to finish this thesis.

The financial support by the missions department, Ministry of Higher Education, Egypt is gratefully acknowledged.



# **CHAPTER ONE**

---

## **INTRODUCTION**

### **Polymeric Nanoparticles (NPs) as Drug**

### **Delivery Systems**

## **1.1. A Brief Overview of Nanotechnology**

In recent years, significant effort has been devoted to research and applications in the area of nanotechnology. Nanotechnology is the design, characterization, synthesis and application of materials, structures, devices and systems by controlling shape and size at nanometer scale [1]. Nanotechnology is widely applied nowadays to many areas of life as; fiber and textiles [2], agriculture [3], electronics [4], forensic science [5], space [6] and many other industrial applications. Medicine is one of the areas likely benefited from advances in nanotechnology [7-10]. Many applications of nanotechnology in medicine have been investigated so far including drug delivery, both in vitro and in vivo diagnostics, and production of high quality biocompatible materials [11, 12]. It is reported that the global market of nanotechnology is expanding very fast with many expectations that it will reach \$1.5 trillion by year 2012 [13].

## **1.2. Nanotechnology and Drug Delivery**

Development of nanotechnology for drug delivery has attracted a great deal of attention in recent years. Nanotechnology for drug delivery aims at formulating medicinal agents in biocompatible nanocarriers (nanoparticles) for improving their clinical outcomes. The development of nanotechnology products for currently existing drugs may optimize their therapeutic performance, and minimize the need for developing new drugs with better properties. Formulating drugs into nanocarriers has proven successful to achieve all the following tasks [14]. To enhance the solubility and hence; absorption of poorly water-soluble drugs; efficiently target drugs into distant areas in the body; enhance cellular uptake of drugs across tight epithelial and endothelial barriers; efficiently deliver large macromolecular drugs (e.g. proteins, peptides and nucleic acids) to intracellular sites; deliver two or more drugs using the same carrier [15, 16]; and follow drug delivery journey in the body using imaging tools combined with the drug in the same carrier [17].

Nowadays, nanotechnology is widely used for encapsulating many drugs/bioactive moieties onto nanocarriers to improve either their pharmaceutical performance (e.g. bioavailability, stability, and controlled release) or their pharmacological performance (e.g. therapeutic activity, reducing side effects, and effective targeting) [18-20]. Several drugs used for treating incurable diseases like cancer [21], AIDS [22], diabetes [23], malaria [24], prion disease [25] and tuberculosis [26] are in the clinical testing phase and some of them are available in the market

[27, 28]. As a result of the last mentioned applications, nanotechnology holds enormous promise for drug delivery and it is widely expected that nanotechnology will be able to change the landscape of pharmaceutical and biotechnology industries for the foreseeable future [14].

### **1.3. Design of Nanotechnology–Polymeric based Drug Delivery Systems**

There are a number of parameters that need to be considered for the development and manufacturing of successful drug delivery vehicles [29]. These include (a) the use of well-characterized, biodegradable, biocompatible materials; (b) the ability to tune the biophysicochemical properties of the used materials (e.g. hydrophilicity/ hydrophobicity balance, charge, molecular weight) to develop nanocarriers with adjustable properties (e.g. size, surface charge, release behavior); and (c) developing small unit operations amenable to scaling-up (manufacturing large quantities of drug delivery systems) for clinical applications. Numerous classes of drug delivery nanocarriers composed of different materials including lipids, polymers and inorganic materials have been developed, resulting in different delivery systems that vary in their physicochemical properties and thus their pharmaceutical uses.

Growing interest in formulating polymeric nanoparticles is rapidly expanding for the following reasons. Advances in the scientific fields of polymer chemistry and polymer colloid physicochemistry have resulted in the availability of many tailor-made polymers for drug delivery. Polymeric drug delivery systems are often biodegradable, and biocompatible with potential of controlled drug release. They often have a superior drug delivery performance (e.g. size, surface charge, drug release, and cellular uptake properties) relative to other non-polymeric carriers. Moreover, they can be designed with hydrophilic coats, such as poly(ethylene glycol) (PEG), which creates a steric barrier decreasing the adsorption of opsonin proteins onto particle surface. This helps nanoparticles avoid recognition by the mononuclear phagocytic system (MPS) and circulate for prolonged period of time in the blood [30, 31]. Nanoparticles assembled from water soluble polymers usually have a molecular weight above glomerular filtration threshold (42-50 kDa), which is another cofactor for their prolonged circulation in the body [32].

An interesting feature of polymeric carriers is their ability to control the release of a therapeutic agent to achieve desired therapeutic level in certain pathological areas in the body. This could be achieved by the use of stimuli responsive polymers which release their payload under the effect of external stimuli (i.e. change in pH, temperature or ionic strength) [33, 34].

This allows maximum drug release at the target site, achieving optimum therapeutic efficacy [35]. Polymeric nanoparticles can be delivered to distant target sites either by localized delivery using a catheter-based approach [36] or they can be attached to a recognition marker or/ ligand which could direct them to the target area [37]. They usually achieve high drug loading, which maximizes drug/excipients ratio. This results into reducing the frequency of administration and hence, patient expenses, and risks of toxicity could also be reduced.

One of the most distinct advantages of polymeric carriers for drug delivery is their adjustable nanometer size range. Due to their sub-cellular and sub-micron size, polymeric nanoparticles can homogeneously penetrate into tissues, cross the fenestration of the epithelial lining (e.g., liver), and efficiently taken up by the cells [38]. In addition, their nanometer size range allows them to be efficiently captured by some tumor cells particularly solid tumors, infarcts and inflamed tissues. This phenomenon is called enhanced permeability and retention effect (EPR) or passive accumulation of nanocarriers into the tumor tissues [39]. EPR mainly occurs because of the pathophysiological features of tumors vessels that are mainly distinct from normal vessels. Tumor cells are characterized by hypervascularity, incomplete vascular architecture, poorly aligned endothelial cells and wide fenestrations (20 nm-1.2  $\mu$ m) [40, 41]. These features make the vasculature of pathological tissues more “leaky” or more “permeable” than that of normal tissue. This increased permeability or leaky vasculature together with compromised lymphatic drainage facilitates accumulation of macromolecules and nanoparticles in pathological tissues. Based on the EPR effect, drug concentration in the tumor tissues was found to be 10-30 times higher than that in the blood and other normal tissues [42]. To sum up, nanoencapsulation of medicinal drugs using polymeric carriers (nanomedicines) was shown to enhance drug efficacy, specificity, tolerability and therapeutic index of many drugs [43-45].

#### **1.4. Review of Polymeric Nanoparticles as Delivery Systems**

Polymeric nanoparticles are solid or semisolid colloidal particles that vary in size from 10 nm to 1000 nm [46]. They are mainly consisting of macromolecular substances and can be used as drug carrier. The drug is adsorbed, dissolved, entrapped, or encapsulated into the nanoparticles matrix. Either nanospheres or nanocapsules can be obtained from the same polymer depending on the used method of preparation [47, 48]. Nanospheres are matrix systems in which the drug is uniformly dispersed whereas; nanocapsules are vesicular systems in which

the drug is confined to a cavity surrounded by a polymer shell (Fig. 1.1). After preparation, nanoparticles are usually dispersed in aqueous solution. The resultant drug nanoparticle dispersion can be administered to humans by many routes as injection, oral route, or applied topically either to the skin or the eye. Nanoparticles can be also used for pulmonary delivery after being dried to a powder, or can be compressed into tablets or capsules.

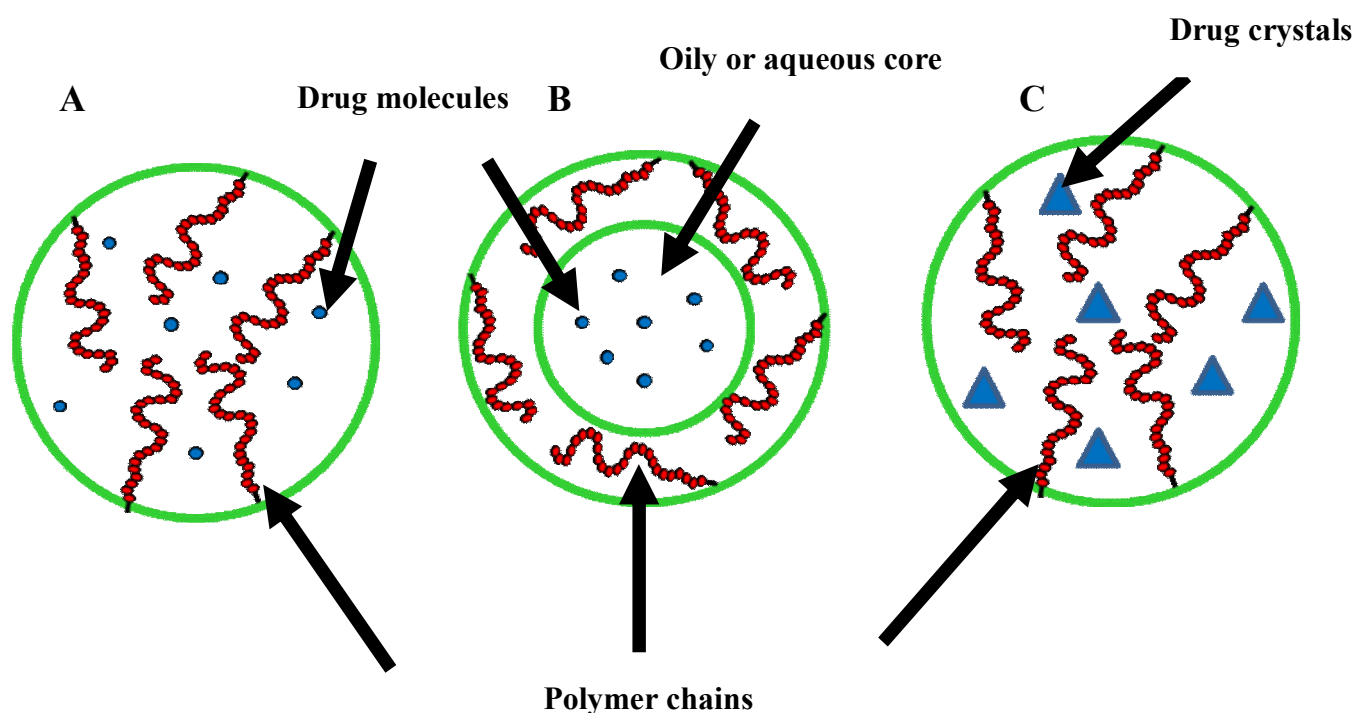


**Fig.1.1.** Schematics of polymeric nanoparticles. A. Matrix type nanosphere, drug molecules are uniformly dispersed in the polymer matrix. B. Core shell nanocapsules, drug molecules are presented in an oily or aqueous core covered with polymeric shell. C. matrix type nanosphere where drug crystals are embedded in a polymer matrix.

### 1.5. Factors affecting Performance of Polymeric Nanoparticles as Delivery Vehicles

Formulation of nanoparticles as delivery vehicles depends on the choice of suitable polymeric substance having acceptable biocompatibility and biodegradability, higher incorporation efficiency, and an extraordinary ability to enhance the drug retention time in vivo. Nanoparticles are superior to conventional drug carriers (e.g. tablets, capsules....etc.) with respect to control release, targeted delivery and therapeutic potential.

Many factors affect the drug delivery performance of polymeric nanoparticles as particle size, surface charge, surface modification, and hydrophobicity (Fig.1.2). Size and size distributions of nanoparticles play an important role in determining their release kinetics as well as their interaction with the cell membrane and their penetration across the biological barriers. The ability of nanoparticles to penetrate different biological barriers is mainly dependent on the particle size, the target tissue biophysiological characteristics e.g. tissue size, tissue thickness, and blood circulation [49]. It has been shown before that large size particles are rapidly cleared by mononuclear phagocytic system (MPS) than smaller size particles [50]. The size of the carrier might have a role in complement activation [51]. For long circulating colloidal nanoparticles, optimum size is favored to be 150-200 nm [52, 53].

Surface charge is also important in determining the in vivo stability as well as cellular interaction of nanoparticles. Surface charge measurement (zeta potential) evaluates whether nanoparticles would aggregate in blood flow or would adhere to, or interact with oppositely charged cells membrane [54]. As a biological rule, to enhance the rate and extent of cellular uptake, positively charged surfaces or cationic surface charges are required as it promotes the interaction of nanoparticles with the negative charges (phospholipids) of the cell membrane [10]. However, cationic charges could enhance the non-specific cell sticking or uptake of the particles. As a result, it is recommended that colloidal carriers should have neutral or near neutral surface charge to avoid both the non specific cell uptake and uncontrolled plasma protein adsorption onto their surfaces [50, 55].

Intravenously (IV) administered nanoparticles are easily recognized by the body immune system, and then massively cleared by the macrophages (MPS) rich organs such as liver, spleen, lungs and bone marrow [56]. The NPs surface hydrophobicity determines the amount of adsorbed blood components, mainly proteins (opsonins) which initiate the phagocytosis process [57]. Hence, to prolong the circulation time of NPs in the blood, it is necessary to minimize the opsonization process (plasma protein adsorption onto NPs surface). This can be achieved by surface modification of hydrophobic particles by coating their surfaces with different hydrophilic molecules such as polyethylene glycol (PEG), polyethylene oxide, polyoxamer, poloxamine and polysorbate 80 (Tween 80) [46, 58].

Finally, the in vivo performance of nanoparticles is affected by morphological characteristics, surface chemistry, and molecular weight. Molecular weight of the carrier can

play a role in modulating the release behavior. For a slow drug release from the particles, high molecular weight of the starting polymer should be used [59]. Careful formulation of polymeric nanoparticles with respect to target and route of administration may solve many pharmaceutical problems of either marketed drugs or newly discovered drugs.

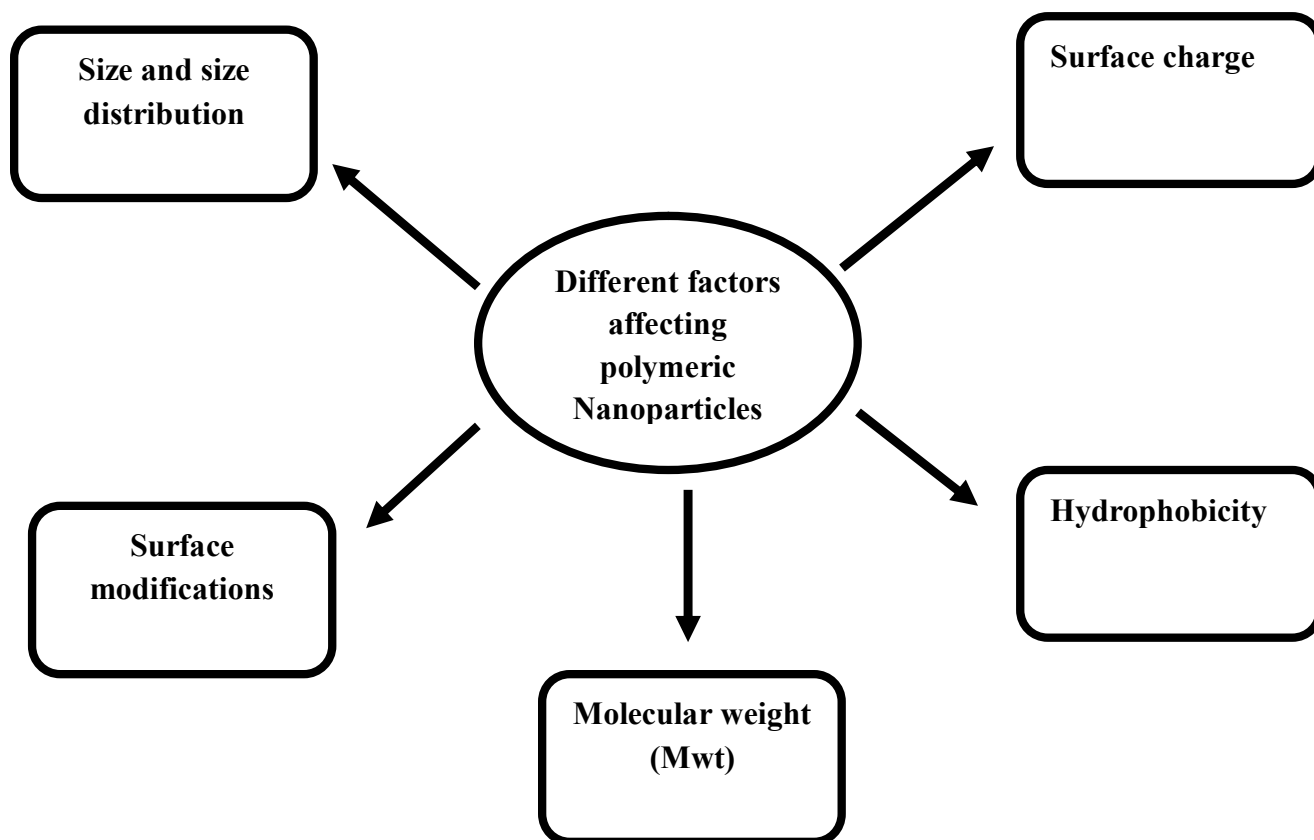


**Fig.1.2.** Factors affecting the drug delivery performance of polymeric nanoparticles

### 1.6. Applications of Polymeric Nanoparticles

Nanoparticles in pharmaceutical applications have gained plenty of research attention during recent decades taking advantage of their small size, and their biodegradable nature [13]. Nanoparticles can be administered orally as a reconstituted aqueous dispersion. NPs dispersion is easily uptaken and absorbed into the systemic circulation across the mucosal epithelium by enterocytes [60]. They could protect the encapsulated active ingredient against the gastro-

intestinal (GI) tract harsh conditions and/or prolong the contact time of its payload on the mucous membrane by efficiently adhering to mucosal surfaces (bioadhesion). Many examples of the oral applications of NPs are reported in the literature particularly for delicate macromolecules e.g. oral delivery of peptides such as salmon calcitonin [61] and elcatonin [62]. NPs were also used as an oral carrier for the delivery of hormones as mifepristone [63] and estradiol [64]. Oral delivery of vaccines by NPs has achieved considerable success through the targeted uptake of the particles in the M cells of peyer's patches. Many examples for the oral immunization using PLGA nanoparticles are also reported such as tetanus toxoid [65], ovalbumin [66] and bovine serum albumin (BSA) [67].

Several applications of stealth (long circulating) nanoparticles can be found in the area of tumor/cancer therapy. The mean residence time, effective concentration, half life of some anticancer drugs loaded into polymeric nanoparticles have been enhanced compared to pure drug e.g. camptothecin [68], and paclitaxel [69].

PLA and PLGA NPs have also been applied for the sustained delivery of many drugs into an intracellular target [70-72]. NPs could enhance the cytoplasmic delivery of many drugs through their marked ability to rapidly escape the endo-lysosomal compartment to the cytoplasmic compartment e.g. PCL nanoparticles [73]. Dexamethasone-loaded nanoparticles has achieved higher antiproliferative activity in vascular smooth muscle cells compared to free dexamethasone due to the enhance uptake of NPs by the glucocorticoid receptors which are cytoplasmic [74].

Another interesting application of nanoparticles is their ability to deliver drugs across the Blood-Brain Barrier (BBB) [75]. Nanoparticles has been shown to sustain the delivery of therapeutic agents to brain tumours following the opening of tight junctions of the BBB by hyperosmotic mannitol [76]. Poly(alkylcyanoacrylate) nanoparticles have been widely investigated as a drug carrier to the brain [77]. Many types of polymeric nanoparticles have also been used for the brain delivery e.g. PLA-PEG nanoparticles functionalized by lectin [78], PLA-PEG nanoparticles bearing cationic BSA coating [79], PLA-polysorbate 80 nanoparticles [80], and PLGA peptide nanoparticles [81]. Loperamide has been loaded into peptide derivatized PLGA NPs then delivered successfully to the central nervous system of rats [82]. Till now, the mechanisms of particle uptake across the BBB are not clearly identified; other processes may be also involved [83].

Nanoparticles with mucoadhesive properties have also been investigated as an ocular drug delivery carrier. They mainly act as an ocular carrier based on their ability to prolong the mean residence time of the drug in the cornea, control its release and reduce irritation after topical application. Flurbiprofen loaded into PLGA nanoparticles exhibited higher anti-inflammatory action upon instillation into the eye than free drug [84]. Similar enhancement of the ocular absorption of acyclovir-loaded PEG-PLA nanoparticles has been observed [85].

In gene delivery studies, non-viral vectors are assembled through the interaction between the negative charge of nucleic acids and the positive charge of the particles. Non viral vectors have been demonstrated a marked ability to encapsulate the entrapped gene, protect it against stressful body conditions, sustain its release, and facilitate its delivery and interaction with the cell membrane. For example, PLA-PEG nanoparticles administered orally have achieved higher transfection efficiency for the encapsulated DNA [86]. PLGA nanoparticles have been used as non viral vector for the sustained release of DNA [87]. Many challenges in nanoparticulate gene delivery applications are faced particularly the key challenge of enhancing the coupling potential between nucleic acid and the polymer while maintain the size of the carrier in the nanometer scale.

Despite the extensive research in the area of nanotechnology and drug delivery, few polymeric nanoparticulate products have marketed so far. A commercialized product, Abraxane™, obtained from the protein albumin bound with paclitaxel, is administered intravenously [88]. Another product, Doxorubicin Transdrug®, consisting of doxorubicin-loaded poly(isohexylcyanoacrylate) nanoparticles is currently investigated clinically [89].

As a general summary of the investigated applications of nanoparticles in the pharmaceutical field, nanoparticles could protect the encapsulated active ingredient, enhance its action, reduce its toxicity and side effects, sustain its release and target it into the desired area. For clinical translation, most of the research is now focused on developing processes for the scaling up of nanoparticles [90]. A range of different types of nanoparticles and their applications are outlined in Table 1.1.

**Table 1.1.** Different applications of polymeric nanoparticles in pharmaceutical field.

<b>Therapeutic application</b>	<b>Carried therapeutic agent/fluorescent marker</b>	<b>Ref.</b>	<b>Advantages</b>
<b>Oral and nasal therapy</b>	Salmon calcitonin Elcatonin Mifepristone Estradiol Tetanus toxoid Oral vaccination, Ova-albumin Bovine serum albumin	[61] [62] [63] [64] [65] [66] [67]	(1) Sustained release of the encapsulated drug. (2) Efficient uptake and transport across the mucosal epithelium. (3) Protect the encapsulated drug against the gastro-intestinal (GI) tract harsh conditions. (4) Prolong the residence time of drug on the mucous membrane (mucoadhesive properties).
<b>Cancer therapy</b>	Camptothecin Paclitaxel Tamoxifen Curcumin Doxorubicin Neocarzinostatin Atinsense oligonucleotides (AONs)	[68] [21, 27] [69] [10] [91] [12] [39] [57]	(1) Enhanced antitumor efficacy. (2) Reduced systemic side effects and toxicity levels. (3) Enhanced tumor specific uptake. (4) Enhanced accumulation into tumor tissues.
<b>Brain therapy</b>	Cisplatin Dalargin hexapeptide 6-Coumarin FITC-Dextran Fluorescein Loperamide/ Rhodamine B	[76] [77] [78, 79] [80] [81] [82]	(1) Efficient passage across the blood brain barrier (BBB). (2) Effective targeting of the brain endothelium. (3) Sustained drug release into the brain cells.
<b>Gene Therapy</b>	DNA DNA vaccine DNA, siRNA, and AONs	[86] [87] [92]	(1) Increased transfection efficiency. (2) Protection of the encapsulated gene against in vivo degradation.
<b>Intraocular delivery</b>	Flurbiprofen Acyclovir	[84] [85]	(1) Prolonging the corneal contact time. (2) Controlled drug release. (3) Reduced ocular irritation.

(FITC-dextran): Fluorescein isothiocyanate-dextran

## 1.7. Preparation of Polymeric Nanoparticles

Polymeric nanoparticles for pharmaceutical applications are prepared from a class of synthetic and natural polymers. Natural polymers are considered safer and more biocompatible than synthetic ones. Synthetic polymers became more acceptable than before in the preparation of NPs due to the greater control over their biophysicochemical properties. Natural polymers include e.g. albumin [93], casein [91], alginate [94], gelatin [95, 96], and chitosan which is considered the most widely used natural polymer for nanoparticle preparation [97, 98]. Synthetic polymers include aliphatic polyesters, polyanhydrides, polyorthoesters, and polycyanoacrylates [46]. Other investigated synthetic polymers include polystyrene [99] and poly(vinyl pyridine) [100].

Two techniques are widely used for nanoparticles preparation; (i) polymerization of monomers and (ii) deposition of an already synthesized or preformed polymer [58, 101]. Nanoparticle preparation from preformed polymers is more common because of the ease of the preparation, more control of the manufacturing process, and reproducibility of the used method. Polymer deposition method mainly depends on dissolving a preformed polymer in a convenient solvent followed by precipitation in a liquid medium leading to nanoparticle formation. The drug intended to be encapsulated in the particles is usually incorporated in the process during the polymer solvation process. Nanoprecipitation, salting-out, emulsification/solvent diffusion, and emulsification/solvent evaporation methods are widely applied techniques used for nanoparticles preparation by polymer deposition method [46, 102-104].

Nanoprecipitation method was introduced and patented by Fessi and co-workers [105]. In this method, particles are formed spontaneously by precipitation and subsequent solidification of the polymer upon rapid solvent diffusion. The polymer is dissolved in a water miscible organic solvent (or solvent mixture) and poured under magnetic stirring into a non solvent (usually water containing surfactant), in which the organic solvent diffuses. The mechanism of formation of NPs by this technique has been explained by the interfacial turbulence generated at the interface of the solvent and non-solvent. Thus, the process is often called solvent displacement or interfacial deposition. In the salting-out method, nanoparticle formation is based on the separation of a water-miscible solvent containing the polymer from aqueous solutions via a salting-out effect. Acetone is commonly used as the water-miscible solvent because of its

solubilizing efficiency and rapid separation from aqueous solutions by salting-out effect with electrolytes. In emulsification/solvent diffusion method, nanoparticle formation starts when the saturation limit of a partially water-miscible solvent (e.g. benzyl alcohol) is exceeded by addition of water. In both techniques, vigorous stirring is a prerequisite for inducing the phase separation. The emulsification solvent evaporation method is presented in section 1.7.5. Another widely used technique nowadays for nanoparticles preparation is supercritical fluid technology [106, 107]. Nanoparticles can also be prepared directly from monomers using different polymerization techniques as described in those reviews [46, 102]. A list of some used polymers and the commonly used methods to prepare nanoparticles are summarized in Table 1.2.

Nanoparticles are usually prepared as an aqueous dispersion. If nanoparticles are stored in an aqueous medium, polymer degradation, drug leakage, and/ or drug degradation may occur [108]. In addition, handling (storage, transportation) of a liquid particle system is inconvenient. To improve the physicochemical stability of nanoparticles, freeze-drying is usually performed to conserve the structure of particles, facilitate handling and transport, and help the further processing of particles into other dosage forms (e.g. tablets, capsules, and powder).

### **1.7.1. Classification of Copolymers used for Nanoparticles Formation**

Nanoparticles have been formulated using a wide range of polymers. Copolymers are widely used than homopolymers in NPs preparation due to their tunable properties. Copolymers can be divided into 4 main types based on their architecture (how the building blocks are connected together) (Fig.1.3):

1. Block copolymers: linear copolymers where the end group of one chain is covalently attached to the head of another chain giving diblock or triblock architectures [109].
2. Graft copolymers: branched copolymers with a comb-like architecture where different branches emanate from one main chain.
3. Random copolymers: linear copolymers with the building blocks arranged randomly [110].
4. Alternating copolymers: linear copolymers with perfectly alternating arrangement of their building blocks.

### 1.7.2. Polyesters

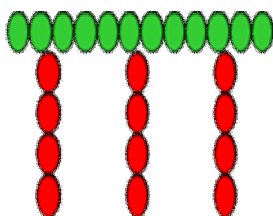
Biodegradable polyesters (e.g. PLA, PGA, PLGA and PCL) are, so far, the most extensively used biomaterials for biomedical applications. They are the preferred synthetic polymers for nanoparticle preparation for the following reasons. They are mainly characterized by their biocompatibility and their controlled degradation to biocompatible monomers [111]. They are degraded by bulk hydrolysis of their ester bonds [112]. Their degradation products (e.g. lactic acid or glycolic acid) are eliminated from the body by citric acid cycle [113], hence, they do not require any kind of surgery to be removed from the body. They are easily synthesized through ring opening polymerization of cyclic lactones. They could efficiently protect the entrapped drug against degradation and control its site specific delivery. They are more efficient for encapsulation of many drugs particularly hydrophobic drugs. Encapsulated drugs are slowly released from polyester based matrices upon the controlled degradation of the polymeric materials.



**Diblock copolymer**



**Mutliblock copolymer**



**Graft copolymer**



**Random copolymer**



**Alternating copolymer**

**Fig.1.3.** Architectures of different copolymers used in the preparation of polymeric nanoparticles.

**Table 1.2.** Polymers and methods widely used in nanoparticle preparation.

<b>Polymer class</b>	<b>Examples</b>	<b>Drug/application</b>	<b>Preparation method</b>	<b>Ref.</b>
<b>Natural polymers</b>	Albumins	Ganciclovir	Coacervation	[93]
	Casein	Curcumin	Centrifugation redispersion	[91]
	Alginate	Antitubercular drugs (Isoniazide, Rifampicin, and Pyrazinamide)	Cation induced gelation	[94]
	Gelatin	Paclitaxel	Desolvation method	[95]
	Chitosan	Bovine serum albumin	Ionic gelation	[97]
<b>Synthetic polymers</b>	Poly(alkyl cyanoacrylate)	Tissue adhesives	Polymerization method	[46]
	Poly(alkyl methacrylate)	Tissue adhesives	Polymerization method	[46]
	Polystyrene	Progesterone	Emulsification/solvent evaporation method	[99]
	Poly(vinyl pyridine)	Tebuconazole	Emulsification/solvent diffusion method	[100]
	Poly( $\epsilon$ -caprolactone) (PCL)	Many anti-cancer drugs and model proteins	Different Techniques are described in the cited review	[112]
	Polylactic acid (PLA)	Bovine serum albumin	Emulsification/solvent evaporation method	[114]
	Poly(lactic-co-glycolic acid) (PLGA)	Bovine serum albumin and 6-coumarin	Emulsification/solvent evaporation method	[74]

### 1.7.3. Poly(lactic acid) (PLA)

Poly(lactic acid) (PLA) belongs to the family of linear aliphatic polyesters commonly made from  $\alpha$ -hydroxy acids. PLA mainly obtained from lactic acid monomers (Fig. 1.4.). Being biodegradable polyester, PLA is widely used nowadays for nanoparticle preparation. PLA is also used for the manufacture of resorbable sutures, bone implants, artificial organs, tissue screws, and contraceptive implants [115, 116].

PLA is the simplest hydroxy acid with an asymmetric carbon atom and exists in two optically active configurations. Polymers of L(+) lactic acid and D(-) lactic acid are partially crystalline, while the racemic poly(D,L-lactic acid) is amorphous. The self-condensation of lactic acid results in low molecular weight (Mwt) PLAs, whereas ring opening polymerization of lactide usually results into higher Mwt PLA polymers [117]. PLAs are insoluble in water and ethanol, but they are soluble in organic solvents such as dichloromethane and chloroform [117-119].

PLA undergoes hydrolytic degradation of its ester bond in an aqueous medium [120]. The degradation products are biocompatible and metabolizable; they are removed from the body by the citric acid cycle. PLA degradation rate is mainly controlled by these factors; (i) Mwt (high Mwt PLAs degrade slower); (ii) crystallinity (amorphous PLA degrades faster); (iii) environmental conditions (pH, ionic strength, temperature); (iv) particle morphology (porous particles degrade faster); (v) size of the particles (small size particles degrade faster) [121]. Drugs encapsulated into PLA particles also could affect its degradation rate. Both acidic and basic drugs may catalyze the degradation of PLA polymeric carriers either microparticles or nanoparticles.

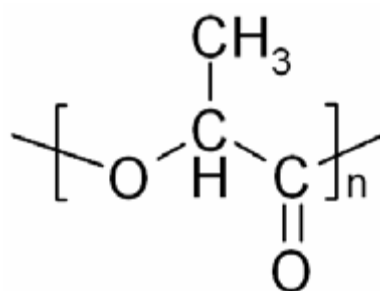


**Fig. 1.4.** Chemical structure of poly(lactic acid).

#### 1.7.4. Functionalized Polyesters for Nanoparticles Preparation

Extensive work has been recently devoted towards functionalizing polyesters in order to enhance the drug delivery behavior of the obtained nanoparticles, increase the number of drugs that can be encapsulated into the polymeric particles and finally to efficiently control the drug release pattern. Most polyesters do not have significant number of functional groups that could enhance their potential applications. Such applications are greatly widened when functional pendant groups are incorporated into the polymer backbone.

Introduction of functional groups that can be easily substituted or conjugated with the compound of interest is a challenge. Many synthetic protocols were tried in the past for the synthesis of functionalized polyesters with better characteristics [122-124]. Most of these trials were complex including various tedious steps and the process itself was not reproducible and out of control in many cases. For example, functionalized malolactonate copolymers were synthesized with low yields (12–45%) and polymerization reactions were very slow (over 4–30 days) [122]. PLA grafted polysaccharide copolymers were also synthesized with a multistep method that required protection/deprotection step [125]. Moreover, most of the polyesters developed had molecular weights that are usually not high enough to be used for nanoparticles preparation [126]. Thus, there are very few methods that could be regarded as easy and efficient for the synthesis of functionalized polyesters. An efficient method for the synthesis of functionalized PCL and PLLA with controlled molecular weight and low polydispersity was previously reported [124].

In our study, nanoparticles were prepared from novel functionalized PLA copolymers. Those copolymers were developed by grafting different functional substituent as poly(ethylene glycol), PEG onto PLA backbone according to a previously reported method by our group [127]. This method simply depends on the development of versatile copolymers of PLA and allyl glycidyl ether. The grafted PLA with allyl group is undergoing subsequent steps to convert the allyl group into hydroxyl and then carboxyl groups to which various functional groups could be grafted easily to the polymer backbone. Various bioactive molecules like salens [128] or ligands for E-selectin and for P glycoprotein were successfully grafted onto PLA Backbone. Also, methoxy PEG-g-PLA has been previously synthesized by our group using the same principle and successfully used to prepare colloidal nanoparticles for sustained drug release [129].

### 1.7.5. Emulsification Solvent Evaporation

The emulsification solvent evaporation method was early described by Niwa *et al* and has been widely used to prepare NPs from a range of polymeric materials, particularly PLA and PLGA [130]. In this method, the polymer is first dissolved in a water immiscible, volatile organic solvent (e.g. chloroform, methylene chloride or ethyl acetate) then emulsified into an aqueous phase as shown in Fig.1.5. Emulsification can be achieved with the help of mechanical stirring, sonication or a high-energy source such as ultrasound or homogenization [Fig. 1.5]. The aqueous phase usually containing a surfactant like poly(vinyl alcohol), PVA to stabilize the system and help the formation of relatively small sized particles with uniform size distribution [131]. Nanoparticles tend to precipitate into the aqueous phase in the form of solid particles after the organic solvent has been removed under reduced pressure. This technique has been widely used for encapsulating hydrophobic drugs. The procedure has been modified to help encapsulating hydrophilic compounds and large macromolecules as peptides and proteins. The modified protocol depends on the use of the double or multiple emulsion technique (w/o/w) instead of the single emulsion (o/w). Simply, a water soluble drug and a surfactant are dissolved in water. The primary emulsion is prepared by dispersing the aqueous phase into an organic solvent containing a dissolved polymer. This is then re-emulsified in an outer aqueous phase also containing surfactant [132-134]. From here, the procedure for obtaining the nanoparticles is similar to the single emulsion technique (o/w) for solvent removal.

Several factors can influence the physicochemical properties of the obtained particles, these include; type and molecular weight of the starting polymer, concentration of polymer in the organic phase, type of organic phase, volume ratio of organic: aqueous phase, nature and concentration of surfactant, and stirring speed.

The main advantages of using this technique is the use of water as the nonsolvent; this is reduces the cost of production, facilitates the washing step of the particles, facilitates the further processing of particles [102]. However, there are some major disadvantages associated with the use of this method to prepare NPs. First of all, residual chlorinated solvents have serious toxicity potential. Second, the excess surfactant used is difficult to remove. Poly(vinyl alcohol), PVA is the most widely used stabilizer to prepare nanoparticles. However, PVA remains adsorbed at the surface of the nanoparticles and is difficult to be removed by multiple washing steps. It is

reported that PVA adsorbed at the surface of nanoparticles could change biodegradability, biodistribution, NPs cellular uptake, and drug-release pattern [135]. Third, this procedure is good for a laboratory-scale, but not for a large-scale pilot production.

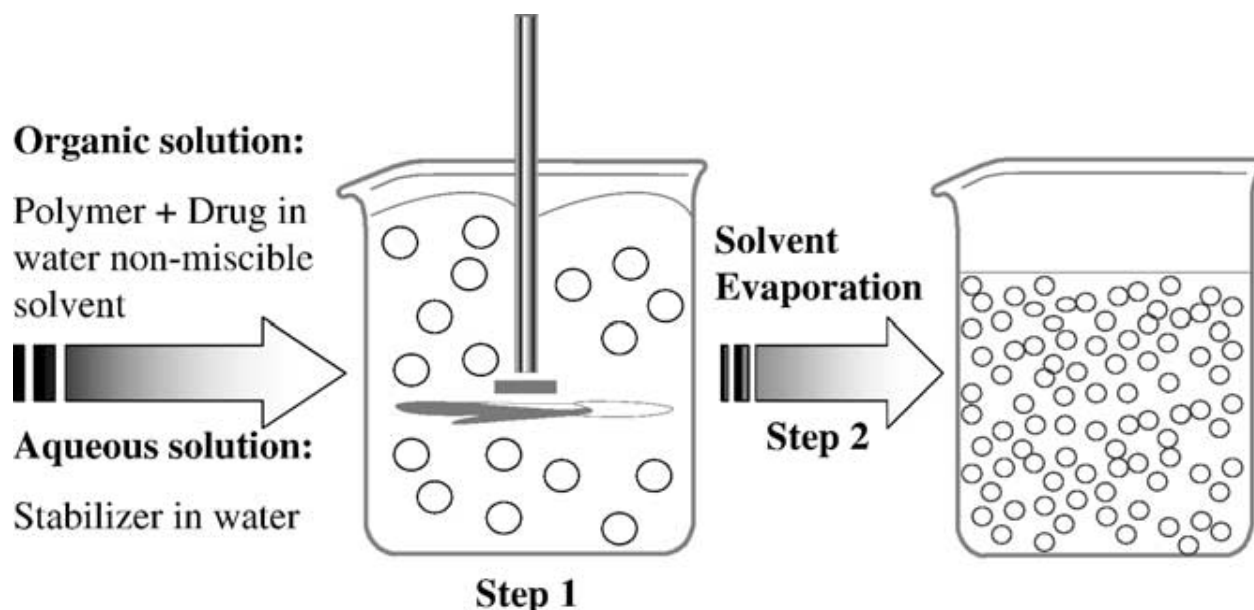


**Fig.1.5.** Schematic representation of the emulsification- evaporation technique (taken from ref. [102]).

## 1.8. NPs Characterization

Nanoparticles as colloidal dispersions differ remarkably from other macroscopic dispersions. Nanoparticles have some unique physicochemical properties related to their sub-micron size as high surface area and surface free energy, and movement of particles by random motion (Brownian diffusion). Different physicochemical methods are being used specifically for NPs characterization to help understand their performance in vivo.

### 1.8.1. Size and Morphology

Particle size affects release kinetics, biodistribution potential and cellular uptake properties of NPs [46, 136]. Therefore, it is crucial to measure the size of the particles before conducting any further characterization. A detailed knowledge of the NPs size could help identify the

success of the used preparation method and give an idea about the in vivo performance of the particles. Optical light microscopy is not suitable for nanoparticle characterization since its resolution limit is about 500 nm. The most commonly used techniques for the characterization of nanoparticle size and morphology are scanning electron microscopy (SEM) [137, 138], transmission electron microscopy (TEM) [105, 139], and atomic force microscopy (AFM) [15, 129].

Atomic force microscopy (AFM) (scanning probe microscopy) enables the visualization of NPs at the atmospheric pressure without gold coating [140, 141]. Nevertheless, the resolution of AFM is still lower than that with SEM. Visualization of NPs using AFM can be done by three modes; contact, non-contact, and tapping mode. Tapping mode AFM (TM-AFM) is more preferred than contact and no-contact modes because of the ability of that mode to probe soft samples like biological and polymeric materials under ambient conditions [142, 143]. In tapping mode, the cantilever oscillates close to its bending mode resonance frequency so that tip makes contact with the sample for only short period of time during each oscillation cycle. As the tip approaches the sample, the tip-sample interactions alter the amplitude, frequency, and the phase angle of the oscillating cantilever. During scanning, the amplitude at the operating frequency is maintained at the constant level, called the set-point amplitude by adjusting the relative position of the tip with respect to the sample. This operating method results in lower surface forces, particularly lateral forces causing less surface damage [142].

One recent approach in TM-AFM is the use of the changes in the phase angle of the cantilever probe to produce phase image. An interesting application of TM-AFM in nanoparticle field is to visually investigate the mode of chain organization of the used polymer during NPs formation. Phase imaging is based on the use of changes in the phase angle of cantilever probe. This image shows more contrast than the topographic one as well as more sensitivity to material surface properties such as stiffness, viscoelasticity, and chemical composition [142, 144, 145]. Depending on the viscoelastic differences between PLA and PEG chains, phase imaging could be done to directly examine PEG on the surface of pegylated NPs.

Photon correlation spectroscopy (PCS) is the most commonly used tool in size determinations of nanoparticles [15, 129, 139, 146]. PCS is mainly based on the principle of laser light scattering by particles in colloidal dispersion. It can be used for size measurement between 5 nm and 2  $\mu\text{m}$ . The size or diameter obtained by PCS is a value that refers to how a

particle diffuses within a fluid so it is referred to as a hydrodynamic diameter. The hydrodynamic diameter is the diameter of a sphere that has the same translational diffusion coefficient as the particle. Simply, PCS detects the intensity variation of laser light scattered by the random motion of the particles (Brownian motion), and relates it to the particle size with the help of an autocorrelation function [147]. PCS allows the determination of the size distribution of mono and multidispersed particles. The advantage of this method is ease of sample preparation, fast technique, sensitive to nanoscale particles, and provides information about the whole colloidal dispersion. To be analyzed, the particles dispersion needs to be diluted, sometimes filtered to remove any dust particles that might interfere with the accuracy of results. Microscopic visualization and PCS should be used together in NPs size determinations. PCS is a computational technique that presumes that the particles are spherical and the size results are based on this assumption which might not be true in many cases. Instead, AFM/SEM provides visual and descriptive information, a real overview about the nanoparticles population.

### **1.8.2. Surface Characteristics and Stability**

Surface charge determines the stability of particles either in vitro or in vivo and also affects their cellular interaction in the body [58]. Colloidal dispersions are mainly stabilized either by electrostatic forces (surface charge) or by steric forces (polymers or surfactants at the particle surface), or by both forces [148, 149]. Information about the particle surface charge are usually obtained by zeta ( $\zeta$ ) potential measurement [150]. Stability for nanoparticle dispersion is usually achieved by high  $\zeta$ -potential values. Particles with zeta potentials more positive than +30 mV or more negative than -30 mV are normally considered stable, as the surface charge prevents aggregation of the particles [151]. Zeta ( $\zeta$ ) potential reflects the electric potential of the particles. It is the charge at the electrical double layer, created by ions of the liquid, which exists around each particle.

Zeta ( $\zeta$ ) potential measurement depends on determining the mobility of charged particles under the effect of electric potential (electrophoretic mobility). The electrophoretic mobility can be transferred to  $\zeta$ -potential by applying Smoluchowski's equation. Zeta-potential is mainly affected by the conditions of the dispersing medium as pH and electrolyte concentration [152]. PLA NPs are mainly stabilized by ionization of carboxylic acid groups at basic pH which shifts the zeta potential towards the negative side (around -40 mV or more) [153, 154]. Zeta-potential

values can be altered by surface modification [155] or stabilizer concentration [156]. It can also be used to determine whether a charged drug is entrapped into NPs or adsorbed onto the surface [58].

Another widely used surface characterization technique particularly used for PLA nanoparticles modified with PEG [157] is the X-ray photoelectron spectroscopy (XPS). This technique, also known as ESCA (electron spectroscopy for chemical analysis), is a surface sensitive technique that could give information about the chemical composition and structure of the particles surface qualitatively and quantitatively by measuring the binding energy of electrons associated with the atoms in a 5–10 nm depth of the NP surface. Other widely used tools for investigating the chemical composition of NPs include Fourier-transform infrared spectroscopy (FTIR) [158] and nuclear magnetic resonance spectroscopy (NMR) [159].

### **1.8.3. Drug-Polymer Interactions**

It is crucial during NPs preparation to identify any possible drug polymer-interactions. Drug loading can be done by two methods: (i) adding drug during NPs preparation (incorporation method); (ii) adsorbing drug onto the surface of preformed particles (adsorption technique). Drug loading efficiency depend greatly on the solid-state drug solubility in polymeric matrix (solid solution or dispersion), which is related to the polymer composition, the molecular weight, the drug polymer interaction and the presence of end functional groups (ester or carboxyl) [139, 160, 161]. Two types of drug polymer interactions exist either physical interaction (e.g. weak van der waals attraction) or chemical interaction (e.g. strong ionic interaction). As a result of drug-polymer interactions, drug can be adsorbed onto the particle surface [162] or bound chemically within the nanoparticles [163].

Physical state of the drug inside the particles also affects the drug diffusion and hence drug release from the particles. Amorphous materials have higher solubility and hence faster release rate compared to crystalline substances. Crystalline drugs need to be first dissolved before diffusing through the NPs matrix and hence, the release pattern would be slower. The preparation process of NPs can play a role in modifying the final state of drug in the particles.

Differential scanning calorimetry (DSC), (powder) x-ray diffractometry (PXRD) and FTIR are commonly used techniques to identify the final state of encapsulated drug, and to investigate any physicochemical interaction between the drug and the matrix polymer. DSC detects changes

in heat flow between a sample and reference upon heating both substances at a constant heating rate. DSC is widely used to detect phase transitions such as glass transition, exothermic transitions (e.g. crystallization) and endothermic transitions (e.g. melting) [164]. PXRD analysis is based on determining the diffraction pattern of the x-rays from a sample as a function of scattering angle. It is used to investigate the crystalline properties of drugs [165]. Absence of the drug melting peak and diffraction peaks of the crystal structure of the drug in DSC thermogram and PXRD pattern, respectively, are usually signs of amorphous or solid solution state of the drug within the polymer [166, 167]. FTIR can be used for identifying any chemical interaction between the drug and the polymer. An FTIR vibrational spectrum, characteristics for a given structure, is usually obtained [168]. Any reduction or disappearance of the FTIR characteristics peaks of the encapsulated drug indicates an interaction between the drug and the polymer might have occurred.

#### 1.8.4. Drug Loading

After NPs preparation, it is of prime importance to determine whether the preparation procedure used for incorporating a drug into NPs was efficient or not. This point is also important when dealing with expensive drugs to be encapsulated into NPs. To this end, two main parameters are usually calculated to govern the process of drug loading; drug entrapment or encapsulation efficiency (% EE) and the loading efficiency (or drug loading, % DL).

$$\% \text{ EE} = \frac{\text{Weight of drug entrapped in NPs}}{\text{Initial weight of drug added}} \times 100 \quad (1)$$

$$\% \text{ DL} = \frac{\text{Weight of drug entrapped in NPs}}{\text{Weight of NPs}} \times 100 \quad (2)$$

Because of the small size of nanoparticles, determinations of drug encapsulation, or drug loading are not always an easy task. Separation of free drug from bound or entrapped drug is firstly done by ultracentrifugation or ultrafiltration. Drug loading is then estimated either from the supernatant or after dissolution of the NPs sediment in an appropriate solvent [169-171]. In case of freeze-dried NPs, the particles are first dissolved then drug content can be easily analyzed [62, 85, 139, 172]. Depending on the loaded drug, various analytical methods can be used for drug determination such as spectrophotometry, spectrofluorometry, and high performance liquid chromatography (HPLC). For example, UV spectroscopy was used to estimate drug loading efficiency of PLGA NPs containing procaine hydrochloride after dissolving of NPs in acetonitrile [139]. In another case, high performance liquid chromatography (HPLC) was used to quantify acyclovir loaded into D,L-PLA NPs [85].

### **1.8.5. Drug Release**

In general, drug release from NPs is mainly governed by the following factors: (1) drug solubility; (2) desorption of the surface bound drug; (3) drug diffusion through the NPs matrix; (4) NPs matrix erosion; and (5) combination of erosion/diffusion process [58]. In case of uniformly distributed drug into the NPs matrix, the release occurs by diffusion or erosion of the matrix. In case of a crystalline drug being entrapped into the NPs matrix, drug dissolution occurs first followed by diffusion to initiate drug release. The rapid initial release or 'burst' is mainly attributed to desorption of the weakly bound or adsorbed drug close to the NPs surface.

Unfortunately, the *in vivo* drug release environment is complex and may be difficult to simulate. However, *in vitro* release kinetics could be useful for quality control purposes and the prediction of *in vivo* release kinetic. Several techniques can be used to study the *in vitro* release pattern of the drug. Ultracentrifugation is widely used for studying the *in vitro* drug release [85, 173-175]. Simply, it depends on stirring drug loaded NPs in a buffer solution mimicking blood components as phosphate buffer saline (PBS, pH 7.4) [175]. At predetermined intervals, a sample is withdrawn and ultracentrifuged. Then the drug content is analyzed from the supernatant by a suitable analytical method. Similarly, ultrafiltration can be used to separate the free drug from NPs [139, 176].

Dialysis bags are also used for studying the *in vitro* drug release. They are generally preferred over other methods because they save time and facilitate the separation of

nanoparticles from release media. NPs are immersed either in small dialysis bags in a stirred receptor (aqueous) medium [137, 146, 177] or in the medium containing drug-free dialysis bags (reverse dialysis) [171, 178]. The dialysis bag is impermeable to the NPs. The released drug could permeate the bag easily depending on the used molecular weight cutoff. Diffusion cells can also be used to monitor the drug diffusion from one compartment to another. Both compartments are separated from each other with a membrane that provides a possibility of drug not NPs permeation [179, 180].

## **1.9. Thesis Rationale and Research Objectives**

### **1.9.1. Rationale**

Poly(lactic acid) (PLA) is a well-known biocompatible and biodegradable polyester polymer that is widely used in the medical field [46, 103, 181]. Different kinds of PLA-based drug carrier systems, such as nanoparticles, microparticles, nanocapsules, hydrogels and polymersomes have been prepared and investigated as a carrier for the delivery of numerous drugs. Among these different carriers, nanoparticles are considered the most promising ones because of their superior performance either *in vitro* or *in vivo*. Nanoparticles made from biodegradable polymers or solid polymeric NPs including both nanospheres and nanocapsules offer some specific advantages over other nanoparticulate carriers. For instance, those polymeric NPs help to increase the stability of encapsulated drugs, and possess useful controlled release (CR) properties [58].

NPs made from PLA might suffer many drawbacks as their rapid uptake by the reticuloendothelial system after intravascular administration, low drug loading efficiency, inability to encapsulate a wide range of drugs particularly hydrophilic drugs, and in many cases inability to release their payload completely. Low drug incorporation of PLA usually leads to large drug loss during NP formulation, and hence, encapsulating insufficient drug amounts for therapeutic efficacy [137, 139]. The former situation necessitates the use of high polymer levels that might exceed their safety profile. Another drawback of PLA is that an initial burst release of drug can be observed in most loaded NPs, which may result in a loss of much of the therapeutic dose before the target site is reached by the NPs [58, 182]. Despite those drawbacks, little work was devoted to the development of functionalized PLA polymers in attempt to avoid the limitations of PLA homopolymer as drug carrier.

Functionalized poly(D,L-lactide) (PLA) nanoparticles development mainly depend on introducing a flexible moiety onto PLA hydrophobic cores in attempt to improve the drug delivery properties of the obtained NPs. A variety of pendant substituents e.g. PEG, and palmitic acid could be grafted onto PLA to generate polymers of different physicochemical properties and hence different drug incorporation behavior than PLA itself. NPs formulated using those functionalized polymers is expected to have better delivery performance than PLA itself. Introduction of PEG into PLA cores could prolong the circulation time of PLA NPs in blood, enhance the encapsulation efficiency of PLA for many drugs particularly hydrophilic drugs, and enhance the drug release from PLA matrices.

Another interesting benefit from grafting PEG over PLA is to achieve small size particles benefiting from the surfactant properties of PEG-PLA polymers. This could be an advantage since the optimum size required to achieve an effective targeting is proposed to be 150-200 nm [52, 53]. Moreover, in order to achieve prolonged circulation of NPs in the blood, nanoparticles diameter should be  $\leq 200$  nm since the sub-200 nm size along with biocompatibility allows nanoparticles to avoid recognition by the MPS cells [183, 184]. Although the smallest capillaries in the body are 5-10  $\mu$ m in diameter, the size of nanoparticles intended for parenteral administration and any possible aggregates should be far below this size to avoid blocking blood vessels and emboli formation [185]. Grafting PLA with palmitic acid moiety is expected to enhance the drug loading efficiency for hydrophobic drugs, change the release pattern of PLA particles since palmitate is expected to be embedded inside PLA domain lowering its chain rigidity. Fatty acid esters were found to have a remarkable plasticizing actions on PLA chains [186].

It was the overall aim of this project to develop polymeric nanoparticles based on functionalized PLA polymers that could be used as an alternative to PLA homopolymer for the encapsulation of different drugs. Physicochemical properties of NPs, as well as their performance as drug delivery systems are affected; to a great extent by the properties of the copolymers used to formulate them [110, 187, 188]. Thus, chemical structure and surface properties of polymer biomaterials have been shown to affect NPs delivery performance either in vitro or in vivo [189, 190]. We believe that an understanding of the effects of polymer architecture on the properties of NPs in general and PLA in particular will result in the predictable improvement of existing biopolymers and the design of new biocompatible polymers.

To reveal the effect of these parameters on the properties of PLA NPs, we developed four functionalized PLA polymers: (i) two copolymers identical in terms of the grafting density (i.e. % of grafted moiety or pendant substituent inserted onto PLA backbone), but different in terms of the solubility of grafted moiety; and (ii) two copolymers identical in terms of the length of PEG blocks, but different in terms of the chain organization of the PEG block. The ability of these four copolymers to act as drug carrier was investigated using a model drug, ibuprofen. Moreover, the effect of polymer architecture on the physicochemical properties of PLA NPs was investigated in comparison to PLA itself. NPs were analyzed for the major physicochemical parameters such as encapsulation efficiency, size and size distribution, surface charge, thermal properties, surface chemistry, % poly(vinyl alcohol) (PVA) adsorbed at the surface of NPs, and drug release pattern. Surface chemistry analysis using x-ray photoelectron spectroscopy (XPS), and phase imaging AFM were used to study the chain organization behavior of each functionalized NPs during NPs formulation. Special emphasis was devoted to PEG-g-PLA polymers trying to optimize their drug delivery performance. The effect of different PEG grafting densities over PLA backbone on the properties of PEG-g-PLA NPs either physicochemical or biological properties was investigated to reveal the optimal PEG grafting density required to develop stealth particles. Finally, functionalized PEG/PLA polymer that showed the most satisfactory results in terms of various drug delivery aspects, such as small size, neutral surface charge, high drug loading, and controlled drug release was chosen for encapsulation of itraconazole in attempt to improve its aqueous solubility, bioavailability and hence its fungal properties.

### 1.9.2. Research Objectives

1. Synthesis and characterization of functionalized PLA polymers according to a previously published protocol by our group [127].

**Summary:** Various linear and branched poly(D,L-lactide) (PLA) based polymers, namely, PLA homopolymer, poly(ethylene glycol) (PEG) grafted on PLA backbone at 2.5% & 7% grafting density (PEG2.5%-g-PLA and PEG7%-g-PLA, respectively), palmitic acid grafted on PLA backbone at 2.5% grafting density (palmitic acid2.5%-g-PLA), and multiblock copolymer of PLA and PEG, (PLA-PEG-PLA)<sub>n</sub> were synthesized.

2. Studying the effect of aqueous solubility of grafted moiety on the physicochemical properties of Poly (D,L-lactide) (PLA) based nanoparticles (research paper published in International Journal of Pharmaceutics).

**Summary:** In this part, the effect of grafting PLA backbone with two substituents of nearly similar grafting density but having different solubility profile, on the physicochemical properties of PLA NPs was investigated. The polymers used in this part are; PEG2.5%-g-PLA, and palmitic acid2.5%-g-PLA.

3. Studying the effect of polyethylene glycol (PEG) chain organization on the physicochemical properties of Poly (D,L-lactide) (PLA) based nanoparticles (research paper published in European Journal of Pharmaceutics and Biopharmaceutics).

**Summary:** In this part, a comparative study of the physicochemical properties of NPs obtained from two PEG/PLA copolymers of different architecture and nearly similar PEG chain length, PEG7%-g-PLA and (PLA-PEG-PLA)<sub>n</sub> polymers was done. Mode of PEG chains organization on the surface of PLA NPs was also investigated using XPS and phase imaging AFM.

4. Characterization of rhodamine loaded PEG-g-PLA nanoparticles (NPs): Effect of poly(ethylene glycol) grafting density (research paper published in International Journal of Pharmaceutics).

**Summary:** In this part, the effect of PEG grafting density (1, 7, or 20 % mol/mol of lactic acid monomer) on both physicochemical and biological properties (mainly plasma protein binding and in vitro macrophage uptake) of PEG-g-PLA NPs was studied. The optimal PEG grafting density required to develop stealth PEG-g-PLA NPs suitable for parenteral administration was also investigated.

5. Improved antifungal activity of itraconazole loaded PEG/PLA nanoparticles (research paper to be submitted).

**Summary:** In this part, a nanocarrier drug delivery system based on PEG/PLA copolymers was developed for the encapsulation of the antifungal drug, itraconazole (ITZ). NPs were developed to provide a controlled release pattern of ITZ as well as to improve its aqueous

solubility and hence enhance its antifungal action. The antifungal capability of ITZ loaded NPs was investigated using both *Candida* and *Aspergillus* species. Two PEG modified PLA polymers (PEGylated polymers) were used in this part; PEG7%-g-PLA, and multiblock copolymer of PLA and PEG, (PLA-PEG-PLA)<sub>n</sub> with nearly similar PEG insertion ratio and the same PEG chain length.

### 1.10. References

1. Horton, M.A., Khan, A., 2006. Medical nanotechnology in the UK: a perspective from the London Centre for Nanotechnology. *Nanomedicine: Nanotechnology, Biology and Medicine* 2, 42-48.
2. Gittard, S., Hojo, D., Hyde, G., Scarel, G., Narayan, R., Parsons, G., 2010. Antifungal Textiles Formed Using Silver Deposition in Supercritical Carbon Dioxide. *Journal of Materials Engineering and Performance* 19, 368-373.
3. Lai, F., Wissing, S.A., Muller, R.H., Fadda, A.M., 2006. *Artemisia arborescens* L essential oil-loaded solid lipid nanoparticles for potential agricultural application: Preparation and characterization. *Aaps Pharmscitech* 7, E10-E18.
4. Huang, D., Liao, F., Molesa, S., Redinger, D., Subramanian, V., 2003. Plastic-compatible low resistance printable gold nanoparticle conductors for flexible electronics. *Journal of the Electrochemical Society* 150, G412-G417.
5. Choi, M.J., McDonagh, A.M., Maynard, P., Roux, C., 2008. Metal-containing nanoparticles and nano-structured particles in fingerprint detection. *Forensic Science International* 179, 87-97.
6. Liu, T.M., Musinski, L.D., Patel, P.R., Gallimore, A.D., Gilchrist, B.E., Keidar, M., 2007. Nanoparticle electric propulsion for space exploration. *Space Technology and Applications International Forum - STAIF 2007* 880, 787-794.
7. Barauskas, J., Johnsson, M., Tiberg, F., 2005. Self-assembled lipid superstructures: Beyond vesicles and liposomes. *Nano Letters* 5, 1615-1619.
8. Bender, A.R., vonBriesen, H., Kreuter, J., Duncan, I.B., RubsamenWaigmann, H., 1996. Efficiency of nanoparticles as a carrier system for antiviral agents in human immunodeficiency virus-infected human monocytes/macrophages in vitro. *Antimicrobial Agents and Chemotherapy* 40, 1467-1471.
9. Jahanshahi, M., Babaei, Z., 2008. Protein nanoparticle: A unique system as drug delivery vehicles. *African Journal of Biotechnology* 7, 4926-4934.
10. Shenoy, D.B., Amiji, M.A., 2005. Poly(ethylene oxide)-modified poly(epsilon-caprolactone) nanoparticles for targeted delivery of tamoxifen in breast cancer. *International Journal of Pharmaceutics* 293, 261-270.

11. Duncan, R., 2003. The dawning era of polymer therapeutics. *Nature Reviews Drug Discovery* 2, 347-360.
12. Ferrari, M., 2005. Cancer nanotechnology: opportunities and challenges. *Nat Rev Cancer* 5, 161-171.
13. Couvreur, P., Vauthier, C., 2006. Nanotechnology: Intelligent design to treat complex disease. *Pharmaceutical Research* 23, 1417-1450.
14. Farokhzad, O.C., Langer, R., 2009. Impact of Nanotechnology on Drug Delivery. *Acs Nano* 3, 16-20.
15. Hammady, T., El-Gindy, A., Lejmi, E., Dhanikula, R.S., Moreau, P., Hildgen, P., 2009. Characteristics and properties of nanospheres co-loaded with lipophilic and hydrophilic drug models. *International Journal of Pharmaceutics* 369, 185-195.
16. Ahmed, F., Pakunlu, R.I., Brannan, A., Bates, F., Minko, T., Discher, D.E., 2006. Biodegradable polymersomes loaded with both paclitaxel and doxorubicin permeate and shrink tumors, inducing apoptosis in proportion to accumulated drug. *Journal of Controlled Release* 116, 150-158.
17. Liong, M., Lu, J., Kovichich, M., Xia, T., Ruehm, S.G., Nel, A.E., Tamanoi, F., Zink, J.I., 2008. Multifunctional inorganic nanoparticles for imaging, targeting, and drug delivery. *Acs Nano* 2, 889-896.
18. Budhian, A., Siegel, S.J., Winey, K.I., 2005. Production of haloperidol-loaded PLGA nanoparticles for extended controlled drug release of haloperidol. *Journal of Microencapsulation* 22, 773-785.
19. Gomez-Graete, C., Tsapis, N., Besnard, M., Bochot, A., Fattal, E., 2007. Encapsulation of dexamethasone into biodegradable polymeric nanoparticles. *International Journal of Pharmaceutics* 331, 153-159.
20. Cheng, Q.-Y., Feng, J., Li, F.-Z., 2008. Brain delivery of neurotoxin-I-loaded nanoparticles through intranasal administration. *Yao Xue Xue Bao* 43, 431-4.
21. Mu, L., Feng, S.S., 2003. A novel controlled release formulation for the anticancer drug paclitaxel (Taxol®): PLGA nanoparticles containing vitamin E TPGS. *Journal of Controlled Release* 86, 33-48.

22. Coester, C., Kreuter, J., von Briesen, H., Langer, K., 2000. Preparation of avidin-labelled gelatin nanoparticles as carriers for biotinylated peptide nucleic acid (PNA). *International Journal of Pharmaceutics* 196, 147-149.
23. Damgé, C., Maincent, P., Ubrich, N., 2007. Oral delivery of insulin associated to polymeric nanoparticles in diabetic rats. *Journal of Controlled Release* 117, 163-170.
24. Date, A.A., Joshi, M.D., Patravale, V.B., 2007. Parasitic diseases: Liposomes and polymeric nanoparticles versus lipid nanoparticles. *Advanced Drug Delivery Reviews* 59, 505-521.
25. Calvo, P., Gouritin, B., Brigger, I., Lasmezas, C., Deslys, J.-P., Williams, A., Andreux, J.P., Dormont, D., Couvreur, P., 2001. PEGylated polycyanoacrylate nanoparticles as vector for drug delivery in prion diseases. *Journal of Neuroscience Methods* 111, 151-155.
26. Ahmad, Z., Pandey, R., Sharma, S., Khuller, G.K., 2006. Pharmacokinetic and pharmacodynamic behaviour of antitubercular drugs encapsulated in alginate nanoparticles at two doses. *International Journal of Antimicrobial Agents* 27, 409-416.
27. Kim, S.Y., Lee, Y.M., 2001. Taxol-loaded block copolymer nanospheres composed of methoxy poly(ethylene glycol) and poly( $\epsilon$ -caprolactone) as novel anticancer drug carriers. *Biomaterials* 22, 1697-1704.
28. Lee, K., Chung, H., Im, S., Park, Y., Kim, C., Kim, S.-B., Rha, S., Lee, M., Ro, J., 2008. Multicenter phase II trial of Genexol-PM, a Cremophor-free, polymeric micelle formulation of paclitaxel, in patients with metastatic breast cancer. *Breast Cancer Research and Treatment* 108, 241-250.
29. Gu, F., Zhang, L., Teply, B.A., Mann, N., Wang, A., Radovic-Moreno, A.F., Langer, R., Farokhzad, O.C., 2008. Precise engineering of targeted nanoparticles by using self-assembled biointegrated block copolymers. *Proceedings of the National Academy of Sciences* 105, 2586-2591.
30. Gref, R., Lück, M., Quellec, P., Marchand, M., Dellacherie, E., Harnisch, S., Blunk, T., Müller, R.H., 2000. 'Stealth' corona-core nanoparticles surface modified by polyethylene glycol (PEG): influences of the corona (PEG chain length and surface density) and of the core composition on phagocytic uptake and plasma protein adsorption. *Colloids and Surfaces B: Biointerfaces* 18, 301-313.

31. Peracchia, M.T., Gref, R., Minamitake, Y., Domb, A., Lotan, N., Langer, R., 1997. PEG-coated nanospheres from amphiphilic diblock and multiblock copolymers: Investigation of their drug encapsulation and release characteristics. *Journal of Controlled Release* 46, 223-231.
32. Osada, K., Christie, R.J., Kataoka, K., 2009. Polymeric micelles from poly(ethylene glycol)-poly(amino acid) block copolymer for drug and gene delivery. *Journal of The Royal Society Interface* 6, S325-S339.
33. Motornov, M., Roiter, Y., Tokarev, I., Minko, S., Stimuli-responsive nanoparticles, nanogels and capsules for integrated multifunctional intelligent systems. *Progress in Polymer Science* 35, 174-211.
34. Kohori, F., Sakai, K., Aoyagi, T., Yokoyama, M., Sakurai, Y., Okano, T., 1998. Preparation and characterization of thermally responsive block copolymer micelles comprising poly(N-isopropylacrylamide-b-lactide). *Journal of Controlled Release* 55, 87-98.
35. Makhlof, A., Tozuka, Y., Takeuchi, H., 2009. pH-Sensitive nanospheres for colon-specific drug delivery in experimentally induced colitis rat model. *European Journal of Pharmaceutics and Biopharmaceutics* 72, 1-8.
36. Song, C., Labhasetwar, V., Cui, X., Underwood, T., Levy, R.J., 1998. Arterial uptake of biodegradable nanoparticles for intravascular local drug delivery: Results with an acute dog model. *Journal of Controlled Release* 54, 201-211.
37. Moghimi, S.M., Hunter, A.C., Murray, J.C., 2001. Long-circulating and target-specific nanoparticles: theory to practice. *Pharmacol Rev* 53, 283-318.
38. Vinogradov, S.V., Bronich, T.K., Kabanov, A.V., 2002. Nanosized cationic hydrogels for drug delivery: preparation, properties and interactions with cells. *Advanced Drug Delivery Reviews* 54, 135-147.
39. Matsumura, Y., Maeda, H., 1986. A New Concept for Macromolecular Therapeutics in Cancer Chemotherapy: Mechanism of Tumor-tropic Accumulation of Proteins and the Antitumor Agent Smancs. *Cancer Research* 46, 6387-6392.
40. Gaucher, G., Dufresne, M.-H., Sant, V.P., Kang, N., Maysinger, D., Leroux, J.-C., 2005. Block copolymer micelles: preparation, characterization and application in drug delivery. *Journal of Controlled Release* 109, 169-188.

41. Kataoka, K., Harada, A., Nagasaki, Y., 2001. Block copolymer micelles for drug delivery: design, characterization and biological significance. *Advanced Drug Delivery Reviews* 47, 113-131.
42. Maeda, H., Bharate, G.Y., Daruwalla, J., 2009. Polymeric drugs for efficient tumor-targeted drug delivery based on EPR-effect. *European Journal of Pharmaceutics and Biopharmaceutics* 71, 409-419.
43. Safra, T., Muggia, F., Jeffers, S., Tsao-Wei, D.D., Groshen, S., Lyass, O., Henderson, R., Berry, G., Gabizon, A., 2000. Pegylated liposomal doxorubicin (doxil): Reduced clinical cardiotoxicity in patients reaching or exceeding cumulative doses of 500 mg/m<sup>2</sup>. *Annals of Oncology* 11, 1029-1033.
44. Schroeder, U., Sommerfeld, P., Ulrich, S., Sabel, B.A., 1998. Nanoparticle technology for delivery of drugs across the blood–brain barrier. *Journal of Pharmaceutical Sciences* 87, 1305-1307.
45. Raghuvanshi, R.S., Katare, Y.K., Lalwani, K., Ali, M.M., Singh, O., Panda, A.K., 2002. Improved immune response from biodegradable polymer particles entrapping tetanus toxoid by use of different immunization protocol and adjuvants. *International Journal of Pharmaceutics* 245, 109-121.
46. Soppimath, K.S., Aminabhavi, T.M., Kulkarni, A.R., Rudzinski, W.E., 2001. Biodegradable polymeric nanoparticles as drug delivery devices. *Journal of Controlled Release* 70, 1-20.
47. Letchford, K., Burt, H., 2007. A review of the formation and classification of amphiphilic block copolymer nanoparticulate structures: micelles, nanospheres, nanocapsules and polymersomes. *European Journal of Pharmaceutics and Biopharmaceutics* 65, 259-269.
48. Barratt, G.M., 2000. Therapeutic applications of colloidal drug carriers. *Pharmaceutical Science & Technology Today* 3, 163-171.
49. Brannon-Peppas, L., Blanchette, J.O., 2004. Nanoparticle and targeted systems for cancer therapy. *Advanced Drug Delivery Reviews* 56, 1649-1659.
50. Owens Iii, D.E., Peppas, N.A., 2006. Opsonization, biodistribution, and pharmacokinetics of polymeric nanoparticles. *International Journal of Pharmaceutics* 307, 93-102.

51. Lück, M., Schröder, W., Paulke, B.R., Blunk, T., Müller, R.H., 1999. Complement activation by model drug carriers for intravenous application: determination by two-dimensional electrophoresis. *Biomaterials* 20, 2063-2068.
52. Lian, T., Ho, R.J.Y., 2001. Trends and developments in liposome drug delivery systems. *Journal of Pharmaceutical Sciences* 90, 667-680.
53. Awasthi, V.D., Garcia, D., Goins, B.A., Phillips, W.T., 2003. Circulation and biodistribution profiles of long-circulating PEG-liposomes of various sizes in rabbits. *International Journal of Pharmaceutics* 253, 121-132.
54. Feng, S.-S., 2004. Nanoparticles of biodegradable polymers for new-concept chemotherapy. *Expert Review of Medical Devices* 1, 115-125.
55. Alexis, F., Pridgen, E., Molnar, L.K., Farokhzad, O.C., 2008. Factors Affecting the Clearance and Biodistribution of Polymeric Nanoparticles. *Molecular Pharmaceutics* 5, 505-515.
56. Müller, R.H., Wallis, K.H., 1993. Surface modification of i.v. injectable biodegradable nanoparticles with poloxamer polymers and poloxamine 908. *International Journal of Pharmaceutics* 89, 25-31.
57. Brigger, I., Dubernet, C., Couvreur, P., 2002. Nanoparticles in cancer therapy and diagnosis. *Advanced Drug Delivery Reviews* 54, 631-651.
58. Mohanraj, V.J., Chen, Y., Nanoparticles - A review. 2007, Association of Crop Science, Uganda.
59. Zambaux, M.F., Bonneaux, F., Gref, R., Dellacherie, E., Vigneron, C., 1999. Preparation and characterization of protein C-loaded PLA nanoparticles. *Journal of Controlled Release* 60, 179-188.
60. Florence, A.T., 1997. The Oral Absorption of Micro- and Nanoparticulates: Neither Exceptional Nor Unusual. *Pharmaceutical Research* 14, 259-266.
61. Sang Yoo, H., Gwan Park, T., 2004. Biodegradable nanoparticles containing protein-fatty acid complexes for oral delivery of salmon calcitonin. *Journal of Pharmaceutical Sciences* 93, 488-495.
62. Kawashima, Y., Yamamoto, H., Takeuchi, H., Kuno, Y., 2000. Mucoadhesive D,L-Lactide/Glycolide Copolymer Nanospheres Coated with Chitosan to Improve Oral Delivery of Elcatonin. *Pharmaceutical Development and Technology* 5, 77-85.

63. He, W., Horn, S.W., Hussain, M.D., 2007. Improved bioavailability of orally administered mifepristone from PLGA nanoparticles. *International Journal of Pharmaceutics* 334, 173-178.
64. Hariharan, S., Bhardwaj, V., Bala, I., Sitterberg, J., Bakowsky, U., Ravi Kumar, M., 2006. Design of Estradiol Loaded PLGA Nanoparticulate Formulations: A Potential Oral Delivery System for Hormone Therapy. *Pharmaceutical Research* 23, 184-195.
65. Vila, A., Sánchez, A., Tobío, M., Calvo, P., Alonso, M.J., 2002. Design of biodegradable particles for protein delivery. *Journal of Controlled Release* 78, 15-24.
66. Garinot, M., Fiévez, V., Pourcelle, V., Stoffelbach, F., des Rieux, A., Plapied, L., Theate, I., Freichels, H., Jérôme, C., Marchand-Brynaert, J., Schneider, Y.-J., Prétat, V., 2007. PEGylated PLGA-based nanoparticles targeting M cells for oral vaccination. *Journal of Controlled Release* 120, 195-204.
67. Gutierro, I., Hernández, R.M., Igartua, M., Gascón, A.R., Pedraz, J.L., 2002. Size dependent immune response after subcutaneous, oral and intranasal administration of BSA loaded nanospheres. *Vaccine* 21, 67-77.
68. Kunii, R., Onishi, H., Machida, Y., 2007. Preparation and antitumor characteristics of PLA/(PEG-PPG-PEG) nanoparticles loaded with camptothecin. *European Journal of Pharmaceutics and Biopharmaceutics* 67, 9-17.
69. Dong, Y., Feng, S.-S., 2007. In vitro and in vivo evaluation of methoxy polyethylene glycol-poly(lactide) (MPEG-PLA) nanoparticles for small-molecule drug chemotherapy. *Biomaterials* 28, 4154-4160.
70. Panyam, J., Labhasetwar, V., 2003. Biodegradable nanoparticles for drug and gene delivery to cells and tissue. *Advanced Drug Delivery Reviews* 55, 329-347.
71. Barrera, D.A., Zylstra, E., Lansbury, P.T., Langer, R., 1993. Synthesis and RGD peptide modification of a new biodegradable copolymer: poly(lactic acid-co-lysine). *Journal of the American Chemical Society* 115, 11010-11011.
72. Davda, J., Labhasetwar, V., 2002. Characterization of nanoparticle uptake by endothelial cells. *International Journal of Pharmaceutics* 233, 51-59.
73. Woodward, S.C., Brewer, P.S., Moatamed, F., Schindler, A., Pitt, C.G., 1985. The intracellular degradation of poly( $\epsilon$ -caprolactone). *Journal of Biomedical Materials Research* 19, 437-444.

74. Panyam, J., Zhou, W.-Z., Prabha, S., Sahoo, S.K., Labhasetwar, V., 2002. Rapid endo-lysosomal escape of poly(D,L-lactide-co-glycolide) nanoparticles: implications for drug and gene delivery. *The FASEB Journal* 16, 1217-1226.
75. Lockman, P.R., Mumper, R.J., Khan, M.A., Allen, D.D., 2002. Nanoparticle Technology for Drug Delivery Across the Blood-Brain Barrier. *Drug Development and Industrial Pharmacy* 28, 1-13.
76. Avgoustakis, K., Beletsi, A., Panagi, Z., Klepetsanis, P., Karydas, A.G., Ithakissios, D.S., 2002. PLGA-mPEG nanoparticles of cisplatin: in vitro nanoparticle degradation, in vitro drug release and in vivo drug residence in blood properties. *Journal of Controlled Release* 79, 123-135.
77. Kreuter, J., 2001. Nanoparticulate systems for brain delivery of drugs. *Advanced Drug Delivery Reviews* 47, 65-81.
78. Gao, X., Chen, J., Tao, W., Zhu, J., Zhang, Q., Chen, H., Jiang, X., 2007. UEA I-bearing nanoparticles for brain delivery following intranasal administration. *International Journal of Pharmaceutics* 340, 207-215.
79. Lu, W., Zhang, Y., Tan, Y.-Z., Hu, K.-L., Jiang, X.-G., Fu, S.-K., 2005. Cationic albumin-conjugated pegylated nanoparticles as novel drug carrier for brain delivery. *Journal of Controlled Release* 107, 428-448.
80. Sun, W., Xie, C., Wang, H., Hu, Y., 2004. Specific role of polysorbate 80 coating on the targeting of nanoparticles to the brain. *Biomaterials* 25, 3065-3071.
81. Costantino, L., Gandolfi, F., Tosi, G., Rivasi, F., Vandelli, M.A., Forni, F., 2005. Peptide-derivatized biodegradable nanoparticles able to cross the blood-brain barrier. *Journal of Controlled Release* 108, 84-96.
82. Tosi, G., Costantino, L., Rivasi, F., Ruozi, B., Leo, E., Vergoni, A.V., Tacchi, R., Bertolini, A., Vandelli, M.A., Forni, F., 2007. Targeting the central nervous system: In vivo experiments with peptide-derivatized nanoparticles loaded with Loperamide and Rhodamine-123. *Journal of Controlled Release* 122, 1-9.
83. Garcia-Garcia, E., Andrieux, K., Gil, S., Couvreur, P., 2005. Colloidal carriers and blood-brain barrier (BBB) translocation: A way to deliver drugs to the brain? *International Journal of Pharmaceutics* 298, 274-292.

84. Vega, E., Egea, M.A., Valls, O., Espina, M., García, M.L., 2006. Flurbiprofen loaded biodegradable nanoparticles for ophthalmic administration. *Journal of Pharmaceutical Sciences* 95, 2393-2405.
85. Giannavola, C., Bucolo, C., Maltese, A., Paolino, D., Vandelli, M.A., Puglisi, G., Lee, V.H.L., Fresta, M., 2003. Influence of preparation conditions on acyclovir-loaded poly-D,L-lactic acid nanospheres and effect of PEG coating on ocular drug bioavailability. *Pharmaceutical Research* 20, 584-590.
86. Chen, J., Tian, B., Yin, X., Zhang, Y., Hu, D., Hu, Z., Liu, M., Pan, Y., Zhao, J., Li, H., Hou, C., Wang, J., Zhang, Y., 2007. Preparation, characterization and transfection efficiency of cationic PEGylated PLA nanoparticles as gene delivery systems. *Journal of Biotechnology* 130, 107-113.
87. Ribeiro, S., Rijpkema, S.G., Durrani, Z., Florence, A.T., 2007. PLGA-dendron nanoparticles enhance immunogenicity but not lethal antibody production of a DNA vaccine against anthrax in mice. *International Journal of Pharmaceutics* 331, 228-232.
88. Haley, B., Frenkel, E., Nanoparticles for drug delivery in cancer treatment. *Urologic Oncology: Seminars and Original Investigations* 26, 57-64.
89. Merle, P., Si Ahmed, S., Habersetzer, F., Abergel, A., Taieb, J., Bonyhay, L., Costantini, D., Dufour-Lamartinie, J., Trepo, C., 2006. Phase 1 study of intra-arterial hepatic (IAH) delivery of doxorubicin-transdrug (DT) for patients with advanced hepatocellular carcinoma (HCC). *ASCO Meeting Abstracts* 24, 14094.
90. Galindo-Rodríguez, S.A., Puel, F., Briançon, S., Allémann, E., Doelker, E., Fessi, H., Comparative scale-up of three methods for producing ibuprofen-loaded nanoparticles. *European Journal of Pharmaceutical Sciences* 25, 357-367.
91. Sahu, A., Kasoju, N., Bora, U., 2008. Fluorescence Study of the Curcumin–Casein Micelle Complexation and Its Application as a Drug Nanocarrier to Cancer Cells. *Biomacromolecules* 9, 2905-2912.
92. Pinto Reis, C., Neufeld, R.J., Ribeiro, A.J., Veiga, F., 2006. Nanoencapsulation II. Biomedical applications and current status of peptide and protein nanoparticulate delivery systems. *Nanomedicine: Nanotechnology, Biology and Medicine* 2, 53-65.

93. Merodio, M., Arnedo, A., Renedo, M.J., Irache, J.M., 2001. Ganciclovir-loaded albumin nanoparticles: characterization and in vitro release properties. *European Journal of Pharmaceutical Sciences* 12, 251-259.
94. Zahoor, A., Sharma, S., Khuller, G.K., 2005. Inhalable alginate nanoparticles as antitubercular drug carriers against experimental tuberculosis. *International Journal of Antimicrobial Agents* 26, 298-303.
95. Lu, Z., Yeh, T.-K., Tsai, M., Au, J.L.S., Wientjes, M.G., 2004. Paclitaxel-Loaded Gelatin Nanoparticles for Intravesical Bladder Cancer Therapy. *Clinical Cancer Research* 10, 7677-7684.
96. Cascone, M.G., Lazzeri, L., Carmignani, C., Zhu, Z., 2002. Gelatin nanoparticles produced by a simple W/O emulsion as delivery system for methotrexate. *Journal of Materials Science: Materials in Medicine* 13, 523-526.
97. Zhang, H., Oh, M., Allen, C., Kumacheva, E., 2004. Monodisperse Chitosan Nanoparticles for Mucosal Drug Delivery. *Biomacromolecules* 5, 2461-2468.
98. Agnihotri, S.A., Mallikarjuna, N.N., Aminabhavi, T.M., 2004. Recent advances on chitosan-based micro- and nanoparticles in drug delivery. *Journal of Controlled Release* 100, 5-28.
99. Venier-Julienne, M.C., Benoît, J.P., 1996. Preparation, purification and morphology of polymeric nanoparticles as drug carriers. *Pharmaceutica Acta Helvetiae* 71, 121-128.
100. Liu, Y., Yan, L., Heiden, P., Laks, P., 2001. Use of nanoparticles for controlled release of biocides in solid wood. *Journal of Applied Polymer Science* 79, 458-465.
101. Vauthier, C., Bouchemal, K., 2009. Methods for the Preparation and Manufacture of Polymeric Nanoparticles. *Pharmaceutical Research* 26, 1025-1058.
102. Pinto Reis, C., Neufeld, R.J., Ribeiro, A.J., Veiga, F., 2006. Nanoencapsulation I. Methods for preparation of drug-loaded polymeric nanoparticles. *Nanomedicine: Nanotechnology, Biology and Medicine* 2, 8-21.
103. Hans, M.L., Lowman, A.M., 2002. Biodegradable nanoparticles for drug delivery and targeting. *Current Opinion in Solid State and Materials Science* 6, 319-327.
104. Quintanar-Guerrero, D., Allémann, E., Fessi, H., Doelker, E., 1998. Preparation Techniques and Mechanisms of Formation of Biodegradable Nanoparticles from Preformed Polymers. *Drug Development and Industrial Pharmacy* 24, 1113-1128.

105. Fessi, H., Puisieux, F., Devissaguet, J.P., Ammoury, N., Benita, S., 1989. Nanocapsule formation by interfacial polymer deposition following solvent displacement. *International Journal of Pharmaceutics* 55, R1-R4.
106. Jarmer, D.J., Lengsfeld, C.S., Randolph, T.W., 2003. Manipulation of particle size distribution of poly(-lactic acid) nanoparticles with a jet-swirl nozzle during precipitation with a compressed antisolvent. *The Journal of Supercritical Fluids* 27, 317-336.
107. He, W., Jiang, Z., Suo, Q., Li, G., 2010. Mechanism of dispersing an active component into a polymeric carrier by the SEDS-PA process. *Journal of Materials Science* 45, 467-474.
108. Tsiontides, S.C., Rajniak, P., Pham, D., Hunke, W.A., Placek, J., Reynolds, S.D., 2004. Freeze drying--principles and practice for successful scale-up to manufacturing. *International Journal of Pharmaceutics* 280, 1-16.
109. Kakizawa, Y., Kataoka, K., 2002. Block copolymer micelles for delivery of gene and related compounds. *Advanced Drug Delivery Reviews* 54, 203-222.
110. Qiu, L.Y., Bae, Y.H., 2006. Polymer architecture and drug delivery. *Pharm Res* 23, 1-30.
111. Singh, R., Singh, S., Lillard, J.W., 2008. Past, present, and future technologies for oral delivery of therapeutic proteins. *Journal of Pharmaceutical Sciences* 97, 2497-2523.
112. Sinha, V.R., Bansal, K., Kaushik, R., Kumria, R., Trehan, A., 2004. Poly-[epsilon]-caprolactone microspheres and nanospheres: an overview. *International Journal of Pharmaceutics* 278, 1-23.
113. Kannan, R.M., Pillai Perumal, O., Kannan, S., Cellular Interactions of Nano Drug Delivery Systems. *Force Microscopy*. 2005: John Wiley & Sons, Inc. 113-136.
114. Ropert, C., Bazile, D., Bredenbach, J., Marlard, M., Veillard, M., Spenlehauer, G., 1993. Fate of <sup>14</sup>C radiolabeled poly(dl-lactic acid) nanoparticles following oral administration to rats. *Colloids and Surfaces B: Biointerfaces* 1, 233-239.
115. Middleton, J.C., Tipton, A.J., 2000. Synthetic biodegradable polymers as orthopedic devices. *Biomaterials* 21, 2335-2346.
116. Ambrose, C.G., Clanton, T.O., 2004. Bioabsorbable Implants: Review of Clinical Experience in Orthopedic Surgery. *Annals of Biomedical Engineering* 32, 171-177.
117. Södergård, A., Stolt, M., 2002. Properties of lactic acid based polymers and their correlation with composition. *Progress in Polymer Science* 27, 1123-1163.

118. Schliecker, G., Schmidt, C., Fuchs, S., Kissel, T., 2003. Characterization of a homologous series of  $\epsilon$ -lactic acid oligomers; a mechanistic study on the degradation kinetics in vitro. *Biomaterials* 24, 3835-3844.
119. Park, T.G., 1994. Degradation of poly(D,L-lactic acid) microspheres: effect of molecular weight. *Journal of Controlled Release* 30, 161-173.
120. Grizzi, I., Garreau, H., Li, S., Vert, M., 1995. Hydrolytic degradation of devices based on poly( $\epsilon$ -lactic acid) size-dependence. *Biomaterials* 16, 305-311.
121. Belbella, A., Vauthier, C., Fessi, H., Devissaguet, J.-P., Puisieux, F., 1996. In vitro degradation of nanospheres from poly(D,L-lactides) of different molecular weights and polydispersities. *International Journal of Pharmaceutics* 129, 95-102.
122. Bizzarri, R., Chiellini, F., Solaro, R., Chiellini, E., Cammas-Marion, S., Guerin, P., 2002. Synthesis and Characterization of New Malolactonate Polymers and Copolymers for Biomedical Applications. *Macromolecules* 35, 1215-1223.
123. Tian, D., Dubois, P., Grandfils, C., Jerome, R., 1997. Ring-Opening Polymerization of 1,4,8-Trioxaspiro[4.6]-9-undecanone: A New Route to Aliphatic Polyesters Bearing Functional Pendent Groups. *Macromolecules* 30, 406-409.
124. Anna Finne, A.-C.A., 2004. New functionalized polyesters to achieve controlled architectures. *Journal of Polymer Science Part A: Polymer Chemistry* 42, 444-452.
125. Ouchi, T., Ohya, Y., 2004. Design of lactide copolymers as biomaterials. *Journal of Polymer Science Part A: Polymer Chemistry* 42, 453-462.
126. Ni, Q., Yu, L., 1998. Synthesis of Novel Poly( $\epsilon$ -caprolactone)s Functionalized with a Thioester End-Group via a Living Ring Opening Polymerization and Their Application in Chemoselective Ligation with Compounds Containing a Cysteine Terminal. *Journal of the American Chemical Society* 120, 1645-1646.
127. Nadeau, V., Leclair, G., Sant, S., Rabanel, J.-M., Quesnel, R., Hildgen, P., 2005. Synthesis of new versatile functionalized polyesters for biomedical applications. *Polymer* 46, 11263-11272.
128. Nadeau, V., Hildgen, P., 2005. AFM study of a New Carrier Based on PLA and Salen Copolymers for Gene Therapy. *Molecules* 10, 105-113.

129. Sant, S., Nadeau, V., Hildgen, P., 2005. Effect of porosity on the release kinetics of propafenone-loaded PEG-g-PLA nanoparticles. *Journal of Controlled Release* 107, 203-214.
130. Niwa, T., Takeuchi, H., Hino, T., Nohara, M., Kawashima, Y., 1995. Biodegradable submicron carriers for peptide drugs: Preparation of poly(D,L-lactide/glycolide) copolymer (PLGA) nanospheres with nafarelin acetate by a novel emulsion-phase separation method in an oil system. *International Journal of Pharmaceutics* 121, 45-54.
131. Sahoo, S.K., Panyam, J., Prabha, S., Labhasetwar, V., 2002. Residual polyvinyl alcohol associated with poly (D,L-lactide-co-glycolide) nanoparticles affects their physical properties and cellular uptake. *Journal of Controlled Release* 82, 105-114.
132. Ruan, G., Feng, S.-S., 2003. Preparation and characterization of poly(lactic acid)-poly(ethylene glycol)-poly(lactic acid) (PLA-PEG-PLA) microspheres for controlled release of paclitaxel. *Biomaterials* 24, 5037-5044.
133. Hagan, S.A., Coombes, A.G.A., Garnett, M.C., Dunn, S.E., Davies, M.C., Illum, L., Davis, S.S., Harding, S.E., Purkiss, S., Gellert, P.R., 1996. Polylactide–Poly(ethylene glycol) Copolymers as Drug Delivery Systems. 1. Characterization of Water Dispersible Micelle-Forming Systems. *Langmuir* 12, 2153-2161.
134. Herrero-Vanrell, R., Rincón, A.C., Alonso, M., Reboto, V., Molina-Martinez, I.T., Rodríguez-Cabello, J.C., 2005. Self-assembled particles of an elastin-like polymer as vehicles for controlled drug release. *Journal of Controlled Release* 102, 113-122.
135. Scholes, P.D., Coombes, A.G.A., Illum, L., Davis, S.S., Watts, J.F., Ustariz, C., Vert, M., Davies, M.C., 1999. Detection and determination of surface levels of poloxamer and PVA surfactant on biodegradable nanospheres using SSIMS and XPS. *Journal of Controlled Release* 59, 261-278.
136. Gaumet, M., Vargas, A., Gurny, R., Delie, F., 2008. Nanoparticles for drug delivery: The need for precision in reporting particle size parameters. *European Journal of Pharmaceutics and Biopharmaceutics* 69, 1-9.
137. Leo, E., Brina, B., Forni, F., Vandelli, M.A., 2004. In vitro evaluation of PLA nanoparticles containing a lipophilic drug in water-soluble or insoluble form. *International Journal of Pharmaceutics* 278, 133-141.

138. Galindo-Rodriguez, S., Allémann, E., Fessi, H., Doelker, E., 2004. Physicochemical Parameters Associated with Nanoparticle Formation in the Salting-Out, Emulsification-Diffusion, and Nanoprecipitation Methods. *Pharmaceutical Research* 21, 1428-1439.
139. Govender, T., Stolnik, S., Garnett, M.C., Illum, L., Davis, S.S., 1999. PLGA nanoparticles prepared by nanoprecipitation: drug loading and release studies of a water soluble drug. *Journal of Controlled Release* 57, 171-185.
140. Skiba, M., Puisieux, F., Duchene, D., Wouessidjewe, D., 1995. Direct imaging of modified [beta]-cyclodextrin nanospheres by photon scanning tunnelling and scanning force microscopy. *International Journal of Pharmaceutics* 120, 1-11.
141. Gref, R., Minamitake, Y., Peracchia, M.T., Trubetskoy, V., Torchilin, V., Langer, R., 1994. Biodegradable long-circulating polymeric nanospheres. *Science* 263, 1600-1603.
142. Raghavan, D., Gu, X., Nguyen, T., VanLandingham, M., Karim, A., 2000. Mapping Polymer Heterogeneity Using Atomic Force Microscopy Phase Imaging and Nanoscale Indentation. *Macromolecules* 33, 2573-2583.
143. Kopp-Marsaudon, S., Leclere, P., Dubourg, F., Lazzaroni, R., Aime, J.P., 2000. Quantitative Measurement of the Mechanical Contribution to Tapping-Mode Atomic Force Microscopy Images of Soft Materials. *Langmuir* 16, 8432-8437.
144. Paredes, J.I., Gracia, M., Martínez-Alonso, A., Tascón, J.M.D., 2005. Nanoscale investigation of the structural and chemical changes induced by oxidation on carbon black surfaces: A scanning probe microscopy approach. *Journal of Colloid and Interface Science* 288, 190-199.
145. Magonov, S.N., Elings, V., Whangbo, M. H., 1997. Phase imaging and stiffness in tapping-mode atomic force microscopy. *Surface Science* 375, L385-L391.
146. Leroueil-Le Verger, M., Fluckiger, L., Kim, Y.-I., Hoffman, M., Maincent, P., 1998. Preparation and characterization of nanoparticles containing an antihypertensive agent. *European Journal of Pharmaceutics and Biopharmaceutics* 46, 137-143.
147. Pecora, R., 2000. Dynamic Light Scattering Measurement of Nanometer Particles in Liquids. *Journal of Nanoparticle Research* 2, 123-131.
148. Evans, R., Napper, D.H., 1973. Steric stabilization I. *Colloid & Polymer Science* 251, 409-414.

149. Overbeek, J.T.G., 1977. Recent developments in the understanding of colloid stability. *Journal of Colloid and Interface Science* 58, 408-422.
150. Webb, P.A., Orr, C., *Analytical Methods in Fine Particle Technology*. 1997: Micromeritics Instrument Corp. :Norcross. 273-280.
151. Benita, S., Levy, M.Y., 1993. Submicron emulsions as colloidal drug carriers for intravenous administration: Comprehensive physicochemical characterization. *Journal of Pharmaceutical Sciences* 82, 1069-1079.
152. Ishikawa, Y., Katoh, Y., Ohshima, H., 2005. Colloidal stability of aqueous polymeric dispersions: Effect of pH and salt concentration. *Colloids and Surfaces B: Biointerfaces* 42, 53-58.
153. Vila, A., Gill, H., McCallion, O., Alonso, M.J., 2004. Transport of PLA-PEG particles across the nasal mucosa: effect of particle size and PEG coating density. *Journal of Controlled Release* 98, 231-244.
154. Tobío, M., Gref, R., Sánchez, A., Langer, R., Alonso, M.J., 1998. Stealth PLA-PEG Nanoparticles as Protein Carriers for Nasal Administration. *Pharmaceutical Research* 15, 270-275.
155. Sukhorukov, G.B., Donath, E., Lichtenfeld, H., Knippel, E., Knippel, M., Budde, A., Möhwald, H., 1998. Layer-by-layer self assembly of polyelectrolytes on colloidal particles. *Colloids and Surfaces A: Physicochemical and Engineering Aspects* 137, 253-266.
156. Alonso, M.J., Sanchez, A., Torres, D., Seijo, B., Vila-Jato, J.L., 1990. Joint effects of monomer and stabilizer concentrations on physico-chemical characteristics of poly(butyl 2-cyanoacrylate) nanoparticles. *Journal of Microencapsulation* 7, 517-526.
157. Dong, Y., Feng, S.-S., 2004. Methoxy poly(ethylene glycol)-poly(lactide) (MPEG-PLA) nanoparticles for controlled delivery of anticancer drugs. *Biomaterials* 25, 2843-2849.
158. Feng, S.S., Mu, L., Win, K.Y., Huang, G.F., 2004. Nanoparticles of biodegradable polymers for clinical administration of paclitaxel. *Current Medicinal Chemistry* 11, 413-424.
159. Das, S.K., Tucker, I.G., Hill, D.J.T., Ganguly, N., 1995. Evaluation of Poly(isobutylcyanoacrylate) Nanoparticles for Mucoadhesive Ocular Drug Delivery. I.

- Effect of Formulation Variables on Physicochemical Characteristics of Nanoparticles. *Pharmaceutical Research* 12, 534-540.
160. Govender, T., Riley, T., Ehtezazi, T., Garnett, M.C., Stolnik, S., Illum, L., Davis, S.S., 2000. Defining the drug incorporation properties of PLA-PEG nanoparticles. *International Journal of Pharmaceutics* 199, 95-110.
  161. Panyam, J., Williams, D., Dash, A., Leslie-Pelecky, D., Labhasetwar, V., 2004. Solid-state solubility influences encapsulation and release of hydrophobic drugs from PLGA/PLA nanoparticles. *Journal of Pharmaceutical Sciences* 93, 1804-1814.
  162. Illum, L., Khan, M.A., Mak, E., Davis, S.S., 1986. Evaluation of carrier capacity and release characteristics for poly( butyl 2-cyanoacrylate) nanoparticles. *International Journal of Pharmaceutics* 30, 17-28.
  163. Page-Clisson, M.E., Pinto-Alphandary, H., Ourevitch, M., Andreumont, A., Couvreur, P., 1998. Development of ciprofloxacin-loaded nanoparticles: physicochemical study of the drug carrier. *Journal of Controlled Release* 56, 23-32.
  164. Dubernet, C., 1995. Thermoanalysis of microspheres. *Thermochimica Acta* 248, 259-269.
  165. Suryanarayanan, R., X-Ray Powder Diffractometry. in *Physical Characterization of Pharmaceutical Solids*, ed. Brittain, H.G. Vol. 70. 1995, New York.: Marcel Dekker, Inc. 187-221.
  166. Benoit, J.P., Courteille, F., Thies, C., 1986. A physicochemical study of the morphology of progesterone-loaded poly (D,L-lactide) microspheres. *International Journal of Pharmaceutics* 29, 95-102.
  167. Wichert, B., Rohdewald, P., 1990. A new method for the preparation of drug containing polylactic acid microparticles without using organic solvents. *Journal of Controlled Release* 14, 269-283.
  168. Brittain, H.G., Bogdanowich, S.J., Bugay, D.E., DeVincentis, J., Lewen, G., Newman, A.W., 1991. *Physical Characterization of Pharmaceutical Solids*. *Pharmaceutical Research* 8, 963-973.
  169. Saez, A., Guzmán, M., Molpeceres, J., Aberturas, M.R., 2000. Freeze-drying of polycaprolactone and poly(-lactic-glycolic) nanoparticles induce minor particle size changes affecting the oral pharmacokinetics of loaded drugs. *European Journal of Pharmaceutics and Biopharmaceutics* 50, 379-387.

170. Bivas-Benita, M., Romeijn, S., Junginger, H.E., Borchard, G., 2004. PLGA-PEI nanoparticles for gene delivery to pulmonary epithelium. *European Journal of Pharmaceutics and Biopharmaceutics* 58, 1-6.
171. De Campos, A.M., Sánchez, A., Gref, R., Calvo, P., Alonso, M.J., 2003. The effect of a PEG versus a chitosan coating on the interaction of drug colloidal carriers with the ocular mucosa. *European Journal of Pharmaceutical Sciences* 20, 73-81.
172. Riley, T., Govender, T., Stolnik, S., Xiong, C.D., Garnett, M.C., Illum, L., Davis, S.S., 1999. Colloidal stability and drug incorporation aspects of micellar-like PLA-PEG nanoparticles. *Colloids and Surfaces B: Biointerfaces* 16, 147-159.
173. Redhead, H.M., Davis, S.S., Illum, L., 2001. Drug delivery in poly(lactide-co-glycolide) nanoparticles surface modified with poloxamer 407 and poloxamine 908: in vitro characterisation and in vivo evaluation. *Journal of Controlled Release* 70, 353-363.
174. Ferranti, V., Marchais, H., Chabenat, C., Orecchioni, A.M., Lafont, O., 1999. Primidone-loaded poly-[var epsilon]-caprolactone nanocapsules: incorporation efficiency and in vitro release profiles. *International Journal of Pharmaceutics* 193, 107-111.
175. Leroux, J.-C., Allémann, E., De Jaeghere, F., Doelker, E., Gurny, R., 1996. Biodegradable nanoparticles -- From sustained release formulations to improved site specific drug delivery. *Journal of Controlled Release* 39, 339-350.
176. Ahlin, P., Kristl, J., Kristl, A., Vrecer, F., 2002. Investigation of polymeric nanoparticles as carriers of enalaprilat for oral administration. *International Journal of Pharmaceutics* 239, 113-120.
177. Alvarez-Román, R., Barré, G., Guy, R.H., Fessi, H., 2001. Biodegradable polymer nanocapsules containing a sunscreen agent: preparation and photoprotection. *European Journal of Pharmaceutics and Biopharmaceutics* 52, 191-195.
178. Teixeira, M., Alonso, M.J., Pinto, M.M.M., Barbosa, C.M., 2005. Development and characterization of PLGA nanospheres and nanocapsules containing xanthone and 3-methoxyxanthone. *European Journal of Pharmaceutics and Biopharmaceutics* 59, 491-500.
179. Grazia Cascone, M., Zhu, Z., Borselli, F., Lazzeri, L., 2002. Poly(vinyl alcohol) hydrogels as hydrophilic matrices for the release of lipophilic drugs loaded in PLGA nanoparticles. *Journal of Materials Science: Materials in Medicine* 13, 29-32.

180. Niwa, T., Takeuchi, H., Hino, T., Kunou, N., Kawashima, Y., 1993. Preparations of biodegradable nanospheres of water-soluble and insoluble drugs with D,L-lactide/glycolide copolymer by a novel spontaneous emulsification solvent diffusion method, and the drug release behavior. *Journal of Controlled Release* 25, 89-98.
181. Cheng, Y., Deng, S., Chen, P., Ruan, R., 2009. Polylactic acid (PLA) synthesis and modifications: a review. *Frontiers of Chemistry in China* 4, 259-264.
182. Magjarevic, R., Ling, Y., Huang, Y., Preparation and Release Efficiency of Poly (lactic-co-glycolic) Acid Nanoparticles for Drug Loaded Paclitaxel, in 7th Asian-Pacific Conference on Medical and Biological Engineering, Peng, Y., Weng, X., Editors. 2008, Springer Berlin Heidelberg, p. 514-517.
183. Stolnik, S., Illum, L., Davis, S.S., 1995. Long circulating microparticulate drug carriers. *Advanced Drug Delivery Reviews* 16, 195-214.
184. Nishiyama, N., Kataoka, K., 2006. Current state, achievements, and future prospects of polymeric micelles as nanocarriers for drug and gene delivery. *Pharmacology & Therapeutics* 112, 630-648.
185. Tathagata, D., Narendra, K.J., Nigel, A.J.M., Harendra, S.P., 2010. RETRACTED: Dendrimer nanocarriers as versatile vectors in gene delivery. *Nanomedicine : nanotechnology, biology, and medicine* 6, 25-34.
186. Jacobsen, S., Fritz, H.G., 1999. Plasticizing polylactide- The effect of different plasticizers on the mechanical properties. *Polymer Engineering and Science* 39, 1303-1310.
187. Mittal, G., Sahana, D.K., Bhardwaj, V., Ravi Kumar, M.N.V., 2007. Estradiol loaded PLGA nanoparticles for oral administration: Effect of polymer molecular weight and copolymer composition on release behavior in vitro and in vivo. *Journal of Controlled Release* 119, 77-85.
188. Wang, Y.-X., Robertson, J.L., Spillman, W.B., Claus, R.O., 2004. Effects of the Chemical Structure and the Surface Properties of Polymeric Biomaterials on Their Biocompatibility. *Pharmaceutical Research* 21, 1362-1373.
189. Choi, S.-W., Kim, W.-S., Kim, J.-H., 2003. Surface Modification of Functional Nanoparticles for Controlled Drug Delivery. *Journal of Dispersion Science and Technology* 24, 475 - 487.

190. Nasongkla, N., Chen, B., Macaraeg, N., Fox, M.E., Fréchet, J.M.J., Szoka, F.C., 2009. Dependence of Pharmacokinetics and Biodistribution on Polymer Architecture: Effect of Cyclic versus Linear Polymers. *Journal of the American Chemical Society* 131, 3842-3843.

## CHAPTER TWO

---

### RESEARCH PAPER

#### **Effect of Aqueous Solubility of Grafted Moiety on The Physicochemical Properties of Poly(D,L-lactide) (PLA) based Nanoparticles<sup>1</sup>.**

Sherief Essa, Jean Michel Rabanel, and Patrice Hildgen.

Faculty of Pharmacy, Université de Montréal, CP 6128, Succursale Centre Ville,  
Montréal, QC, Canada, H3C 3J7

**International Journal of Pharmaceutics 388 (2010) 263-273**

---

<sup>1</sup> My contribution included designing the experiments, polymer synthesis, nanoparticles preparation and characterization, interpreting the results and writing the paper, which was supervised by Dr. Patrice Hildgen. Jean Michel Rabanel contribution was technical assistance using laboratory equipments.

## 2.1. Abstract

In order to evaluate the solubility effect of grafted moiety on the physicochemical properties of poly(D,L-lactide) (PLA) based nanoparticles (NPs), two materials of completely different aqueous solubility, polyethylene glycol (PEG) and palmitic acid were grafted on PLA backbone at nearly the same grafting density, 2.5% (mol of grafted moiety/mol of lactic acid monomer). Blank and ibuprofen-loaded NPs were fabricated from both polymers and their properties were compared to PLA homopolymer NPs as a control. NPs were analyzed for major physicochemical parameters such as encapsulation efficiency, size and size distribution, surface charge, thermal properties, surface chemistry, % poly(vinyl alcohol) (PVA) adsorbed at the surface of NPs, and drug release pattern. Encapsulation efficiency of ibuprofen was found to be nearly the same for both polymers ~ 36 % and 39 % for PEG2.5%-g-PLA and palmitic acid2.5%-g-PLA NPs, respectively. Lyophilized NPs of palmitic acid2.5%-g-PLA either blank or loaded showed larger hydrodynamic diameter (~ 180 nm) than PEG2.5%-g-PLA NPs (~ 135 nm). PEG2.5%-g-PLA NPs showed lower % of PVA adsorbed at their surface (~ 5% w/w) than palmitic acid2.5%-g-PLA NPs (~ 10 % w/w). Surface charge of palmitic acid2.5%-g-PLA NPs seems to be influenced by the large amount of PVA remains associated within their matrix. Thermal analysis using DSC revealed possible drug crystallization inside NPs. Both AFM phase imaging and XPS studies revealed the tendency of PEG chains to migrate towards the surface of PEG2.5%-g-PLA NPs. While, XPS analysis of palmitic acid2.5%-g-PLA NPs showed the tendency of palmitate chains to position themselves into the inner core of the forming particle avoiding facing the aqueous phase during NPs preparation using O/W emulsion method. The in vitro release

pattern showed that PEG2.5%-g-PLA NPs exhibited faster release rates than palmitic acid2.5%-g-PLA NPs. PEG and palmitate chains when grafted onto PLA backbone, different modes of chain organization during NPs formation were obtained, affecting the physicochemical properties of the obtained NPs. The obtained results suggest that the properties of PLA- based NPs can be tuned by judicious selection of both chemistry and solubility profile of grafted material over PLA backbone.

## **2.2. Keywords**

Poly(D,L-lactide), PEG-PLA NPs, palmitic acid-PLA NPs, chain organization, X-ray photo-electron spectroscopy (XPS) , phase imaging atomic force microscopy (AFM).

## **2.3. Introduction**

Controlled release technology began in 1970s and since that time great interest has been paid to this technology. Recently, colloidal drug carriers are widely used for the development of controlled release systems for large number of drugs. Those carriers possess important applications in the pharmaceutical field. Moreover, they offer numerous advantages over conventional drug delivery systems such as controlled drug release rate, improved therapeutic efficiency, prolonged biological activity and decreased administration frequency [1]. They may also act as stabilizer protecting entrapped drugs against degradation. A way of modifying the original pharmacokinetics and biodistribution of drugs is to incorporate them in submicroscopic colloidal carriers. Numerous classes of colloidal carriers composed of different materials including lipids, polymers and inorganic materials have been developed, resulting in different delivery

systems that vary in their physicochemical properties and thus their pharmaceutical uses. Growing interest in formulating NPs from synthetic polymers with tunable properties is rapidly expanding.

Despite the identification of various factors that might influence the properties of polymeric NPs such as the physicochemical properties of polymer and the drug [2], their interaction with each other [3], drug load [4], drug distribution inside the carrier, and size and morphology of the carrier [5], chemical constitution effect and solubility profile of grafted moiety of the used polymer on various drug delivery aspects remains to be adequately addressed. Although different nanosystems have been developed, the effect of grafting the starting polymer with various grafted moieties needs to be realized and emphasized for each nanosystem. In fact, grafting the same polymer with different materials will not only affect the physicochemical properties of the polymer, but also various drug delivery facets including, drug release rate, pharmacokinetics and biodistribution of the carrier, and even cellular uptake of the nanocarrier in vivo. It was previously shown that the molecular architecture of the polymer affects the cellular interaction of NPs prepared from different polymers [6].

This work is the first in-depth study of the effect of chain organization of the grafted moiety of the starting polymer on the major physicochemical aspects of drug delivery from PLA-based NPs e.g. size of the carrier, surface charge, matrix erosion, and drug release profile. NPs formulated using PLA-b-PEG block copolymers were extensively investigated in the past [7-9]. Up to now, however, relatively fewer studies have focused on grafted pegylated copolymer of PLA and PEG, used in our study.

Objective of the present work is to compare the effect of two grafted materials of different composition and aqueous solubility on the physicochemical properties of PLA-based NPs. Effect of grafted moiety on polymer chains organization during NPs formation was also investigated using relatively new techniques like XPS and phase imaging-AFM. PLA homopolymer was proposed as the control NPs and either hydrophilic (PEG) or hydrophobic (palmitic acid) substance was grafted onto PLA backbone at nearly the same grafting density 2.5 % (mol/mol of lactic acid monomer), according to a previously published method by our group [10]. Ibuprofen was used as a model lipophilic drug to be encapsulated by PLA and grafted PLA NPs. NPs were prepared using (O/W) emulsion solvent evaporation method. PVA was used as an emulsifier during NPs preparation since it aids the formation of relatively small sized particles with uniform size distribution [11].

## **2.4. Material and methods:**

### **2.4.1. Materials:**

D,L-dilactide, poly(ethylene glycol) methyl ether (MePEG; 2000 Da) , allyl glycidyl ether, tetraphenyltin, polyvinyl alcohol (PVA, average  $M_w$  9000-10,000 Da, 80% hydrolyzed), pyridine, acetone, diethyl ether, thionyl chloride, borane-tetrahydrofuran complex (1 M), and palmitoyl chloride were purchased from Aldrich Chemical Company Inc., Milwaukee, USA. Ibuprofen was obtained from Medisca Pharmaceutical Inc., Montreal, Quebec, Canada. Sodium hydroxide pellets were purchased from Anachemia Canada Inc. and dichloromethane (DCM) was purchased from Laboratoire Mat Inc., Montreal, Quebec, Canada.

#### 2.4.2. Synthesis of Polymers.

Poly(D,L)-lactide (PLA) was synthesized by ring-opening polymerization of dilactide in argon atmosphere, using tetraphenyltin as the catalyst. Briefly, dilactide was crystallized from toluene solution and dried under vacuum before use. A weighed amount of purified dilactide was then placed in a round-bottom flask and purged thoroughly with argon. Bulk polymerization was carried at 180 °C for 6 h. The polymer thus obtained was dissolved in acetone and was purified by precipitating in water.

Polymer with poly(ethylene glycol)-grafted randomly on poly(D,L)-lactide (PEG2.5%-g-PLA) (PEG; *M<sub>w</sub>* 2000 Da) was synthesized in our laboratory as reported earlier [10]. Briefly, D,L-dilactide (21.5 g, 97.5 mol %) was polymerized in the presence of allyl glycidyl ether (0.872 g, 2.5 mol %) with tetraphenyltin as the catalyst (1:10 000 mol with regards to D,L-dilactide) at 180 °C for 6 h under argon. Polylactic acid with allyl groups was purified by dissolving in acetone and precipitating in water. The allyl groups were converted to hydroxyl groups by hydroboration with an equimolar quantity of borane in tetrahydrofuran, followed by oxidation in the presence of hydrogen peroxide under alkaline conditions (1.5 mol of 3 N sodium hydroxide). The hydroxyl groups were oxidized to carboxylic acid groups using Jones reagent, which was further converted to an acid chloride using thionyl chloride (1:1000 M). Finally, methoxy-PEG was grafted onto the polymer backbone by the reaction between acid chloride and the hydroxyl groups of methoxy-PEG (2000 Da) in the presence of pyridine. The final polymer was purified by evaporating pyridine and washing with distilled water.

Palmitic acid grafted on PLA backbone at 2.5% grafting density, palmitic acid 2.5%-g-PLA was synthesized as follows, to a solution of PLA grafted with 2.5 % hydroxyl pendant groups (1g, 0.136 mmol) in 50 mL pyridine, palmitoyl chloride (1.8 g, 6 mmol) was added. The solution was stirred for 3h and then, 10 mL water was added. The solvent was evaporated and the product was crystallized in diethyl ether to obtain a yellow product.  $^1\text{H}$  NMR spectra were recorded on a Bruker ARX 400 spectrometer (Bruker Biospin, Billerica, MA). Chemical shifts ( $\delta$ ) were measured in parts per million (ppm) using tetramethylsilane (TMS) as an internal reference. Gel permeation chromatography (GPC) was performed on a Water Associate chromatography system (Waters, Milford, MA) equipped with a refractive index detector and a Phenomenex Phenogel 5  $\mu$  column. Polystyrene standards were used for calibration with THF as the mobile phase at a flow rate of 0.6 mL/min.

#### **2.4.3. Preparation of nanoparticles (NPs)**

NPs were prepared using an (O/W) emulsion-solvent evaporation method. For blank NPs, each polymer (1 g) was dissolved in 35 mL DCM and emulsified in 100 mL PVA solution (0.5% w/v) as an external aqueous phase using high-pressure homogenizer (Emulsiflex C30, Avestin, Ottawa, Canada) at a pressure of 10,000 psi for 5 min. The emulsion was collected by washing with another 100 mL 0.5% PVA. The DCM was evaporated under reduced pressure with constant stirring to obtain the NPs. Finally, NPs obtained as a suspension were then collected by centrifugation at 18500 rpm for 1 hr at 4 °C (Sorval® Evolution<sub>RC</sub>, Kendro, USA), washed four times with distilled water, then lyophilized to obtain dry NPs (Freeze Dry System, Lyph.Lock 4.5, Labconco) and stored

at 4 °C until further use. Ibuprofen loaded NPs were prepared in a similar manner to that of blank NPs using initial loading of 10% w/w of each polymer. Ibuprofen was first dissolved in the organic phase followed by dissolution of the polymer. The emulsification and purification steps procedure were repeated as before.

#### **2.4.4. Characterization of NPs**

##### **2.4.4.1. Particle size and zeta ( $\zeta$ ) potential measurements**

The mean hydrodynamic diameters ( $d_h$ ) and the polydispersity indices (PDIs) of NPs were measured by DLS with a Malvern Autosizer 4800 instrument (Malvern Instruments, Worcestershire, UK) before and after lyophilization. For all samples, fresh NP suspensions (0.1 mL) or lyophilized NPs (1 mg) were diluted 10 times with Milli-Q Water. Measurements were taken at a fixed scattering angle of 90° and at 25° C. The CONTIN program was used to extract size distributions from the autocorrelation functions. Zeta-potential measurements of NPs suspended in 0.25% w/v saline solution (pH 7.4) were done on Malvern ZetaSizer Nanoseries ZS (Malvern Instruments, Worcestershire, UK). Both measurements were performed in triplicate

##### **2.4.4.2. Determination of residual PVA**

A colorimetric analysis was used for determination of PVA amount remaining in the NPs. The method is simply based on the formation of a colored complex between two adjacent hydroxyl groups of PVA and an iodine molecule [11] . For surface associated PVA, certain weight of NPs was suspended in distilled water followed by vigorous vortexing for 10 min., then fixed volumes of all formulations were taken followed by addition of 5 mL of saturated solution of boric acid and 0.5 mL iodine (0.1 N), and the

volume was made up to 10 mL with distilled water. The absorbance of the formed complex was measured at 660 nm against similarly treated blank. Whereas for the total amount of PVA associated with the particles (amount entrapped inside the matrix as well as present on the surface), NPs were digested in 1 N NaOH then neutralized by 1 N HCl followed by stirring for 1 h and the volume was made up to 5 mL with distilled water. To this, 3 mL of saturated solution of boric acid and 0.5 mL iodine (0.1 N) were added, and the volume was made up to 10 mL with distilled water. The absorbance was measured as before. PVA actual amount was calculated by using a calibration curve of PVA prepared under the same conditions.

#### **2.4.4.3. NPs surface morphology and phase image analysis**

Nanoscope IIIa Dimension 3100 atomic force microscope (Digital Instruments, Santa Barbara, CA, USA) was used to study both surface morphology and phase imaging of lyophilized NPs. Samples were prepared by deposition of particles suspension in Milli-Q Water on freshly cleaved mica followed by air-drying for 10 min at room temperature. Topography and phase images of these samples were captured simultaneously using TappingMode™ etched silicon probes (TESP7) with tip radius of 5–10 nm, spring constant of 20–100 N/m and resonance frequency of 200–500 kHz. Cantilever length was 125 μm.

#### **2.4.4.4. Encapsulation efficiency (EE)**

For ibuprofen loaded NPs of PLA homopolymer and PEG2.5%-g-PLA, weighed amount of NPs was digested in 1 N NaOH for 1 h. Ibuprofen concentration was measured

by spectrophotometry at 264 nm (U-2001 UV/Visible spectrophotometer, Hitachi). While, for palmitic acid 2.5%-g-PLA loaded NPs, weighed NPs were also suspended in 1 N NaOH for 1 h to which chloroform was added followed by vigorous stirring for another 3 h to extract ibuprofen into the chloroform layer. Then, the chloroform layer was collected and ibuprofen concentration was measured by spectrophotometry at 263 nm. Percent encapsulation efficiency (% EE) and % actual loading efficiency (% LE) were calculated based on the following equations:

$$\% \text{ EE} = \frac{\text{Amount of drug entrapped in NPs}}{\text{Initial amount of drug added}} \times 100 \quad (1)$$

$$\% \text{ LE} = \frac{\text{Amount of drug entrapped in NPs}}{\text{Total amount of NPs}} \times 100 \quad (2)$$

#### 2.4.4.5. Differential Scanning Calorimetry (DSC)

The thermal properties of polymers and drug in the physical mixture and NPs were characterized by DSC analysis (DSC 30, Mettler TA 4000, Schwerzenbach, Switzerland) with refrigerated cooling. Measurements were done (n =2) on all investigated samples. Physical mixtures were prepared by triturating polymer and ibuprofen in a ratio similar to drug loaded NPs. In brief, weighed samples were sealed in crimped aluminum pans with

lids and heated at a rate of 10 °C/min from -50 to 200 °C for polymers and physical mixtures, while for NPs the samples were heated from -50 to 90 °C at the same heating rate.

#### **2.4.4.6. XPS analysis**

X-ray photoelectron spectroscopy, XPS (VG Scientific ESCALAB MK II) with a monochromatized Mg Ka X-rays (hv 1253.6 eV) and an electron take off angle of 0° was used to study the surface chemistry of pure materials, polymers, blank, and drug-loaded NPs. A single survey scan spectrum (0–1000 eV) and narrow scans for C1s (210–305 eV) and O1s (525–550 eV) were recorded for each sample with a pass energy of 1 and 0.5 eV, respectively. Acquisition and data analysis were performed by a VGS 5000 data system. Peak fitting of the C1s envelope was as described by Shakesheff et al [12].

#### **2.4.4.7. <sup>1</sup>H NMR spectroscopy**

50 mg of lyophilized NPs of each polymer was suspended in deuterium Oxide (D<sub>2</sub>O). <sup>1</sup>H NMR spectra were recorded on a Bruker ARX 400 spectrometer (Bruker Biospin, Billerica, MA). Chemical shifts (δ) were measured in parts per million (ppm) using tetramethylsilane (TMS) as an internal reference.

#### **2.4.4.8. Erosion study**

Mass losses of PLA (A), PEG2.5%-g-PLA (B), and Palmitic acid2.5%-g-PLA (C) NPs were done by suspending 50 mg of NPs for each time interval in 10 mL PBS, pH 7.4 at 37 °C in shaking water bath. The study was terminated at 0, 5, 14, 25, 35 and 45

days. Samples were centrifuged (5000rpm, 10 min) at the end of each time interval. The residues were washed two times with water to remove phosphate buffer and lyophilized for 24 h. The final mass of NPs was determined at each time point.

#### **2.4.4.9. In vitro drug release study**

NPs formulations prepared using different polymers were tested for in vitro release of ibuprofen in triplicates in phosphate buffered saline (PBS, 10 mM, pH 7.4.). 150 mg NPs were suspended in 3.5 mL PBS in a dialysis tubing (Spectra Por 1 membrane, 6–8 kDa cut-off). This dialysis tubing was placed in a screw-capped tube containing 10 mL PBS. The tubes were shaken at 200 rpm on a horizontal water bath shaker (Orbit Shaker Bath, Labline) maintained at  $37\pm 0.5$  °C. At predetermined time intervals, the whole medium in the tube was withdrawn and replaced by fresh PBS to maintain sink conditions. The aliquots were assayed for the concentration of ibuprofen released by spectrophotometry at 262 nm.

### **2.5. Results and discussion:**

#### **2.5.1. Characterization of Polymers.**

Gel permeation chromatography (GPC) was used to measure molecular weight and molecular weight distribution of the synthesized polymers. Results are shown in Table 2.1. The polydispersity was calculated by the ratio of  $M_w$  to  $M_n$  from the GPC data. All the synthesized polymers exhibited uniform molecular weight distribution as revealed by the narrow polydispersity index values. Unimodal mass distribution ruled out the possibility of the presence of unreacted MePEG or palmitoyl chloride with Poly(D,L-

lactide). Typical spectrum was obtained for PLA homopolymer with a characteristic peak at 5.2 ppm corresponding to the tertiary PLA proton (m, -CH), and another peak at 1.5 ppm for the pendant methyl group of the PLA chain (m, -CH<sub>3</sub>) (spectrum not shown). <sup>1</sup>H NMR spectra and chemical structures of PEG2.5%-g-PLA and palmitic acid2.5%-g-PLA polymers are shown in Figure 2.1. A characteristic peak at 5.2 ppm corresponding to the tertiary PLA proton (m, -CH) was observed. Another characteristic peak at 3.6 ppm for the protons of the repeating units in the PEG chain (m, OCH<sub>2</sub>-CH<sub>2</sub>O), a peak at 4.3 ppm for the PEG connecting unit to the PLA block (m, CH<sub>2</sub>-OCO), and a peak at 1.5 ppm for the pendant methyl group of the PLA chain (m, -CH<sub>3</sub>) were also observed. The grafting density of PEG over the PLA backbone was calculated by comparing the peak intensity ratios of PEG (3.6 ppm) to that of PLA (5.2 ppm). The actual PEG grafting density was found to be 2.3 % that is close to the initial feed ratio of PEG as shown in Table 2.1. For palmitic acid2.5%-g-PLA polymer, the signal observed at 1.2–1.3 ppm corresponds to the twelve hydrogens of the palmitate CH<sub>2</sub>. The signal at 0.8– 0.9 ppm is due to the palmitate CH<sub>3</sub>. Palmitate grafting density was calculated by comparing peak intensity ratio of palmitate CH<sub>3</sub> (0.9 ppm) and PLA (5.2 ppm). The final palmitic acid grafting percentage was 1.02 % that is also close to the initial feed ratio as shown in Table 2.1.

### 2.5.2. Particle size and size distribution

Dynamic light scattering (DLS) data showed unimodal distribution for freshly prepared and lyophilized NPs in all batches. Different blank formulations showed nearly similar particle size to that of loaded ones for all NPs types in the range of 120–200 nm (Table 2.2).

**Table 2.1.** Polymers characterization by <sup>1</sup>H NMR, DSC, and Gel Permeation Chromatography (GPC).

Polymer	Mn <sup>a</sup>	Mw <sup>a</sup>	Mw/Mn <sup>a</sup>	PEG/Palmitate (mol%) <sup>b</sup>	Mn ( <sup>1</sup> H NMR) <sup>b</sup>	Tg <sup>c</sup>
PLA	40,318	56,171	1.4	N/A	N/A	46.4 °C
PEG2.5%-g-PLA	4706	5171	1.1	2.3 %	8209	50 °C
Palmitic acid2.5%-g-PLA	10,185	14,050	1.4	1.02 %	14,514	19 °C

N/A: not analyzed.

<sup>a</sup> Determined by GPC analysis using narrow molecular weight polystyrene standards.

<sup>a</sup> Mw/Mn = Polydispersity index of the polymers (PDI).

<sup>b</sup> Calculated from peak intensity ratios of PEG (3.6 ppm) in PEG2.5%-g-PLA or palmitate CH<sub>3</sub> (0.9 ppm) in palmitic acid2.5%-g-PLA and PLA (5.2 ppm) from <sup>1</sup>H NMR data analysis.

<sup>c</sup> Calculated from the second run of DSC as half of the extrapolated tangents in case of PLA and palmitic acid2.5%-g-PLA or as an endothermic peak in case of PEG2.5%-g-PLA.

This might indicate that drug loading had no observable effect on NPs size, suggesting that the size was mainly controlled by homogenization parameters during NPs preparation. Lyophilized palmitic acid2.5%-g-PLA NPs either blank or loaded seems to have larger hydrodynamic diameters than those obtained with PEG2.5%-g-PLA NPs as shown in Table 2.2. This could be explained by the fact that palmitic acid2.5%-g-PLA NPs is more hydrophobic compared to PEG2.5%-g-PLA NPs. The hydrophobic nature of the obtained particles might induce their aggregating tendency due to hydrophobic interactions. The aggregating tendency of palmitic acid2.5%-g-PLA NPs was confirmed later by AFM surface analysis (Fig. 2.2(c), left panel, T). While in PEG2.5%-g-PLA, the

polymer architecture will allow PEG chains to migrate freely towards the surface of NPs during NPs preparation by O/W emulsion method. This would create a steric barrier reducing NPs aggregating tendency.

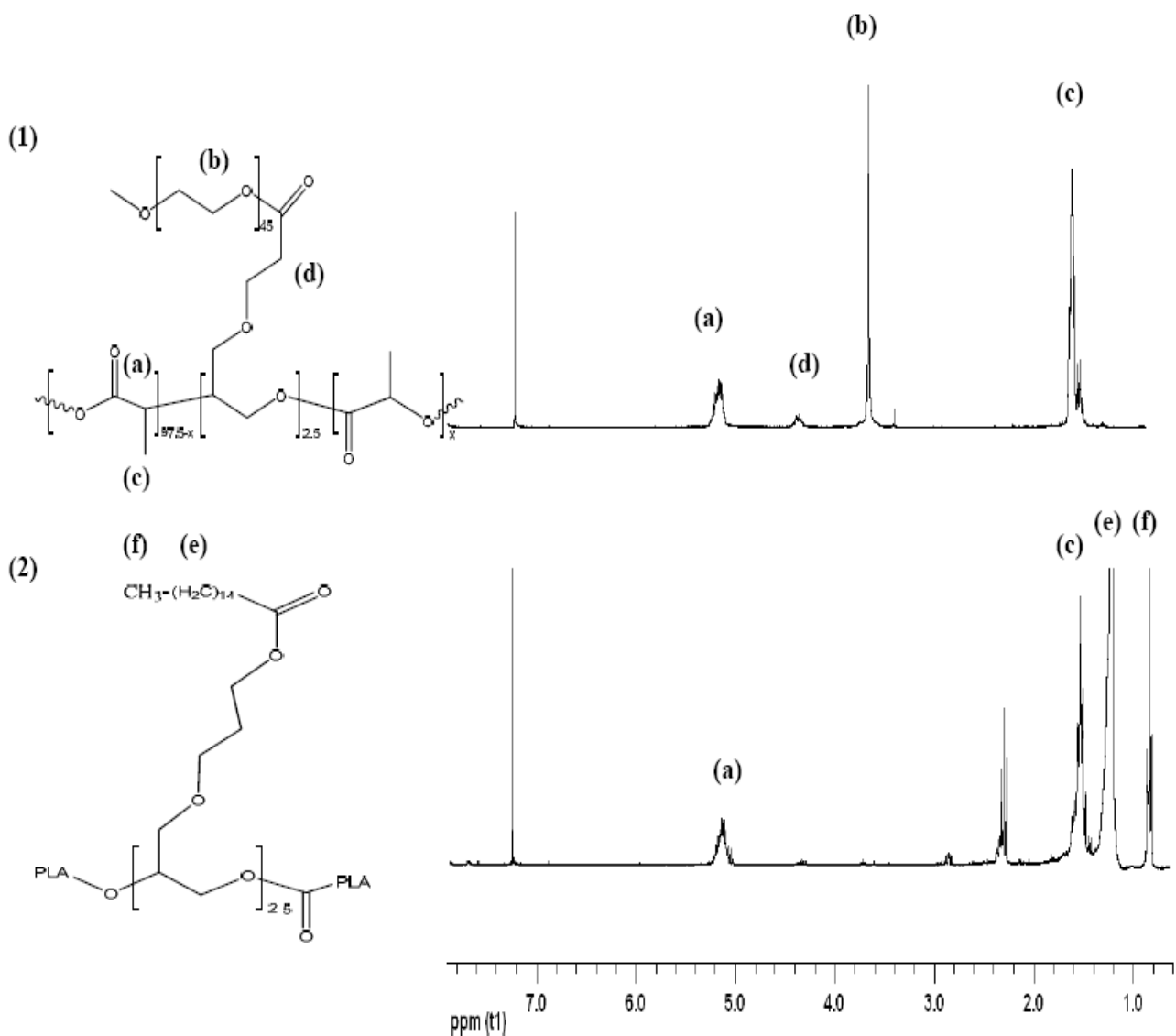


**Figure 2.1.**  $^1\text{H}$  NMR spectra and chemical structures of PEG2.5%-g-PLA (1), and palmitic acid2.5%-g-PLA (2).

### 2.5.3. Zeta ( $\zeta$ ) potential measurements

PLA and palmitic acid2.5%-g-PLA blank NPs showed lower zeta potential (close to zero) values than expected, -3.5 mV and -0.4 mV, respectively. This low  $\zeta$ -potential for both NPs could be attributed to the effective adsorption of PVA on the surface of NPs as will be seen in the next section which could mask the surface charge of PLA and/ or palmitic acid in case of PLA and palmitic acid2.5%-g-PLA NPs, respectively.  $\zeta$ -Potential value of palmitic acid2.5%-g-PLA NPs were lower than PLA NPs and this might be due to higher amount of PVA adsorbed onto the surface (8.6 % w/w) compared to PLA NPs (6.7 % w/w) (Table 2.2). Loaded NPs of both polymers also showed low zeta potential values explained by the same reason. Zambaux et al. also obtained a low zeta potential value of -4 mV for PLA NPs prepared with PVA as an emulsifier [13]. PEG2.5%-g-PLA NPs had also low zeta potential and this could be attributed to shielding action of PEG on the surface charge. Similar results to ours were reported earlier by other authors [14-16]. Moreover, the greater reduction in zeta potential value of PEG2.5%-g-PLA NPs compared to other PEG-PLA NPs reported in the last cited references could be explained by the existence of PVA at the surface of NPs which played also a role in masking their actual surface charge. PEG2.5%-g-PLA NPs showed a remarkable adsorption of 5% w/w PVA onto their surface as shown in Table 2.2.

### 2.5.4. Residual PVA

One of the drawbacks of NPs formulation using emulsion solvent evaporation method is the residual surfactant remaining in NPs suspension after particles precipitation in the aqueous phase. Residual surfactant becomes adsorbed onto the surface of freeze

dried nanoparticles irrespective of the number of washing steps performed to remove it. This might lead to alteration of NPs physicochemical properties such as particle size, hydrophilicity, release kinetics, cellular uptake, etc. [11]. PVA amount remained attached to the nanoparticles needed to be evaluated to detect whether they are affected by the composition and the architecture of the starting polymer or not. It could be seen that a different amount of PVA remained in all the formulations even after 4 washings (Table 2.2). It was found that the highest amounts of PVA remained attached to NPs matrix were 9.8 % and 6.8 % w/w for palmitic acid2.5%-g-PLA and PLA NPs, respectively (Table 2.2). This might be attributed to the enhanced hydrophobic interaction between acetate group of PVA and the hydrophobic PLA matrix as reported before by other authors [11, 17]. Similar findings were obtained before by other authors. When 1% w/v PVA was used as an external aqueous phase emulsifier, 5–6% w/w PVA remained attached within PLA NPs even after 3 washings [13]. PLGA NPs also exhibited a remarkable adsorption of 6.15% w/w PVA into their matrix when 5% w/v PVA solution was used as an emulsifier. Since palmitic acid2.5%-g-PLA is expected to be more hydrophobic than PLA so more interaction with acetate group of PVA might take place. PEG2.5%-g-PLA exhibited less PVA adsorption (5% w/w, Table 2.2) onto their surface and this might be due to their PEG content which offered a certain degree of hydrophilicity to the NPs matrix so a less favored interaction with PVA should be expected. PVA amount adsorbed at the surface of more hydrophilic PLGA microspheres was found to be less than PLGA microspheres [12]. Also, blank NPs showed similar amount of PVA adsorbed on their surfaces as loaded NPs indicating that drug loading had no apparent effect on the amount of PVA associated within the NPs matrix. An attempt was made to evaluate whether

PVA was present either inside the polymeric matrix or on the surface of the particles. Nearly the same amount of PVA was present in the given NPs formulations by both assays confirming that the amount of PVA was mainly associated with the surface of the particles (data not shown).

### 2.5.5. Surface morphology and phase analysis

Tapping mode atomic force microscopy (TM-AFM) was used for analysis of surface morphology of NPs. TM-AFM revealed that both PLA and PEG2.5%-g-PLA NPs were spherical with smooth surfaces. While palmitic acid2.5%-g-PLA NPs seems to have some irregularities at their surface. This might indicated their aggregating tendency (Fig. 2.2(c), left panel, T) confirming the size data obtained by DLS. Phase image analysis was done to investigate the surface chemistry of the obtained particles. It shows more sensitivity to material surface properties such as stiffness, viscoelasticity, and chemical composition [18-20]. Phase imaging is based on the use of changes in the phase angle of cantilever probe. Figure 2.2 shows TM-AFM topography (left panel, T) and their corresponding phase images (right panel, P) of PLA, PEG2.5%-g-PLA, and palmitic acid2.5%-g-PLA NPs, respectively. It is evident from Figure 2.2 that phase images displayed more contrast than the respective topographic images. Phase images of PLA NPs didn't show any clear phase separation evidenced by no colour contrast was observed [Fig.2.2(a); right panel, P]. On the other hand, PEG2.5%-g-PLA NPs showed the presence of an observable phase contrast at the surface of NPs revealed by some dark layers at the surface of bright cores [Fig.2.2(b); right panels, P]. PEG molecules of lower  $M_w$  2000 (used in our study) have smaller Young's modulus than PLA so they are

expected to be softer than PLA [21]. Those mechanical differences between PLA and PEG will result in such phase contrast. Thus, it was expected that PEG molecule will result into darker regions for PEG in the phase images. This was investigated before for poly(styrene-*b*-ethylene oxide) polymer films, where softer PEG segments appeared as darker regions embedded in lighter polystyrene domain [22]. The immiscibility of both PEG and PLA blocks would result in separation of both components during NPs formation. Thus, PEG2.5%-*g*-PLA NPs will be predominantly consisting of hydrophobic PLA cores surrounded by hydrophilic PEG chains on the surface (Figure 2.2(b), phase image, P). While, in case of palmitic acid2.5%-*g*-PLA (Fig.2.2(c), NPs appear as if they were collapsed together with some deformation. This might be due to energy dissipation during tip-sample interaction. The last finding could be explained on the basis of the soft nature of the polymer resulted from grafting palmitic acid over PLA backbone. Palmitate chains are expected to lower the chain rigidity of PLA domains evidenced by the lower  $T_g$  of the polymer (19 °C) compared to PLA homopolymer (46.4 °C ) as will be revealed from DSC data (Table 2.1). Another predisposing factor for palmitic acid-*g*-PLA NPs deformation by AFM tip is that they were dried at room temperature above their  $T_g$  (19 °C). This might favored the existence of the polymer chains in their mobile rubbery state.

#### **2.5.6. Encapsulation efficiency (EE)**

As seen from Table 2.2, % EE of ibuprofen was found to be 36.6 % and 39.5 % for PEG2.5%-*g*-PLA, and palmitic acid2.5%-*g*-PLA NPs, respectively. No marked difference between both polymers ability to encapsulate the drug was detected. This might be due to small grafting density of each polymer since 2.5 % (mol of grafted subs.

/mol of lactic acid) might not be big enough to affect the loading level of PLA NPs. Another possible reason is the larger surface area of the obtained NPs that resulted from the smaller particle size of either PEG2.5%-g-PLA (135 nm) or palmitic acid2.5%-g-PLA NPs (147 nm), readily result in higher drug diffusion to the aqueous phase and hence, limited drug loading (Table 2.2) [23]. Moreover, grafting palmitate over PLA backbone might decreased the density of the obtained NPs (evidenced by low  $M_w$  of palmitic acid2.5%-g-PLA compared to high  $M_w$  PLA, Table 2.1) leading to slower precipitation of NPs compared to the denser PLA and this might give a chance for the drug to diffuse freely into the aqueous phase.

#### 2.5.7. DSC

DSC was used to detect the effect of grafted substance of the used polymer on the thermal properties of NPs. DSC was also used for investigating any possible interaction between the drug and the polymeric matrix. PLA showed glass transition ( $T_g$ ) at 46.4 °C (Table 2.1). Random grafting of PEG on the PLA backbone resulted in an increased  $T_g$  value (by about 4 °C) due to enhanced chain rigidity (Table 2.1 and Figure 2.3.a). For palmitic acid2.5%-g-PLA, the glass transition of the polymer was found to be 19 °C with the existence of an endothermic peak at 58 °C corresponding to the melting peak of the palmitic acid crystals (Table 2.2 and Fig.2.3.b). The melting endotherm of palmitic acid was shifted by 4 °C lower compared to pure palmitic acid indicating the possibility of physical interaction (hydrophobic interaction) between the grafted palmitic acid group and PLA.

**Table 2.2.** Characteristics of different NPs formulation.

<b>Formulation</b>	<b>Size (<math>d_h</math>) before freeze drying (nm)<sup>a, d</sup></b>	<b>PDI<sup>b</sup></b>	<b>Size (<math>d_h</math>) after freeze drying (nm)<sup>a, d</sup></b>	<b>PDI<sup>b</sup></b>	<b>Actual loading (% w/w)<sup>d</sup></b>	<b>% EE<sup>c, d</sup></b>	<b>Zeta potential (mV)<sup>a, d</sup></b>	<b>Surface adsorbed PVA (%w/w)<sup>d</sup></b>
<b>PLA (*)</b>	<b>184±20.8</b>	<b>0.13</b>	<b>161±18.4</b>	<b>0.01</b>	<b>N/A</b>	<b>N/A</b>	<b>-3.50 ± 3.1</b>	<b>6.76±0.4</b>
<b>PLA (**)</b>	<b>194±30.0</b>	<b>0.08</b>	<b>162±22.3</b>	<b>0.09</b>	<b>4.50±0.2</b>	<b>45.0±2.2</b>	<b>-0.18 ± 3.2</b>	<b>6.80±0.2</b>
<b>PEG2.5%-g-PLA (*)</b>	<b>122±31.6</b>	<b>0.14</b>	<b>145±24.7</b>	<b>0.03</b>	<b>N/A</b>	<b>N/A</b>	<b>-1.30 ± 3.5</b>	<b>4.87±0.4</b>
<b>PEG2.5%-g-PLA (**)</b>	<b>135±22.9</b>	<b>0.11</b>	<b>135±32.7</b>	<b>0.01</b>	<b>3.56±0.1</b>	<b>36.6±1.5</b>	<b>-0.60 ± 3.9</b>	<b>5.00±0.7</b>
<b>Palmitic acid2.5%-g-PLA (*)</b>	<b>176±19.7</b>	<b>0.04</b>	<b>181 ±30.8</b>	<b>0.13</b>	<b>N/A</b>	<b>N/A</b>	<b>-0.40 ± 3.1</b>	<b>8.60±0.4</b>
<b>Palmitic acid2.5%-g-PLA (**)</b>	<b>147±22.4</b>	<b>0.06</b>	<b>183±22.2</b>	<b>0.12</b>	<b>3.86±0.2</b>	<b>39.5±0.7</b>	<b>-0.14 ± 3.7</b>	<b>9.80±0.5</b>

<sup>a</sup> median.

<sup>b</sup> refers to polydispersity index.

<sup>c</sup> refers to encapsulation efficiency.

<sup>d</sup> All values indicate mean±S.D. for n=3 independent measurements.

N/A: not analyzed.

(\*) refers to blank NPs (unloaded).

(\*\*) refers to Loaded NPs.

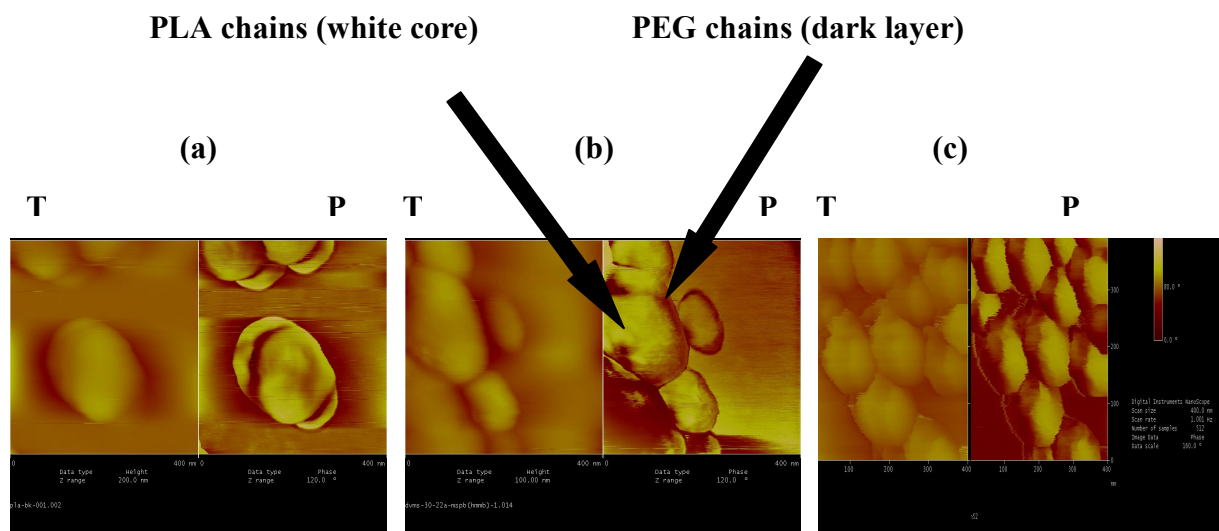


**Figure 2.2.** Tapping mode AFM images of NPs, left panel shows topography (T) and right panel shows corresponding phase images (P); all images are acquired in air. Scan size [400 nm  $\times$  400 nm]; PLA (a), PEG2.5%-g-PLA (b), palmitic acid2.5%-g-PLA (c).

Also, this might indicate that some of palmitate chains are embedded inside PLA domain lowering its chain rigidity evidenced by the lower  $T_g$  of the polymer (19 °C) compared to PLA homopolymer (46.4 °C). Fatty acid esters were found to have a remarkable plasticizing actions on PLA chains [24]. Ibuprofen showed an endothermic peak at 78 °C corresponding to the melting of ibuprofen crystals (Fig.2.3.a). As shown in Fig. 2.3.a, DSC curve of PEG2.5%-g-PLA/ibuprofen physical mixture showed an endothermic peak corresponding to the glass transition ( $T_g$ ) at  $\sim$  50 °C. The melting endotherm of ibuprofen crystals could also be detected at 74 °C. The drug melting peak was shifted by 4 °C lower with some broadening of the peak, indicating the possibility of an interaction between drug and polymer. After encapsulation of ibuprofen in the NPs,  $T_g$  was found to be

reduced by 15 °C lower (~ 35 °C) and this due to the effect of formulation parameters. Surprisingly, the melting endotherm of ibuprofen crystals could also be detected at 74 °C with some broadening (Fig.2.3.a). For more verification, lyophilized loaded NPs were washed five times with water then centrifuged to remove the surface associated drug followed by their lyophilization. DSC scans were done again, surprisingly; the melting endotherm of ibuprofen still exists. This might indicate the detected melting endotherm is for encapsulated ibuprofen which was dispersed in a crystalline form (solid dispersion) not molecular dispersion into PLA matrix. Moreover, the shift and broadening of the melting peak also indicated that an interaction between the drug in its crystalline state and the polymer might take place. Similar observations were noticed with PLA (DSC figure not shown), and palmitic acid 2.5%-g-PLA (Fig.2.3.b) in both physical mixtures and NPs with the consideration of different  $T_g$  for each investigated polymer. Similar finding to ours was obtained when lidocaine was embedded into PEG-PLGA nanospheres. Lidocaine exhibited an endothermic peak at lower temperature or broadened melting peak compared to lidocaine alone. The authors also suggested that there is an interaction between lidocaine and the polymeric carrier [25].

#### **2.5.8. XPS analysis**

Surface chemistry analysis of NPs prepared from both polymers was investigated by means of X-ray photoelectron spectroscopy (XPS) technique. It is possible to determine the surface chemical composition at a depth in the range of 1-10 nm. Any possible interaction between PLA and PVA at the surface of NPs could also be detected in that range. PVA polymer showed three main characteristic peaks corresponding to C-

C/C-H (285 eV), C-OH (286.7 eV) and O-C=O (289 eV) components (Table 2.3). XPS spectrum of PEG showed one characteristic peak corresponding to ether carbons (286.5 eV, Table 3). For PLA homopolymer, the best envelop fit was obtained using three main peaks corresponding to C-C/C-H (285 eV), C-OH (287 eV) and O-C=O (289 eV) (Table 2.3) as previously reported [12]. Ibuprofen could not be experimentally analyzed because it sublimates under the high vacuum of the equipment. Theoretically, ibuprofen has two main characteristic peaks corresponding to C-C/C-H (285 eV), and O-C=O (289 eV) components (Table 2.3).

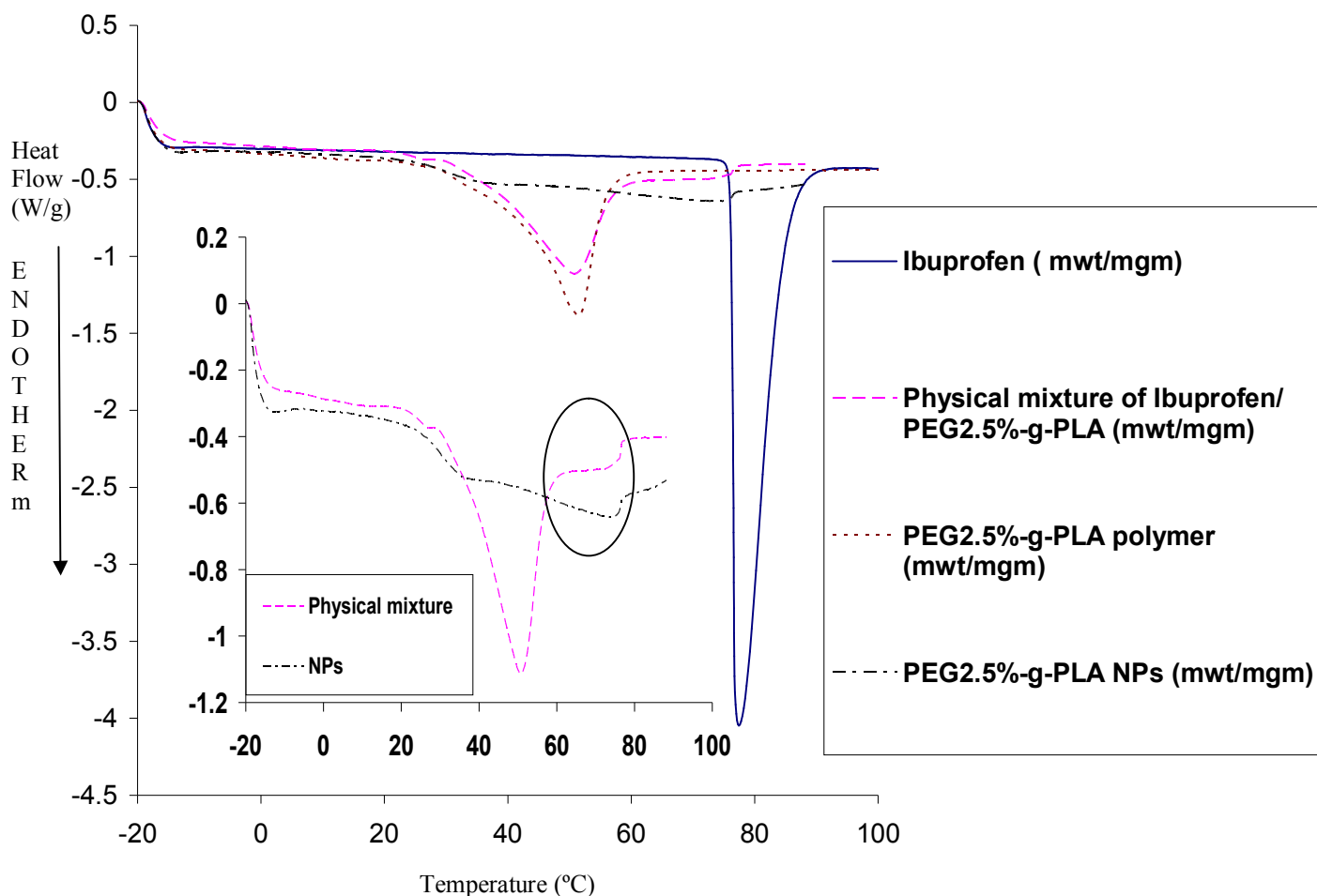


**Figure 2.3.a.** DSC curves of ibuprofen, physical mixture of PEG2.5%-g-PLA with ibuprofen, PEG2.5%-g-PLA polymer, and ibuprofen loaded NPs. Inset inside the figure shows clear thermograms for both physical mixtures and NPs, Ibuprofen melting peak is encircled.

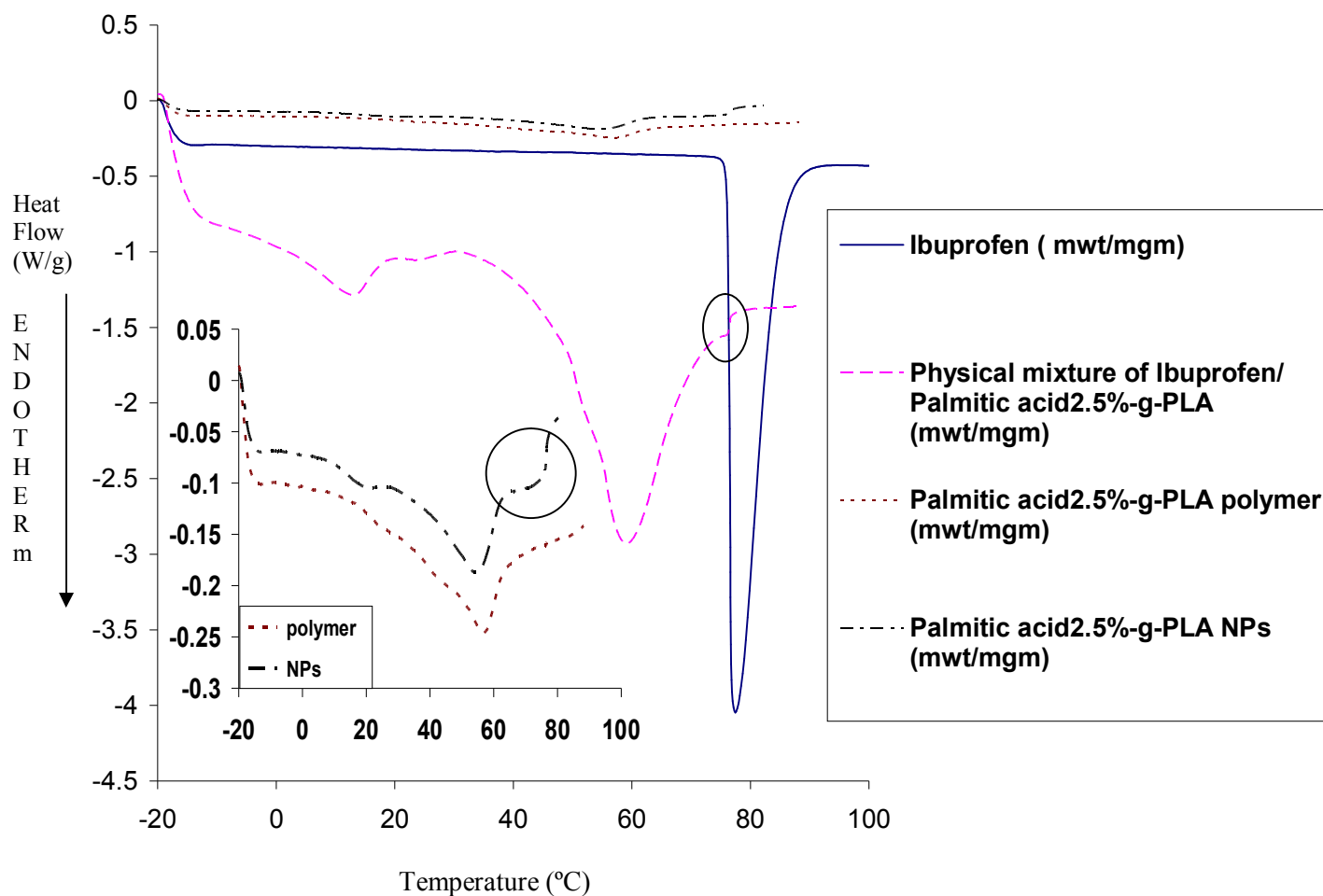


**Figure 2.3.b.** DSC curves of ibuprofen, physical mixture of palmitic acid2.5%-g-PLA with ibuprofen, palmitic acid2.5%-g-PLA polymer, and ibuprofen loaded NPs. Inset inside the figure shows clear thermograms for both pure polymer and NPs. Ibuprofen melting peak is encircled.

It should be mentioned that for ibuprofen to be detected at the surface of loaded NPs, an increase in atomic percentages of both its characteristic peaks mainly C-C/C-H (285 eV) is expected to be found. Both ibuprofen loaded and blank NPs of **PEG2.5%-g-PLA** grafted polymer as well as the polymer itself showed the existence of PEG chains on the

surface as seen by the presence of a characteristic peak corresponding to ether carbons (286.5 eV, Table 2.4). However, the atomic % of PEG decreased when the polymer (9.5 %) was formulated into NPs either blank (5.4 %) or loaded NPs (5 %) as shown in Table 2.4. This might be due to surface adsorption of PVA in case of blank NPs as shown before in PVA analysis section. While in loaded NPs, both PVA and ibuprofen might be adsorbed at the surface of NPs as evidenced from the increase in atomic % of C-C (285 eV) in case of loaded NPs (10.8%) compared to blank NPs (7.3 %) [Table 2.4]. Such an adsorption might decrease the PEG content at the surface. Also, it could be seen from Table 2.4 that the atomic % of C-C (285 eV) decreases from the polymer (10%) to blank (7.3%) and then increased again in case of loaded NPs (10.8%). This might be due to presence of more PLA chains collapsed inside the NPs core (oil phase) during NPs chain organization by O/W emulsion method with less existence of PLA and hence, the C-C functional component at the NPs surface. This C-C content lowering was compensated by drug adsorption (rich in C-C component) at the surface in case of loaded NPs. Moreover, to get the best envelop fit of both NPs, two additional peaks had to be added corresponding to C-O-\*C=O (287.6 eV) and \*C-O-C=O (286.2 eV) components (Table 2.4). These new peaks obtained in both types of NPs could be the result of chemical interaction between PLA-COOH end and PVA-OH during NP formation. The last finding also supports the effective masking of negative charge of these NPs by both PEG and PVA chains at the surface of such NPs as shown in Table 2.2. It was shown before that despite of several washing steps of the separated NPs pellets, there is always a fraction of PVA remains associated with the NPs and this has been attributed to the hydrophobic interactions between vinyl acetate segment of PVA and PLA/ PLGA core [11]. O-C=O

functional component (289 eV) was detected also in the XPS spectrum of the PEG2.5%-g-PLA polymer, both its blank and loaded NPs. This might be due to the presence of COOH functional group in the polymer structure (Fig.2.1) or due to adsorption of PVA (partially hydrolyzed) and ibuprofen (weak acid) at the surface of blank and loaded NPs, respectively. In case of **palmitic acid2.5%-g-PLA** polymer and its both NPs types, there was a marked decrease in C-C components (285 eV) atomic % from the polymer (63.8%) to blank (49.1%) and then to loaded NPs (42.8%). This might be due to chain organization during NPs formation by O/W emulsion method in such a way that showed the migration of palmitate (hydrophobic chain) towards NPs core (oil phase) to avoid facing the external aqueous phase. This process might force palmitate chains to be embedded into NPs core and hence decreasing the C-C content at the surface. Although we expected an increase in the atomic % of C-C (285 eV) from blank to loaded NPs as shown before with PEG2.5%-g-PLA loaded NPs, a decrease in the atomic % (from 49.1% to 42.8%) of that component was surprisingly detected and this might be due to the possibility of hydrophobic interaction between ibuprofen and palmitic acid which forces the drug to be embedded inside the core of NPs. The last hypothesis was supported by another finding that the atomic % of O-C=O (289 eV) [also characteristic for the drug] was very low (2.2%) in case of loaded NPs (Table 2.4). This indicates that some interaction might occur between the drug and polymer shielding the drug functional groups from the surface. It also should be mentioned that the existence of that functional gp, O-C=O (289 eV) in the polymer and blank NPs spectra (4.6% and 5.7%, respectively) might be due to COOH of both PLA and PVA (partially hydrolyzed), respectively. Also, the existence of two new peaks at C-O-\*C=O (287.6 eV) and \*C-O-C=O (286.2 eV)

might confirmed PVA interaction with PLA in such kind of polymer. This finding was also supported by the high % residual PVA detected at the NPs surface as shown in Table 2.4.

**Table 2.3.** Relative atomic percentages calculated from XPS Surface Analysis of pure materials used in NPs preparation.

<b>Binding Energy (functional component)</b>	<b>Atomic Percentage (%)</b>			
	<b>Ibuprofen</b>	<b>PLA</b>	<b>PVA</b>	<b>PEG</b>
<b>285 (C-C)</b>	<b>92.4</b>	<b>22.3</b>	<b>37.1</b>	<b>-</b>
<b>286.5 (C-O)</b>	<b>-</b>	<b>-</b>	<b>-</b>	<b>100</b>
<b>286.7 (C-O)</b>	<b>-</b>	<b>-</b>	<b>23</b>	<b>-</b>
<b>287 (C-O)</b>	<b>-</b>	<b>28.9</b>	<b>-</b>	<b>-</b>
<b>289 (O-C=O)</b>	<b>7.6</b>	<b>13.9</b>	<b>4.3</b>	<b>-</b>

N.B: Relative percentage of each functional component is calculated from the area under the curve from their respective peaks in XPS analysis.

### 2.5.9. <sup>1</sup>H-NMR of NPs in D<sub>2</sub>O

<sup>1</sup>H-NMR analysis of NPs in D<sub>2</sub>O was done to confirm the core-corona structure of PEG2.5%-g-PLA NPs and compare it with palmitate2.5%-g-PLA NPs structure. <sup>1</sup>H-NMR spectra of PEG2.5%-g-PLA NPs in D<sub>2</sub>O showed presence of methylene protons of PEG chains at 3.6 ppm (Fig.2.4). Signals from PLA methyl or methylene protons were absent or diminished in intensity. Also both signals corresponding to the twelve hydrogens of the palmitate CH<sub>2</sub> and the palmitate CH<sub>3</sub> were completely absent in <sup>1</sup>H-NMR spectra of palmitic acid2.5%-g-PLA.

**Table 2.4.** Relative atomic percentages calculated from XPS Surface Analysis of synthesized polymers and formulated NPs using those polymers.

B.E. (functional component)	Atomic Percentage (%)					
	PEG2.5%- g-PLA BK NPs	PEG2.5%-g- PLA LD NPs	PEG2.5%-g- PLA polymer	Palmitate 2.5%-g- PLA BK NPs	Palmitate 2.5%-g- PLA LD NPs	Palmitate 2.5%-g- PLA polymer
285 (C-C)	7.3	10.8	10.0	49.1	42.8	63.8
286.2 (*C-O-C=O)	2.1	2.5	-	8.6	13.9	-
286.5 (C-O)	5.4	5.0	9.5	-	-	-
287.6 (C-O-*C=O)	4.2	3.5	-	5.3	5.0	-
289 (O-C=O)	5.5	4.1	5.0	5.7	2.2	4.6

(B.E.) refers to the binding energy  
 (BK) refers to blank NPs  
 (LD) refers to loaded NPs

This might indicate that both PLA and palmitate protons are in solid environment and can't be detected whereas PEG chains must be in mobile state. Core-corona structure of PLA-PEG diblock NPs was confirmed before from  $^1\text{H-NMR}$  analysis of NPs in  $\text{D}_2\text{O}$  [26].  $^1\text{H-NMR}$  analysis was also used to confirm poly-(ethylene glycol)-*b*-(styrene-*r*-benzocyclobutene) block copolymer (PEG-*b*-(S-*r*-BCB) NPs formation after intramolecular cross-linking of the S-*r*-BCB block to form a linear-nanoparticle structure.  $^1\text{H-NMR}$  spectra of NPs showed complete disappearance of the aliphatic benzocyclobutene protons at 3.05 ppm upon formation of the cross-linked nanoparticles [27]. Our results are in accordance with the above-cited references suggesting NPs made

of PLA and PEG corona in case of PEG2.5%-g-PLA NPs. Thus,  $^1\text{H-NMR}$  analysis together with XPS data of NPs might indicate that hydrophilic polymer parts (PEG) are oriented towards the outer phase (water) during precipitation and NP hardening whereas the more lipophilic polyester (either PLA or PLA and palmitate) residues form the inner core. A schematic representation of different chain organization of NPs depending on both their polymer composition and polymer architecture is shown in Figure 2.5. For PEG2.5%-g-PLA NP, enhanced phase separation of both components during NPs formation was observed as confirmed from AFM phase imaging, XPS and  $^1\text{H-NMR}$  data. Thus, easy migration of PEG chains towards the surface of NPs will be favored while the cores will be predominantly hydrophobic. On the contrary, palmitic acid2.5%-g-PLA NPs showed the migration of palmitate chains into PLA core avoiding facing the aqueous phase during NPs preparation.

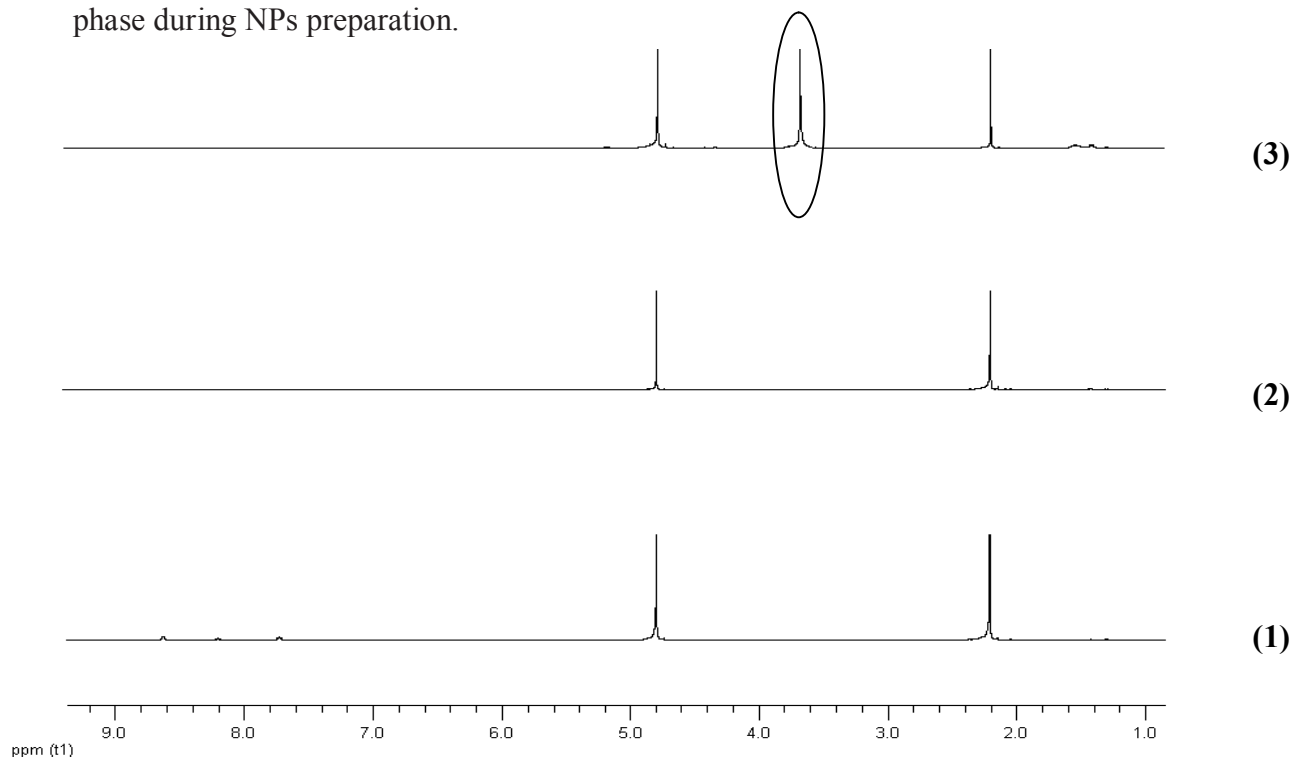


**Figure 2.4.**  $^1\text{H-NMR}$  of blank NPs of PLA (1), palmitic acid2.5%g-PLA (2), and PEG2.5%-g-PLA (3) in D<sub>2</sub>O. PEG peaks at 3.6 ppm are encircled.

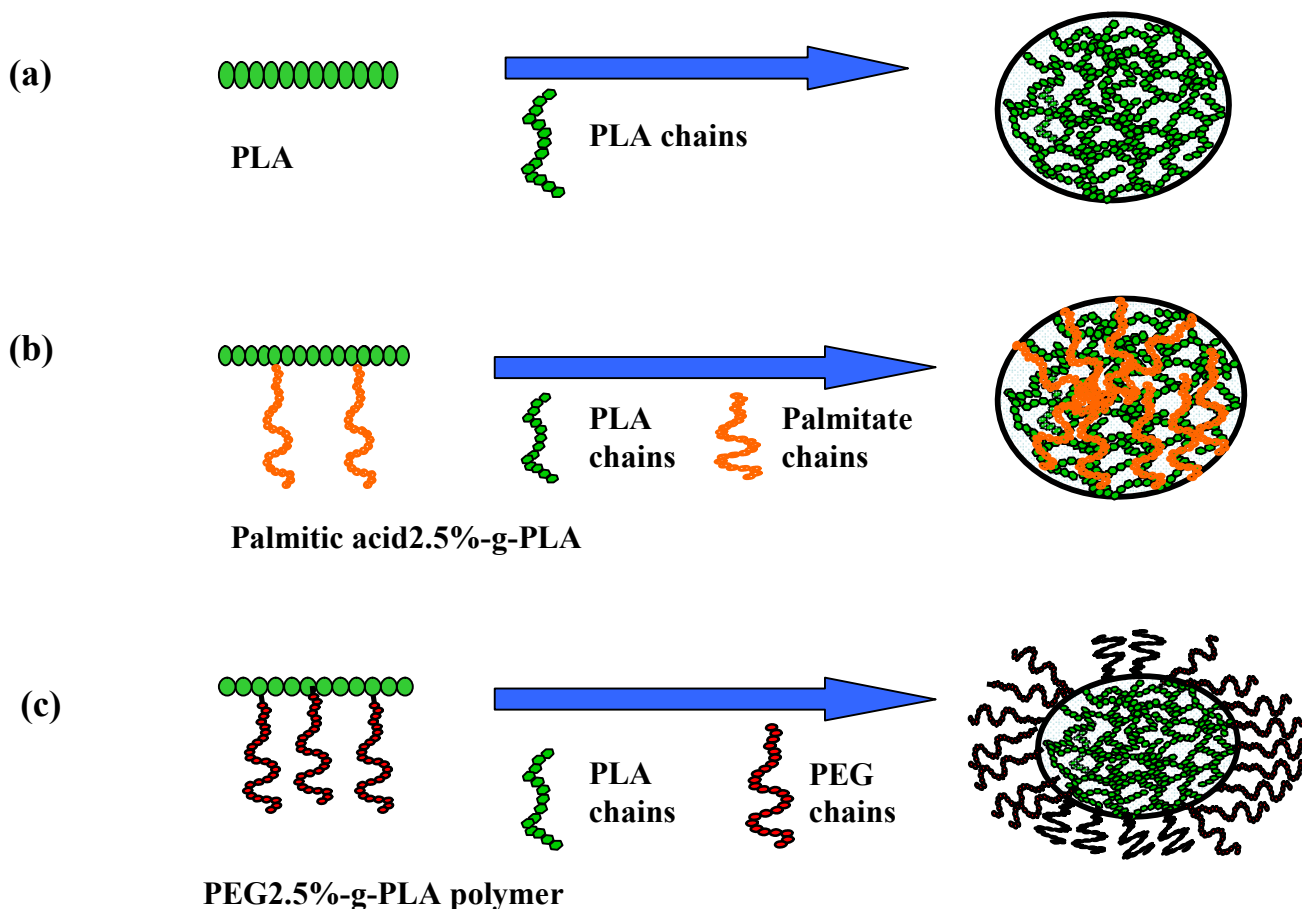


**Figure 2.5.** Schematic representation of polymer chain organization inside the NPs: PLA (a), Palmitic acid2.5%-g-PLA (b), PEG2.5%-g-PLA (c).

### 2.5.10. Erosion study

This study was conducted to investigate the effect of polymer grafting on the in vitro degradation rate of PLA based NPs under conditions similar to physiological ones. Mass loss of copolymer in phosphate buffer started after 5 days for all the investigated NPs. A noticeable difference in mass loss is observed between PEG2.5%-g-PLA and

palmitic acid2.5%-g-PLA NPs after 10 days of incubation. PEG2.5%-g-PLA exhibited faster erosion rate ~ 43 % compared to both PLA and palmitic acid2.5%-g-PLA NPs which showed slower rates around 17% and 32 %, respectively after 45 days. This pattern is shown in Figure 2.6. Mass loss of polyester copolymers is usually enhanced by ester hydrolysis and transesterification mechanisms [28]. NPs erosion was initiated by wateruptake followed by random hydrolytic chain scission of PLA block with release of lactide oligomers. The more hydrophilic PEG2.5%-g-PLA initially swells to a much greater degree than other polymers of lower hydrophilic content, allowing more water uptake into the matrix, further increasing the rate of hydrolysis and breakdown of NPs [29, 30]. Thus PEG grafting over PLA backbone was observed to increase the degradation rate of PLA. The possible reason that palmitic acid2.5%-g-PLA NPs showed faster degradation rates than PLA NPs is that palmitic acid2.5%-g-PLA polymer has lower Mw compared to PLA homopolymer (Table 2.1).

#### **2.5.11. In Vitro Drug Release.**

One of the main purposes of this study is to compare and study the effect of the aqueous solubility of grafted substance over PLA backbone on drug release profiles from modified PLA NPs. Ibuprofen showed much more rapid release from solution than its release from the NPs indicating that drug diffusion through the dialysis bag was not the release rate-limiting step (Fig. 2.7). Different NPs formulations were compared for their in vitro release behavior as shown in Fig.2.7. It could be seen that all formulations exhibited biphasic release phenomenon.

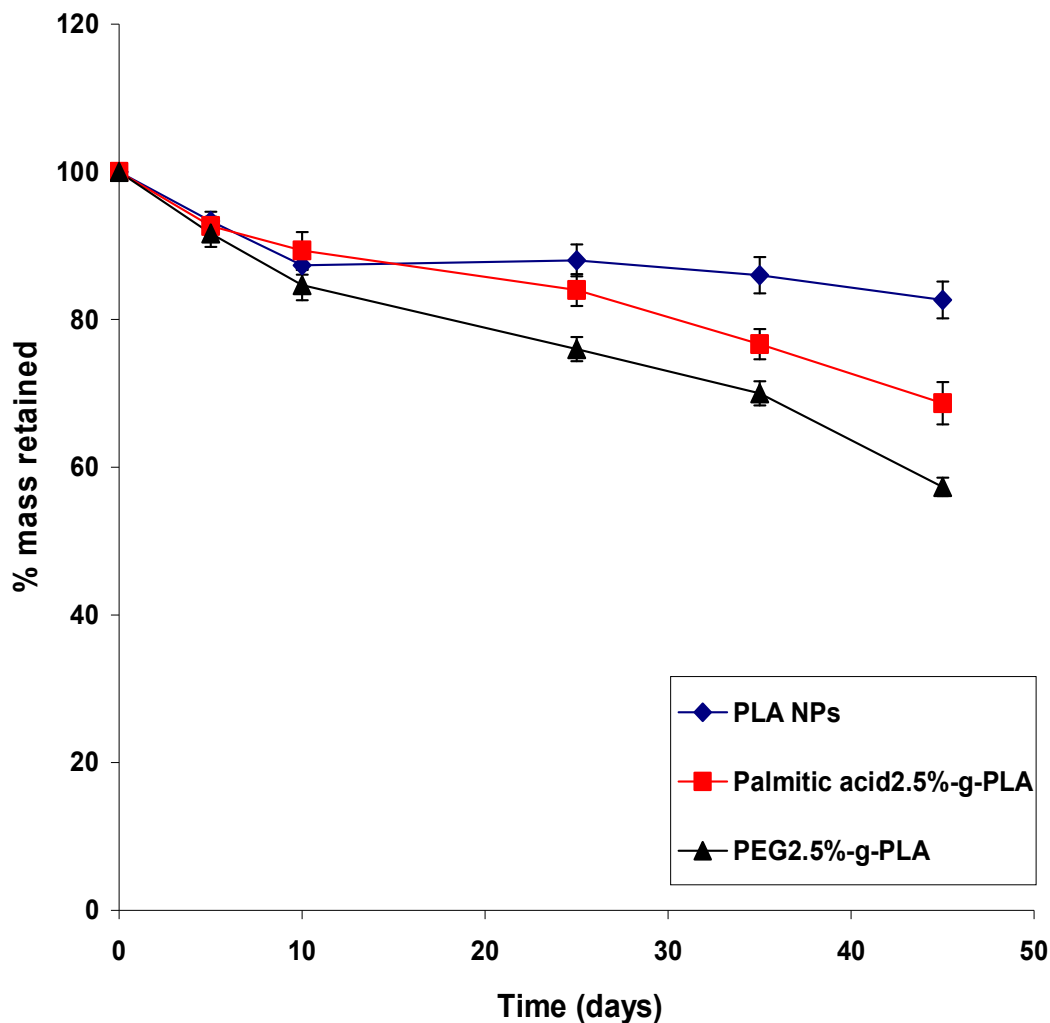


**Figure 2.6.** Erosion of different ibuprofen loaded NPs in phosphate buffer saline (PBS, pH 7.4) at 37 °C.

A rapid initial burst release varied from 10 % to 20 % of their payload and this might be due to the immediate release of drug particles adsorbed at or near the surface of NPs [31]. This phase was followed by sustained release of the drug over 300 h. Drug release during that phase is mainly controlled by solubility of the drug in the matrix, diffusion of drug into the matrix, and matrix erosion [32, 33]. The physical state of the drug inside the NPs matrix might have an influence on the in vitro and in vivo release behaviour of the drug. DSC indicated that ibuprofen mostly exists in a crystalline state inside all NPs

irrespective of their polymer content. The last finding indicates that the main rate limiting step affecting drug release will be the dissolution of drug crystals into the polymeric matrix followed by their diffusion out of the matrix into the release media. This finding also confirmed the role of NPs core wetting in enhancing drug dissolution and hence drug release. PEG2.5%-g-PLA NPs showed faster drug release rates compared to other formulations and this could be attributed to their PEG content that might led to rapide core wetting resulting in faster drug dissolution followed by its rapide diffusion and/or more enhancement of matrix erosion. On the other hand, palmitic acid2.5%-g-PLA NPs showed faster drug release compared to PLA NPs although the former is expected to be more hydrophobic and hence more interaction with drug will be favored. This is could be explained on the basis that PLA polymer had large molecular weight compared to palmitic acid2.5%-g-PLA polymer as shown before from GPC data (Table 2.1) and this might slow the process of matrix erosion [25]. Erosion study showed that PEG2.5%-g-PLA NPs exhibited faster degradation rate (Fig. 2.6) than other NPs supporting the faster release behaviour exhibited by those NPs. These results showed that the hydrophilicity of the matrix is one of the major factors that markedly influence its hydration and, in turn, the drug release profile [34, 35]. It also should be mentioned that both erosion and release rates could be affected by the size of the particle tested. However, the small size differences between the three tested loaded batches (PLA,  $162 \pm 22.3$  nm), (PEG-g-PLA,  $135 \pm 32.7$  nm), and (palmitic acid-g-PLA,  $183 \pm 22.2$  nm) might not be fully responsible for such big differences in both release and erosion.

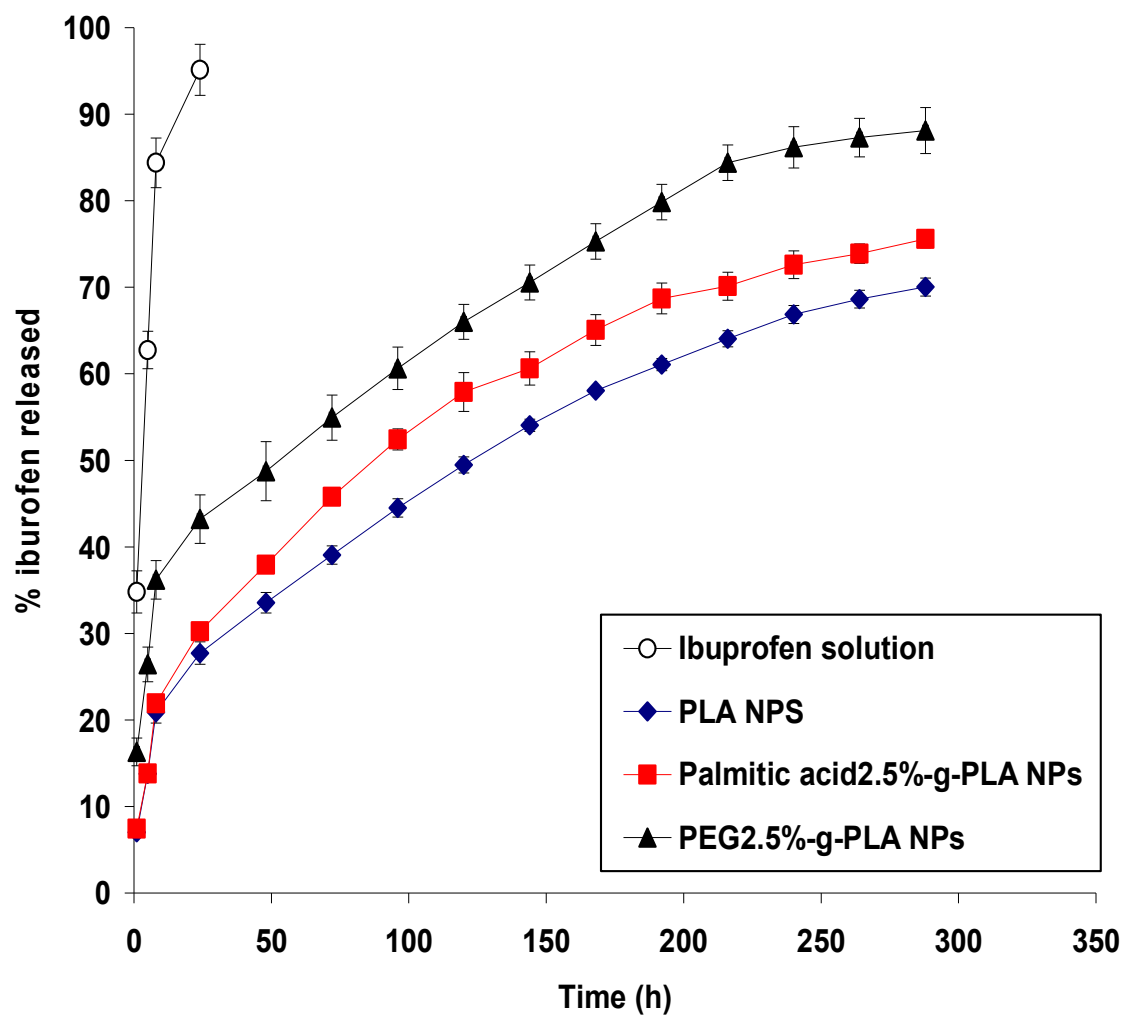


**Figure 2.7.** Effect of PLA grafting on the in vitro release behavior of ibuprofen loaded NPs; values are represented as mean  $\pm$ S.D. of three independent experiments.

## 2.6. Conclusion

NPs were fabricated using grafted copolymers of PLA with two grafted substances of different aqueous solubility. PEG2.5%-g-PLA NP and palmitic acid2.5%-g-PLA polymers were synthesized and fabricated into NPs. NPs were compared for the effect of

the aqueous solubility of grafted substance of the polymer on their physicochemical properties. Mode of chain organization of each polymer was also investigated. Both AFM phase imaging and XPS studies showed the existence of PEG chains on the surface of PEG2.5%-g-PLA NPs. This resulted in rapide core wetting, faster degradation of the polymeric matrix and faster drug release from NPs. On the contrary, palmitic acid2.5%-g-PLA NPs showed the existence of palmitate chains embedded inside NPs core. This organization affected some major physicochemical properties of NPs. Our future work will focus on studying the cellular uptake of rhodamine encapsulated NPs made from different architectures. In brief, the aqueous solubility of grafted material over the polymer backbone is an important parameter controlling surface characteristics of NPs which in turn determine their physicochemical properties like % PVA adsorbed at the surface of NPs, zeta potential, thermal characteristic, NPs surface organization and drug release kinetics.

## **2.7. Acknowledgment**

The work was supported in part by a grant of Fonds de la recherche en santé Québec (FRSQ) to Dr. Hildgen. The authors wish to thank Mme. Suzie poulin, research associate at École Polytechnique, University of Montreal for her help in the data analysis of the XPS experiments. Sherief Abdel-Azeez thanks the Ministry of Higher Education, Egypt for granting him a scholarship during his Ph.D.

## 2.8. References

1. Letchford, K., Burt, H., 2007. A review of the formation and classification of amphiphilic block copolymer nanoparticulate structures: micelles, nanospheres, nanocapsules and polymersomes. *European Journal of Pharmaceutics and Biopharmaceutics* 65, 259-269.
2. Frank, A., Rath, S.K., Venkatraman, S.S., 2005. Controlled release from bioerodible polymers: effect of drug type and polymer composition. *Journal of Controlled Release* 102, 333-344.
3. Jeong, Y.-I., Cheon, J.-B., Kim, S.-H., Nah, J.-W., Lee, Y.-M., Sung, Y.-K., Akaike, T., Cho, C.-S., 1998. Clonazepam release from core-shell type nanoparticles in vitro. *Journal of Controlled Release* 51, 169-178.
4. Chorny, M., Fishbein, I., Danenberg, H.D., Golomb, G., 2002. Lipophilic drug loaded nanospheres prepared by nanoprecipitation: effect of formulation variables on size, drug recovery and release kinetics. *Journal of Controlled Release* 83, 389-400.
5. Gorner, T., Gref, R., Michenot, D., Sommer, F., Tran, M.N., Dellacherie, E., 1999. Lidocaine-loaded biodegradable nanospheres. I. Optimization of the drug incorporation into the polymer matrix. *Journal of Controlled Release* 57, 259-268.
6. Sant, S., Poulin, S., Hildgen, P., 2008. Effect of polymer architecture on surface properties, plasma protein adsorption, and cellular interactions of pegylated nanoparticles. *Journal of Biomedical Materials Research Part A* 87A, 885-895.
7. Govender, T., Riley, T., Ehtezazi, T., Garnett, M.C., Stolnik, S., Illum, L., Davis, S.S., 2000. Defining the drug incorporation properties of PLA-PEG nanoparticles. *International Journal of Pharmaceutics* 199, 95-110.
8. Vila, A., Gill, H., McCallion, O., Alonso, M.J., 2004. Transport of PLA-PEG particles across the nasal mucosa: effect of particle size and PEG coating density. *Journal of Controlled Release* 98, 231-244.
9. Heald, C.R., Stolnik, S., Kujawinski, K.S., De Matteis, C., Garnett, M.C., Illum, L., Davis, S.S., Purkiss, S.C., Barlow, R.J., Gellert, P.R., 2002. Poly(lactic acid)-Poly(ethylene oxide) (PLA-PEG) Nanoparticles: NMR Studies of the Central Solidlike PLA Core and the Liquid PEG Corona. *Langmuir* 18, 3669-3675.

10. Nadeau, V., Leclair, G., Sant, S., Rabanel, J.-M., Quesnel, R., Hildgen, P., 2005. Synthesis of new versatile functionalized polyesters for biomedical applications. *Polymer* 46, 11263-11272.
11. Sahoo, S.K., Panyam, J., Prabha, S., Labhasetwar, V., 2002. Residual polyvinyl alcohol associated with poly (D,L-lactide-co-glycolide) nanoparticles affects their physical properties and cellular uptake. *Journal of Controlled Release* 82, 105-114.
12. Shakesheff, K.M., Evora, C., Soriano, I., Langer, R., 1997. The Adsorption of Poly(vinyl alcohol) to Biodegradable Microparticles Studied by X-Ray Photoelectron Spectroscopy (XPS). *Journal of Colloid and Interface Science* 185, 538-547.
13. Zambaux, M.F., Bonneaux, F., Gref, R., Maincent, P., Dellacherie, E., Alonso, M.J., Labrude, P., Vigneron, C., 1998. Influence of experimental parameters on the characteristics of poly(lactic acid) nanoparticles prepared by a double emulsion method. *Journal of Controlled Release* 50, 31-40.
14. Quesnel, R., P., Hildgen, 2005. Synthesis of PLA-b-PEG multiblock copolymers for stealth drug carrier preparation. *Molecules* 10, 98-104.
15. Beletsi, A., Panagi, Z., Avgoustakis, K., 2005. Biodistribution properties of nanoparticles based on mixtures of PLGA with PLGA-PEG diblock copolymers. *International Journal of Pharmaceutics* 298, 233-241.
16. Gref, R., Lück, M., Quellec, P., Marchand, M., Dellacherie, E., Harnisch, S., Blunk, T., Müller, R.H., 2000. 'Stealth' corona-core nanoparticles surface modified by polyethylene glycol (PEG): influences of the corona (PEG chain length and surface density) and of the core composition on phagocytic uptake and plasma protein adsorption. *Colloids and Surfaces B: Biointerfaces* 18, 301-313.
17. Scholes, P.D., Coombes, A.G.A., Illum, L., Davis, S.S., Watts, J.F., Ustariz, C., Vert, M., Davies, M.C., 1999. Detection and determination of surface levels of poloxamer and PVA surfactant on biodegradable nanospheres using SSIMS and XPS. *Journal of Controlled Release* 59, 261-278.

18. Raghavan, D., Gu, X., Nguyen, T., VanLandingham, M., Karim, A., 2000. Mapping Polymer Heterogeneity Using Atomic Force Microscopy Phase Imaging and Nanoscale Indentation. *Macromolecules* 33, 2573-2583.
19. Paredes, J.I., Gracia, M., Martínez-Alonso, A., Tascón, J.M.D., 2005. Nanoscale investigation of the structural and chemical changes induced by oxidation on carbon black surfaces: A scanning probe microscopy approach. *Journal of Colloid and Interface Science* 288, 190-199.
20. Magonov, S.N., Elings, V., Whangbo, M. H., 1997. Phase imaging and stiffness in tapping-mode atomic force microscopy. *Surface Science* 375, L385-L391.
21. Donald, G., William, D., Randal, S., John, L., Willett, J.L., 2003. Mechanical and thermal properties of starch-filled poly(D,L-lactic acid)/poly(hydroxy ester ether) biodegradable blends. *Journal of Applied Polymer Science* 88, 1775-1786.
22. Wang, H., Djuricic, A.B., Chan, W.K., Xie, M.H., 2005. Factors affecting phase and height contrast of diblock copolymer PS-b-PEO thin films in dynamic force mode atomic force microscopy. *Applied Surface Science* 252, 1092-1100.
23. Mohanraj, V.J., Chen, Y., Nanoparticles - A review. 2007, Association of Crop Science, Uganda.
24. Jacobsen, S., Fritz, H.G., 1999. Plasticizing polylactide - The effect of different plasticizers on the mechanical properties. *Polymer Engineering and Science* 39, 1303-1310.
25. Peracchia, M.T., Gref, R., Minamitake, Y., Domb, A., Lotan, N., Langer, R., 1997. PEG-coated nanospheres from amphiphilic diblock and multiblock copolymers: Investigation of their drug encapsulation and release characteristics. *Journal of Controlled Release* 46, 223-231.
26. Riley, T., Stolnik, S., Heald, C.R., Xiong, C.D., Garnett, M.C., Illum, L., Davis, S.S., Purkiss, S.C., Barlow, R.J., Gellert, P.R., 2001. Physicochemical evaluation of nanoparticles assembled from poly(lactic acid)-poly(ethylene glycol) (PLA-PEG) block copolymers as drug delivery vehicles. *Langmuir* 17, 3168-3174.
27. Kim, Y., Pyun, J., Frechet, J.M.J., Hawker, C.J., Frank, C.W., 2005. The Dramatic Effect of Architecture on the Self-Assembly of Block Copolymers at Interfaces. *Langmuir* 21, 10444-10458.

28. von Burkersroda, F., Gref, R., Göpferich, A., 1997. Erosion of biodegradable block copolymers made of poly(-lactic acid) and poly(ethylene glycol). *Biomaterials* 18, 1599-1607.
29. Siparsky, G.L., Voorhees, K.J., Dorgan, J.R., Schilling, K., 1997. Water transport in polylactic acid (PLA), PLA/polycaprolactone copolymers, and PLA polyethylene glycol blends. *Journal of Environmental Polymer Degradation* 5, 125-136.
30. Clapper, J.D., Skeie, J.M., Mullins, R.F., Guymon, C.A., 2007. Development and characterization of photopolymerizable biodegradable materials from PEG-PLA-PEG block macromonomers. *Polymer* 48, 6554-6564.
31. Magenheim, B., Levy, M.Y., Benita, S., 1993. A new in-vitro technique for the evaluation of drug-release profile from colloidal carriers - ultrafiltration technique at low-pressure. *International Journal of Pharmaceutics* 94, 115-123.
32. Panyam, J., Dali, M.M., Sahoo, S.K., Ma, W., Chakravarthi, S.S., Amidon, G.L., Levy, R.J., Labhasetwar, V., 2003. Polymer degradation and in vitro release of a model protein from poly(D,L-lactide-co-glycolide) nano- and microparticles. *Journal of Controlled Release* 92, 173-187.
33. Mittal, G., Sahana, D.K., Bhardwaj, V., Ravi Kumar, M.N.V., 2007. Estradiol loaded PLGA nanoparticles for oral administration: Effect of polymer molecular weight and copolymer composition on release behavior in vitro and in vivo. *Journal of Controlled Release* 119, 77-85.
34. Sung, K.C., Han, R.-Y., Hu, O.Y.P., Hsu, L.-R., 1998. Controlled release of nalbuphine prodrugs from biodegradable polymeric matrices: influence of prodrug hydrophilicity and polymer composition. *International Journal of Pharmaceutics* 172, 17-25.
35. Sinha Roy, D., Rohera, B.D., 2002. Comparative evaluation of rate of hydration and matrix erosion of HEC and HPC and study of drug release from their matrices. *European Journal of Pharmaceutical Sciences* 16, 193-199.

## **CHAPTER THREE**

---

### **RESEARCH PAPER**

**Effect of Polyethylene Glycol (PEG) Chain Organization on the  
Physicochemical Properties of Poly(D,L-lactide) (PLA) based  
Nanoparticles<sup>1</sup>.**

Sherief Essa, Jean Michel Rabanel, and Patrice Hildgen.

**European Journal of Pharmaceutics and Biopharmaceutics  
75 (2010) 96-106**

---

<sup>1</sup> My contribution included designing the experiments, polymer synthesis, nanoparticles preparation and characterization, interpreting the results and writing the paper, which was supervised by Dr. Patrice Hildgen. Jean Michel Rabanel contribution was technical assistance using laboratory equipments.

### 3.1. Abstract:

The aim of the present study is to evaluate the effect of polyethylene glycol (PEG) chain organization on various physicochemical aspects of drug delivery from poly(D,L-lactide) (PLA) based nanoparticles (NPs). To reach that goal, two different pegylated polymers of poly(D,L-lactide) (PLA) were synthesized. Polymers used in this study are grafted one in which PEG was grafted on PLA backbone at 7% (mol/mol of lactic acid monomer), PEG7%-g-PLA, and multiblock copolymer of both PLA and PEG, (PLA-PEG-PLA)<sub>n</sub> with nearly similar PEG insertion ratio and the same PEG chain length. Blank and ibuprofen-loaded NPs were prepared from both polymers and their properties were compared to PLA homopolymer NPs as a control. Encapsulation efficiency of ibuprofen was found to be ~ 25% for (PLA-PEG-PLA)<sub>n</sub> NPs and ~ 80% for PEG7%-g-PLA NPs. (PLA-PEG-PLA)<sub>n</sub> NPs either blank or loaded showed larger hydrodynamic diameter (~ 200 nm) than PEG7%-g-PLA NPs (~ 135 nm). A significant difference was observed in the amount of PVA associated with the surface of both NPs where 3.6 and 0.4 % (wt/wt) were found on the surface of PEG7%-g-PLA and (PLA-PEG-PLA)<sub>n</sub> NPs, respectively. No observed difference in zeta potential values for both NPs formulations was found. DSC showed the existence of the drug in a crystalline state inside NPs matrix irrespective of the type of polymer used with either shifting or/ and broadening of the drug melting endotherm. Both AFM phase imaging and XPS studies revealed the possibility of existence of more PEG chains at the surface of grafted polymer NPs than (PLA-PEG-PLA)<sub>n</sub> during NPs formation. The in vitro release behavior showed that (PLA-PEG-PLA)<sub>n</sub> NPs exhibited faster release rates than PEG7%-g-PLA NPs. The

physicochemical differences obtained between both polymers were probably due to different chain organization during NPs formulation. Such pegylated NPs made from these two different polymers might find many applications, being able to convert poorly soluble, poorly absorbed substances into promising drugs, improving their therapeutic performance, and helping them reach adequately their target area. Our results suggest that the properties of pegylated PLA-based NPs can be tuned by proper selection of both polymer composition and polymer architecture.

### **3.2. Keywords**

Poly(D,L-lactide), polymer architecture, graft polymers, multiblock, chain organization, X-ray photoelectron spectroscopy ( XPS), atomic force microscopy (AFM) phase imaging.

### **3.3. Introduction:**

Over the past few decades, there has been an intensive research on the development of biodegradable nanoparticles (NPs) as a suitable means for controlled drug release and targeting [1-3] Nanoparticles (NPs) are colloidal systems that vary in size from 10 to 1000 nm. The drug is either dissolved, entrapped, encapsulated or attached to a nanoparticle matrix [4]. Poly(lactic acid) (PLA) or poly(lactide-co-glycolide) (PLGA) have been widely used to fabricate NPs owing to excellent biocompatibility, biodegradability and high encapsulation capability for hydrophobic drugs. However, uptake of such naked NPs by the reticuloendothelial system after intravascular administration presented a major problem for achieving effective targeting to specific

sites in the body other than liver and spleen [5]. Therefore, the design of long-circulating NPs or stealth NPs has emerged as an attempt to escape recognition by phagocytic cells of the blood. The most commonly used strategy for designing stealth NPs is reliant upon introducing flexible hydrophilic coat onto hydrophobic surfaces, shielding them against plasma protein adsorption, which is the first step of particle clearance mechanism by blood phagocytes. Covalently grafted PEG strategy was proven stable and more successful than physical adsorption of PEG containing surfactants onto NPs surface. Generally, covalent copolymers of PLA (A) and PEG (B) can be divided into single-sided grafted defined as grafted or diblock copolymer (A-B) and double-sided grafted denoted as triblock copolymer (A-B-A) or multiblock copolymer (A-B-A)<sub>n</sub>. Many attempts have been made in the past to fabricate NPs using diblock copolymers of either PLA-PEG or PLGA-PEG [3, 6]. Up to now, however, relatively fewer studies have focused on grafted pegylated and multiblock copolymers of PLA and PEG. In this study we are hypothesizing that it is difficult for hydrophilic PEG domains of multiblock copolymer NPs to move freely towards NPs surface as PEG-g-PLA NPs. The major objective of this study was first to optimize NPs formulation using two pegylated polymers of different PEG chain organization, one is grafted, PEG7%-g-PLA and the second is multiblock copolymer of PLA and PEG, (PLA-PEG-PLA)<sub>n</sub>. Second to study the effect of PEG chain organization on the physicochemical properties of the obtained NPs. Poly (lactic acid) (PLA) homopolymer was proposed as the hydrophobic control in our study. Ibuprofen was used as a model lipophilic drug to be encapsulated by PLA and PEG-modified PLA NPs. NPs were formulated using emulsion-solvent evaporation method and poly(vinyl

alcohol) (PVA) was mainly used as an emulsifier to stabilize the emulsion droplets since it aids the formation of relatively small sized particles with uniform size distribution [7].

### **3.4. Material and methods:**

#### **3.4.1. Materials:**

D,L-dilactide, poly(ethylene glycol) methyl ether (MePEG; 2000 Da), poly(ethylene glycol) (PEG, 1500 Da), allyl glycidyl ether, tetraphenyltin, polyvinyl alcohol (PVA, average  $M_w$  9000-10,000 Da, 80% hydrolyzed), succinic acid, 1-ethyl-3-[3-dimethylaminopropyl]-carbodiimide (EDC), 4-dimethylaminopyridine (4-DMAP), pyridine, acetone, chloroform, diethyl ether, and N,N-dimethylformamide were purchased from Aldrich Chemical Company Inc., Milwaukee, USA. Ibuprofen was obtained from Medisca Pharmaceutical Inc., Montreal, Quebec, Canada. Sodium hydroxide pellets were purchased from Anachemia Canada Inc. and dichloromethane (DCM) was purchased from Laboratoire Mat Inc., Montreal, Quebec, Canada.

#### **3.4.2. Synthesis of Polymers.**

The homopolymer poly(D,L)-lactide (PLA) was synthesized by ring-opening polymerization of dilactide in argon atmosphere, using tetraphenyltin as the catalyst. Bulk polymerization was carried at 180 °C for 6 h in a round-bottom flask and purged thoroughly with argon. The obtained polymer was dissolved in acetone and then purified by precipitating in water.

Polymer with poly(ethylene glycol)-grafted randomly on poly(D,L)-lactide at 7% grafting density, PEG7%-g-PLA (PEG;  $M_w$  2000 Da) was synthesized in the laboratory as reported earlier by our group [8]. Multiblock copolymer, (PLA-PEG-PLA) $_n$  was also synthesized as previously reported [9] using PEG with  $M_n$  of 1500 and succinic acid was used as condensing agent to link triblock copolymers. (PLA-PEG-PLA) $_n$  was synthesized to yield a PEG (1500)/lactic acid monomer ratio of 7% (mol/mol).  $^1\text{H}$  NMR spectra were recorded on a Bruker ARX 400 spectrometer (Bruker Biospin, Billerica, MA). Chemical shifts ( $\delta$ ) were measured in parts per million (ppm) using tetramethylsilane (TMS) as an internal reference. Gel permeation chromatography (GPC) was performed on a Water Associate chromatography system (Waters, Milford, MA) equipped with a refractive index detector and a Phenomenex Phenogel 5  $\mu$  column. Polystyrene standards were used for calibration with THF as the mobile phase at a flow rate of 0.6 mL/min.

### **3.4.3. Preparation of nanoparticles (NPs)**

NPs were prepared by an (O/W) emulsion-solvent evaporation method. It should be mentioned that NPs could not be prepared using the multiblock copolymer alone due to its low molecular weight as revealed by GPC data (Table 3.1); hence, a 1:1 mixture of PLA and multiblock copolymer was used for the preparation of NPs. For blank NPs, each polymer or polymer blend in case of multiblock (1 g) was dissolved in 35 mL DCM and emulsified in 100 mL PVA solution (0.5% w/v) as an external aqueous phase using high-pressure homogenizer (Emulsiflex C30, Avestin, Ottawa, Canada) at a pressure of 10,000 psi for 5 min. The emulsion was collected by washing with another 100 mL of 0.5% PVA. The DCM was evaporated under reduced pressure with constant stirring to obtain

the NPs. Finally, NPs obtained as a suspension were then collected by centrifugation at 41.340 g for 1 hr at 4 °C (Sorval® Evolution<sub>RC</sub>, Kendro, USA), washed four times with distilled water, then lyophilized in the presence of 5 % w/v sucrose as a cryoprotectant to obtain dry NPs (Freeze Dry System, Lyph.Lock 4.5, Labconco) and stored at 4 °C until further use. Ibuprofen loaded NPs were prepared in a similar manner to that of blank NPs using initial loading of 10% wt/wt of each polymer. Ibuprofen was first dissolved in the organic phase followed by dissolution of the polymer. The emulsification and purification steps procedure were repeated as before.

#### **3.4.4. Characterization of NPs**

##### **3.4.4.1. Particle size and size distribution**

Size and size distribution of NPs were measured by dynamic light scattering (DLS) with a Malvern Autosizer 4800 instrument (Malvern Instruments, Worcestershire, UK) before and after lyophilization. For all batches, fresh NP suspensions (0.1 mL) or lyophilized NPs (1 mg) were diluted 10 times with Milli-Q Water and size measurements were performed at 25 °C and scattering angle of 90°. The CONTIN program was used to extract size distributions from the autocorrelation functions. Measurements were performed in triplicate.

##### **3.4.4.2. NPs surface morphology and phase image analysis**

Surface morphology and phase imaging of NPs were studied using Nanoscope IIIa Dimension 3100 atomic force microscope (Digital Instruments, Santa Barbara, CA,

USA). Samples were prepared by deposition of particles suspension in Milli-Q Water on freshly cleaved mica followed by air-drying. Topography and phase images of these samples were captured simultaneously using TappingMode™ etched silicon probes (TESP7) with tip radius of 5–10 nm, spring constant of 20–100 N/m and resonance frequency of 200–500 kHz. Cantilever length was 125 μm. A set-point ratio (rsp, ratio of engaged oscillation amplitude to free air oscillation amplitude) between 0.5 and 0.7 (moderate tapping mode) was used for all topographic and phase images unless otherwise stated.

#### **3.4.4.3. Zeta ( $\zeta$ ) potential measurements**

NPs were suspended in 0.22 μm filtered 0.25% (w/v) saline solution and  $\zeta$ -potential was measured on Malvern ZetaSizer Nanoseries ZS (Malvern Instruments, Worcestershire, UK) in triplicate.

#### **3.4.4.4. Encapsulation efficiency (EE)**

A weighed amount of NPs was digested in 1 N NaOH for 1 h. Ibuprofen concentration was measured by spectrophotometry at 264 nm (U-2001 UV/Visible spectrophotometer, Hitachi). Percent encapsulation efficiency (% EE) and % drug loading (% DL) were calculated based on the following equations:

$$\% \text{ EE} = \frac{\text{Amount of drug entrapped in NPs}}{\text{Initial amount of drug added}} \times 100 \quad (1)$$

$$\% \text{ DL} = \frac{\text{Amount of drug entrapped in NPs}}{\text{Total amount of NPs}} \times 100 \quad (2)$$

#### 3.4.4.5. Determination of residual PVA

The amount of PVA remaining in the NPs was determined by a colorimetric method based on the formation of a colored complex between two adjacent hydroxyl groups of PVA and an iodine molecule [7]. First to determine the surface associated PVA, certain weight of NPs was suspended in distilled water followed by vigorous vortexing for 10 min., then fixed volumes of all formulations were withdrawn followed by addition of 5 mL of saturated solution of boric acid and 0.5 mL iodine (0.1 N), and the volume was made up to 10 mL with distilled water. The absorbance of the formed complex was measured at 660 nm against similarly treated blank. Whereas for the total amount of PVA associated with the particles (amount entrapped inside the matrix as well as present on the surface), NPs were digested in 1 N NaOH then neutralized by 1 N HCl followed by stirring for 1 h and the volume was made up to 5 mL with distilled water. To this, 3 mL of saturated solution of boric acid and 0.5 mL iodine (0.1 N) were added, and

the volume was made up to 10 mL with distilled water. The absorbance was measured as above. The amount of PVA was calculated by using the calibration curve of PVA prepared under the same conditions.

#### **3.4.4.6. Differential Scanning Calorimetry (DSC)**

The thermal properties of the pure polymers, physical mixtures of ibuprofen with each polymer, and NPs were characterized by DSC analysis (DSC 30, Mettler TA 4000, Schwerzenbach, Switzerland) with refrigerated cooling. The purge gas was purified nitrogen at a pressure of 20 psi. For pure polymers, weighed samples were sealed in crimped aluminum pans with lids using an empty pan as a reference and were heated at a rate of 10 °C/min from -50 to 200 °C (two runs), while for NPs the samples were heated from -50 to 90 °C (two runs) at the same heating rate.

#### **3.4.4.7. XPS analysis**

Surface chemistry of pure materials, polymers, blank, and drug-loaded NPs was characterized by X-ray photoelectron spectroscopy (VG Scientific ESCALAB MK II) with a monochromatized Mg Ka X-rays (hv 1253.6 eV) and an electron take off angle of 0°. A single survey scan spectrum (0–1000 eV) and narrow scans for C1s (210–305 eV) and O1s (525–550 eV) were recorded for each sample with a pass energy of 1 and 0.5 eV, respectively. Acquisition and data analysis were performed by a VGS 5000 data system. Peak fitting of the C1s envelope was as described by Shakesheff et al [10].

#### **3.4.4.8. <sup>1</sup>H NMR spectroscopy**

A weighed amount of nanoparticles lyophilized in presence of sucrose (50 mg) was suspended in 10 mL distilled water, centrifuged (5000rpm, 10 min). The residues were washed three times with water to remove sucrose (cryoprotectant) that might show any interference during <sup>1</sup>H NMR analysis of NPs. Then, NPs were lyophilized for 24 h. Relyophilized NPs were suspended in deuterium Oxide (D<sub>2</sub>O). <sup>1</sup>H NMR spectra were recorded on the same machine used before for analysis of synthesized polymers.

#### **3.4.4.9. Erosion study**

Erosion (mass loss) studies of (A) PLA, (B) PEG7%-g-PLA, and (C) (PLA-PEG-PLA)<sub>n</sub> NPs were done by suspending 50 mg of NPs for each time interval in 10 mL PBS, pH 7.4 at 37 °C in shaking water bath. The study was terminated at 0, 5, 14, 25, 35 and 45 days. Samples were centrifuged (5000rpm, 10 min) at the end of each time interval. The residues were washed two times with water to remove phosphate buffer and lyophilized for 24 h. The final mass of NPs was determined at each time point.

#### **3.4.4.10. In vitro drug release study**

Loaded formulations prepared using different polymers were tested for in vitro release of ibuprofen in triplicates in phosphate buffered saline (PBS, 10 mM, pH 7.4.). 150 mg NPs were suspended in 3.5 mL PBS in a dialysis tubing (Spectra Por 1 membrane, 6–8 kDa cut-off). This dialysis tubing was placed in a screw-capped tube containing 10 mL PBS. The tubes were shaken at 200 rpm on a horizontal water bath shaker (Orbit Shaker Bath, Labline) maintained at 37±0.5 °C. At predetermined time

intervals, the whole medium in the tube was withdrawn and replaced by fresh PBS to maintain sink conditions. The aliquots were assayed for the concentration of ibuprofen released by spectrophotometry at 262 nm.

### **3.5. Results and discussion:**

#### **3.5.1. Characterization of Polymers.**

$^1\text{H}$  NMR spectroscopy and gel permeation chromatography (GPC) were used to measure the number average ( $M_n$ ) and weight average molecular weights ( $M_w$ ) of the synthesized polymers. The polydispersity was calculated by the ratio of  $M_w$  to  $M_n$  from the GPC data. All the synthesized polymers exhibited uniform molecular weight distribution as revealed by the narrow polydispersity index values (Table 3.1). Unimodal mass distribution ruled out the possibility of the presence of unreacted MePEG or Poly(D,L-lactide) in case of PEG7%-g-PLA. The results are summarized in Table 3.1. Typical  $^1\text{H}$  NMR spectrum was obtained for PLA homopolymer with a characteristic peak at 5.2 ppm corresponding to the tertiary PLA proton (m, -CH), and another peak at 1.5 ppm for the pendant methyl group of the PLA chain (m, -CH<sub>3</sub>). Moreover, the integration ratio of those two characteristic peaks was 3:1 that is also a characteristic feature for the protons of PLA homopolymer (data not shown).  $^1\text{H}$  NMR spectra and chemical structures of PEG7%-g-PLA, and (PLA-PEG-PLA)<sub>n</sub> polymers are shown in Figure 3.1. Also typical spectrum for PEG7%-g-PLA was obtained with a peak at 5.2 ppm corresponding to the tertiary PLA proton (m, -CH), a peak at 3.6 ppm for the protons of the repeating units in the PEG chain (m, OCH<sub>2</sub>-CH<sub>2</sub>O), a peak at 4.3 ppm for

the PEG connecting unit to the PLA block (m, CH<sub>2</sub>-OCO), and a peak at 1.5 ppm for the pendant methyl group of the PLA chain (m, -CH<sub>3</sub>). While, for the multiblock copolymer, an additional peak could be seen at around 2.7 ppm corresponding to the protons of the succinic acid group (m, CH<sub>2</sub>-COO) used to link the triblock chains during multiblock synthesis. The actual PEG insertion ratio of PEG7%-g-PLA, and (PLA-PEG-PLA)<sub>n</sub> was calculated by comparing the peak intensity ratios of PEG (3.6 ppm) to that of PLA (5.2 ppm). The final PEG insertion ratio in both polymers was close to the initial feed ratio as shown in Table 3.1.

### 3.5.2. Particle size and size distribution

Particle size distribution by dynamic light scattering (DLS) showed unimodal distribution for freshly prepared as well as lyophilized NPs. Freshly prepared (PLA-PEG-PLA)<sub>n</sub> NPs either blank or loaded showed larger hydrodynamic diameter (~ 200 nm) than PEG7%-g-PLA NPs (~ 132 nm) as shown in Table 3.2. The last finding could be attributed to the difference in PEG chain organization during NPs formation between both formulations. In PEG7%-g-PLA, PEG chains are expected to be more mobile creating a steric barrier around PLA core preventing particle aggregation. While, for multiblock copolymer, the polymer architecture allows some PEG chains to be embedded inside PLA core leaving some uncovered areas at the surface that might showed some aggregating tendency due to hydrophobic interactions. Moreover, the higher PEG content of multiblock copolymer (8.9 %, Table 3.1) might favor the swelling of NPs in aqueous media to a much degree than PEG7%-g-PLA NPs which contains lower PEG ratio (4.1 %, Table 3.1).

**Table 3.1.** Polymers characterization by  $^1\text{H}$  NMR, DSC, and Gel Permeation Chromatography (GPC).

Polymer	Mn <sup>a</sup>	Mw <sup>a</sup>	Mw/Mn <sup>a</sup>	PEG insertion (mol%) <sup>b</sup>	Mn ( $^1\text{H}$ NMR) <sup>b</sup>	Tg <sup>c</sup>
PLA	40318	56171	1.4	N/A	N/A	46.4 °C
PEG7%-g-PLA	3752	8392	2.2	4.1 %	8336	53 °C
(PLA-PEG-PLA) <sub>n</sub>	3508	3982	1.2	8.9 %	3780	39 °C

N/A: not analyzed.

<sup>a</sup> Determined by GPC analysis using narrow molecular weight polystyrene standards.

<sup>a</sup> Mw/Mn = Polydispersity index of the polymers (PDI).

<sup>b</sup> Calculated from peak intensity ratios of PEG (3.6 ppm) and PLA (5.2 ppm) by  $^1\text{H}$  NMR.

<sup>c</sup> Calculated from the second run of DSC as half of the extrapolated tangents in case of PLA and (PLA-PEG-PLA)<sub>n</sub> or as an endothermic peak in case of PEG7%-g-PLA .

Blank formulations showed nearly similar particle size to that of loaded ones for all NPs types in the range of 135–200 nm (Table 3.2). Thus, drug loading level had no apparent effect on particle size, suggesting that the size was largely controlled by the emulsification process during NPs preparation. Also, it could be noticed that the size of most lyophilized NPs after resuspension into Milli-Q Water was smaller with narrow polydispersity compared to the freshly prepared NPs suspension. The possible reason behind that is the tendency of freshly prepared PLA particles particularly pegylated ones to uptake water, allowing more swelling of the NPs matrix [11, 12], further increasing the size of the particles. While, after lyophilization, the size of the particles was reduced due to shrinkage of the swollen cores after removal of entrapped water by sublimation. The

narrow polydispersity values indicate the ability of the used cryoprotectant used (sucrose) to prevent particle aggregation. It was previously reported that cryoprotectants could efficiently prevent NPs aggregation and protect them against the mechanical stress of ice crystals due to the immobilization of nanoparticles within their glassy matrices [13]. Particle size distribution data by DLS were also supplemented with a visual method like tapping mode AFM as will be revealed in the next section.

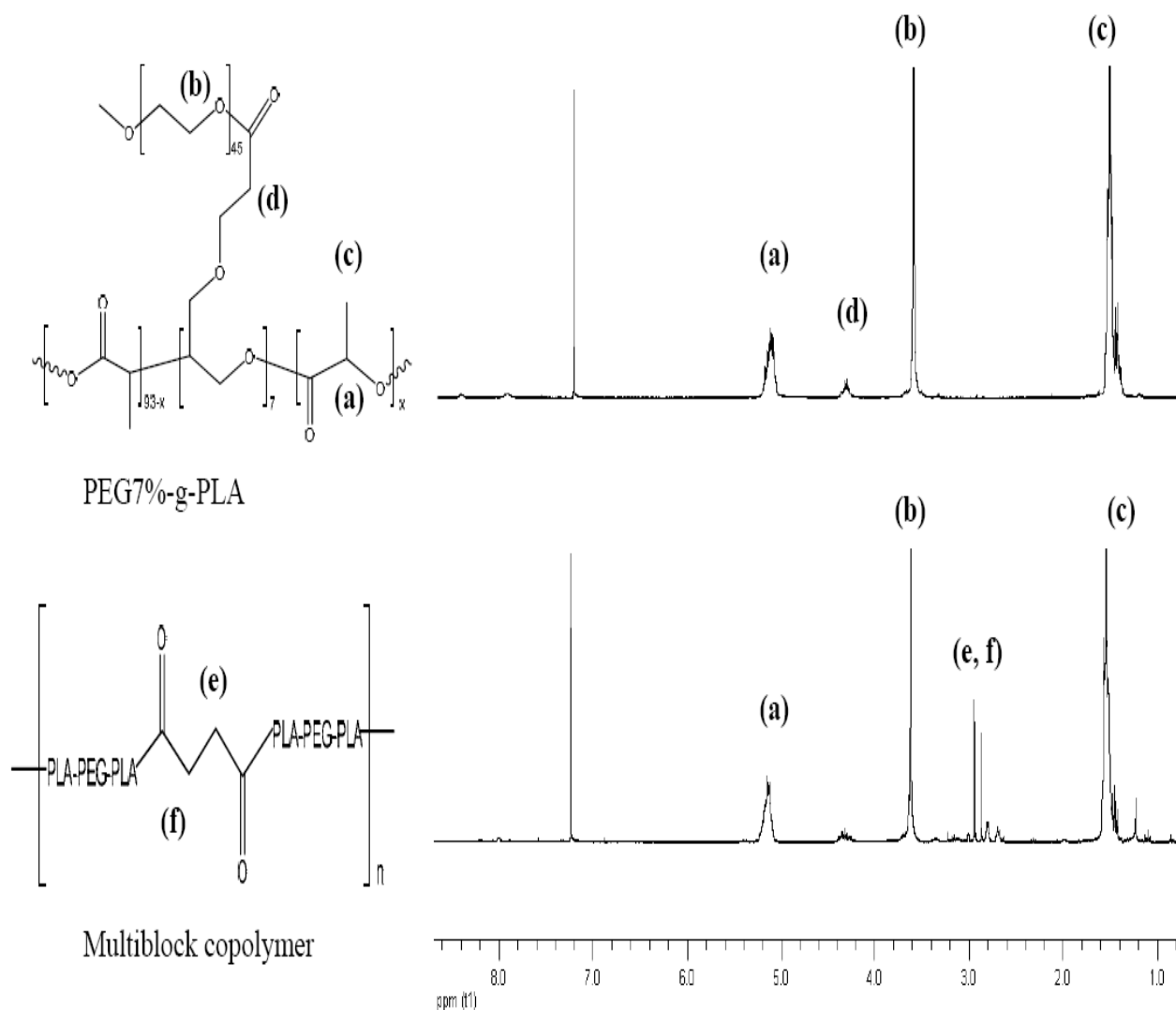


**Figure 3.1.**  $^1\text{H}$  NMR spectra and chemical structures of PEG7%-g-PLA, and multiblock copolymer, (PLA-PEG-PLA) $_n$ .

### 3.5.3. Surface morphology and phase analysis

Tapping mode atomic force microscopy (TM-AFM) is a versatile technique, which allows probing soft samples such as biological and polymeric materials [14, 15]. TM-AFM surface analysis revealed that all lyophilized NPs were nearly spherical with smooth surface and displayed less aggregating tendency with a size range 100- 200 nm (Fig. 3.2, left panels, T) confirming the size data obtained by DLS. Phase image analysis using the same (TM-AFM) was done on NP samples to visually examine PEG chains at the surface of pegylated NPs. Phase imaging is based on the use of changes in the phase angle of cantilever probe. This image shows more contrast than the topographic one as well as more sensitivity to material surface properties such as stiffness, viscoelasticity, and chemical composition [14, 16, 17]. Figure 3.2 shows TM-AFM topography (left panel, T) and their corresponding phase images (right panel, P) of PLA, PEG7%-g-PLA, and multiblock copolymer, respectively acquired at moderate tapping force. It can be seen that PLA particles had nearly homogenous surface without any clear phase separation [Fig. 3.2(a); right panel, P]. Therefore, no contrast was observed in phase images of PLA NPs. On the other hand, both pegylated NPs showed the presence of an observable phase contrast at the surface of NPs that varies in degree from grafted to multiblock [Fig. 3.2(b, and c); right panels, P]. This might be due mechanical differences between PLA and PEG that result in such phase contrast. PEG molecule is expected to be softer than PLA since PEG molecules of lower  $M_w$  2000 or 1500 (used in our study) have smaller Young's modulus than PLA [18]. Thus, it was expected that PEG molecule will appear as darker regions in the phase images due to negative phase shift. This has already been shown before for poly(styrene-b-ethylene oxide) polymer films, where softer PEG

segments appeared as darker regions embedded in lighter polystyrene domain [19]. In the case of PEG7%-g-PLA, highly intense dark coat surrounds the surface of brighter core could be seen indicating the existence of hydrophilic PEG chains around hydrophobic PLA chains that represents the core. The immiscibility of these two blocks should result in separation of both components during NPs formation. Thus, grafted copolymer NPs will be predominantly consisting of hydrophobic PLA cores surrounded by hydrophilic PEG chains on the surface (Figure 3.2 b, phase image, P). In the case of the (PLA-PEG-PLA)<sub>n</sub> multiblock copolymer, few dark regions are found at the surface of NPs without complete coverage of the surface as seen with grafted polymer. This might be due to the peculiar architecture of the polymer itself that mainly consist of PEG chain covalently linked with two PLA chains. This might affect mobility of PEG chains towards the aqueous phase of the O/W emulsion during NPs formation. It was shown before in a previous study that multiblock copolymers of PLA and PEG exhibited enhanced miscibility of the two blocks compared to grafted copolymers [20].

#### **3.5.4. Encapsulation efficiency (EE)**

As seen from Table 3.2, % EE of ibuprofen was found to be 25.3 % and 79.7 % for multiblock and PEG7%-g-PLA NPs, respectively. PEG7%-g-PLA showed better % EE than multiblock copolymers. The last finding could be attributed to the enhanced steric hindrance of the more mobile PEG chains at NPs surface in the case of the grafted copolymers, thus reducing premature diffusion of ibuprofen into the external aqueous phase during solidification of the NPs. This was confirmed before by AFM phase

imaging where PEG chains were found to completely cover the entire NPs surface. The higher encapsulation efficiency obtained with PEG7%-g-PLA may have significant implications on the feasibility of development of PLA-PEG nanoparticulate formulations optimized with regard to both the longer circulation behavior and the drug loading properties by judicious selection of both the composition and the suitable architecture of the nanoparticles. Thus, the obtained data suggest that it is possible to prepare nanoparticles with low PEG content, which would generate favorable conditions for the entrapment of a hydrophobic drug, without compromising the prolonged blood circulation properties of the nanoparticles.

### 3.5.5. Zeta ( $\zeta$ ) potential measurements

Although zeta potential measurements didn't show big differences between different formulations but two findings worthy of note were observed in Table 3.2 : 1) PLA showed low zeta potential (close to zero) values than expected, -3.5 mV. This lower  $\zeta$ -potential for NPs could be attributed to the effective adsorption of PVA on the surface of NPs as will be seen in the next section which could mask the surface charge of PLA. Zambaux et al. also obtained a low zeta potential value of -4 mV for PLA NPs prepared with PVA as an emulsifier [21]. 2) Pegylated polymers either grafted or block had also low zeta potential values for both blank and loaded NPs as shown in Table 3.2. This could be attributed to the shielding action of PEG on the surface charge even if most of PEG chains were found embedded into the NPs matrix as in case of multiblock copolymer. Since some of the PEG chains would be present at the surface, the copolymer might also keep its stealth behavior. Similar results to ours were reported earlier by other

authors [9, 22, 23]. Moreover, the greater reduction in zeta potential values of pegylated NPs compared to other PEG-PLA NPs reported in the last cited references could be explained by the existence of a fraction of PVA at the surface of NPs which played also a role in masking their actual surface charge (Table 3.2). It also should be mentioned that zeta potential measurements were done again in 0.5 mM NaCl solution in order to clearly find significant differences between different NPs formulations. However, nearly similar zeta potential values to the ones observed with 0.25 % w/v NaCl were obtained (data not shown).

### **3.5.6. Residual PVA**

It is widely reported that although the several washing steps of nanoparticles, yet some residual surfactant remains in the suspension and becomes adsorbed onto surface of freeze dried nanoparticles and this might lead to alteration of their physicochemical properties such as particle size, hydrophilicity, release kinetics, cellular uptake, etc. [7]. So, one of our goals was to evaluate the amount of PVA remained attached to the nanoparticles and whether they are affected by different PEG chain organization of the polymer or not. It was observed that a variable amount of PVA remained in all the formulations even after 4 washings (Table 3.2). An attempt was made to evaluate whether PVA was present either inside the polymeric matrix or on the surface of the particles. Nearly the same amount of PVA was present in the given NPs formulations by both assays confirming that the amount of PVA was mainly associated with the surface of the particles (data not shown). It was found that the highest amount of PVA remained attached to NPs matrix was 6.7 % wt/wt for PLA NPs (Table 3.2). This might be

attributed to the enhanced hydrophobic interaction between acetate group of PVA and the hydrophobic PLA matrix as reported before by other authors [7, 24]. This result is in accordance with other previous studies by other authors. Sahoo et al.[7] have determined 6.15% wt/wt PVA remaining associated within PLGA NPs matrix when they used 5% PVA solution as external aqueous phase. Another study done by Zambaux et al. showed also that 5–6% wt/wt PVA remained attached within PLA NPs after 3 washings when 1% PVA was used as an external aqueous phase [21]. For all the other pegylated polymers either graft or block, they exhibited less adsorption of PVA than PLA NPs as shown in Table 3.2. This might be due to the PEG content which offered a certain degree of hydrophilicity to the NPs matrix so a less favored interaction with PVA should be expected. Similar results were obtained before where the amount of adsorbed PVA decreased with increased PEG content within the NPs matrix [10]. Multiblock copolymer NPs showed less PVA adsorption ~ 0.5 % compared to PEG7%-g-PLA which showed ~ 3.5 % wt/wt. The reason behind that is the possibility of a chemical interaction between PVA-OH and PLA-COOH and this interaction might be less favored in case of multiblock copolymer NPs as will be revealed by XPS data. Also, blank NPs showed similar amount of PVA adsorbed on their surfaces as loaded NPs indicating that drug loading had no apparent effect on the amount or the orientation of PVA within the NPs matrix.

### **3.5.7. DSC**

DSC was used to detect the effect of molecular structure of the used polymer on the thermal properties of NPs. Moreover, DSC was also used for detecting the state of the

encapsulated drug inside the NPs matrix as well as investigating any possible interaction between the drug and the polymeric matrix. PLA showed glass transition ( $T_g$ ) at 46.4 °C (Table 3.1). Grafting PEG on the PLA backbone resulted in an increased  $T_g$  value (by about 7 °C) due to enhanced chain rigidity (Table 3.1 and Fig. 3.3.a).

**Table 3.2.** Characteristics of different NPs formulation.

<i>Formulation</i>	<i>Size before freeze drying (nm)</i> <small>a, d</small>	<i>PI</i> <sup>b</sup>	<i>Size after freeze drying (nm)</i> <sup>a, d</sup>	<i>PI</i> <sup>b</sup>	<i>Actual loading (% wt/wt)</i> <sup>d</sup>	<i>% EE</i> <sup>c, d</sup>	<i>Zeta potential (mV)</i> <sup>a, d</sup>	<i>Surface associated PVA (%wt/wt)</i> <sup>d</sup>
PLA BK <sup>e</sup>	184±20.8	0.13	161±18.4	0.01	N/A	N/A	-3.5 ±3.1	6.76±0.40
PLA LD <sup>f</sup>	194±30.0	0.08	162±22.3	0.09	4.5±0.22	45±2.24	-0.18 ± 3.2	6.80±0.20
PEG7%-g-PLA BK <sup>e</sup>	132±28.0	0.16	166±30.5	0.01	N/A	N/A	-2.2 ± 3.0	3.57±0.60
PEG7%-g-PLA LD <sup>f</sup>	145±34.0	0.07	137±82.1	0.04	7.9±0.04	79.7±0.56	-0.2 ± 3.1	3.79±0.50
(PLA-PEG-PLA)n BK <sup>e</sup>	202±21.2	0.01	168±42.1	0.01	N/A	N/A	-1.0± 3.5	0.40±0.50
(PLA-PEG-PLA)n LD <sup>f</sup>	199±19.8	0.10	158±31.9	0.02	2.5±0.12	25.3±1.20	-0.24 ± 3.2	0.70±0.60

N/A: not analyzed.

<sup>a</sup> median

<sup>b</sup> refers to polydispersity index.

<sup>c</sup> refers to encapsulation efficiency.

<sup>d</sup> All values indicate mean±S.D. for n=3 independent measurements for the same particle preparation.

<sup>e</sup> Blank NPS

<sup>f</sup> Loaded NPS

N.B: (PLA-PEG-PLA)n consists of 1:1 mixture of PLA: (PLA-PEG-PLA)n.

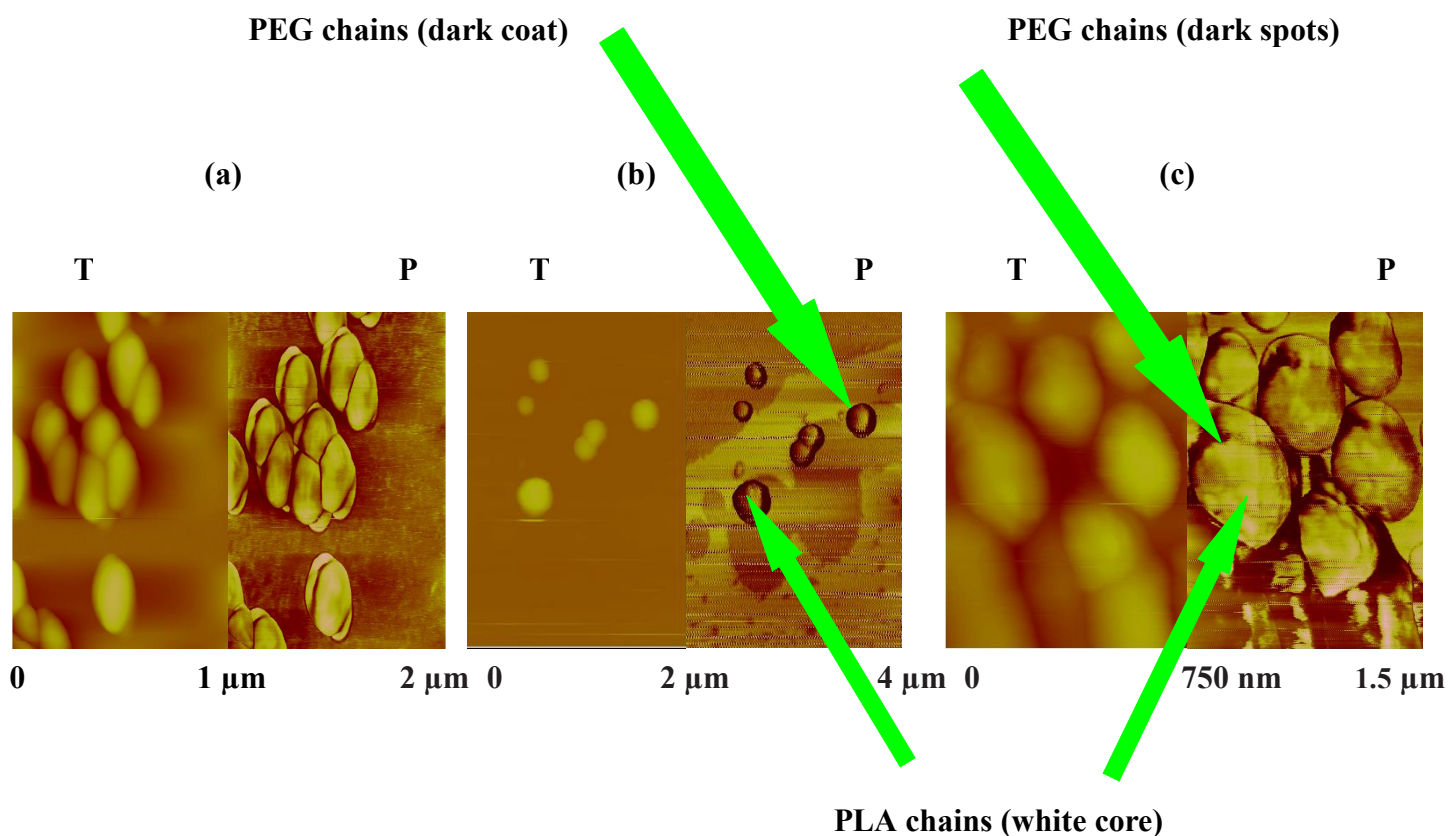


**Figure 3.2.** Tapping mode AFM images of NPs, left panel shows topography (T) and right panel shows corresponding phase images (P); all images are acquired in air. PLA (a) [Scan size: 1 μm × 1 μm], PEG7%-g-PLA (b) [Scan size: 2 μm × 2 μm], and (PLA-PEG-PLA)<sub>n</sub> (c) [Scan size: 750 nm × 750 nm].

Similar findings were previously reported for hyperbranched polymers and dendrimers over their linear chain analogues [25]. However, multiblock copolymer showed lower  $T_g$  values at 39 °C, compared to grafted polymer (Table 3.1 and Figure 3.3.b). This might be attributed to their actual higher PEG content 8.9 mol % and/or low molecular weight as compared to the grafted polymers (Table 3.1). Also, this might indicate the presence of some PEG chains inside the core of PLA. The high PEG content embedded inside PLA chains might enhance the chain mobility of PLA due to its plasticization effect on PLA chains resulting in a lower  $T_g$ , as reported earlier [26, 27]. Thus, the effect of branching

was predominant for PEG grafting over PLA backbone, whereas the possibility of PEG chains entrapment inside PLA domains might lead to a predominant plasticizer effect. Ibuprofen showed an endothermic peak at 78 °C corresponding to the melting of ibuprofen crystals (Fig. 3.3.a, and b). As shown in Fig. 3.3.a, DSC curve of PEG7%-g-PLA/ibuprofen physical mixture showed an endothermic peak corresponding to the glass transition ( $T_g$ ) at ~ 52 °C. The melting endotherm of ibuprofen crystals could also be detected at 74 °C. The drug melting peak was shifted by 4 °C lower with some broadening of the peak, indicating the possibility of a weak interaction between the drug and the polymer. After encapsulation of ibuprofen into the NPs,  $T_g$  was found to be ~ 20 °C, which might be due to process formulation parameters. Surprisingly, the melting endotherm of the drug was clearly observed with also some broadening of its melting peak (Fig. 3.3.a). This phenomenon has been related recently to the size of the nanocrystals obtained after the process of encapsulation [28]. For more verification of the final state of ibuprofen inside NPs, x-ray diffraction analysis (XRD) was carried out for ibuprofen loaded NPs and compared to both pure ibuprofen crystals and physical mixture of the polymer with the drug having the same ratio as in NPs. Ibuprofen loaded NPs showed the presence of crystalline ibuprofen but with slight reduction in the intensity of its diffraction peaks (Figure 3.S in the supporting information). XRD data confirmed DSC findings. Similar observations were also noticed with (PLA-PEG-PLA)<sub>n</sub>, in both physical mixtures and NPs with the consideration of different  $T_g$  for multiblock copolymer ~ 39 °C (Fig.3.3.b). Similar finding to ours was obtained when lidocaine embedded into PEG-PLGA nanospheres. Lidocaine exhibited an endothermic peak at

lower temperature or broadened melting peak compared to lidocaine alone. The authors also suggested that there is an interaction between lidocaine and the polymeric carrier [2].

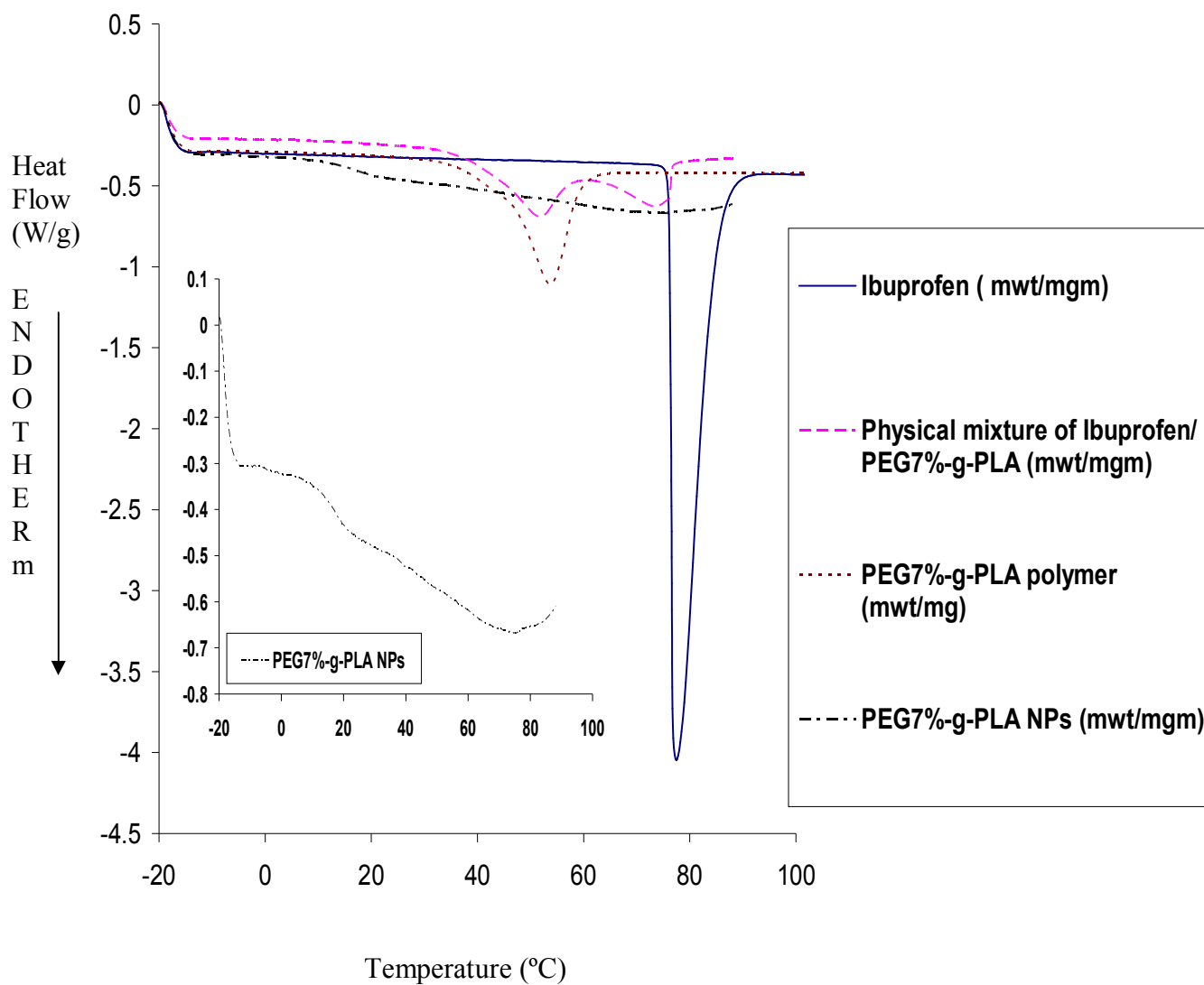


**Figure 3.3.a.** DSC curves of ibuprofen, physical mixture of PEG7%-g-PLA with ibuprofen, PEG7%-g-PLA polymer, and ibuprofen loaded NPs. Inset inside the figure shows clear thermogram for NPs.

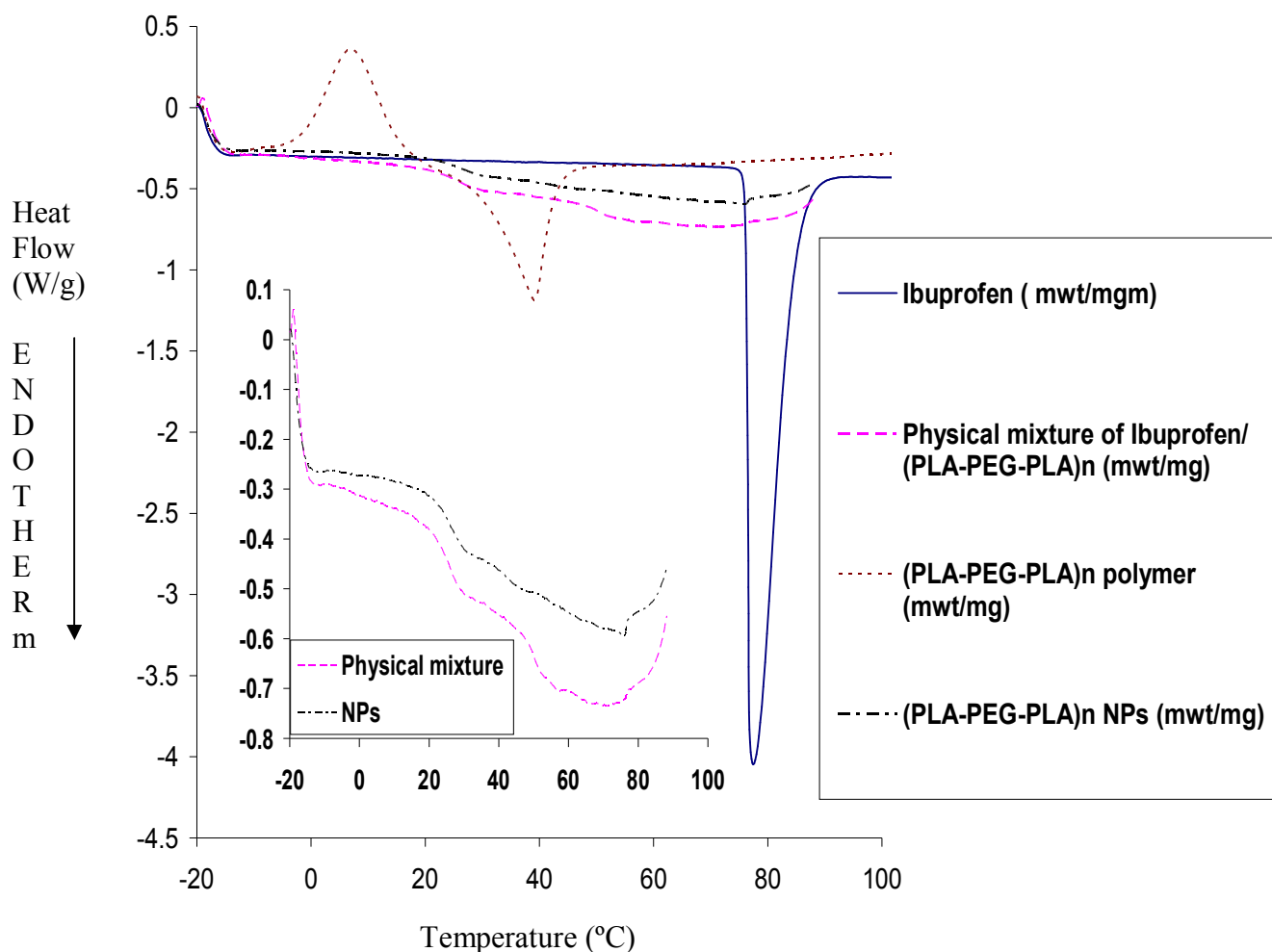


**Figure 3.3.b.** DSC curves of ibuprofen, physical mixture of (PLA-PEG-PLA)<sub>n</sub> with ibuprofen, (PLA-PEG-PLA)<sub>n</sub> polymer, and ibuprofen loaded NPs. Inset inside the figure shows clear thermograms for both physical mixtures and NPs.

### 3.5.8. XPS analysis

XPS analysis was done to investigate the surface chemistry of NPs prepared from different polymers and to detect any possible interaction between PLA and PVA on their surface. XPS spectrum of PEG showed one characteristic peak corresponding to ether carbons (286.5 eV, Table 3.3). PVA polymer showed three main characteristic peaks

corresponding to C-C/C-H (285 eV), C-OH (286.7 eV) and O-C=O (289 eV) components (Table 3.3). For synthesized PLA homopolymer, the best envelop fit was obtained using three main peaks corresponding to C-C/C-H (285 eV), C-OH (287 eV) and O-C=O (289 eV) (Table 3.3). Similar results were obtained before with Shakesheff et al.[10]. Ibuprofen could not be experimentally analyzed since it was found to sublime under the high vacuum of the equipment. Based on theoretical estimation, ibuprofen has two main characteristic peaks corresponding to C-C/C-H (285 eV), and O-C=O (289 eV) components (Table 3.3).

**Table 3.3.** Relative atomic percentages calculated from XPS Surface Analysis of pure materials used in NPs formulation.

<b>Binding Energy (functional component)</b>	<b>Atomic Percentage (%)</b>			
	<b>Ibuprofen</b>	<b>PLA</b>	<b>PVA</b>	<b>PEG</b>
<b>285 (C-C)</b>	<b>92.4</b>	<b>22.3</b>	<b>37.1</b>	-
<b>286.5 (C-O)</b>	-	-	-	<b>100</b>
<b>286.7 (C-O)</b>	-	-	<b>23</b>	-
<b>287 (C-O)</b>	-	<b>28.9</b>	-	-
<b>289 (O-C=O)</b>	<b>7.6</b>	<b>13.9</b>	<b>4.3</b>	-

N.B: Relative percentage of each functional component is calculated from the area under the curve from their respective peaks in XPS analysis.

It should be mentioned that for ibuprofen to be detected at the surface of loaded NPs, an increase in atomic percentages of both its characteristic peaks mainly C-C/C-H (285 eV) is expected to be found. Both ibuprofen loaded and blank NPs of **PEG7%-g-PLA** grafted

polymer as well as the polymer itself showed the existence of PEG chains on the surface as seen by the presence of a characteristic peak corresponding to ether carbons (286.5 eV, Table 3.4). However, the atomic % of PEG decreases from the polymer (16.9 %) to blank (11.8%) then to loaded NPs (8%) as shown in Table 3.4. This might be due to adsorption of PVA in case of blank NPs. While in loaded NPs, both PVA and ibuprofen might be adsorbed at the surface of NPs as evidenced from the increase in atomic % of C-C (285 eV) in case of loaded NPs (18.6%) compared to blank NPs (13.1%) [Table 3.4]. Such an adsorption might decrease the PEG content at the surface. Also, it could be seen from Table 3.4 that the atomic % of C-C (285 eV) decreases from the polymer (18%) to blank (13.1%) and then increased again in case of loaded NPs (18.6%). This order might be due to chain organization during NPs formation by O/W emulsion method in such a way that PLA chains (rich in C-C) will be collapsed inside the oil droplets (internal phase) while PEG chains will be facing the external aqueous phase. Oil droplets tend to form the internal NPs core upon organic solvent removal and particle precipitation. This process will lower PLA chains and hence, C-C content at the NPs surface. This C-C content lowering was compensated by drug adsorption (also rich in C-C component as shown in Table 3.3) at the surface in case of loaded NPs as stated before. Moreover, to get the best envelop fit of both NPs, two additional peaks had to be added corresponding to C-O-C=O (287.6 eV) and \*C-O-C=O (286.2 eV) components (Table 3.4). These new peaks obtained in both types of NPs could be the result of chemical interaction between PLA-COOH end and PVA-OH during NP formation. The last finding also supports the effective masking of negative charge of these NPs by both PEG and PVA chains at the surface of such NPs as shown in Table 3.2. The increase in atomic % of O-C=O (289 eV)

from the polymer (5%) to both blank and loaded NPs (7.1% and 6.9%, respectively) might be due to PVA (partially hydrolyzed) and ibuprofen (weak acid) adsorption at the surface of blank and loaded NPs types, respectively. This O-C=O (289 eV) component was also detected in the XPS spectrum of the polymer itself due to the presence of COOH functional group in the polymer structure (Fig.3.1). On the other hand, both drug loaded and blank NPs of **(PLA-PEG-PLA)<sub>n</sub>** polymer as well as the polymer itself showed also the existence of PEG chains on the surface as evidenced from the presence of the same characteristic peak corresponding to ether carbons of PEG (286.5 eV, Table 3.4). However, the atomic % of PEG was markedly decreased upon NPs formation compared to grafted polymer. PEG atomic % detected in the polymer was (31.2%) compared to blank (13%) and loaded NPs (11.6%). Taking into account that minimal amount of PVA was detected at the surface of multiblock NPs (~ 0.5% wt/wt, Table 3.2), so the last finding indicates that only a small fraction of the total PEG content of the multiblock copolymer exists at the surface of NPs while the remaining PEG chains might be entrapped inside NPs core. This could be also due to chain organization during NPs formation by O/W emulsion method in such a way that showed the difficulty of PEG chains migration towards the surface of NPs. In fact the peculiar architecture of the multiblock copolymer (PLA-PEG-PLA)<sub>n</sub> shows that PEG chains are covalently linked between two neighboring PLA chains. That is why PEG chains are not easy to orientate towards the surface of NPs facing the aqueous phase and most of them is orientated or stretched more towards the core. AFM phase images of multiblock copolymer showed the existence of few PEG chains at the surface of NPs compared to grafted polymer confirming XPS findings (Fig.3.2). Moreover, no additional peaks were needed to

complete the fit indicating the absence of PLA interaction with PVA in multiblock copolymer NPs. This might be due to the lower number of free COOH end components available for reaction with PVA-OH components in multiblock copolymer NPs in contrast to grafted polymers. Since multiblock copolymer has been synthesized by the condensation of triblock copolymer, the number of available COOH components was expected to be low. The last hypothesis was supported by the lower atomic % of O-C=O (289 eV) component at the surface of the polymer (2.1 %), blank (2.3 %), and loaded NPs (3.2 %), respectively. The atomic % of C-C (285 eV) was detected in the XPS spectrum of blank NPs in a similar value to that of the polymer (19%) due to presence of some PLA chains (rich in C-C) at the NPs surface since PEG doesn't cover the NPs surface completely. While, the increase in atomic % of C-C components (285 eV) in case of loaded NPs (21.8%) confirms the possibility of drug existence at the surface of NPs.

### 3.5.9. <sup>1</sup>H-NMR of NPs in D<sub>2</sub>O

<sup>1</sup>H-NMR analysis was done on NPs in attempt to investigate the core-corona structure of pegylated NPs. <sup>1</sup>H-NMR spectra of all pegylated NPs in D<sub>2</sub>O showed presence of methylene protons of PEG chains at 3.6 ppm (Fig.3.4). Signals from PLA methyl or methylene protons were absent or diminished in intensity. This might indicate that PLA protons are in solid environment and can't be detected whereas PEG chains must be in mobile state. <sup>1</sup>H-NMR analysis for PLA-PEG diblock NPs confirmed their core-corona structure [29]. Similar finding was obtained for NPs made from comb polyesters of PVA-g-PLGA in water showing reduced signal intensity of the more hydrophobic PLGA chains compared to hydroxyl terminated end groups of PVA [30].

**Table 3.4.** Relative atomic percentages calculated from XPS Surface Analysis of synthesized polymers and formulated NPs using those polymers.

B.E. (functional component)	Atomic percentage (%)					
	PEG7%- g-PLA BK NPs	PEG7%- g-PLA LD NPs	PEG7%- g-PLA polymer	(PLA- PEG- PLA)n BK NPs	(PLA- PEG- PLA)n LD NPs	(PLA- PEG- PLA)n polymer
285 (C-C)	13.1	18.6	18	19	21.8	19.2
286.2 (*C-O-C=O)	10.1	10.4	-	-	-	-
286.5 (C-O)	11.8	8	16.9	13	11.6	31.2
287.6 (C-O-*C=O)	7.1	6.9	-	-	-	-
289 (O-C=O)	7.1	6.9	5	2.3	3.2	2.1

(B.E.) refers to the binding energy  
 (BK) refers to blank NPs  
 (LD) refers to loaded NPs

Our results are in accordance with the above-cited reference suggesting NPs made of PLA core and PEG corona. Thus, <sup>1</sup>H-NMR analysis of NPs might indicate that hydrophilic polymer parts (PEG) are oriented towards the outer phase (water) during precipitation and NP hardening whereas the more lipophilic polyester PLA residues form the inner core. However, these studies are not quantitative to comment whereas all the PEG chains constitute the corona and to determine the amount of PEG exactly at the surface for both grafted and block pegylated NPs.

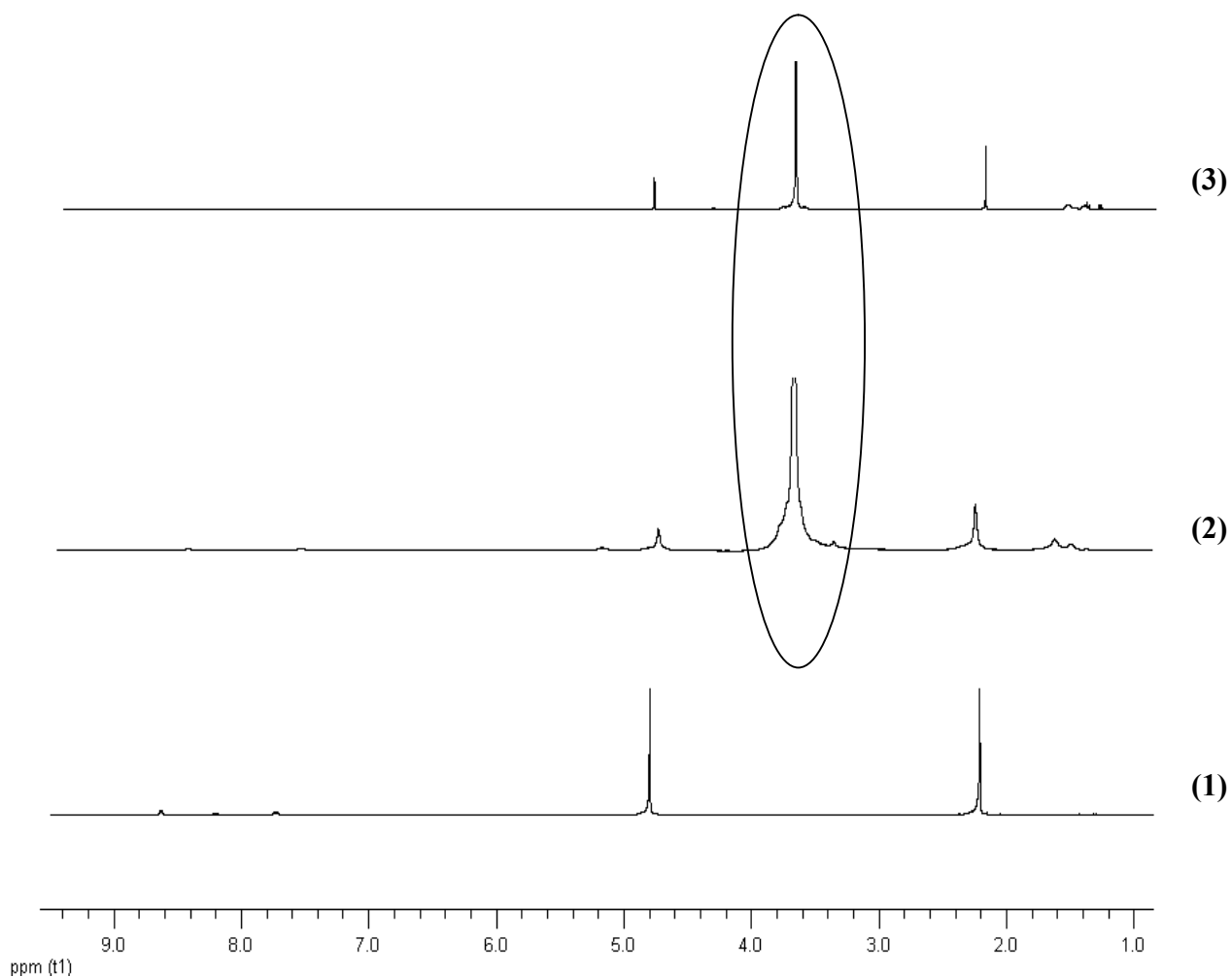


**Figure 3.4.** <sup>1</sup>H-NMR of blank NPs of PLA (1), PEG7%-g-PLA (2), and (PLA-PEG-PLA)<sub>n</sub> (3) in D<sub>2</sub>O. PEG peaks at 3.6 ppm are encircled.

### 3.5.10. Erosion study

This study was conducted to investigate the effect of PEG chain organization on the degradation rate of PLA based NPs under conditions similar to physiological ones. Mass loss of copolymer in phosphate buffer started after 5 days for all the investigated NPs. Pegylated NPs showed faster degradation rates (30 %, and 44 % for PEG7%-g-

PLA, and (PLA-PEG-PLA)<sub>n</sub>, respectively) compared to PLA NPs which showed slower degradation rates around 12% after 25 days. This pattern is shown in Figure 3.5. Ester hydrolysis and transesterification mechanisms are both responsible for mass loss of polyester copolymers [31]. NPs erosion was initiated by water uptake followed by random hydrolytic chain scission of PLA block with release of lactide oligomers. So it might be expected that the more hydrophilic polymer initially swells to a much greater degree than other polymers of lower hydrophilic content, allowing more water uptake into the matrix, further increasing the rate of hydrolysis and breakdown of NPs [11, 32]. Cleavage of the ester bonds between the PLA-PEG backbone leads to free PEG units that will be formed and diffuse out of the matrix. With the loss of PEG from the backbone, degradation of the matrix is dominated by PLA with an increase of the internal matrix-surface in contact with water leading to higher degradation rates than that of homopolymer [33]. The faster degradation rate of (PLA-PEG-PLA)<sub>n</sub> NPs (44%) compared to PEG7%-g-PLA (30%) after 25 days emphasizes the rapid core (PLA) wetting in the multiblock copolymer NPs. This might be due to entrapment of most of PEG chains into the NPs core while in case of grafted PEG7%-g-PLA polymer, most of PEG was found to be at the surface of NPs as shown before by AFM phase imaging and XPS studies.

### **3.5.11. In Vitro Drug Release.**

In order to study the effect of PEG chain organization on drug release profiles from different PLA NPs, ibuprofen loaded NPs were compared for their in vitro release behavior as shown in Fig. 3.6. It could be seen that all formulations exhibited biphasic

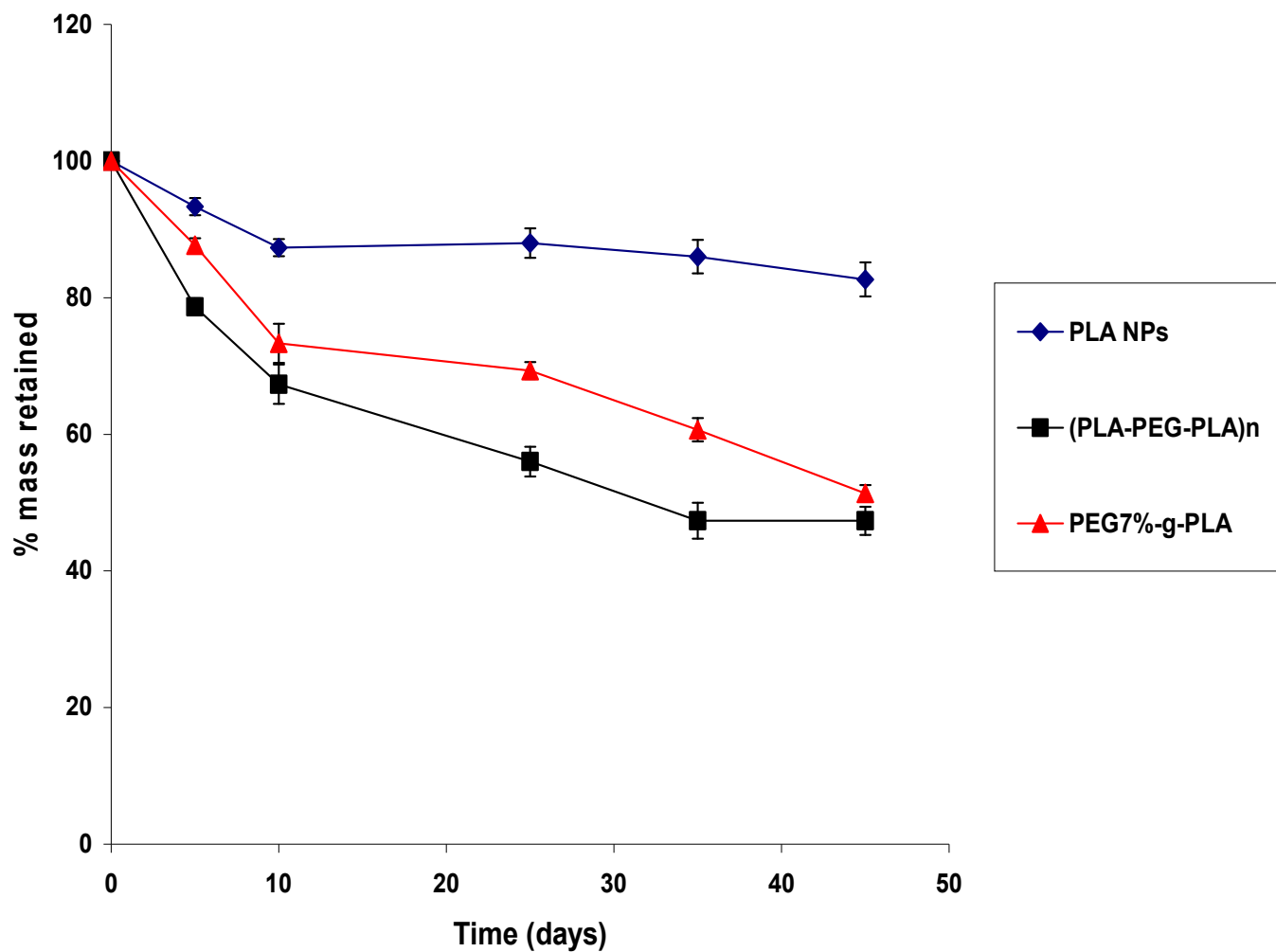


**Figure 3.5.** Erosion of different ibuprofen loaded NPs in phosphate buffer saline (PBS, pH 7.4) at 37 °C.

release phenomenon. After 8 h of NPs immersion into the release medium, a rapid initial burst of ibuprofen varied from 20 % to 53 % of the drug content was clearly observed in all batches. This finding might be due to the desorption of the drug particles adsorbed at or close to the surface of NPs [34] followed by sustained release of the drug over 300 h. This second sustained release phase would mainly depend on both drug diffusion and the

matrix erosion that was a slower process [35, 36]. In such case, the effects of porosity of the nanoparticles on the release property should be verified. As mentioned above in experimental section, that we used 5% w/v sucrose as cryoprotectant to prevent NPs aggregation during lyophilization. Such higher concentration was found to have pore blocking action particularly surface pores, an effect caused by the precipitation of cryoprotectant on nanoparticle surface [37]. So, we expected that NPs porosity might have a minor effect on ibuprofen release from NPs.

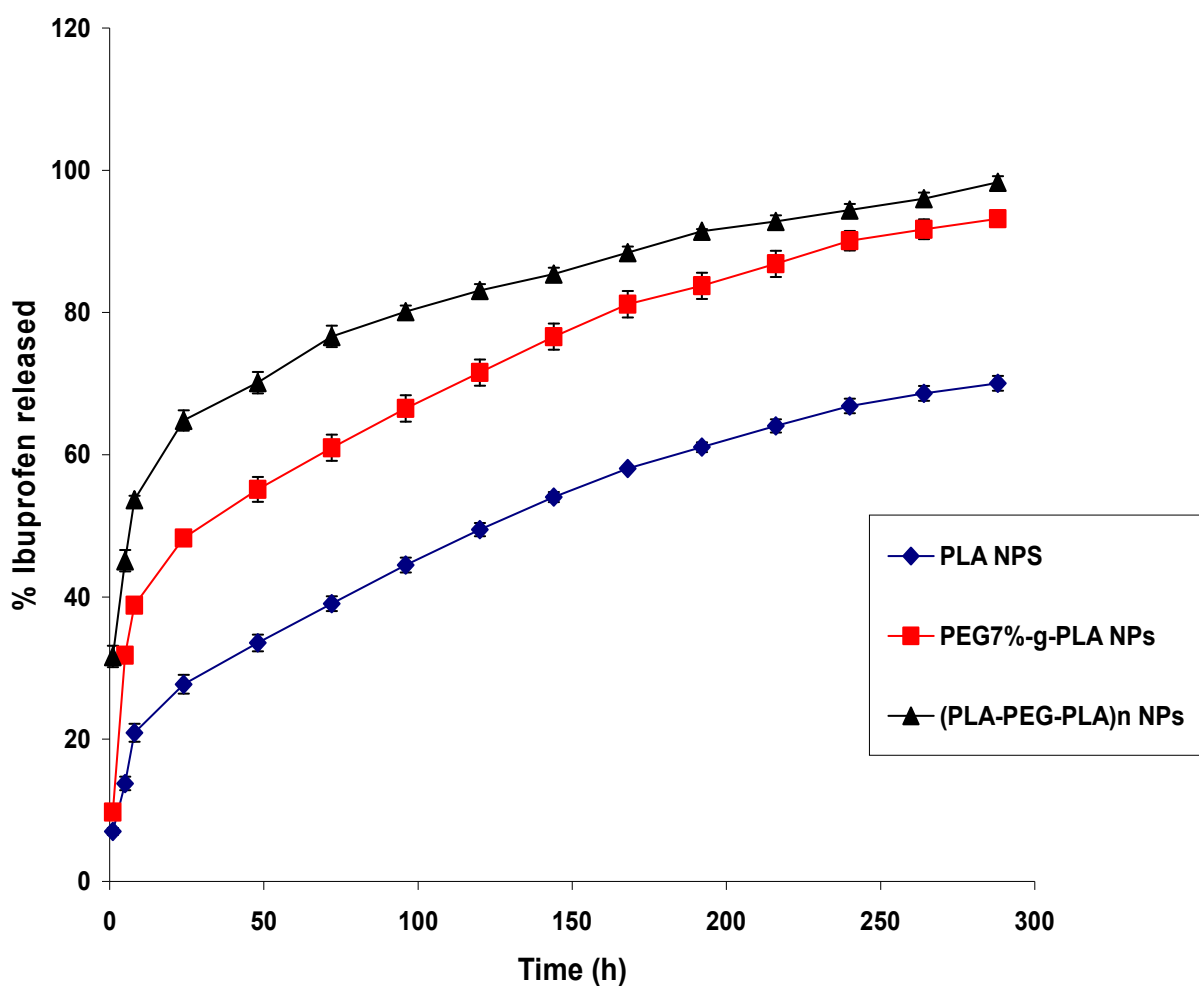


**Figure 3.6.** Effect of PEG chain organization on the in vitro release behavior of ibuprofen loaded NPs; values are represented as mean  $\pm$  S.D. of three independent experiments.

Thus, the last hypothesis might support that the slow release of drug might be mainly controlled by both solubility of the drug in the matrix and matrix erosion mechanism. The physical state of the drug inside the NPs matrix was investigated before using DSC since this would have an influence on the in vitro and in vivo release characteristics of the drug. DSC indicated that ibuprofen exists in a crystalline state inside all NPs irrespective of their polymer content. The last finding indicates that the main rate limiting step affecting drug release will be the dissolution of drug crystals into the polymeric matrix followed by their diffusion out of the matrix into the release media. This finding also confirmed the role of NPs core wetting in enhancing drug dissolution and hence drug release. Thus, the polymer that favors more water uptake and hence rapid core wetting would facilitate drug dissolution and hence faster drug release. The release pattern for all NPs formulations showed good correlation coefficient ( $R^2$  was close to 1) when fitted to Higushi square root equation of diffusion (data not shown) indicating that release will be mainly dominated by the diffusion of the solubilized drug crystals through the NPs matrix with some contribution from degradation decreasing in importance upon increasing the molecular weight of the polymer [36]. It could be seen that multiblock copolymers NPs showed faster drug release compared to PEG7%-g-PLA NPs. The possible reason behind that is the peculiar polymer architecture of the multiblock copolymer allows a major portion of PEG to be entrapped inside the core during NP formation as revealed from XPS and phase imaging data and hence, rapide wetting of the core will take place compared to grafted NPs. When PEG7%-g-PLA NPs are suspended into the release medium, a major fraction of PEG will be migrated easily towards the surface while the cores will be predominantly hydrophobic. In case of multiblock, a

considerable amount of PEG is expected to be embedded into the PLA core due to the covalent linkage of PEG with two PLA blocks as stated before which might hinder PEG chains to be migrated towards the surface. The hydrophilicity of the matrix is one of the major factors that markedly influence its hydration and, in turn, the drug release profile [38, 39]. Multiblock copolymer NPs were shown in the last section to erode faster than PEG7%-g-PLA NPs confirming the faster release rate obtained with such NPs. Another previous study showed that multiblock copolymers of PEG and PLA exhibited faster drug release compared to their PLA homopolymer and the authors attributed this also to the marked hydrophilic properties of multiblock copolymers [40, 41]. These results showed that core wetting is an important factor influencing the drug release kinetics. A schematic representation of different NPs chain organization depending on both their polymer composition and architecture is shown in Figure 3.7. This difference in chain organization was found to have an effect on the release kinetics of the encapsulated drug from NPs. Generally speaking, our results suggest the possibility of use of such pegylated NPs as drug carrier for poorly soluble drugs. Also, they could have the potential of targeting the encapsulated drugs into certain tissues depending on their ability to circulate for longer periods of time without being recognized by the immune system. It should also be mentioned that the use of multiblock copolymer would facilitate the encapsulation of hydrophilic drugs into their NPs matrix due to the formation of small pockets of PEG that might create an aqueous phase embedded inside a hydrophobic polymeric matrix.

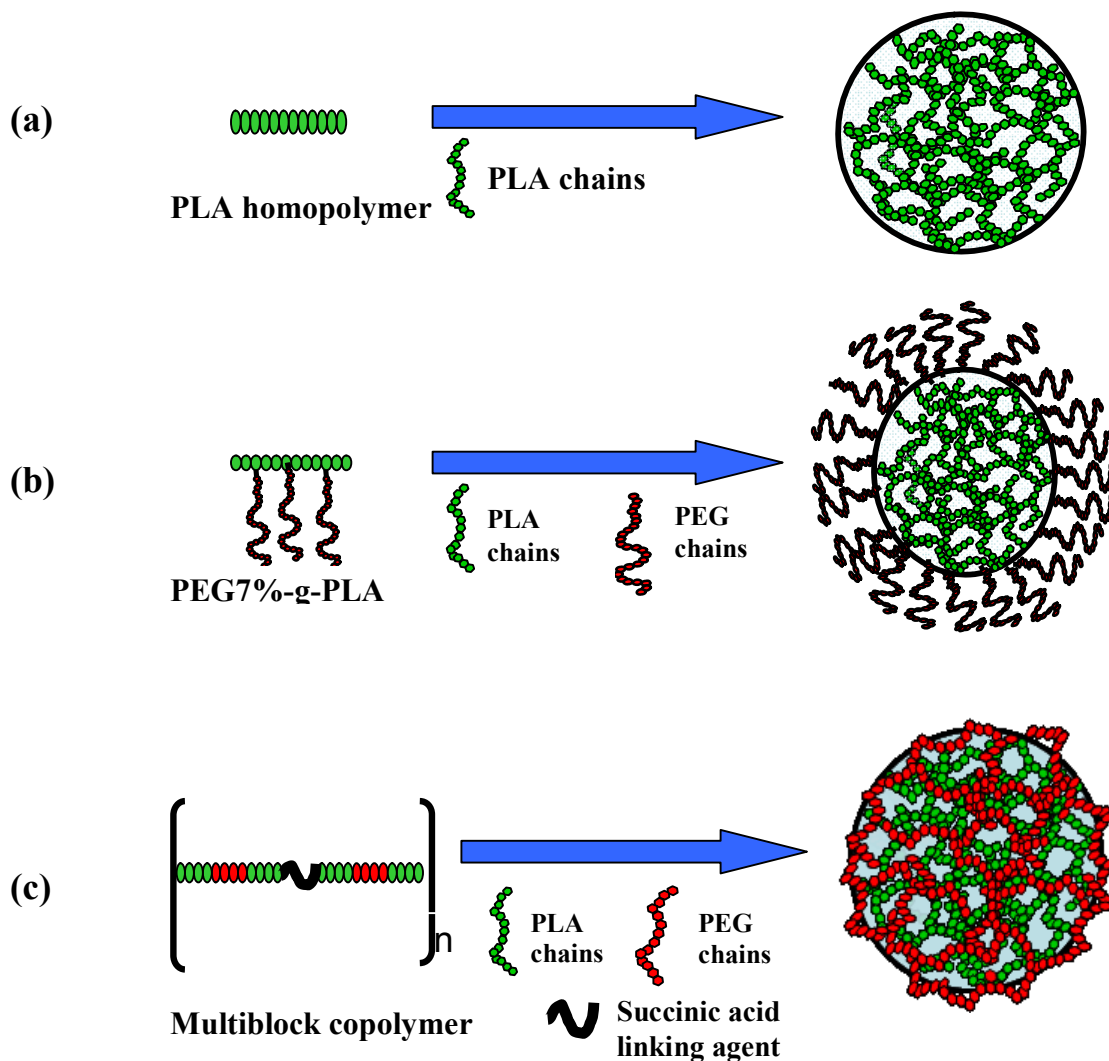


**Figure 3.7.** Schematic representation of polymer chain organization inside the NPs: PLA (a), PEG7%-g-PLA (b), and multiblock copolymers (PLA-PEG-PLA)<sub>n</sub> (c).

### 3.6. Conclusion

NPs were fabricated using novel copolymers of PEG-modified PLA polymers with different PEG chain organization. Both AFM phase imaging and XPS studies showed the existence of PEG chains on the surface of grafted pegylated NPs. Both studies also showed that multiblock copolymer displayed less amount of PEG on the surface due to

the possibility of PEG chains interpenetration inside the PLA core of NPs. This resulted in lower  $T_g$ , rapid degradation of the polymeric matrix, and faster drug release from NPs. On the contrary, grafted pegylated copolymer showed enhanced immiscibility of both PEG and PLA blocks resulting in enhanced phase separation of both components during NPs formation and hence, easy migration of PEG chains towards the surface of NPs while the cores will be predominantly hydrophobic. Our future work will focus on studying the cellular uptake of rhodamine encapsulated NPs made from different polymers with different PEG chain organization. In brief, the way PEG chain organized onto PLA backbone is an important parameter controlling surface characteristics of NPs which in turn determine their physicochemical properties like encapsulation efficiency, % PVA adsorbed at the surface of NPs, zeta potential, thermal characteristic, and drug release kinetics.

### **3.7. Appendix A. Supplementary material**

Supplementary data associated with this article can be found, in the online version, at [doi:10.1016/j.ejpb.2010.03.002](https://doi.org/10.1016/j.ejpb.2010.03.002)

### **3.8. Acknowledgment**

The work was supported in part by a grant of Fond Quebecois de la Recherche en Nature et Technologie (FQRNT). The authors wish to thank Mme. Suzie Poulin, research associate at École Polytechnique, University of Montreal for her help in the data analysis of the XPS experiments. Sherief Essa thanks the Ministry of Higher Education, Egypt for granting him a scholarship during his Ph.D.

### 3.9. References

1. Popielarski, S.R., Pun, S.H., Davis, M.E., 2005. A Nanoparticle-Based Model Delivery System To Guide the Rational Design of Gene Delivery to the Liver. 1. Synthesis and Characterization. *Bioconjugate Chemistry* 16, 1063-1070.
2. Peracchia, M.T., Gref, R., Minamitake, Y., Domb, A., Lotan, N., Langer, R., 1997. PEG-coated nanospheres from amphiphilic diblock and multiblock copolymers: Investigation of their drug encapsulation and release characteristics. *Journal of Controlled Release* 46, 223-231.
3. Li, Y.-P., Pei, Y.-Y., Zhang, X.-Y., Gu, Z.-H., Zhou, Z.-H., Yuan, W.-F., Zhou, J.-J., Zhu, J.-H., Gao, X.-J., 2001. PEGylated PLGA nanoparticles as protein carriers: synthesis, preparation and biodistribution in rats. *Journal of Controlled Release* 71, 203-211.
4. Soppimath, K.S., Aminabhavi, T.M., Kulkarni, A.R., Rudzinski, W.E., 2001. Biodegradable polymeric nanoparticles as drug delivery devices. *Journal of Controlled Release* 70, 1-20.
5. Moghimi, S.M., Hunter, A.C., Murray, J.C., 2001. Long-circulating and target-specific nanoparticles: theory to practice. *Pharmacol Rev* 53, 283-318.
6. Govender, T., Riley, T., Ehtezazi, T., Garnett, M.C., Stolnik, S., Illum, L., Davis, S.S., 2000. Defining the drug incorporation properties of PLA-PEG nanoparticles. *International Journal of Pharmaceutics* 199, 95-110.
7. Sahoo, S.K., Panyam, J., Prabha, S., Labhasetwar, V., 2002. Residual polyvinyl alcohol associated with poly (D,L-lactide-co-glycolide) nanoparticles affects their physical properties and cellular uptake. *Journal of Controlled Release* 82, 105-114.
8. Nadeau, V., Leclair, G., Sant, S., Rabanel, J.-M., Quesnel, R., Hildgen, P., 2005. Synthesis of new versatile functionalized polyesters for biomedical applications. *Polymer* 46, 11263-11272.
9. Quesnel, R., P., Hildgen, 2005. Synthesis of PLA-b-PEG multiblock copolymers for stealth drug carrier preparation. *Molecules* 10, 98-104.

10. Shakesheff, K.M., Evora, C., Soriano, I., Langer, R., 1997. The Adsorption of Poly(vinyl alcohol) to Biodegradable Microparticles Studied by X-Ray Photoelectron Spectroscopy (XPS). *Journal of Colloid and Interface Science* 185, 538-547.
11. Siparsky, G.L., Voorhees, K.J., Dorgan, J.R., Schilling, K., 1997. Water transport in polylactic acid (PLA), PLA/polycaprolactone copolymers, and PLA polyethylene glycol blends. *Journal of Environmental Polymer Degradation* 5, 125-136.
12. Proikakis, C.S., Mamouzelos, N.J., Tarantili, P.A., Andreopoulos, A.G., 2006. Swelling and hydrolytic degradation of poly(D,L-lactic acid) in aqueous solutions. *Polymer Degradation and Stability* 91, 614-619.
13. Abdelwahed, W., Degobert, G., Fessi, H., 2006. Investigation of nanocapsules stabilization by amorphous excipients during freeze-drying and storage. *European Journal of Pharmaceutics and Biopharmaceutics* 63, 87-94.
14. Raghavan, D., Gu, X., Nguyen, T., VanLandingham, M., Karim, A., 2000. Mapping Polymer Heterogeneity Using Atomic Force Microscopy Phase Imaging and Nanoscale Indentation. *Macromolecules* 33, 2573-2583.
15. Kopp-Marsaudon, S., Leclere, P., Dubourg, F., Lazzaroni, R., Aime, J.P., 2000. Quantitative Measurement of the Mechanical Contribution to Tapping-Mode Atomic Force Microscopy Images of Soft Materials. *Langmuir* 16, 8432-8437.
16. Paredes, J.I., Gracia, M., Martínez-Alonso, A., Tascón, J.M.D., 2005. Nanoscale investigation of the structural and chemical changes induced by oxidation on carbon black surfaces: A scanning probe microscopy approach. *Journal of Colloid and Interface Science* 288, 190-199.
17. Magonov, S.N., Elings, V., Whangbo, M. H., 1997. Phase imaging and stiffness in tapping-mode atomic force microscopy. *Surface Science* 375, L385-L391.
18. Donald, G., William, D., Randal, S., John, L., Willett, J.L., 2003. Mechanical and thermal properties of starch-filled poly(D,L-lactic acid)/poly(hydroxy ester ether) biodegradable blends. *Journal of Applied Polymer Science* 88, 1775-1786.

19. Wang, H., Djuricic, A.B., Chan, W.K., Xie, M.H., 2005. Factors affecting phase and height contrast of diblock copolymer PS-b-PEO thin films in dynamic force mode atomic force microscopy. *Applied Surface Science* 252, 1092-1100.
20. Wang, S.G., Cui, W.J., Bei, J.Z., 2005. Bulk and surface modifications of polylactide. *Analytical and Bioanalytical Chemistry* 381, 547-556.
21. Zambaux, M.F., Bonneaux, F., Gref, R., Maincent, P., Dellacherie, E., Alonso, M.J., Labrude, P., Vigneron, C., 1998. Influence of experimental parameters on the characteristics of poly(lactic acid) nanoparticles prepared by a double emulsion method. *Journal of Controlled Release* 50, 31-40.
22. Beletsi, A., Panagi, Z., Avgoustakis, K., 2005. Biodistribution properties of nanoparticles based on mixtures of PLGA with PLGA-PEG diblock copolymers. *International Journal of Pharmaceutics* 298, 233-241.
23. Gref, R., Lück, M., Quellec, P., Marchand, M., Dellacherie, E., Harnisch, S., Blunk, T., Müller, R.H., 2000. 'Stealth' corona-core nanoparticles surface modified by polyethylene glycol (PEG): influences of the corona (PEG chain length and surface density) and of the core composition on phagocytic uptake and plasma protein adsorption. *Colloids and Surfaces B: Biointerfaces* 18, 301-313.
24. Scholes, P.D., Coombes, A.G.A., Illum, L., Davis, S.S., Watts, J.F., Ustariz, C., Vert, M., Davies, M.C., 1999. Detection and determination of surface levels of poloxamer and PVA surfactant on biodegradable nanospheres using SSIMS and XPS. *Journal of Controlled Release* 59, 261-278.
25. Merino, S., Brauge, L., Caminade, A.M., Majoral, J.P., Taton, D., Gnanou, Y., 2001. Synthesis and characterization of linear, hyperbranched, and dendrimer-like polymers constituted of the same repeating unit. *Chemistry-a European Journal* 7, 3095-3105.
26. Kulinski, Z., Piorkowska, E., Gadzinowska, K., Stasiak, M., 2006. Plasticization of poly(L-lactide) with poly(propylene glycol). *Biomacromolecules* 7, 2128-2135.
27. Piorkowska, E., Kulinski, Z., Galeski, A., Masirek, R., 2006. Plasticization of semicrystalline poly(L-lactide) with poly(propylene glycol). *Polymer* 47, 7178-7188.

28. Shrivastava, K.N., 2002. Melting temperature, Brillouin shift, and density of states of nanocrystals. *Nano Letters* 2, 519-523.
29. Riley, T., Stolnik, S., Heald, C.R., Xiong, C.D., Garnett, M.C., Illum, L., Davis, S.S., Purkiss, S.C., Barlow, R.J., Gellert, P.R., 2001. Physicochemical evaluation of nanoparticles assembled from poly(lactic acid)-poly(ethylene glycol) (PLA-PEG) block copolymers as drug delivery vehicles. *Langmuir* 17, 3168-3174.
30. Jung, T., Breitenbach, A., Kissel, T., 2000. Sulfobutylated poly(vinyl alcohol)-graft-poly(lactide-co-glycolide)s facilitate the preparation of small negatively charged biodegradable nanospheres. *Journal of Controlled Release* 67, 157-169.
31. von Burkersroda, F., Gref, R., Göpferich, A., 1997. Erosion of biodegradable block copolymers made of poly(D,L-lactic acid) and poly(ethylene glycol). *Biomaterials* 18, 1599-1607.
32. Clapper, J.D., Skeie, J.M., Mullins, R.F., Guymon, C.A., 2007. Development and characterization of photopolymerizable biodegradable materials from PEG-PLA-PEG block macromonomers. *Polymer* 48, 6554-6564.
33. Youxin, L., Volland, C., Kissel, T., 1994. In-vitro degradation and bovine serum albumin release of the ABA triblock copolymers consisting of poly (L(+)) lactic acid, or poly(L(+)) lactic acid-co-glycolic acid) A-blocks attached to central polyoxyethylene B-blocks. *Journal of Controlled Release* 32, 121-128.
34. Magenheim, B., Levy, M.Y., Benita, S., 1993. A new in-vitro technique for the evaluation of drug-release profile from colloidal carriers - ultrafiltration technique at low-pressure. *International Journal of Pharmaceutics* 94, 115-123.
35. Panyam, J., Dali, M.M., Sahoo, S.K., Ma, W., Chakravarthi, S.S., Amidon, G.L., Levy, R.J., Labhasetwar, V., 2003. Polymer degradation and in vitro release of a model protein from poly(D,L-lactide-co-glycolide) nano- and microparticles. *Journal of Controlled Release* 92, 173-187.
36. Mittal, G., Sahana, D.K., Bhardwaj, V., Ravi Kumar, M.N.V., 2007. Estradiol loaded PLGA nanoparticles for oral administration: Effect of polymer molecular weight and copolymer composition on release behavior in vitro and in vivo. *Journal of Controlled Release* 119, 77-85.

37. Rizkalla, N., Range, C., Lacasse, F.X., Hildgen, P., 2006. Effect of various formulation parameters on the properties of polymeric nanoparticles prepared by multiple emulsion method. *Journal of Microencapsulation* 23, 39-57.
38. Sinha Roy, D., Rohera, B.D., 2002. Comparative evaluation of rate of hydration and matrix erosion of HEC and HPC and study of drug release from their matrices. *European Journal of Pharmaceutical Sciences* 16, 193-199.
39. Sung, K.C., Han, R.-Y., Hu, O.Y.P., Hsu, L.-R., 1998. Controlled release of nalbuphine prodrugs from biodegradable polymeric matrices: influence of prodrug hydrophilicity and polymer composition. *International Journal of Pharmaceutics* 172, 17-25.
40. Luo, W.J., Li, S.M., Bei, J.Z., Wang, S.G., 2002. Synthesis and characterization of poly(L-lactide)- poly(ethylene glycol) multiblock copolymers. *Journal of Applied Polymer Science* 84, 1729-1736.
41. Chen, W.N., Luo, W.J., Wang, S.G., Bei, J.Z., 2003. Synthesis and properties of poly(L-lactide)-poly (ethylene glycol) multiblock copolymers by coupling triblock copolymers. *Polymers for Advanced Technologies* 14, 245-253.

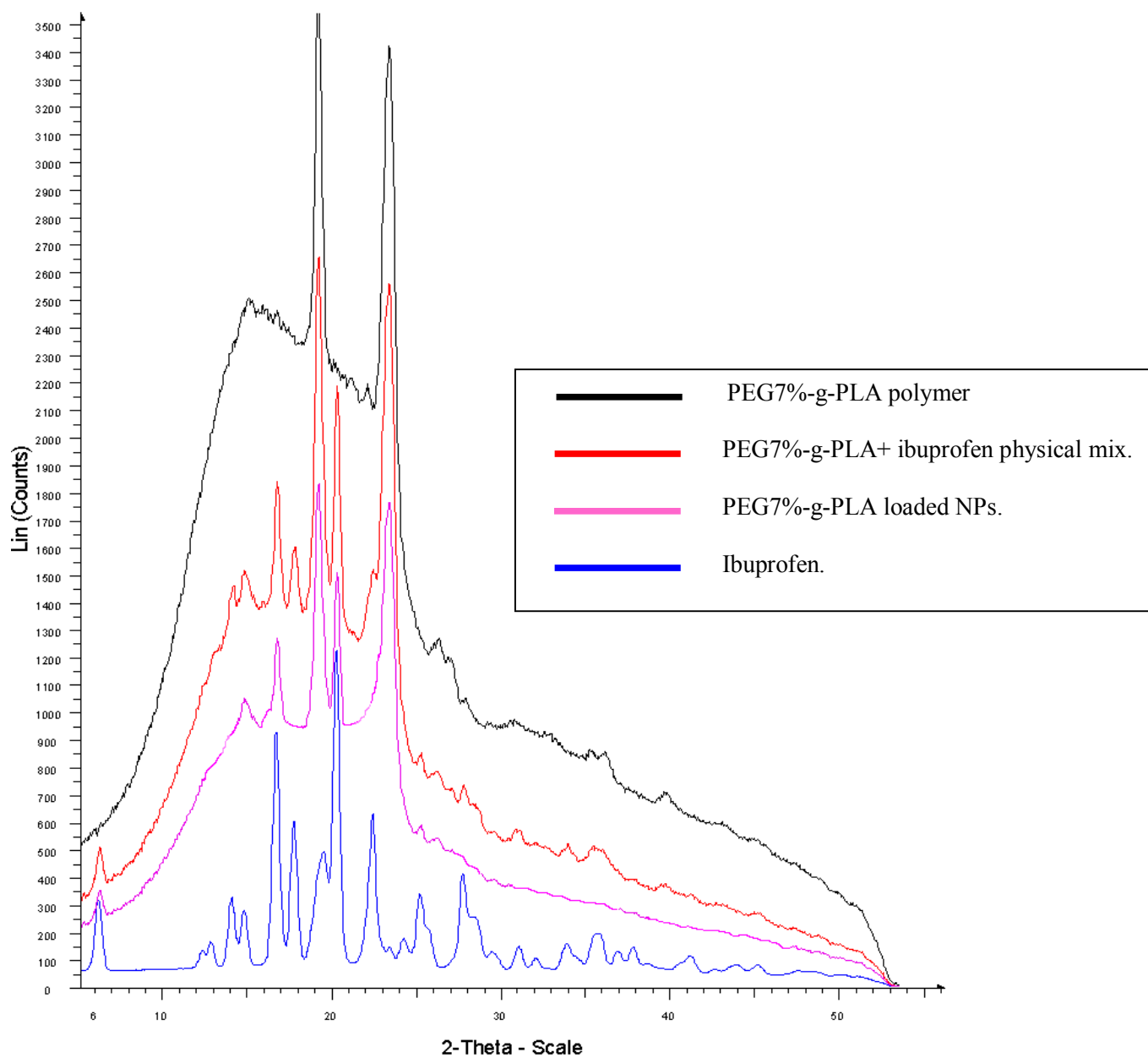


**Figure 3.S (supporting information):** XRD spectra of ibuprofen, physical mixture of PEG7%-g-PLA with ibuprofen, PEG7%-g-PLA polymer, and ibuprofen loaded NPs.

## CHAPTER FOUR

---

### RESEARCH PAPER

#### **Characterization of Rhodamine Loaded PEG-g-PLA Nanoparticles (NPs): Effect of Poly(ethylene glycol) Grafting Density<sup>1</sup>.**

Sherief Essa, Jean Michel Rabanel, and Patrice Hildgen.

Faculty of Pharmacy, Université de Montréal, CP 6128, Succursale Centre Ville,  
Montréal, QC, Canada, H3C 3J7

**International Journal of Pharmaceutics**

**In press, [doi:10.1016/j.ijpharm.2011.02.039](https://doi.org/10.1016/j.ijpharm.2011.02.039)**

---

<sup>1</sup> My contribution included designing the experiments, polymer synthesis, nanoparticles preparation and characterization, interpreting the results and writing the paper, which was supervised by Dr. Patrice Hildgen. Jean Michel Rabanel contribution was technical assistance using laboratory equipments.

#### 4.1. Abstract:

In our previous study, PEG-g-PLA nanoparticles were developed and characterized. The aim of the present work is to investigate the effect of PEG grafting density (% PEG inserted onto poly(D,L)-lactide, PLA backbone) on both physicochemical and biological properties (mainly plasma protein binding and in vitro macrophage uptake) of PEG-g-PLA NPs. Rhodamine B (RHO) loaded NPs were prepared from a 1:1 (wt/wt) blend of PLA and PEG-g-PLA copolymer of varying PEG grafting density (1, 7, or 20 % mol/mol of lactic acid monomer) by an o/w emulsion solvent evaporation method. These NPs were characterized with regard to their morphology, size, surface charge, loading efficiency, and rhodamine release. The extent of protein adsorption to the surface of different NPs was qualitatively investigated by dynamic light scattering technique. Additionally, the in vitro macrophage uptake following incubation of RAW 264.7 cells with rhodamine loaded PEG-g-PLA and PLA particles was investigated by confocal laser scanning microscopy (CLSM). The amount of NPs phagocytosed following incubation of RAW 264.7 cells with different concentrations of rhodamine loaded PLA or pegylated NPs for 24 h at 37 °C was also determined by fluorescence spectroscopy. ALL lyophilized NPs showed larger diameter in the range of 300–400 nm compared to freshly prepared NPs suspension indicating particle aggregation upon lyophilization. % EE of rhodamine was found to be between 10% and 68% wt/wt depending on PEG grafting density. The higher the grafting density of PEG over PLA backbone, the more the entrapment efficiency. All pegylated NPs showed low zeta potential (close to zero) values. In vitro release analysis revealed that rhodamine leaked from all nanoparticles at a very slow rate at physiological pH, thus making it suitable for both imaging and uptake studies with RAW 264.7 cells. All PEG-g-PLA NPs of different PEG grafting density were well tolerated and exhibited no toxicity to RAW 264.7 cells as seen by cell proliferation assays. Cellular uptake of NPs was mainly dependent on polymer type as well as PEG grafting density. Grafted copolymer NPs resulted in lower degree of macrophage uptake compared to PLA NPs in macrophages cell lines. The higher the PEG grafting density, the lower the uptake of NPs by macrophage cells. Minimum NPs uptake for all the investigated concentrations was achieved when the PEG grafting density was 7% mol/mol of lactic acid. When increasing the PEG grafting density in the nanoparticles

above 7 %, no significant reduction in NPs phagocytosis was achieved. Thus, this study shows that the optimal PEG density required for designing stealth PEG-g-PLA NPs suitable for drug delivery applications might vary from 4-7%.

#### **4.2. Keywords**

Nanoparticles, PEG-PLA, grafting density, rhodamine, macrophage, plasma proteins.

#### **4.3. Introduction**

Biodegradable nanoparticles are promising carriers to improve the administration of certain drugs, vaccines, nucleic acid and therapeutic proteins [1-4]. Benefits offered by biodegradable nanoparticles include improved therapeutic efficiency, enhanced protection of the active moiety from degradation, maintenance of drug concentrations within acceptable therapeutic limits, the need for fewer doses thus reducing dose-limiting side effects, prolonged biological activity, and finally better patient compliance [5, 6].

Poly(lactic acid) (PLA) or poly(lactide-co-glycolide) are the most widely used polymers in drug delivery systems. However, NPs formulated using either PLA or PLGA might suffer many drawbacks as their rapid uptake by the reticuloendothelial system after intravascular administration, low drug loading efficiency, inability to encapsulate a wide range of drugs particularly hydrophilic drugs, and in many cases inability to release their payload completely [7]. Low drug incorporation of PLGA and PLA usually leads to large drug loss during NP formulation, and hence, encapsulating insufficient drug amounts for therapeutic efficacy [8, 9]. The former situation necessitates the use of high polymer levels that might exceed their safety profile. Another drawback of PLGA and PLA is that an initial burst release of drug can be observed in most loaded NPs, which may result in a loss of much of the therapeutic dose before the target site is reached by the NPs [10, 11]. With these drawbacks of PLGA/PLA, a novel biodegradable polymer, PEG-g-PLA was early developed by our group [12]. Our previous work focused mainly on the development and characterization of functionalized poly(D,L)-lactide (PLA) nanoparticles in order to improve the drug delivery behavior of PLA nanoparticles [13, 14]. Functionalized poly(D,L)- lactide (PLA) nanoparticles development mainly depend on introducing a flexible moiety onto PLA hydrophobic cores in attempt to improve the

drug delivery properties of the obtained NPs. A variety of pendant substituents could be grafted onto PLA to generate polymers of different physicochemical properties and hence different drug incorporation behavior than PLA itself. In the same work, we have reported the development and characterization of PEG-g-PLA NPs with some optimal properties ideal for drug delivery applications. Those properties were uniform size with narrow size distribution (~150-200 nm), neutral surface charge, higher encapsulation efficiency, and finally their ability to control the release of the entrapped model drug, ibuprofen for a period of two weeks.

In this part, we are attempting to study the effect of PEG grafting density over PLA backbone on the properties of PEG-g-PLA NPs either physicochemical or biological properties mainly in vitro plasma protein adsorption and macrophage cellular uptake. Another aim is to investigate the optimal PEG grafting density required to develop stealth particles from such type of grafted copolymers. In order to reach these goals, we prepared NPs encapsulating rhodamine B (RHO) as a fluorescent marker using grafted pegylated polymer; PEG-g-PLA with different PEG grafting densities (1, 7, or 20% mol/mol of lactic acid monomer). RHO was loaded into NPs in order to have labeled formulations suitable for investigating the cellular uptake of NPs by macrophage cell lines, RAW 264.7. It is important that the marker used is incorporated into the NPs at a sufficient level to give good detection by the used analytical methods. Thus, a 1:1 wt/wt blend of PLA: PEG-g-PLA of different PEG density was used to efficiently entrap RHO into NPs matrix. An o/w emulsion solvent evaporation method was used to prepare RHO loaded NPs. RHO should remain associated with the NPs so that we follow the fate of the NPs rather than the marker itself. Accordingly the drug incorporation and release of the marker from NPs were determined.

#### **4.4. Material and methods**

##### **4.4.1. Materials**

D,L-Lactide, poly(ethylene glycol) methyl ether (MePEG; 2000 Da), allyl glycidyl ether, tetraphenyltin, polyvinyl alcohol (PVA, average  $M_w$  9000-10,000 Da, 80% hydrolyzed), borane-tetrahydrofuran complex (1 M), acetone, toluene, pyridine,

chloroform, thionyl chloride, rhodamine B (RHO), and albumin bovine were purchased from Aldrich Chemical Company Inc., Milwaukee, USA. Sodium hydroxide pellets were purchased from Anachemia Canada Inc. and dichloromethane (DCM) was purchased from Laboratoire Mat Inc., Montreal, Quebec, Canada. Fetal bovine serum and all other materials for cell culture were purchased from Invitrogen (Burlington, ON, Canada) unless otherwise stated.

#### 4.4.2. Synthesis of Polymers.

Poly(D,L)-lactide (PLA) was synthesized by ring-opening polymerization of dilactide in argon atmosphere, using tetraphenyltin as the catalyst. Briefly, dilactide was crystallized from toluene solution and dried under vacuum before use. A weighed amount of purified dilactide was then placed in a round-bottom flask and purged thoroughly with argon. Bulk polymerization was carried at 180 °C for 6 h. The polymer thus obtained was dissolved in acetone and was purified by precipitating in water.

Polymer with poly(ethylene glycol)-grafted randomly on poly(D,L)-lactide (PEG7%-g-PLA) (PEG;  $M_w$  2000 Da) was synthesized as reported earlier [12]. Briefly, D,L-dilactide (21.5 g, 93 mol %) was polymerized in the presence of allyl glycidyl ether (2.6 g, 7 mol %) with tetraphenyltin as the catalyst (1:10 000 mol with regards to D,L-dilactide) at 180 °C for 6 h under argon. Polylactic acid with allyl groups was purified by dissolving in acetone and precipitating in water. The allyl groups were converted to hydroxyl groups by hydroboration with an equimolar quantity of borane in tetrahydrofuran, followed by oxidation in the presence of hydrogen peroxide under alkaline conditions (1.5 mol of 3 N sodium hydroxide). The hydroxyl groups were oxidized to carboxylic acid groups using Jones reagent, which was further converted to an acid chloride using thionyl chloride (1:1000 M). Finally, methoxy-PEG was grafted

onto the polymer backbone by the reaction between acid chloride and the hydroxyl groups of methoxy-PEG (2000 Da) in the presence of pyridine. The final polymer was purified by evaporating pyridine and washing with distilled water. For the 1%, and 20% PEG-grafted polymers (PEG1%-g-PLA, and PEG20%-g-PLA, respectively) the concentrations of D,L-lactide and allyl glycidyl ether were adjusted to give the desired ratios with the remaining synthesis procedure being the same.  $^1\text{H}$  NMR spectra were recorded on a Bruker ARX 400 spectrometer (Bruker Biospin, Billerica, MA). Chemical shifts ( $\delta$ ) were measured in parts per million (ppm) using tetramethylsilane (TMS) as an internal reference. Gel permeation chromatography (GPC) was performed on a Water Associate chromatography system (Waters, Milford, MA) equipped with a refractive index detector and a Phenomenex Phenogel 5  $\mu$  column. Polystyrene standards were used for calibration with THF as the mobile phase at a flow rate of 0.6 mL/min.

#### **4.4.3. Preparation of nanoparticles (NPs)**

RHO loaded NPs were prepared by an O/W emulsion-solvent evaporation method. It should be mentioned that NPs were prepared using a 1:1 blend of high *Mwt* PLA (*Mwt* =56.000 Da, Table 4.1) with each pegylated polymer, PEG-g-PLA of different PEG grafting density (1, 7, or 20% mol/mol of lactic acid monomer) to ensure high retaining ability of NPs for rhodamine B (RHO). RHO loaded NPs were prepared using an initial loading of 0.24% wt/wt of each polymer blend. Rhodamine (RHO) was first dissolved in the organic phase, 10 mL DCM followed by dissolution of each polymer blend (1 g) in the same phase. The organic phase was then emulsified into 30 mL PVA solution (0.5% w/v) as an external aqueous phase using high-pressure homogenizer (Emulsiflex C30, Avestin, Ottawa, Canada) at a pressure of 10,000 psi for 5 min. The O/W emulsion was

collected by washing with another 30 mL 0.5% PVA. The DCM was evaporated under reduced pressure with constant stirring to obtain the NPs. Finally, NPs obtained as a suspension were then collected by centrifugation at 18500 rpm for 30 min. at 4 °C (Sorval® Evolution<sub>RC</sub>, Kendro, USA), washed four times with distilled water, then lyophilized to obtain dry NPs (Freeze Dry System, Lyph.Lock 4.5, Labconco) and stored at 4 °C until further use. Small samples of the nanoparticle suspension were taken before lyophilization step in order to identify the original size of the particles obtained after homogenization and organic solvent evaporation.

#### **4.4.4. Characterization of NPs**

Size and size distribution of NPs were measured by dynamic light scattering (DLS) with a Malvern Autosizer 4800 instrument (Malvern Instruments, Worcestershire, UK) before and after lyophilization. DLS uses photon correlation spectroscopy to determine particle size from the temporal variation of light scattering caused by Brownian motion of the suspended particles. For all batches, fresh NP suspensions (0.1 mL) or lyophilized NPs (1 mg) were diluted 10 times with Milli-Q Water and size measurements were performed at 25 °C and scattering angle of 90°. The CONTIN program was used to extract size distributions from the autocorrelation functions. Measurements were performed in triplicate. The zeta potential of the nanoparticles was measured with Malvern ZetaSizer Nanoseries ZS (Malvern Instruments, Worcestershire, UK). Freeze dried NPs were suspended in 0.22 µm filtered 0.25% (w/v) saline solution (pH 7.4) and zeta potential was measured in triplicate. Nanoparticle morphology was studied using atomic force microscopy technique (AFM). AFM was performed with Nanoscope IIIa, Dimension<sup>TM</sup> 3100 (Digital Instruments, Santa Barbara, CA) in tapping mode. Samples were prepared by suspending the nanoparticles in water at a concentration of 10 mg/mL. These samples were deposited on freshly cleaved mica surface and were allowed to dry at room temperature. Subsequently, they were imaged in air at ambient conditions using etched silicon probes with tip radius of 5-10 nm and spring constant in

the range of 20-100 N/m, oscillated at its fundamental resonant frequency (200-400 KHz).

#### 4.4.5. Encapsulation efficiency (EE)

A weighed amount of NPs was dissolved into dichloromethane (DCM) followed by 5 min. vortexing and then stirring for 1 h. Rhodamine (RHO) concentration was measured by spectrofluorimetry at excitation ( $\lambda_{ex}$ ) and emission ( $\lambda_{em}$ ) wavelengths of 552 and 585 nm, respectively, using a Tecan Safire plate reader (Durham, NC). Percent encapsulation efficiency (% EE) and percent drug loading (% DL) were calculated based on the following equations:

$$\% \text{ EE} = \frac{\text{Drug entrapped in NPs}}{\text{Initial amount of drug added}} \times 100 \quad (1)$$

$$\% \text{ DL} = \frac{\text{Drug entrapped in NPs}}{\text{Weight of NPs}} \times 100 \quad (2)$$

#### 4.4.6. In vitro drug release study

All formulations prepared using different polymers were tested for in vitro release in triplicates in phosphate buffered saline (PBS, 10 mM, pH 7.4.). 30 mg NPs were suspended in 10 mL PBS in a dialysis tubing (Spectra Por 1 membrane, 6–8 kDa cut-off). This dialysis tubing was placed in a screw-capped tube containing 40 mL PBS. The tubes were shaken at 200 rpm on a horizontal water bath shaker (Orbit Shaker Bath, Labline) maintained at  $37 \pm 0.5$  °C. At predetermined time intervals, 15 mL of the external medium was withdrawn and replaced by fresh PBS to maintain sink conditions. The aliquots were assayed for the concentration of RHO released by spectrophotometry at 552 nm (U-2001 UV/Visible spectrophotometer, Hitachi).

#### **4.4.7. Evaluation of protein adsorption to NPs surface**

Dynamic light scattering (DLS) was used for measurement of the size of different NPs incubated with either 5 % fetal bovine serum (FBS) or 2 % bovine serum albumin (BSA). A weighed amount of NPs in 5 mL of either 5% FBS or 2% BSA was incubated at 37 °C for 24 h. Controls included the incubation of serum alone and RHO-loaded NPs alone with only distilled water for the same period of time. Samples were analyzed by DLS (n=3) at the end of the incubation period to determine if there is any change in the size distribution pattern of different NPs.

#### **4.4.8. Cell culture**

Macrophage cell line, RAW 264.7 was grown in Dulbecco's modified Eagle cell culture medium (DMEM) containing 10% (v/v) heat-inactivated fetal bovine serum, 100 U/mL penicillin-G, and 100 mg/mL streptomycin (Invitrogen, Burlington, ON, Canada) in an atmosphere of 5% CO<sub>2</sub> and 95% relative humidity. The cells were routinely passaged at 90–95% confluence.

##### **4.4.8.1. Evaluation of cellular toxicity of PEG-g-PLA NPs**

Inhibition of cell proliferation was assessed by tetrazolium salt 3-(4,5-dimethylthiazol-2-yl)-2,5-diphenyl tetrazolium bromide (MTT) assay. Briefly,  $1 \times 10^5$  RAW 264.7 cells were seeded in 96-well flat bottom plates (Costar, Corning, NY) and allowed to grow for 24 h. The cells were then incubated with increasing concentrations of each PEG-g-PLA NPs of different PEG grafting density for 24 h. Cell layers were washed with cold PBS and further incubated with 10  $\mu$ L of MTT solution (5 mg/mL in PBS) for 4 h at 37°C. Formazan crystals formed were then dissolved along with the cell layers and absorbance was measured on microplate reader at 570 nm. Cell viability was calculated with respect to PBS as control.

##### **4.4.8.2. Cellular interaction with RAW 264.7: CLSM study**

RAW 264.7 cells (a murine macrophage-like cell line) were seeded in eight-well chamber plate that contained a pre-sterilized coverslip at a concentration of  $1 \times 10^5$  cells per well and allowed to adhere overnight in DMEM with 10% serum at 37°C. Next day,

the medium was removed; the cells were washed with a sterile Hanks balanced salt solution (HBSS). Then cells were incubated in RPMI 1640 medium with RHO-encapsulated nanoparticles (ensuring that rhodamine content is the same for all NPs batches based on the actual RHO loading) for 24h at 37°C. Next, the cells were washed six times with HBSS and were fixed with 4% paraformaldehyde solution. Coverslips were then mounted onto microscopy slides using Gel-Tol mounting medium (Thermo Scientific, Pittsburgh, PA, USA) to protect the samples. Microscopy slides were observed with an inverted Olympus IX71 microscope (Olympus Canada Inc., Markham, ON) and an Evolution VF camera (MediaCybernetics, Bethesda, MD) with the same 60× objective lens and exposure time to allow comparison of measurements. Laser sources at 476, 488 and 496 nm were used to excite RHO and the fluorescence signal were detected in the 550–650 nm range. All microscopy gain and offset settings were maintained constant throughout the study. All images were processed with ImagePro software (MediaCybernetics, Bethesda, MD).

#### **4.4.8.3. Cellular interaction with RAW 264.7: Fluorimetry analysis**

RAW 264.7 cells ( $1 \times 10^5$  cells/ well) were plated in 24- well flat bottom plates (Costar, Corning, NY) and allowed to adhere overnight in DMEM with 10% serum. Next day, the medium was removed and replaced by RPMI 1640 without serum. The cells were then incubated with different concentrations of RHO encapsulated NPs for 24 h at 37 °C. The cell monolayers were washed four times with cold PBS (pH 7.4) and then lysed with 0.2% Triton-X 100 in 0.2N NaOH solution. The fluorescence was measured on microplate reader at excitation and emission wavelength of 552 and 585 nm, respectively. The amount of NPs phagocytosed was calculated from calibration curve of NPs under the same conditions.

#### **4.4.9. Statistical analysis**

Results were expressed as mean  $\pm$  SD. All data were generated in three independent experiments with two or three repeat. The t-test and the one-way analysis of variance (ANOVA) were performed to compare two or multiple groups, respectively. The difference between treatments was considered to be significant at a level of  $P < 0.05$ .

Statistical analysis was performed for sizing, zeta potential, release, cellular uptake results, and encapsulation efficiency and loading data.

#### **4.5. Results and discussion**

Our previous development of PEG-g-PLA NPs with suitable drug delivery properties e.g. small size, higher encapsulation efficiency, and prolonged release features led us to investigate the effect of PEG coating density on the physicochemical and in vitro macrophage uptake properties of the obtained NPs. We hypothesized that a high PEG coating density on the particles and a small particle size would improve the potential of PEG-g-PLA as a stealth carrier in vivo. The optimal PEG coverage density that could impart stealth behavior for the PEG-g-PLA NPs without compromising NPs properties was investigated in that study. With this purpose in mind, we synthesized PEG-g-PLA copolymers which differ in the PEG grafting density but have the same PEG chain length (2 kDa). Then, PEG-g-PLA nanoparticles of different PEG coating densities loaded with the fluorescent molecule rhodamine (RHO) were prepared as a tool for investigating NPs interaction with Raw 264.7 macrophage cell lines. The extent of cellular uptake of different particles was evaluated by fluorescence microscopy and fluorimetry analysis. RHO was chosen as the fluorescent label because it is more stable than fluorescein to quenching by light [15], efficiently entrapped and molecularly dispersed into NPs matrices [16], easily loaded into NPs either by simple nanoprecipitation [17] or single o/w emulsion solvent/evaporation method [18]. Moreover, the conditions required for obtaining good images for NPs inside the cells by fluorescence microscopy were found to be easily optimized with RHO use [19, 20]. To develop RHO loaded PEG-g-PLA NPs suitable for investigating the cellular interaction, NPs must show high retaining ability for the fluorescent marker. In order to achieve this, a 1:1 wt/wt polymer blend consisting of high *Mwt* PLA with each pegylated polymer, PEG-g-PLA of different PEG density (1, 7, or 20 mol %) was used to prepare NPs.

##### **4.5.1. Characterization of Polymers**

PLA homopolymer and PEG-g-PLA copolymers of different PEG grafting densities were synthesized by ring-opening polymerization method. <sup>1</sup>H NMR

spectroscopy and gel permeation chromatography (GPC) were used to measure the number average ( $M_n$ ) and weight average molecular weights ( $M_w$ ) of the synthesized polymers. The polydispersity was calculated by the ratio of  $M_w$  to  $M_n$  from the GPC data. GPC results are summarized in Table 4.1. All the synthesized polymers exhibited uniform molecular weight distribution as revealed by the narrow polydispersity index values as shown in the same table. Unimodal mass distribution ruled out the possibility of the presence of unreacted MePEG or Poly(D,L-lactide) (data not shown). The molecular weight of PEG-g-PLA copolymer decreases with increasing grafting density of PEG. Similar finding was obtained before with PLA/PEG copolymer prepared by using different initial feed ratios for both PEG and PLA [21].  $^1\text{H}$ NMR spectra and chemical structure of PEG-g-PLA of different PEG grafting densities are shown in Figure 4.1. A typical spectrum for all PEG-g-PLA polymers was obtained with a peak at 5.2 ppm corresponding to the tertiary PLA proton (m, -CH), a peak at 3.6 ppm for the protons of the repeating units in the PEG chain (m, OCH<sub>2</sub>-CH<sub>2</sub>O), and a peak at 1.5 ppm for the pendant methyl group of the PLA chain (m, -CH<sub>3</sub>). The grafting density of PEG over the PLA backbone was determined by comparing the integration ratio of resonances due to PEG blocks at 3.64 ppm (-O-CH<sub>2</sub>-CH<sub>2</sub>-) and to the PLA blocks at 5.17 ppm (Me-CH\* ) in the  $^1\text{H}$  NMR spectra. The actual grafting density of all synthesized polymers seems closer to the initial feed ratio as shown in Table 4.1. Also, it could be seen from Figure 4.1 that the intensity of PLA peak at 5.2 ppm decreased remarkably upon increasing the grafting density and this might indicate the successful grafting of PEG over the PLA backbone.

#### 4.5.2. NPs characterization

RHO loaded PEG-g-PLA nanoparticles were successfully prepared using an O/W emulsion solvent evaporation method by co-dissolving RHO and polymer blend (1:1 wt/wt PLA: PEG-g-PLA) in DCM and precipitating the polymer into nanoparticles in an aqueous phase having 0.5 % PVA as a stabilizer after organic solvent evaporation. Table 4.2 summarizes the size distribution characteristics of RHO loaded PEG-g-PLA NPs of varying PEG densities (1, 7, and 20 mol %). For comparison, RHO loaded PLA was also

included as the control. Particle size distribution by dynamic light scattering (DLS) showed unimodal distribution for freshly prepared NPs dispersion (before lyophilization)

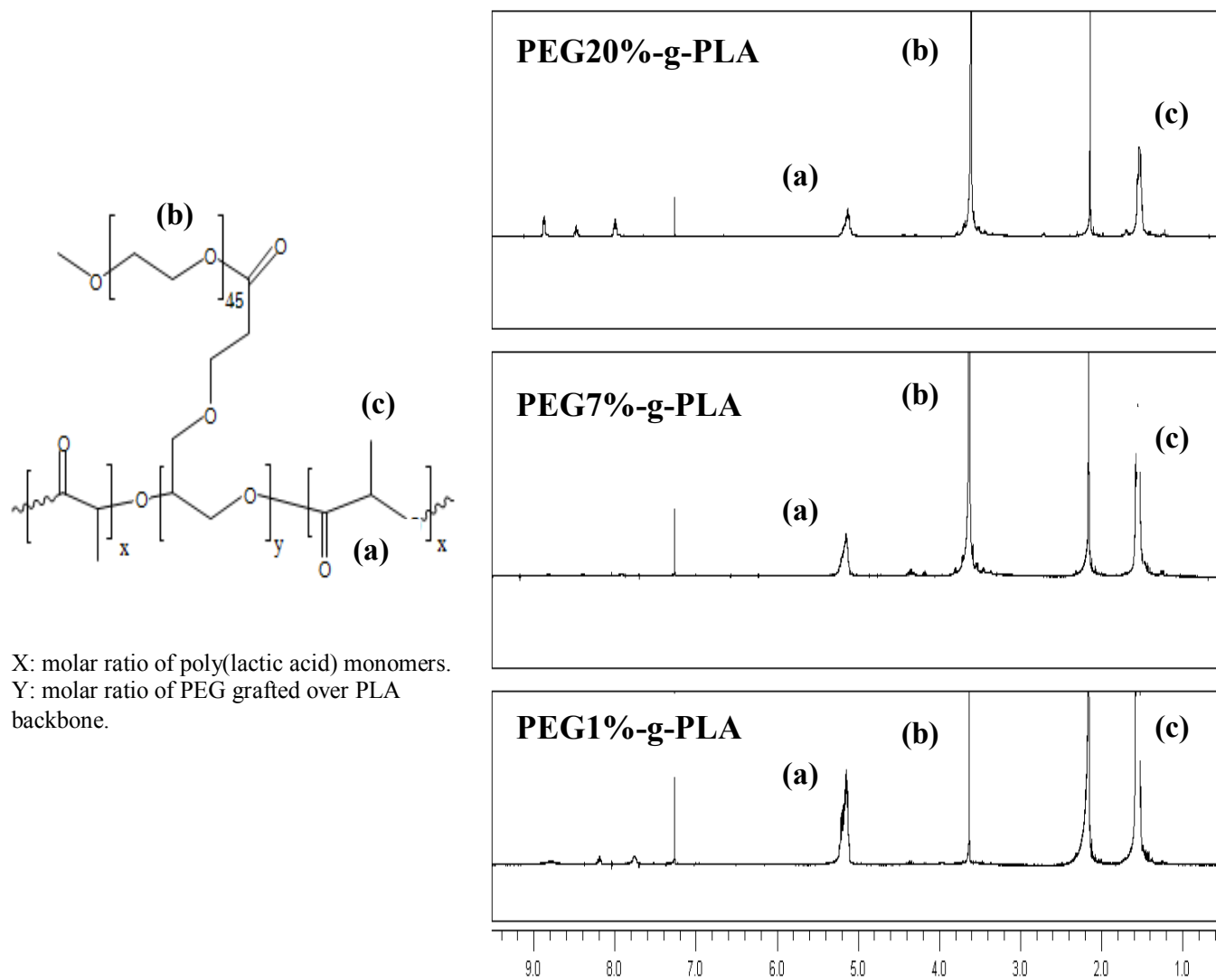


**Figure 4.1.**  $^1\text{H}$  NMR spectra and chemical structure of PEG-g-PLA copolymers of different PEG grafting densities over PLA backbone.

**Table 4.1.** Polymer characterization by  $^1\text{H}$  NMR and Gel Permeation Chromatography (GPC).

<b>Polymer</b>	<b>Mn<sup>a</sup> (Da)</b>	<b>Mw<sup>a</sup> (Da)</b>	<b>Mw/Mn<sup>a</sup></b>	<b>PEG (mol%)<sup>b</sup></b>	<b>Mn (<math>^1\text{H}</math> NMR)<sup>b</sup> (Da)</b>
<b>PLA</b>	<b>40.000</b>	<b>56.000</b>	<b>1.40</b>	<b>N/A</b>	<b>N/A</b>
<b>PEG1%- g-PLA</b>	<b>13.000</b>	<b>17.000</b>	<b>1.30</b>	<b>0.34 %</b>	<b>9.000</b>
<b>PEG7%- g-PLA</b>	<b>4.000</b>	<b>8400</b>	<b>2.10</b>	<b>4.10 %</b>	<b>8.000</b>
<b>PEG20%- g-PLA</b>	<b>2200</b>	<b>2300</b>	<b>1.05</b>	<b>17.00 %</b>	<b>4.000</b>

N/A not analyzed

<sup>a</sup> Determined by GPC analysis using narrow molecular weight polystyrene standards.

<sup>a</sup> Mw/Mn =PDI of the polymers.

<sup>b</sup> Determined from the integration ratio of resonances due to PEG blocks at 3.64 ppm ( $-\text{O}-\text{CH}_2-\text{CH}_2-$ ) and to the PLA blocks at 5.17 ppm ( $\text{Me}-\text{CH}^* \begin{smallmatrix} \diagup \\ \diagdown \end{smallmatrix}$ ) in the  $^1\text{H}$  NMR spectra.

as well as lyophilized NPs. Freshly prepared NPs suspensions were found to be in the size range of 160–230 nm. Furthermore, a clear trend of decreasing the particle size was observed as their PEG content increased. Similar finding was obtained before with diblock copolymer PLA-PEG NPs [22]. The authors related that to the amphiphilic nature of PEG-PLA copolymers thus, reducing the interfacial tension between the aqueous and organic phases. Lyophilized NPs formulations showed larger particle size in the range of 300–400 nm compared to freshly prepared particles (Table 4.2). Thus, lyophilization process might induce particle aggregation. The size of the particles after freeze drying indicates that either a cryoprotectant or vigorous vortexing is needed to maintain the original size of the particles suspension. Vortexing for 5 min. of a suspension of lyophilized NPs in Milli.Q water was successfully able to break the aggregate and reduce

the size of the particles to almost its original size before lyophilization (Table 4.2). Particle size distribution data by DLS were also supplemented with a visual microscopic method like tapping mode atomic force microscopy (TM-AFM). Tapping mode atomic force microscopy (TM-AFM) is a versatile technique, which allows probing soft samples such as biological and polymeric materials [23, 24]. Figure 4.2 displays TM-AFM images of RHO-loaded PEG7%-g-PLA nanoparticles before and after lyophilization. The nanoparticles suspension before lyophilization has a roughly spherical morphology and sizes in the range of 100 and 250 nm, with most particles having a diameter of less than 200 nm [Figure 4.2 (a)]. While after lyophilization, it could be seen that particles showed some aggregating tendency confirming the size data obtained by DLS [Figure 4.2 (b)]. AFM phase image analysis was also done to investigate the surface chemistry of the obtained particles as used before in our previous studies [13, 14]. PEG7%-g-PLA NPs either before or after lyophilization showed the presence of an observable phase contrast at the surface of NPs revealed by some dark layers at the surface of bright cores [Fig. 4.2 (a, b); right panels, P]. These observations confirm the existence of PEG chains at the surface of PLA core. PEG-g-PLA NPs showed lower zeta potential values (close to zero) in comparison to the values reported before by other authors for PEG-b-PLA NPs [25-27] (Table 4.3). The greater reduction in zeta potential values of all PEG-g-PLA NPs of different PEG densities could be explained by the existence of a fraction of PVA at the surface of NPs (data not shown) which might have also played a role in masking the actual surface charge of PLA NPs. No significant difference in the zeta potential values of pegylated NPs of different PEG grafting densities was found (Table 4.3). This could also be explained by the same reason that the residual PVA chains at the NPs surface makes it difficult to estimate the real contribution of PEG coating density to surface charge reduction. What confirms this hypothesis that PLA NPs prepared by the same procedure also showed lower zeta potential values (-0.098 mV, Table 4.3) than expected (-40 mV) [25, 28, 29]. Zambaux et al. also reported a low zeta potential value of -4 mV for PLA NPs prepared with PVA as an emulsifier [30]. The zeta potential findings confirm that residual PVA remained onto NPs surfaces was able to reduce the actual zeta potential values of either PLA or PLA modified NPs (PEG-g-PLA). This could be explained by the ability of PVA to be adsorbed efficiently (not removed by successive

washing steps) onto the NPs surface masking the actual surface charge of PLA (resulted from COOH ionization).

**Table 4.2.** Size distribution characteristics for different NPs after different stages of preparation.

<i>NPs formulation</i>	<i>Size before Freeze drying (nm)<sup>a, b</sup></i>	<i>PDI<sup>c</sup></i>	<i>Size after Freeze drying (nm)<sup>a, b</sup></i>	<i>PDI<sup>c</sup></i>	<i>Size after Vortexing (nm)<sup>a, b</sup></i>	<i>PDI<sup>c</sup></i>
PLA	224.0±27	0.139	381.0±30	0.178	270.0 ±20	0.207
PEG1%-g-PLA	200.6±28	0.002	318.0±20	0.220	250.0 ± 41	0.161
PEG7%-g-PLA	185.6±21	0.161	388.0±14	0.078	230.0 ± 33	0.221
PEG20%-g-PLA	169.5±23	0.092	380.9±21	0.320	211.0 ± 23	0.159

<sup>a</sup> median.

<sup>b</sup> All values indicate mean±S.D. for n=3 independent measurements for the same batch.

<sup>c</sup> refers to polydispersity index.

#### 4.5.3. Encapsulation efficiency (EE)

As seen from Table 4.3, % EE of RHO was found to be between 10% and 68% wt/wt depending on the polymer type. Grafted pegylated polymers showed better % EE than PLA homopolymer. The higher the grafting density, the more the encapsulation efficiency. The last finding could be attributed to the enhanced steric hindrance of the more mobile PEG chains existing at the surface of pegylated NPs, thus reducing premature diffusion of rhodamine into the external aqueous phase during solidification of the NPs. Although higher loading is readily possible since RHO favorably interacts with PLA, this was not necessary as the particles were already easily detected by fluorescence at the concentration levels tested. In a previous study by Sheng et al. [22], haemoglobin

(HbP) was encapsulated into PLA-PEG block copolymer of different PEG contents. The % EE of HbP was found to increase by increasing the PEG content. But further increase of PEG content to 20 wt% caused an obvious decrease of % EE. In our case, increasing the grafting density to 20 mol% resulted in further increase in the % EE. This could be explained by the difference in the polymer architecture between PEG-g-PLA copolymer used in our study compared to PEG-b-PLA. PEG-g-PLA NPs exhibited different PEG chain organization pattern than their corresponding block copolymer NPs as confirmed before by us [13]. PEG chains are easily oriented towards the surface of PEG-g-PLA NPs compared to PEG-b-PLA NPs. This leads to effective surface coverage in case of PEG-g-PLA NPs thus reducing the premature diffusion of drug towards the aqueous phase. While in PEG-b-PLA, some PEG chains might be interpenetrated inside the PLA core particularly at high PEG content (e.g. 20%), enhancing water uptake by the matrix, and hence, facilitating drug diffusion towards the external aqueous phase.

**Table 4.3.** Other physicochemical characteristics for different NPs formulation.

<i>NPs formulation</i>	<i>% EE<sup>a</sup></i>	<i>% Lr (wt/wt)<sup>b</sup></i>	<i>Zeta potential (mV)</i>
<b>PLA</b>	<b>10.01±1.44</b>	<b>0.024±0.003</b>	<b>-0.098±3.78</b>
<b>PEG1%-g-PLA</b>	<b>31.11±2.94</b>	<b>0.073±0.007</b>	<b>0.273±3.27</b>
<b>PEG7%-g-PLA</b>	<b>37.85±0.97</b>	<b>0.090±0.002</b>	<b>0.012±3.72</b>
<b>PEG20%-g-PLA</b>	<b>67.79±0.92</b>	<b>0.163±0.002</b>	<b>0.003±4.42</b>

Targeted loading for all batches=0.24% (wt/wt)

All values indicate mean±S.D. for n=3 independent measurements.

<sup>a</sup> refers to encapsulation efficiency.

<sup>b</sup> refers to actual or real loading.

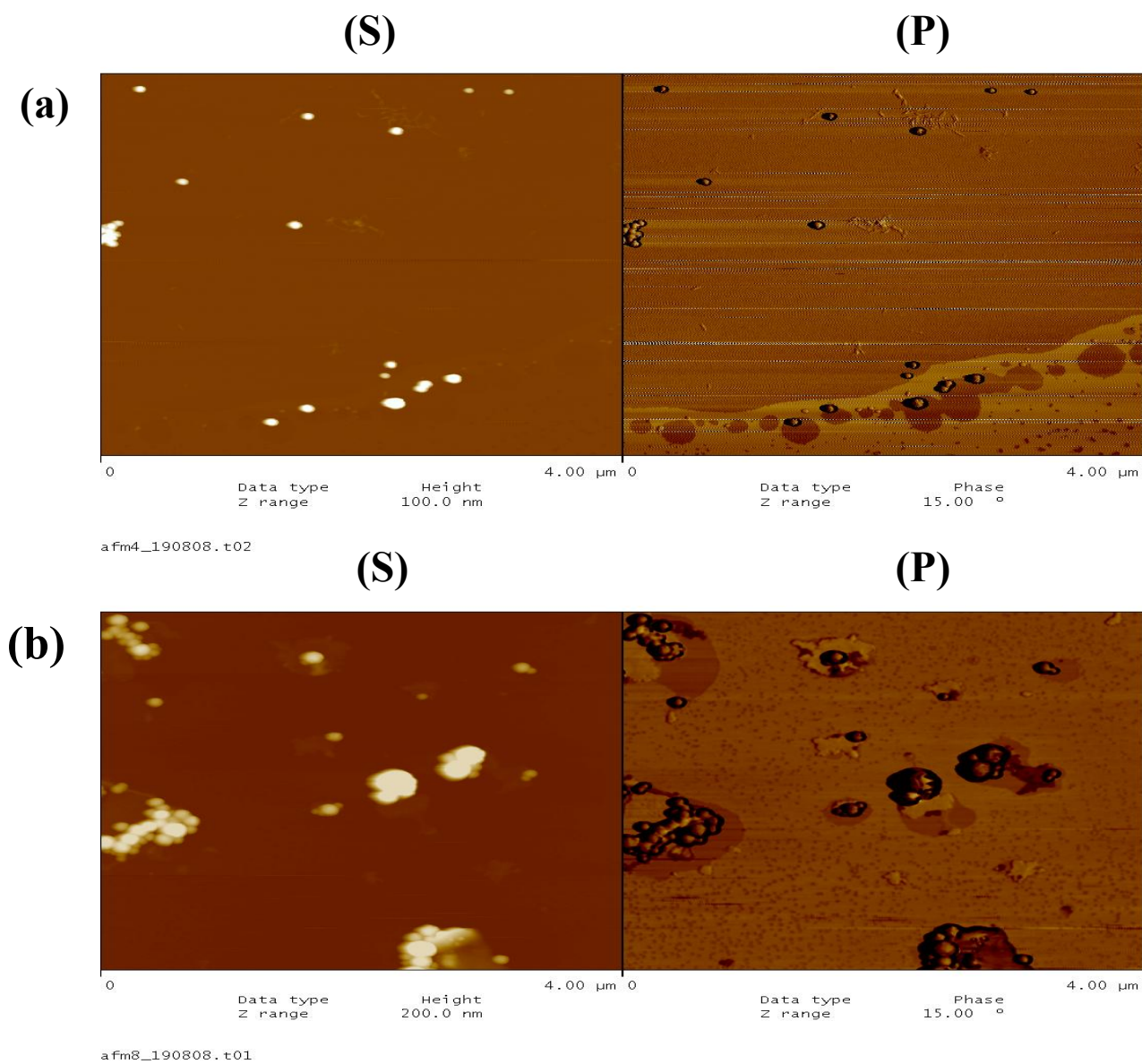


**Figure 4.2.** AFM images of PEG7%-g-PLA NPs encapsulating rhodamine B (RHO), before (a) and after (b) lyophilization; surface morphology (left, S) and phase image (right, P).

#### 4.5.4. In Vitro Drug Release.

An in vitro release study was conducted in PBS at 37  $^{\circ}\text{C}$  in order to evaluate if the fluorescent marker (RHO) remains associated to the particles for a prudential period of time suitable for tracking NPs inside the cells. This could help us decide if RHO loaded NPs formulation were an optimal formulation for cellular uptake studies with RAW264.7 cell lines. RHO release profile over a 15 days period is shown for particles made from

different pegylated polymers compared to PLA homopolymer. RHO was released slowly from different NPs compared to RHO release from solution (Fig. 4.3). Specifically, within 15 h less than 20% of the agent had been released when incubated at 37°C at pH 7.4. No significant difference in the release profile of NPs made from different PEG grating densities was seen. This might indicate the ability of the high  $M_{wt}$  PLA added into each NPs formulation to efficiently trap and control RHO release over a prolonged period of time. Importantly, and as will be described in the cellular uptake section, controlled release of RHO over a time period of 24 h is more than sufficient for studying the interaction and uptake of nanoparticles by cells in vitro.

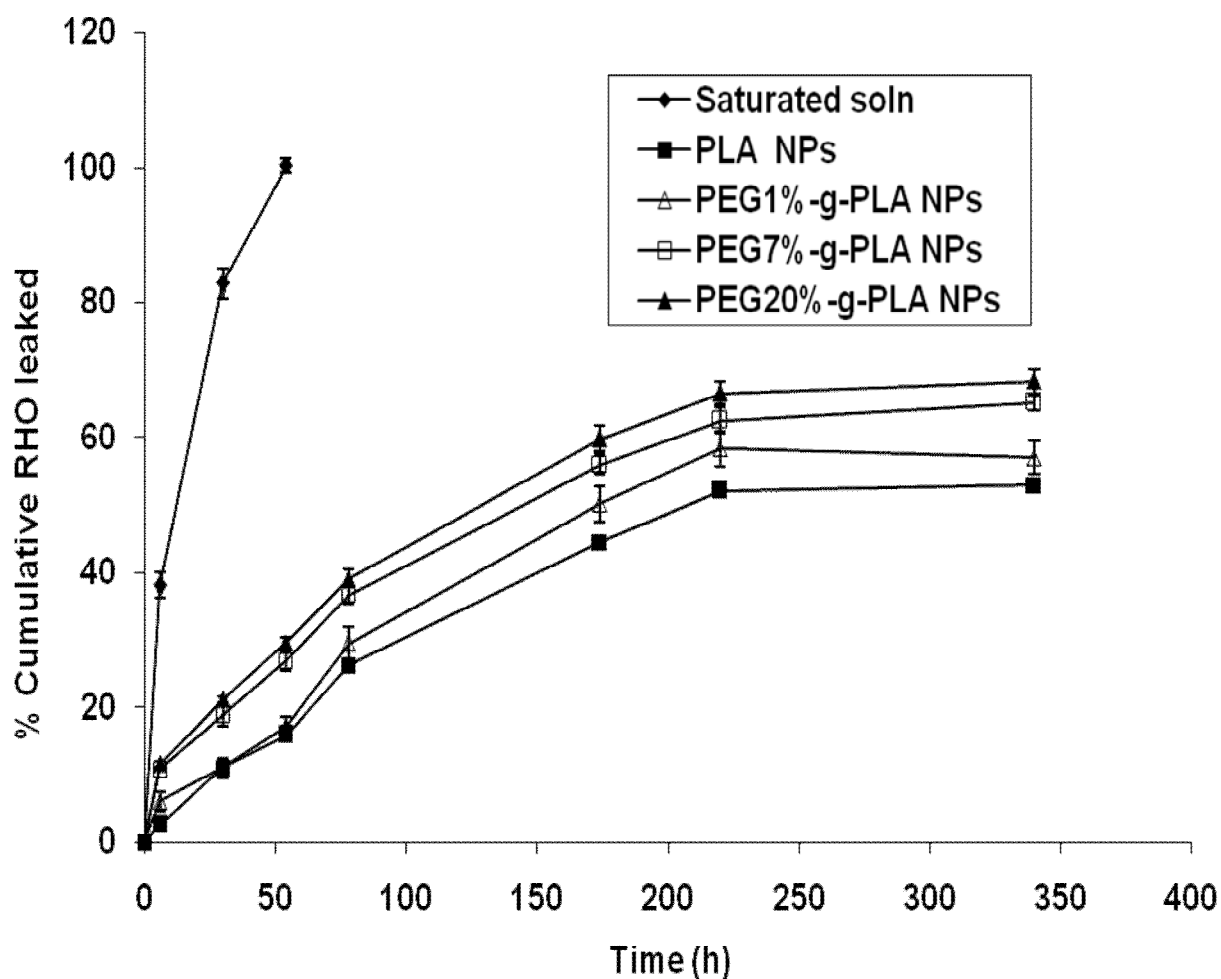


**Figure 4.3.** In vitro release behavior of RHO from different PEG-g-PLA NPs in comparison to PLA NPs and RHO solution; values are represented as mean  $\pm$ S.D. of three independent experiments.

#### 4.5.5. Plasma protein adsorption

It is well established that phagocytosis is a cellular phenomenon mainly initiated by the attachment of the foreign particles to the surface receptors of the phagocytic cells [31]. This phenomenon is facilitated by the adsorption of plasma proteins (opsonins) to the particle surface [32, 33]. Therefore, DLS was used to investigate the possibility of plasma protein (PP) adsorption onto the NPs surface and whether there is any difference between different NPs batches in their ability to adsorb PP. This was simply done by monitoring the size distribution changes of NPs after incubation for a period of time with plasma proteins solution. DLS was used to determine the fate of RHO loaded PEG-g-PLA NPs of different PEG grafting densities, first, in the presence of 5 % fetal bovine serum (5% FBS), and, second, in the presence of 2 % bovine serum albumin (2% BSA). RHO loaded PLA NPs was also included for comparison. DLS analysis was performed on solutions of 5% FBS, RHO loaded NPs in distilled water and RHO loaded NPs in the presence of 5 % FBS following incubation at 37 °C for 24 h. The same procedure was done with 2% BSA. DLS analysis of NPs in the presence of total serum is not possible as some blood proteins (i.e. immunoglobulins) form aggregates in aqueous solution. Size distribution analysis of 5% FBS solution revealed the presence of two size populations at ~ 10, and 66 nm (data not shown). Prior to incubation with 5% FBS the average diameter of all the investigated NPs was ranging from 200-260 nm (Fig.4.4). After 24 h incubation with 5% FBS the average diameter of both PEG7%-g-PLA, and PEG20%-g-PLA NPs remained nearly unchanged. While PLA and PEG1%-g-PLA NPs showed clear aggregating tendency evidenced by the larger size and the broader polydispersity indices obtained after incubation with 5 % FBS for 24 h [Figures 4.4 (a), and 4.S1 (a)]. This might indicate that either PEG7%-g-PLA or PEG20%-g-PLA NPs didn't adsorb significant quantities of plasma proteins compared to either PLA or PEG1%-g-PLA NPs. Bovine serum albumin (BSA) is the most abundant protein in serum. Many studies have shown before that the major protein adsorbed onto NPs surface is albumin [25, 34]. DLS analysis of NPs incubated with 2% BSA was also done under the same conditions as before with 5% FBS. Size distribution analysis of 2% BSA solution revealed the presence of two size populations at ~ 2, and 18 nm (data not shown). And as found with 5 % FBS, PLA and PEG1%-g-PLA NPs showed remarkable aggregating tendency evidenced by

size distribution change after incubation with 2 % BSA for 24 h [ Figures 4.4 (b), and 4.S1 (b)]. These observations confirm that either PEG7%-g-PLA or PEG20%-g-PLA NPs could withstand the serum environment and that protein adsorption onto their surface occurs to a limited extent, if at all [35].

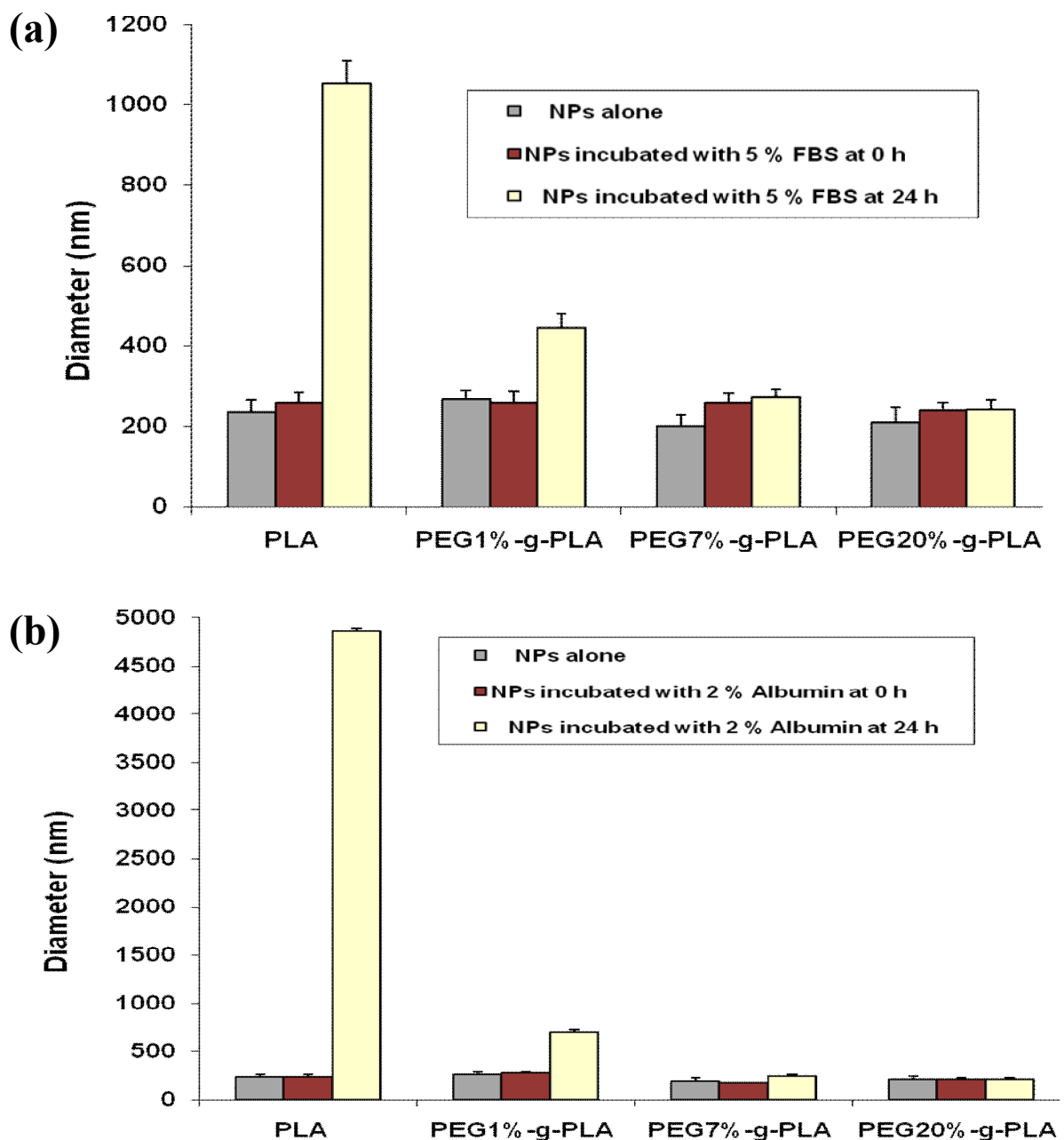


**Figure 4.4.** a): DLS size distribution data (nm) of different NPs upon incubation at 37 °C for 24 h with 5% FBS. b): DLS size data (nm) of NPs upon incubation at 37 °C for 24 h with 2% BSA.

#### 4.5.6. Cellular toxicity and uptake studies

PLA is a well-known biodegradable and biocompatible polymer. NPs made from PEG-g-PLA polymers of different PEG densities were well tolerated and exhibited no adverse effects on the cell viability as shown by cell proliferation assays (Fig. 4.5).

The interaction of RHO encapsulated nanoparticles with macrophage-like cells (RAW 264.7 cells) was first observed by fluorescence microscopy (Fig. 4.6). Microscopy studies showed that a higher fluorescence intensity, corresponding to higher RHO concentration, was observed in cells exposed to both RHO loaded PLA, and PEG1%-g-PLA nanoparticles [Fig. 4.6 (b, and c, respectively)] compared to cells exposed to either RHO loaded PEG7%-g-PLA or PEG20%-g-PLA NPs [Fig. 4.6 (d, and e, respectively)]. This finding might indicate that nanoparticles made with PEG-g-PLA showed less internalization by macrophage cells than PLA nanoparticles. Moreover, to achieve sufficient masking by PEG on the surface of the nanoparticles, PEG grafting density higher than 1 % is usually required to obtain lower internalization by macrophage cells.

To confirm the microscopy study results, estimation of the actual amount of NPs internalized after incubating RAW 264.7 cells for 24 h at 37 °C with different concentrations of RHO loaded NPs was investigated. Similar findings to microscopy results were obtained. Higher uptake was observed for PLA NPs as shown in Figure 4.7. This is the result of the higher hydrophobicity of PLA NPs. Increasing the incubated concentration resulted in an increase in the actual amount internalized. It is interesting to note that PEG-g-PLA NPs of different PEG densities resulted in lower degree of internalization compared to PLA NPs in macrophages cell lines. It also could be seen that the higher the PEG grafting density, the lower the uptake of NPs by macrophage cells. This may be ascribed to surface hydrophilicity and neutral charge of the grafted copolymer NPs. These results are in accordance with other authors [36-38] who have reported that the higher the hydrophilicity of the surface, the lower the adsorption of plasma proteins onto them and hence lower macrophage uptake. However, increasing the grafting density from 7% to 20 % didn't show significant differences in their uptake ability indicating that the steric effect of PEG is concentration dependent [39].

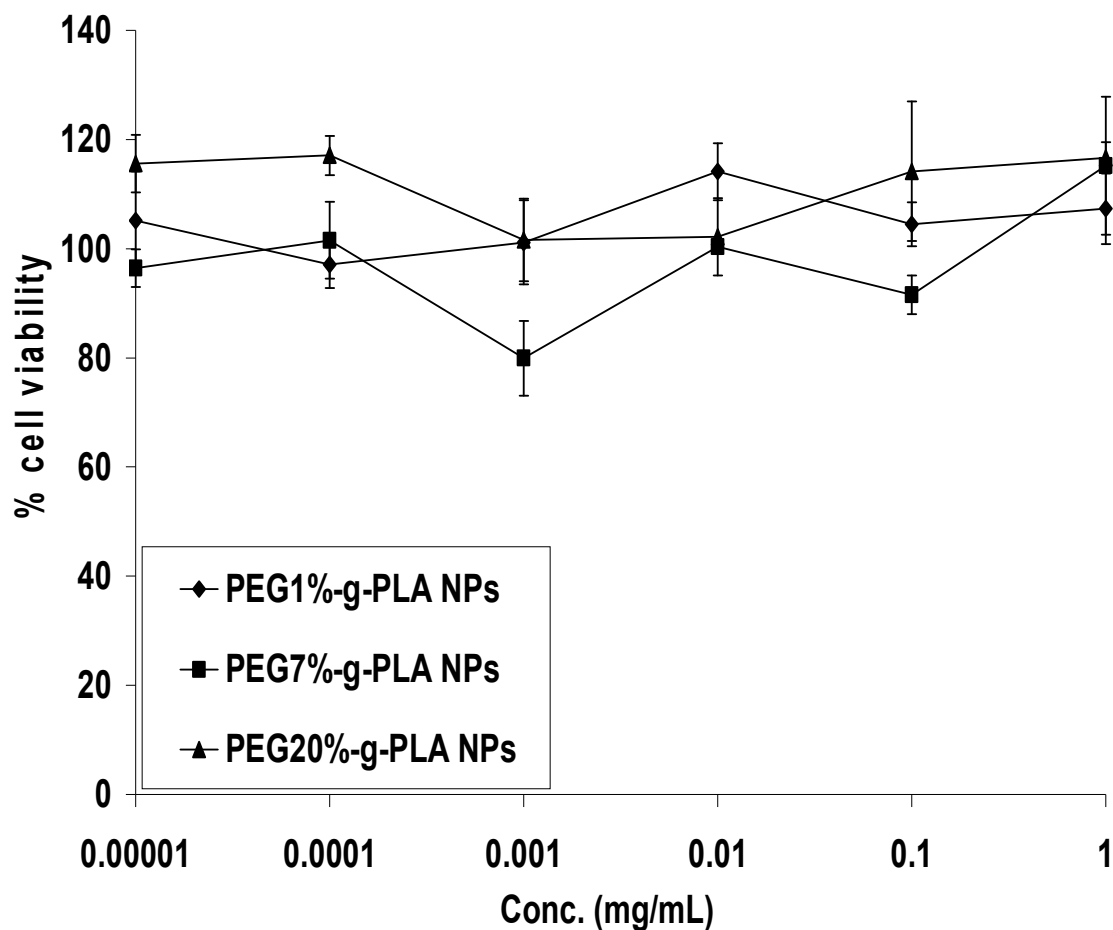


**Figure 4.5.** Cytotoxicity of pegylated NPs of different PEG grafting densities over PLA backbone (1, 7, and 20% mol/mol) in RAW 264.7 cells by MTT assay.

#### 4.6. Conclusions

In the present work, PEG-g-PLA copolymers of different PEG grafting density (1, 7, or 20% mol/mol of lactic acid monomer) were used to prepare nanoparticles loaded with the fluorescent agent RHO. These nanoparticles were designed as models for the study of particles uptake by RAW macrophage cells using confocal microscopy and fluorimetry analysis. An O/W emulsion solvent evaporation technique was utilized for preparation of nanoparticles. Spherical particles with sizes in the range of 150–250 nm were prepared with sufficient RHO encapsulation efficiency. Release studies revealed that RHO nanoparticles were optimal for cellular interaction studies because the agent is

released at a very slow rate. DLS analysis for qualitatively studying the extent of plasma proteins adsorption to nanoparticle surface was also described and showed that PEG-g-PLA NPs might adsorb less amount of PP onto their surface. In vitro cellular studies with RHO nanoparticles revealed that PEG7%-g-PLA NPs showed less internalization by RAW cells as determined by confocal microscopy and fluorimetry analysis. PEG20%-g-PLA did not show significant difference in their phagocytosis tendency compared to PEG7%-g-PLA. The obtained results suggest the possibility of use of grafted copolymer PEG-g-PLA NPs can be used as long-circulating drug carriers for intravenous administration. The optimal PEG grafting density required to achieve that might vary from 4-7 %. However, despite the promising ex vivo data, an actual in vivo data is needed to explore that indeed PEG-g-PLA NPs could exhibit stealth characteristics. A biodistribution study of Itraconazole loaded PEG-g-PLA NPs will be done in the future to support our preliminary data.

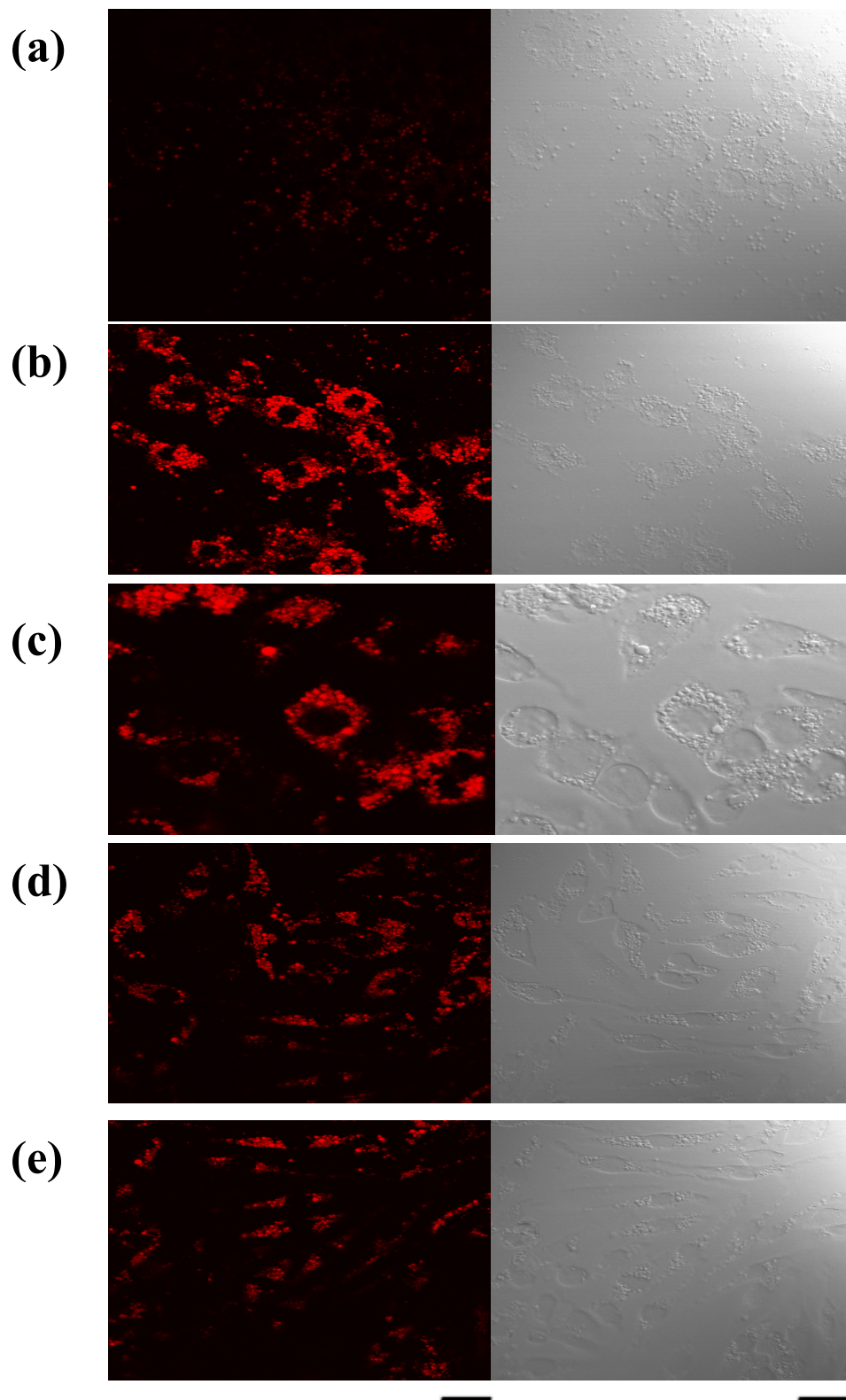


**Figure 4.6.** Fluorescence images (right panels) and their corresponding phase contrast images (left panels) of RAW 264.7 cells after incubation with a) RHO, b) RHO loaded PLA NPs, c) RHO loaded PEG1%-g-PLA NPs, d) RHO loaded PEG7%-g-PLA NPs, and d) RHO loaded PEG20%-g-PLA NPs. red images show RHO. Scale bar=50  $\mu$ m.

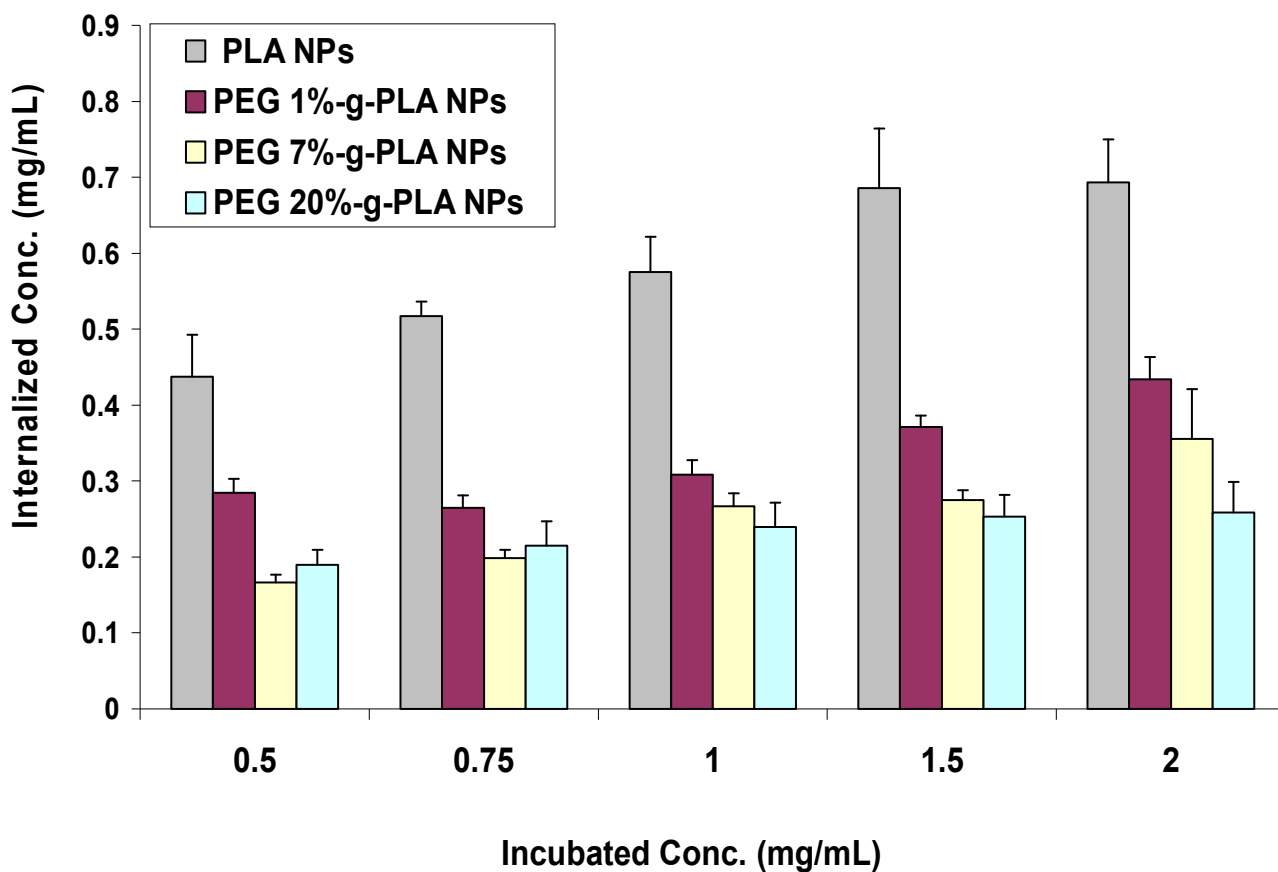


**Figure 4.7.** RAW 264.7 cellular uptake of RHO encapsulated NPs made from PEG-g-PLA copolymer of different PEG grafting densities in comparison to PLA NPs. RAW 264.7 cells were incubated with NPs at 37°C for 24 h.

#### 4.7. Appendix A. Supplementary material

Supplementary data associated with this article can be found, in the online version, at [doi:10.1016/j.ijpharm.2011.02.039](https://doi.org/10.1016/j.ijpharm.2011.02.039).

#### 4.8. Acknowledgment.

The work was supported in part by a grant of Fond Quebecois de la Recherche en Nature et Technologie (FQRNT). The authors wish to thank Prof. Jean François Bouchard, Ecole d'Optométrie, University of Montreal for his technical support using

CLSM. Sherief Essa thanks the Ministry of Higher Education, Egypt for granting him a scholarship during his Ph.D.

#### 4.9. References

1. Soppimath, K.S., Aminabhavi, T.M., Kulkarni, A.R., Rudzinski, W.E., 2001. Biodegradable polymeric nanoparticles as drug delivery devices. *Journal of Controlled Release* 70, 1-20.
2. Hans, M.L., Lowman, A.M., 2002. Biodegradable nanoparticles for drug delivery and targeting. *Current Opinion in Solid State and Materials Science* 6, 319-327.
3. Cohen, H., Levy, R.J., Gao, J., Fishbein, I., Kousaev, V., Sosnowski, S., Slomkowski, S., Golomb, G., 2000. Sustained delivery and expression of DNA encapsulated in polymeric nanoparticles. *Gene Therapy* 7, 1896-1905.
4. des Rieux, A., Fievez, V., Garinot, M., Schneider, Y.-J., Pr eat, V., 2006. Nanoparticles as potential oral delivery systems of proteins and vaccines: A mechanistic approach. *Journal of Controlled Release* 116, 1-27.
5. Panyam, J., Labhasetwar, V., 2003. Biodegradable nanoparticles for drug and gene delivery to cells and tissue. *Advanced Drug Delivery Reviews* 55, 329-347.
6. Wang, M.D., Shin, D.M., Simons, J.W., Nie, S., 2007. Nanotechnology for targeted cancer therapy. *Expert Review of Anticancer Therapy* 7, 833-837.
7. Delie, F., Berton, M., All mann, E., Gurny, R., 2001. Comparison of two methods of encapsulation of an oligonucleotide into poly(D,L-lactic acid) particles. *International Journal of Pharmaceutics* 214, 25-30.
8. Govender, T., Stolnik, S., Garnett, M.C., Illum, L., Davis, S.S., 1999. PLGA nanoparticles prepared by nanoprecipitation: drug loading and release studies of a water soluble drug. *Journal of Controlled Release* 57, 171-185.
9. Leo, E., Brina, B., Forni, F., Vandelli, M.A., 2004. In vitro evaluation of PLA nanoparticles containing a lipophilic drug in water-soluble or insoluble form. *International Journal of Pharmaceutics* 278, 133-141.

10. Mohanraj, V.J., Chen, Y., Nanoparticles - A review. 2007, Association of Crop Science, Uganda.
11. Magjarevic, R., Ling, Y., Huang, Y., Preparation and Release Efficiency of Poly (lactic-co-glycolic) Acid Nanoparticles for Drug Loaded Paclitaxel, in 7th Asian-Pacific Conference on Medical and Biological Engineering, Peng, Y., Weng, X., Editors. 2008, Springer Berlin Heidelberg. p. 514-517.
12. Nadeau, V., Leclair, G., Sant, S., Rabanel, J.-M., Quesnel, R., Hildgen, P., 2005. Synthesis of new versatile functionalized polyesters for biomedical applications. *Polymer* 46, 11263-11272.
13. Essa, S., Rabanel, J.M., Hildgen, P., 2010. Effect of polyethylene glycol (PEG) chain organization on the physicochemical properties of poly(D,L-lactide) (PLA) based nanoparticles. *European Journal of Pharmaceutics and Biopharmaceutics* 75, 96-106.
14. Essa, S., Rabanel, J.M., Hildgen, P., 2010. Effect of aqueous solubility of grafted moiety on the physicochemical properties of poly(D,L-lactide) (PLA) based nanoparticles. *International Journal of Pharmaceutics* 388, 263-273.
15. Meng, W., Parker, T.L., Kallinteri, P., Walker, D.A., Higgins, S., Hutcheon, G.A., Garnett, M.C., 2006. Uptake and metabolism of novel biodegradable poly (glycerol-adipate) nanoparticles in DAOY monolayer. *Journal of Controlled Release* 116, 314-321.
16. Esmaili, F., Ghahremani, M.H., Esmaili, B., Khoshayand, M.R., Atyabi, F., Dinarvand, R., 2008. PLGA nanoparticles of different surface properties: Preparation and evaluation of their body distribution. *International Journal of Pharmaceutics* 349, 249-255.
17. Betancourt, T., Shah, K., Brannon-Peppas, L., 2009. Rhodamine-loaded poly(lactic-co-glycolic acid) nanoparticles for investigation of in vitro interactions with breast cancer cells. *Journal of Materials Science: Materials in Medicine* 20, 387-395.
18. Cartiera, M.S., Johnson, K.M., Rajendran, V., Caplan, M.J., Saltzman, W.M., 2009. The uptake and intracellular fate of PLGA nanoparticles in epithelial cells. *Biomaterials* 30, 2790-2798.

19. Vila, A., Gill, H., McCallion, O., Alonso, M.J., 2004. Transport of PLA-PEG particles across the nasal mucosa: effect of particle size and PEG coating density. *Journal of Controlled Release* 98, 231-244.
20. Ishihara, T., Takahashi, M., Higaki, M., Takenaga, M., Mizushima, T., Mizushima, Y., 2008. Prolonging the in vivo residence time of prostaglandin E-1 with biodegradable nanoparticles. *Pharmaceutical Research* 25, 1686-1695.
21. Park, S.-J., Kim, S.-H., 2004. Preparation and characterization of biodegradable poly(L-lactide)/poly(ethylene glycol) microcapsules containing erythromycin by emulsion solvent evaporation technique. *Journal of Colloid and Interface Science* 271, 336-341.
22. Sheng, Y., Yuan, Y., Liu, C., Tao, X., Shan, X., Xu, F., 2009. In vitro macrophage uptake and in vivo biodistribution of PLA-PEG nanoparticles loaded with hemoglobin as blood substitutes: effect of PEG content. *Journal of Materials Science: Materials in Medicine* 20, 1881-1891.
23. Raghavan, D., Gu, X., Nguyen, T., VanLandingham, M., Karim, A., 2000. Mapping Polymer Heterogeneity Using Atomic Force Microscopy Phase Imaging and Nanoscale Indentation. *Macromolecules* 33, 2573-2583.
24. Kopp-Marsaudon, S., Leclere, P., Dubourg, F., Lazzaroni, R., Aime, J.P., 2000. Quantitative Measurement of the Mechanical Contribution to Tapping-Mode Atomic Force Microscopy Images of Soft Materials. *Langmuir* 16, 8432-8437.
25. Gref, R., Lück, M., Quellec, P., Marchand, M., Dellacherie, E., Harnisch, S., Blunk, T., Müller, R.H., 2000. 'Stealth' corona-core nanoparticles surface modified by polyethylene glycol (PEG): influences of the corona (PEG chain length and surface density) and of the core composition on phagocytic uptake and plasma protein adsorption. *Colloids and Surfaces B: Biointerfaces* 18, 301-313.
26. Beletsi, A., Panagi, Z., Avgoustakis, K., 2005. Biodistribution properties of nanoparticles based on mixtures of PLGA with PLGA-PEG diblock copolymers. *International Journal of Pharmaceutics* 298, 233-241.
27. Govender, T., Riley, T., Ehtezazi, T., Garnett, M.C., Stolnik, S., Illum, L., Davis, S.S., 2000. Defining the drug incorporation properties of PLA-PEG nanoparticles. *International Journal of Pharmaceutics* 199, 95-110.

28. Peracchia, M.T., Gref, R., Minamitake, Y., Domb, A., Lotan, N., Langer, R., 1997. PEG-coated nanospheres from amphiphilic diblock and multiblock copolymers: Investigation of their drug encapsulation and release characteristics. *Journal of Controlled Release* 46, 223-231.
29. Musumeci, T., Ventura, C.A., Giannone, I., Ruozi, B., Montenegro, L., Pignatello, R., Puglisi, G., 2006. PLA/PLGA nanoparticles for sustained release of docetaxel. *International Journal of Pharmaceutics* 325, 172-179.
30. Zambaux, M.F., Bonneaux, F., Gref, R., Maincent, P., Dellacherie, E., Alonso, M.J., Labrude, P., Vigneron, C., 1998. Influence of experimental parameters on the characteristics of poly(lactic acid) nanoparticles prepared by a double emulsion method. *Journal of Controlled Release* 50, 31-40.
31. Pratten, M.K., Lloyd, J.B., 1986. Pinocytosis and phagocytosis: the effect of size of a particulate substrate on its mode of capture by rat peritoneal macrophages cultured in vitro. *Biochimica et Biophysica Acta (BBA) - General Subjects* 881, 307-313.
32. Moghimi, S.M., Patel, H.M., 1998. Serum-mediated recognition of liposomes by phagocytic cells of the reticuloendothelial system - The concept of tissue specificity. *Advanced Drug Delivery Reviews* 32, 45-60.
33. Blunk, T., Hochstrasser, D.F., Sanchez, J.C., Müller, B.W., Müller, R.H., 1993. Colloidal carriers for intravenous drug targeting: Plasma protein adsorption patterns on surface-modified latex particles evaluated by two-dimensional polyacrylamide gel electrophoresis. *ELECTROPHORESIS* 14, 1382-1387.
34. Allémann, E., Gravel, P., Leroux, J.C., Balant, L., Gurny, R., 1997. Kinetics of blood component adsorption on poly(D,L-lactic acid) nanoparticles: Evidence of complement C3 component involvement. *Journal of Biomedical Materials Research* 37, 229-234.
35. Liu, J., Zeng, F., Allen, C., 2005. Influence of serum protein on polycarbonate-based copolymer micelles as a delivery system for a hydrophobic anti-cancer agent. *Journal of Controlled Release* 103, 481-497.
36. Prior, S., Gander, B., Blarer, N., Merkle, H.P., Subirá, M.L., Irache, J.M., Gamazo, C., 2002. In vitro phagocytosis and monocyte-macrophage activation

- with poly(lactide) and poly(lactide-co-glycolide) microspheres. *European Journal of Pharmaceutical Sciences* 15, 197-207.
37. Bazile, D., Prud'homme, C., Bassoullet, M.-T., Marlard, M., Spenlehauer, G., Veillard, M., 1995. Stealth Me.PEG-PLA nanoparticles avoid uptake by the mononuclear phagocytes system. *Journal of Pharmaceutical Sciences* 84, 493-498.
38. Verrecchia, T., Spenlehauer, G., Bazile, D.V., Murry-Brelief, A., Archimbaud, Y., Veillard, M., 1995. Non-stealth (poly(lactic acid/albumin)) and stealth (poly(lactic acid-polyethylene glycol)) nanoparticles as injectable drug carriers. *Journal of Controlled Release* 36, 49-61.
39. Mainardes, R.M., Gremiao, M.P., Brunetti, I.L., da Fonseca, L.M., Khalil, N.M., 2009. Zidovudine-loaded PLA and PLA-PEG blend nanoparticles: influence of polymer type on phagocytic uptake by polymorphonuclear cells. *Journal of Pharmaceutical Sciences* 98, 257-67.

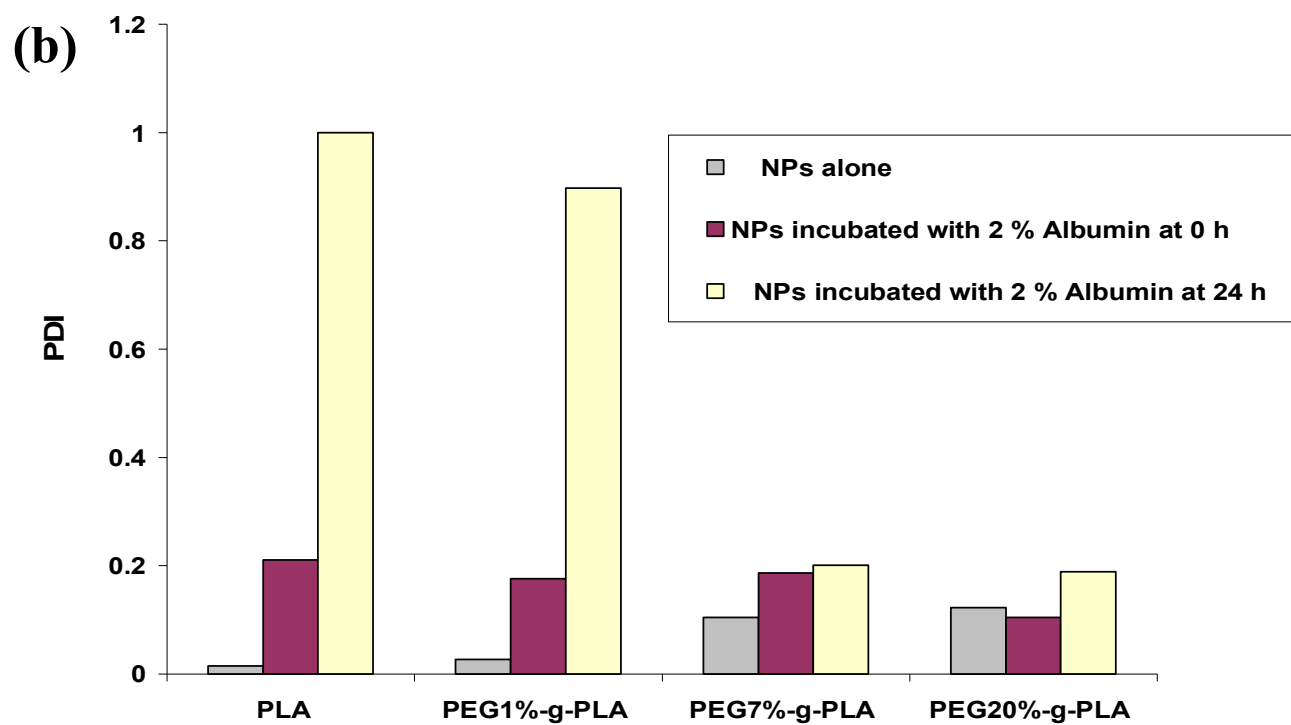


**Figure 4.S1.** a): Polydispersity index values of different NPs upon incubation at 37 °C for 24 h with 5% FBS. b): Polydispersity index values of NPs upon incubation at 37 °C for 24 h with 2%

DC A

## CHAPTER FIVE

---

### RESEARCH PAPER

#### **Improved Antifungal Activity of Itraconazole Loaded PEG/PLA Nanoparticles<sup>2</sup>.**

Sherief Essa<sup>1</sup>, Fatiha Louhichi<sup>2</sup>, Martine Raymond<sup>2</sup>, and Patrice Hildgen<sup>1</sup>.

<sup>1</sup> Faculty of pharmacy and <sup>2</sup> Institute for Research in Immunology and Cancer, Université de Montréal, C.P. 6128, succursale centre-ville, Montréal. Québec, Canada, H3C 3J7

**International Journal of Nanomedicine (To be submitted)**

---

<sup>1</sup> My contribution included designing the experiments, polymer synthesis, nanoparticles preparation and characterization, interpreting the results and writing the paper, which was supervised by Dr. Patrice Hildgen. Fatiha Louichi contribution involved testing the antifungal activity of itraconazole loaded nanoparticle formulations, which was supervised by Dr. Martine Raymond.

## 5.1. Abstract

PEG/PLA nanoparticles containing the hydrophobic antifungal itraconazole (ITZ) were developed to provide a controlled release pattern of ITZ as well as to improve its aqueous dispersability and hence enhance its antifungal action. Two PEG/PLA copolymers (PEGylated PLA polymers) were used in this study; branched PEGylated polymer in which PEG was grafted on PLA backbone at 7% (mol/mol of lactic acid monomer), PEG7%-g-PLA, and multiblock copolymer of PLA and PEG, (PLA-PEG-PLA)<sub>n</sub> with nearly similar PEG insertion ratio and similar PEG chain length. ITZ loaded PLA NPs were also prepared and included in this study as a control. ITZ-NPs were prepared from a 1:1 w/w blend of PLA and each PEGylated polymer either PEG7%-g-PLA or (PLA-PEG-PLA)<sub>n</sub> using an oil-in-water emulsion (O/W) evaporation method. The nanoparticles morphology, size and size distribution, zeta potential, loading efficiency, release profile, and antifungal activity were characterized. All ITZ-NPs were nearly spherical with smooth surface and showed less aggregating tendency with a size range 185- 285 nm. All ITZ-NPs measured nearly neutral zeta potential values close to 0 mV. The % LE of ITZ was ~94% for PEG7%-g-PLA NPs and ~83% for (PLA-PEG-PLA)<sub>n</sub> at 15.3% w/w theoretical loading. PEG/PLA NPs were stable over time regarding size and size distribution, and % ITZ loading efficiency (% LE). ITZ release showed an initial burst followed by a gradual release profile for ITZ-NPs over 5 days. (PLA-PEG-PLA)<sub>n</sub> NPs exhibited faster release rates than PEG7%-g-PLA NPs particularly at the last two days. DSC and PXRD data confirmed that ITZ exists in an amorphous state or a solid solution state into the NPs matrix. FT-IR revealed the possibility of chemical interaction between ITZ and the NPs matrix polymer indicating the successful entrapment of ITZ inside the particles. In Hemolysis test, ITZ-NPs caused mild hemolysis over the concentration range (5-20 µg/mL) compared to free itraconazole (ITZ), indicating better safety profile of ITZ-NPs. ITZ loaded PEG/PLA NPs inhibited fungal growth more efficiently than either free ITZ or ITZ loaded PLA NPs. Our results suggest that PEG/PLA-ITZ could be used efficiently as a nanocarrier to improve the aqueous dispersability of ITZ, control its release over time and thereby enhance its antifungal efficacy.

## 5.2. Keywords

Nanoparticles, PEG-PLA, itraconazole, antifungal, poor solubility, hemolysis.

## 5.3. Introduction

In recent years, fungal infections have become a serious health issue [1, 2], particularly in elderly patients, patients with neoplastic diseases, transplant surgeries, and the acquired immune deficiency syndrome (AIDS). Those patients have in common an immune system compromised by age, aggressive anticancer and antibacterial chemotherapy and long term use of immuno-suppressive agents after oral transplantation [3]. Moreover, spreading of clinical and microbiological resistance to current treatment and emergence of new pathogens have emerged the need for new effective management for those infections.

The widespread use of many available antifungal agents (amphotericin B, flucytosine, miconazole, itraconazole, and ketoconazole) has achieved considerable success in treating fungal infections despite their potential limitations as poor solubility and higher toxicity. Itraconazole (ITZ) is a triazole antifungal agent widely used clinically against a broad spectrum of fungal species such as those commonly caused by *Candida albicans* and *Aspergillus* species [4, 5]. Moreover, ITZ is highly effective for the treatment of both systemic fungal infections and superficial mycoses. Compared with other conventional antifungal agent, itraconazole has less nephrotoxicity than amphotericin B (AmB) [6, 7]. ITZ shows better activity and less resistance by many fungal species in comparison to other azole antifungals, such as fluconazole, voriconazole, and ketoconazole [8]. However, ITZ is poorly absorbed when given orally since ITZ is a hydrophobic weak base with a low aqueous solubility of approximately 1 ng/ml at pH 7 [9]. An acidic medium, such as the gastric environment of the stomach, enhances its solubilization (4 g/ml at pH 1), which in turn increases its absorption [10]. An intravenous formulation for ITZ has been previously developed by complexing the drug with hydroxypropyl- $\beta$ -cyclodextrin (HP- $\beta$ -CD) in an attempt to enhance ITZ aqueous solubility. However, the accumulation of HP- $\beta$ -CD can potentially lead to toxicity limiting the frequency of intravenous doses [11]. This is always a major concern for patients with renal complications, since the reduced clearance rate of HP- $\beta$ -CD could

lead to extensive accumulation of HP- $\beta$ -CD reaching toxic levels [10, 12]. Also, it has been reported that HP- $\beta$ -CD caused pancreatic adenocarcinoma in rat carcinogenicity study [13]. There is an urgent need to develop ITZ formulations able to enhance its solubility, absorption and hence, improve its bioavailability. To address this concern, many formulations of ITZ such as emulsion [11], polymeric micelle [12], nanosuspension [14] and albumin bound nanoparticles [10] have been recently developed and studied.

Polymeric nanoparticles (NPs) prepared using either PLA (polylactic acid) or PLGA (polylactic-*co*-glycolic acid), have been widely used as a drug delivery tool due to their biodegradable and biocompatible nature, and controlled release characteristics [15, 16]. Encapsulating bioactive moieties into these particles is expected to protect them from premature degradation, increase their solubility, and release the drug in a controlled fashion as shown before with other azole antifungal drugs [17]. The combined effect of these factors can lead to increased bioavailability and enhanced antifungal activity. Previous studies have shown improved bioavailability and reduced toxicity of AmB loaded PLGA nanoparticles compared to the commercially available form, Fungizone® [18]. Similarly, the antifungal activity of voriconazole loaded PLGA NPs was enhanced compared to free voriconazole [19]. PEG/PLA NPs has also been used as a nanocarrier for various anticancer and antibacterial agents, achieving sustained and targeted drug concentrations at infected areas [20, 21]. PEG/PLA NPs offers an advantage over naked PLA particles in which the presence of PEG on the surface of PLA could confer a longer circulation of the particles in the blood [22, 23]. Studies have shown enhanced cellular uptake of PEG/PLA nanoparticles by various cancer cell lines, improving drug action and reducing its accumulation in healthy tissue [24-26].

To the best of our knowledge, neither PLA nor PEG/PLA NPs was investigated before as a vector for the delivery of an antifungal drug. The purpose of this study was first to develop a nanocarrier drug delivery system for the encapsulation of the hydrophobic drug, ITZ into either PLA or PEG-modified PLA polymers. Second to test the antifungal capability of ITZ loaded NPs in vitro using both *Candida* and *Aspergillus* species. Two PEG modified PLA polymers (PEGylated polymers) were used in this study; branched PEGylated polymer in which PEG was grafted on PLA backbone at 7% grafting density (mol/mol of lactic acid monomer), PEG7%-g-PLA, and multiblock

copolymer of PLA and PEG, (PLA-PEG-PLA)<sub>n</sub> with nearly similar PEG insertion ratio and similar PEG chain length. The capability of both polymers to act as drug carrier was previously investigated by us using ibuprofen as a model drug [27].

## 5.4. Material and methods:

### 5.4.1. Materials:

D,L-Lactide, poly(ethylene glycol) methyl ether (MePEG; 2000 Da), poly(ethylene glycol) (PEG, 1500 Da), allyl glycidyl ether, tetraphenyltin, polyvinyl alcohol (PVA, average  $M_w$  9000-10,000 Da, 80% hydrolyzed), borane-tetrahydrofuran complex (1 M), acetone, toluene, pyridine, acetonitrile (ACN), chloroform, succinic acid, 1-ethyl-3-[3-dimethylaminopropyl]-carbodiimide (EDC), 4-dimethylaminopyridine (4-DMAP), diethyl ether, N,N-dimethylformamide, Tween® 80, *dimethyl sulfoxide* ([DMSO](#)), and thionyl chloride were purchased from Aldrich Chemical Company Inc., Milwaukee, USA. Itraconazole was purchased from PI chemicals Ltd., Shanghai, China. Sodium hydroxide pellets were purchased from Anachemia Canada Inc. and dichloromethane (DCM) was purchased from Laboratoire Mat Inc., Montreal, Quebec, Canada. *C. albicans* and *A. fumigates* clinical strains were obtained from the Laboratoire de Santé Publique du Québec, Canada.

### 5.4.2. Synthesis of Polymers.

A detailed description of the synthetic protocols used for polymers synthesis was reported earlier by our group [27-29]. Briefly, Poly (D,L)-lactide (PLA) was synthesized by ring opening polymerization of D,L-lactide in argon atmosphere, using tetraphenyltin as the catalyst. The polymerization step was performed at 180 °C for 6 h in a round-bottom flask and purged thoroughly with argon. The final polymer was purified by dissolving in acetone and precipitating in water.

Polymer with poly(ethylene glycol)-grafted randomly on poly(D,L)-lactide at 7% grafting density, PEG7%-g-PLA (PEG;  $M_{wt}$  2000 Da) was synthesized in the laboratory and the detailed procedure can be found in ref. [28]. Multiblock copolymer, (PLA-PEG-PLA) $_n$  was also synthesized as previously reported [30] using PEG with  $M_n$  of 1500 and succinic acid was used as condensing agent to link triblock copolymers. (PLA-PEG-PLA) $_n$  was synthesized to yield a PEG (1500)/lactic acid monomer ratio of 7% (mol/mol).  $^1\text{H}$  NMR spectra were recorded on a Bruker ARX 400 MHz spectrometer (Bruker Biospin, Billerica, MA). Chemical shifts ( $\delta$ ) were measured in parts per million (ppm) using tetramethylsilane (TMS) as an internal reference. Gel permeation chromatography (GPC) was performed on a Water Associate chromatography system (Waters, Milford, MA) equipped with a refractive index detector and a Phenomenex Phenogel 5  $\mu$  column. Polystyrene standards were used for calibration with THF as the mobile phase at a flow rate of 0.6 mL/min.

#### **5.4.3. Preparation of nanoparticles (NPs)**

ITZ loaded NPs were prepared by an O/W emulsion-solvent evaporation method. NPs were prepared using a 1:1 w/w blend of high  $M_{wt}$  PLA with each pegylated polymer either PEG7%-g-PLA or (PLA-PEG-PLA) $_n$  to ensure high retaining ability of NPs for ITZ. ITZ loaded NPs were prepared using an initial loading of 15.3 % w/w of each polymer blend. Briefly, 180 mg ITZ was first dissolved in the organic phase, 10 mL DCM followed by dissolution of each polymer blend (1 g) in the same phase. The organic phase was then emulsified into 30 mL PVA solution (0.5% w/v) as an external aqueous phase using high-pressure homogenizer (Emulsiflex C30, Avestin, Ottawa, Canada) at a pressure of 10,000 psi for 5 min. The O/W emulsion was collected by washing with

another 30 mL of 0.5% PVA. The DCM was evaporated under reduced pressure with constant stirring to obtain the NPs. Finally, NPs obtained as a suspension were then collected by centrifugation at 18500 rpm for 30 min. at 4 °C (Sorval® Evolution<sub>RC</sub>, Kendro, USA), washed four times with distilled water, then lyophilized without adding any cryoprotectant to obtain dry NPs (Freeze Dry System, Lyph.Lock 4.5, Labconco) and stored at 4 °C until further use.

#### **5.4.4. Characterization of NPs**

Dynamic light scattering (DLS) technique; Malvern Autosizer 4800 instrument (Malvern Instruments, Worcestershire, UK) was used for measuring both size and size distribution of NPs. Lyophilized NPs (1 mg) were dispersed into 10 mL Milli-Q Water and size measurements were recorded at a temperature of 25 °C and a scattering angle of 90°. Size distributions data were obtained from the autocorrelation functions using the CONTIN program. Measurements were done in triplicate. Malvern ZetaSizer Nanoseries ZS (Malvern Instruments, Worcestershire, UK) was used to measure the zeta potential of the nanoparticles as follows; Lyophilized NPs were suspended in 0.25% (w/v) saline solution (pH 7.4), sonicated for 1 min. and zeta potential was recorded in triplicate. Atomic force microscopy technique (AFM) was used to examine the nanoparticle morphology. AFM was performed with Nanoscope IIIa, Dimension™ 3100 (Digital Instruments, Santa Barbara, CA) in tapping mode. Samples were prepared by suspending the nanoparticles in water at a concentration of 10 mg/mL. These samples were deposited on freshly cleaved mica surface and were allowed to dry at room temperature. Subsequently, they were imaged in air at ambient conditions using etched silicon probes with tip radius of 5-10 nm and spring constant in the range of 20-100 N/m, oscillated at its fundamental resonant frequency (200-400 KHz).

#### 5.4.5. Loading efficiency (% LE)

A weighed amount of lyophilized NPs was dissolved into acetonitrile (ACN) followed by 5 min. vortexing and then stirring for 1 h to ensure complete dissolution of the particles. Itraconazole (ITZ) absorbance was measured at a wavelength ( $\lambda_{\text{max}}$ ) of 265 nm with a UV/ visible spectrophotometer (U-2001 spectrophotometer, Hitachi). ITZ concentration was determined using a standard curve of ITZ in acetonitrile solution (ACN). Percent loading efficiency (% LE) and percent drug loading (% DL) were calculated based on the following equations:

$$\% \text{ LE} = \frac{\text{Weight of drug entrapped in NPs}}{\text{Initial weight of drug added}} \times 100 \quad (1)$$

$$\% \text{ DL} = \frac{\text{Weight of drug entrapped in NPs}}{\text{Weight of NPs}} \times 100 \quad (2)$$

#### 5.4.6. Stability studies

Physical stability of the developed nanoparticles was monitored by following the particle size, polydispersity index, and loading efficiency (% LE) over time. A weighed amount of nanoparticles was reconstituted in PBS, pH 7.4 then stored for 30 days at room temperature. Size and size distribution was measured by DLS as described above in section 2.4. For loading efficiency, the amount of ITZ remaining in solution was measured using UV spectroscopy after extracting ITZ into ACN and then ITZ concentration was measured as described in section 2.5.

#### **5.4.7. Differential scanning calorimetry (DSC)**

The DSC measurements were performed on a Jade DSC instrument (PerkinElmer, USA). Simply, a weighed amount (5 mg) was sealed in crimped aluminum pans and heated at a rate of 10°C /min from -20° to 200°C. An empty aluminum pan was used as a reference and nitrogen gas was purged at a speed of 20 mL/min.

#### **5.4.8. Powder X-ray diffractometry (PXRD)**

The powder X-ray diffraction patterns were acquired using a powder X-ray diffractometer (D8, Bruker, Germany). X-ray diffraction patterns were carried out for ITZ, ITZ-polymer physical mixtures and ITZ loaded nanoparticles (ITZ-NPs). All experiments were performed at room temperature. The conditions of the operation were as follows: a voltage of 40 kV and a current of 40 mA in the region of  $5^\circ \leq 2\theta \leq 40^\circ$  in step scan mode of 0.02° per second.

#### **5.4.9. Fourier transform infrared spectroscopy (FT-IR) study**

FT-IR spectra were obtained using FT-IR spectrophotometer (Thermo Scientific Nicolet iS10 FT-IR Spectrometer) equipped with attenuated total reflection (ATR) cell. About 10 mg of sample was introduced onto the ATR crystal followed by acquisition of FT-IR spectra over the scanning range of 600–4000  $\text{cm}^{-1}$ .

#### **5.4.10. In vitro drug release study**

In vitro release of itraconazole from ITZ-NPs was performed in triplicates as follows: 5mL of 3.3 mg/mL ITZ-NPs in PBS (10mM, pH 7.4) was sealed in a dialysis bag (Spectra Por 1 membrane, 6–8 kDa cut-off). The dialysis bag was immersed in a screw-capped tube of 45 mL PBS containing 10% (v/v) Tween® 80. The tubes were shaken at 100 rpm on a horizontal water bath shaker (orbit shake bath, Labline) and maintained at  $37 \pm 0.5$  °C. At certain time intervals, sample (5 mL each) was withdrawn from the medium and same volume of fresh medium was added. ITZ solution at 1.5 mg/mL in a solvent mixture of water: DMSO (1:3 v/v) was used as a control. The absorbance of the drug in the release samples was determined by UV spectrophotometry at 263 nm (U-2001 UV/Visible spectrophotometer, Hitachi). The concentration of ITZ

was determined from a calibration curve of ITZ in PBS containing 10% (v/v) Tween® 80.

#### 5.4.11. Hemolysis test

The lysis of erythrocytes by ITZ NPs was determined by incubating NPs with freshly isolated rat RBCs. Blood was collected from Wistar rats in heparinated collection vials as per Canadian guidelines for laboratory animals and animal ethical committee of University of Montreal. It was centrifuged at 5000 rpm for 10 min, washed with 0.1 M phosphate buffered saline (PBS, pH 7.4) three times to obtain RBCs. RBCs were diluted to 10 % with PBS [31]. 0.9 mL of NPs samples in PBS were incubated with 0.1 mL of RBC suspension at 37°C for 2 h. After incubation, tubes were centrifuged at 5000 rpm to remove non-lysed RBCs. Control experiments to determine basal lysis of RBCs by PBS and 100 % lysis by 0.3% Triton X-100 were also carried out. The supernatant was collected and analyzed by UV spectrophotometer at 540 nm to estimate the amount of hemoglobin released. Hemolysis was calculated by the following equation:

$$\% \text{ Hemolysis} = \frac{(\text{Abs}_{\text{sample}}) - (\text{Abs}_{\text{basal}})}{(\text{Abs}_{100\%}) - (\text{Abs}_{\text{basal}})} \times 100 \quad (3)$$

Where,  $\text{Abs}_{\text{sample}}$ ,  $\text{Abs}_{\text{basal}}$  and  $\text{Abs}_{100\%}$  are absorbance values of sample, basal lysis by PBS and 100 % lysis by 0.3% Triton X-100, respectively.

#### 5.4.12. Fungal Growth Inhibition Studies

The antifungal action of ITZ-NPs was tested on fungal growth as follows: growth inhibition on a lawn of conidia in a petri plate of either *Candida albicans* or *Aspergillus fumigatus*. ITZ-NPs were compared against two drug formulations consisting of ITZ in water (ITZ-Water) and an ITZ solution in DMSO (ITZ-DMSO). Stock solutions of ITZ-Water, ITZ-DMSO, and ITZ-NPs in water were prepared at 1 mg/ml. Solvents and blank NPs were used as controls. Actual ITZ concentrations tested against fungal strains were 20 µg/ml for *C.albicans* and 17 µg/ml for *A. fumigatus*.

#### **5.4.13. Strains and growth media**

*Candida albicans* SC5314 clinical strain was used in this study. Cells were grown at 30 °C in YPD (1% yeast extract, 2% Bacto Peptone and 2% glucose), including 2% agar for solid medium. The *Aspergillus fumigatus* MY070968 clinical strain was grown on complete medium (CM) plates (0.1% yeast extract, 0.2% Bacto Peptone, 1% glucose, 0.15% casamino acids, 0.6% NaNO<sub>3</sub>, 0.05% KCl, 0.05% MgSO<sub>4</sub>.7H<sub>2</sub>O, 1% Vitamin stock solution, pH 6.8 and 2% agar).

#### **5.4.14. Petri Plate Culture**

##### **5.4.14.1. *C. albicans***

Cells grown overnight were resuspended in YPD to an optical density at 600 nm (OD<sub>600</sub>) of 0.1 and 150 µl of cells were spread on YPD plates. A filter paper disc was placed in the center of each plate and 12.5 µl of each of the ITZ solutions was added to the disc. The plates were incubated for 2 days at 30 °C before measuring the diameter of the zones of growth inhibition. Digital photos of the cultures were taken after treatments were initiated to assess the antifungal activity.

##### **5.4.14.2. *A. fumigatus***

Cells were thawed from -80 °C glycerol stock onto CM plates and grown for 3 days at 30 °C. Spores were transferred with a toothpick onto equal conc. of ITZ-containing CM plates and incubated at 30 °C for 3 days. Digital photos of the cultures were taken after treatments as before with *C. albicans*.

#### **5.4.15. Statistical analysis**

Results were expressed as mean ± SD. All data were generated in three independent experiments with two or three repeat. The t-test and the one-way analysis of variance (ANOVA) were performed to compare two or multiple groups, respectively. The difference between treatments was considered to be significant at a level of p<0.05. Statistical analysis was performed for sizing, zeta potential, release, and loading efficiency, hemolysis and antifungal activity.

## 5.5. Results and discussion:

Our previous development of PEG/PLA polymeric NPs either made from PEG-g-PLA or (PLA-PEG-PLA)<sub>n</sub> with suitable drug delivery properties e.g. small size, higher loading efficiency, and prolonged release features led us to investigate the applicability of PEG/PLA as an efficient drug carrier [27]. We hypothesized that the presence of PEG on the surface of PLA particles and a small particle size would improve the potential of PEG/PLA as carrier for the hydrophobic drug, ITZ. To achieve this, we first synthesized PEG-g-PLA, and (PLA-PEG-PLA)<sub>n</sub> copolymers with nearly similar PEG insertion ratio and similar PEG chain length to facilitate the comparison between both PEGylated polymers. Then, PEG/PLA nanoparticles loaded with itraconazole (ITZ) were prepared in attempt to investigate the ability of such particles to enhance ITZ dispersability in water, control its release over time and potentially improve its bioavailability. The extent of PEG/PLA particles to enhance the antifungal action of ITZ was tested in vitro using both *Candida* and *Aspergillus* clinical strains.

### 5.5.1. Characterization of Polymers.

The same polymers used in this study were previously described and characterized by us [27]. For a detailed discussion of the characterization results including <sup>1</sup>H-NMR and GPC data, please refer to both Figure 1 and Table 1 in the last cited article.

### 5.5.2. NPs characterization.

ITZ-NPs were successfully prepared using an O/W emulsion solvent evaporation method by co-dissolving ITZ and polymer blend [1:1 w/w of PLA: each PEGylated polymer either PEG7%-g-PLA or (PLA-PEG-PLA)<sub>n</sub> in DCM and precipitating the polymer into nanoparticles in an aqueous phase having 0.5 % PVA as a stabilizer after organic solvent evaporation. Major physicochemical characteristics of ITZ-NPs e.g. loading efficiency (% LE), particle size, PDI and zeta potential are shown in Table 5.1. Particle size distribution by dynamic light scattering (DLS) showed unimodal distribution

**Table 5.1.** Characteristics of different NPs formulations after lyophilization process.

<i>Formulation</i>	<i>Mean diameter (nm)</i>	<i>PDI<sup>a</sup></i>	<i>% DL (% w/w)<sup>c</sup></i>	<i>% LE<sup>b</sup></i>	<i>Zeta-potential (mV)</i>
<b>PLA</b>	<b>284 ± 4</b>	<b>0.18</b>	<b>9.4 ± 0.3</b>	<b>61.7 ± 1.7</b>	<b>0.11 ± 4</b>
<b>PEG7%-g-PLA</b>	<b>197 ± 6</b>	<b>0.08</b>	<b>14.3 ± 0.3</b>	<b>93.6 ± 1.8</b>	<b>0.02 ± 3</b>
<b>(PLA-PEG-PLA)n</b>	<b>185 ± 4</b>	<b>0.05</b>	<b>12.6 ± 0.4</b>	<b>82.7 ± 2.7</b>	<b>0.03 ± 4</b>

<sup>a</sup> refers to polydispersity index.

<sup>b</sup> refers to loading efficiency.

<sup>c</sup> refers to drug loading.

*All values indicate mean±S.D. for n=3 independent measurements for the same particle preparation.*

for lyophilized ITZ-NPs. All ITZ-NPs formulations showed particle size in the range of 185–285 nm (Table 5.1). ITZ loaded PEG/PLA NPs either made from PEG7%-g-PLA, or (PLA-PEG-PLA)n NPs showed smaller size compared to ITZ-PLA NPs as shown in the same table. This could be due to the amphiphilic nature (surfactant effect) of PEG/PLA copolymer thus, reducing the size of the emulsion droplet during the emulsification process [32, 33]. Particle size distribution data and NPs morphology were also investigated using a visual microscopic method like tapping mode atomic force microscopy (TM-AFM). Figure 5.1 displays TM-AFM images of ITZ-loaded PEG7%-g-PLA nanoparticles after lyophilization. Lyophilized NPs were nearly spherical with smooth surface and displayed less aggregating tendency with a size range 150- 250 nm confirming the size data obtained by DLS. As seen from Table 5.1, % LE of ITZ at an initial loading of 15.3% w/w was found to be 82.7 % and 93.6 % for multiblock, (PLA-PEG-PLA)n and PEG7%-g-PLA NPs, respectively. PEG7%-g-PLA showed better % LE than multiblock copolymers. The possible reason behind that is PEG chain organization

in case of branched polymer; PEG7%-g-PLA allows more mobile PEG chains at NPs surface. The PEG chains at the surface might exhibit enhanced steric hindrance, thus reducing premature diffusion of drug into the external aqueous phase during solidification of the NPs. Similar results were obtained before with us for ibuprofen loaded PEG/PLA NPs [27]. The zeta potential values of all ITZ-NPs were almost neutral (close to zero value) as shown in Table 5.1. The greater reduction in zeta potential values of all ITZ-NPs irrespective of the type of polymer used, could be explained by the existence of a fraction of PVA at the surface of NPs (data not shown) which might have a significant role in masking the actual surface charge of PLA NPs. Zambaux et al. also reported a low zeta potential value of -4 mV for PLA NPs prepared with PVA as an emulsifier [34]. PEG chains as well could shield the actual surface charge of PLA in case of PEG/PLA nanoparticles as previously shown [22, 35].

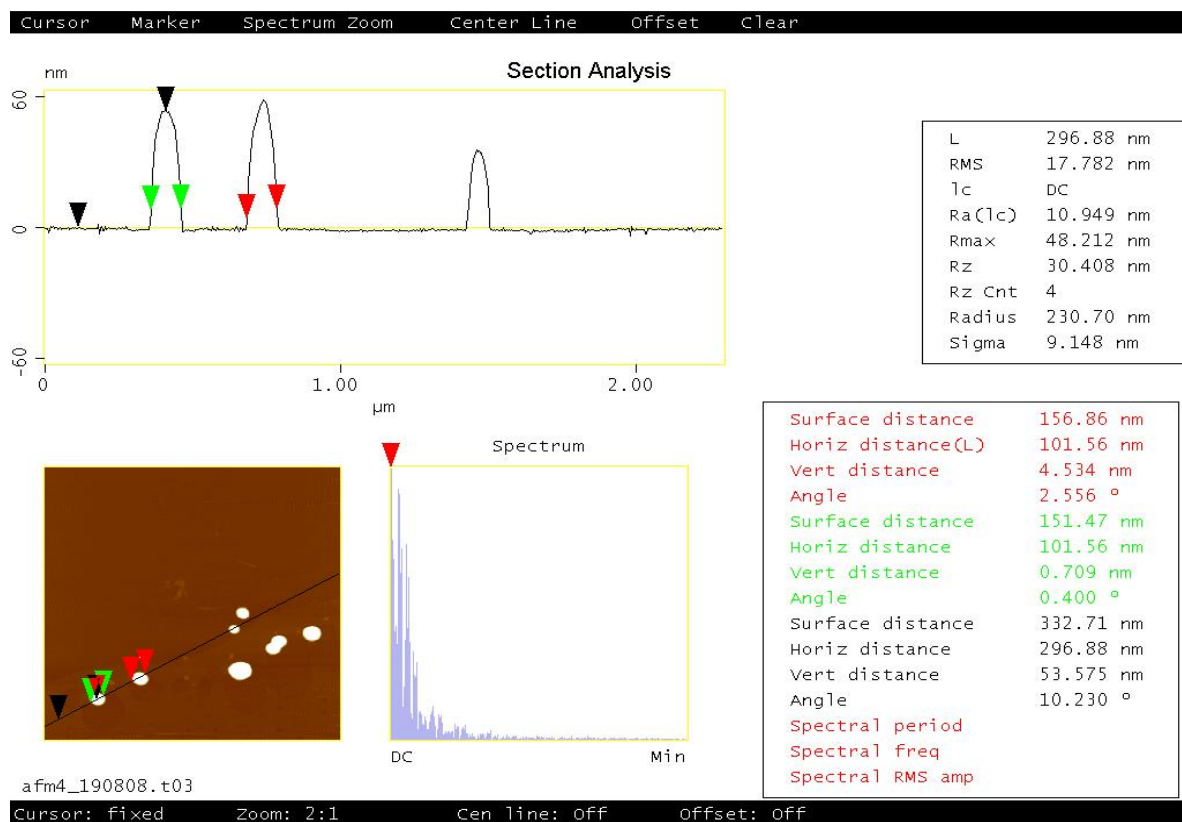
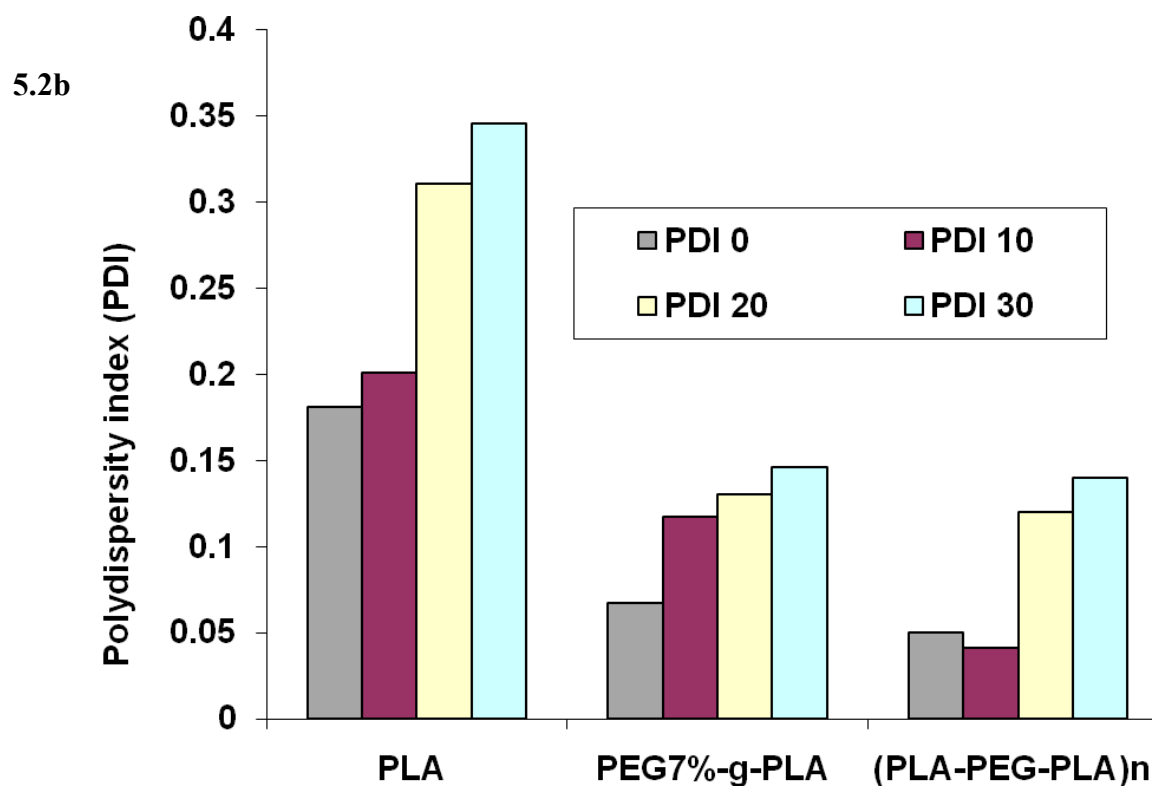
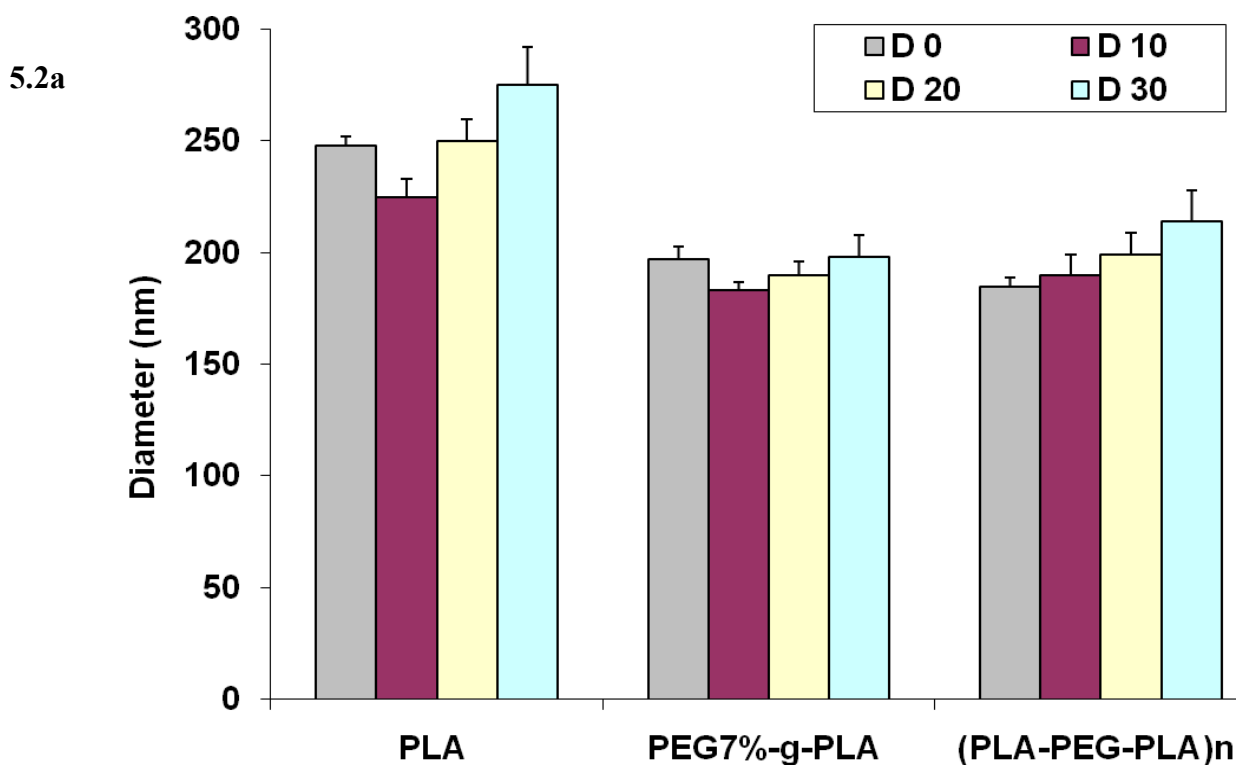


**Figure 5.1.** AFM image of lyophilized ITZ loaded PEG7%-g-PLA NPs

### 5.5.3. Stability studies

One of the major goals of this study was to develop NPs formulations able to efficiently entrap ITZ for sufficient period of time and hence keep it dispersed in aqueous phase taking advantage of their nanosize. To check for NPs ability to perform that, physical stability of the prepared particles was monitored over time by following the changes of particle size, PDI, and % loading efficiency (% LE) during storage for one month after reconstituting ITZ-NPs in PBS. All ITZ-NPs seems stable to some extent in terms of particle size and PDI for 30 days. PLA NPs showed larger particle size and PDI after 30 days of storage (Fig. 5.2a, b); that is, particle size and PDI increased from 248 nm, 0.181 up to 275 nm, and 0.345, respectively. PEG/PLA NPs either made from PEG7%-g-PLA or (PLA-PEG-PLA)<sub>n</sub> looks more stable in terms of particles size and PDI for 30 days at room temperature than PLA particles (Fig.5.2a, b). % LE of all ITZ-NPs was decreased to some extent during storage (Fig. 5.2c). This might be due to ITZ diffusion from NPs over time followed by its precipitation in water. PEG/PLA NPs either made from PEG7%-g-PLA or (PLA-PEG-PLA)<sub>n</sub> showed an observable decrease in terms of % LE after 30 days of storage; that is, % LE decreased from 93 % to 82 % and from 82 % to 71 % for PEG7%-g-PLA, and (PLA-PEG-PLA)<sub>n</sub>, respectively (Fig. 5.2c). PLA NPs showed better stability profile after 30 days in terms of % LE; that is, % LE decreased from 61 % to 54 % compared to PEG/PLA NPs (Fig. 5.2c). The last finding could be attributed to the presence of PEG chains within PLA matrix which might enhance more water uptake into the particles, and hence more ITZ diffusion over time. However, irrespective of that decrease in % LE, the remaining ITZ in NPs seems enough to achieve a therapeutic effect considering dose adjustment. These results suggest that ITZ remains entrapped inside the PEG/PLA particles for a sufficient period of time without changing the particle size, PDI and slight change in % LE.



To be continued in the next

5.2c

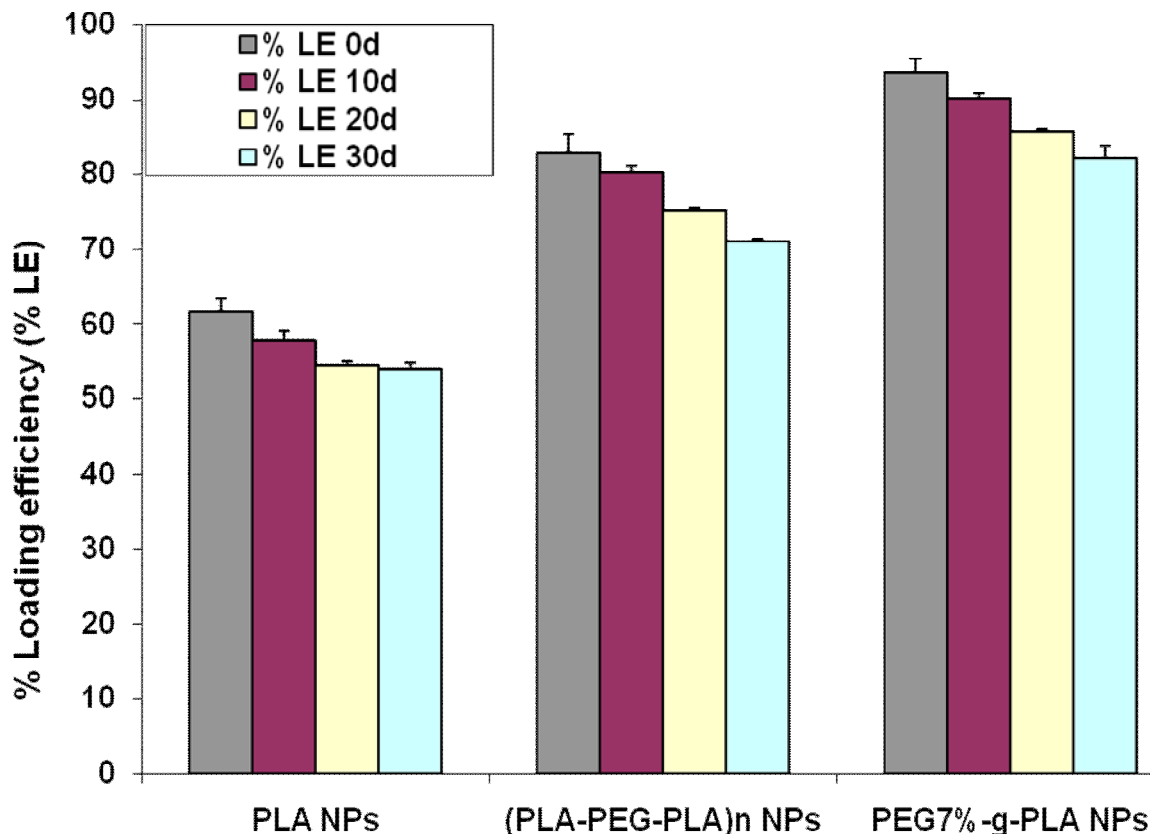


**Figure 5.2.** The stability index of ITZ-NPs in the particle size shown as diameter [D] (a), polydispersity index [PDI] (b), and loading efficiency [% LE] (c) during storage for 30 days [d] at room temperature. Data are expressed as the mean $\pm$ S.D. (n = 3).

#### 5.5.4. Differential scanning calorimetry (DSC)

DSC was used to investigate the physical state of the encapsulated ITZ into ITZ-NPs. As shown in Fig. 5.3a, a sharp endothermic peak characteristic of the melting of ITZ was seen at 167 °C. In the thermogram of lyophilized ITZ loaded (PLA-PEG-PLA)<sub>n</sub> NPs, the endothermic peak of ITZ completely disappeared. This indicates that ITZ exists in a non crystalline state inside NPs. The physical mixture of itraconazole and (PLA-PEG-PLA)<sub>n</sub> copolymer showed both endothermic characters of both the bulk drug and the polymer. In case of ITZ loaded PEG7%-g-PLA NPs (Fig. 5.3b), the endothermic peak of ITZ was still observed but with significantly reduced intensity compared to the same weight of either pure ITZ or ITZ/PEG7%-g-PLA physical mixture. This indicated also

that PEG7%-g-PLA NPs were able to significantly reduce ITZ crystallinity compared to pure ITZ drug.

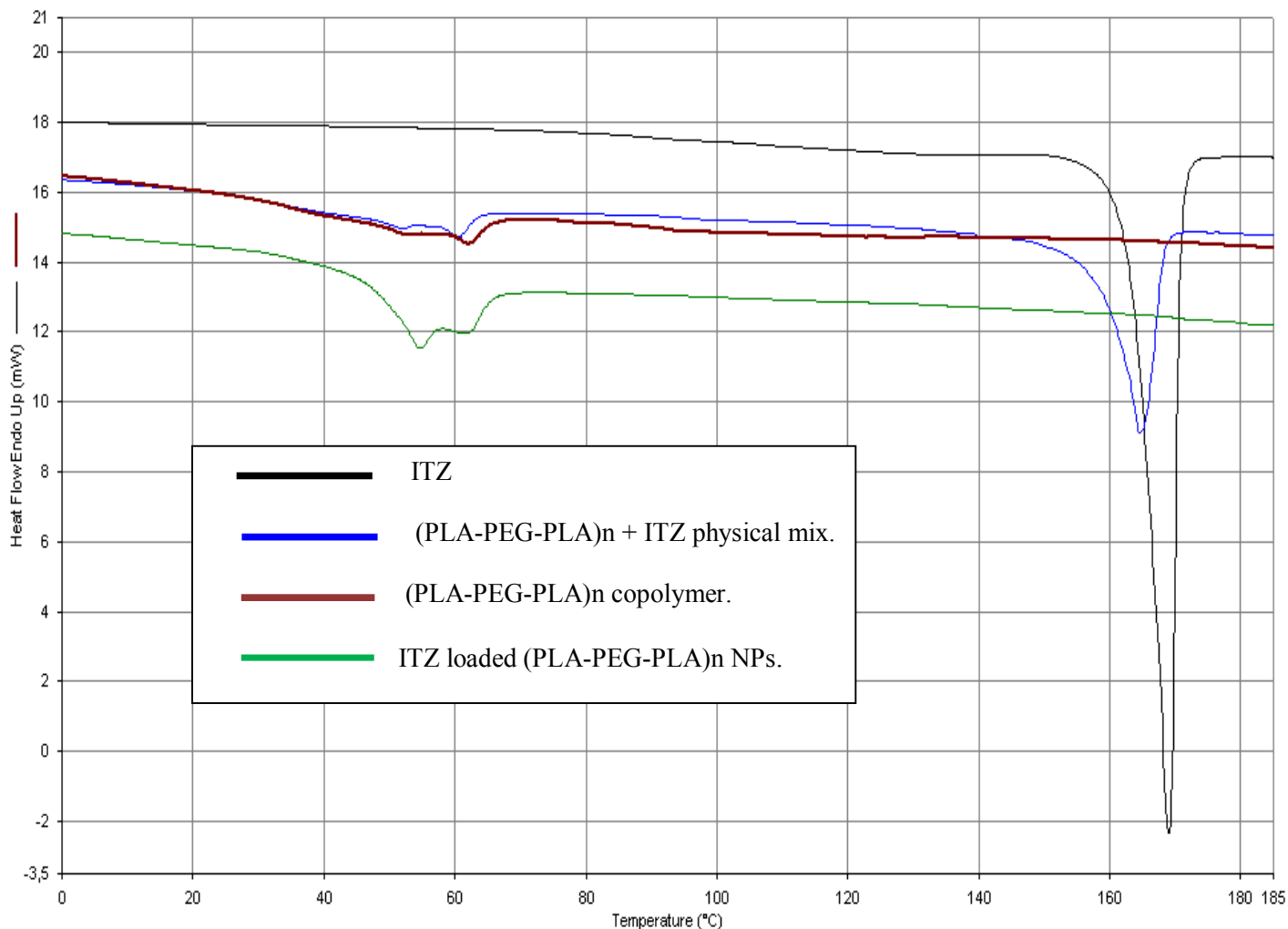


**Figure 5.3a.** DSC curves of ITZ, physical mixture of (PLA-PEG-PLA) $_n$  with ITZ, (PLA-PEG-PLA) $_n$  copolymer, and ITZ loaded (PLA-PEG-PLA) $_n$  NPs.

### 5.5.5. Powder X-ray diffractometry (PXRD)

For more verification of the final state of ITZ encapsulated into NPs, powder X-ray diffractometry (PXRD) was used to investigate the crystalline structure of ITZ in ITZ-NPs compared to bulk ITZ as previously used by other authors [36-38]. It can be seen from (Figs. 5.4a, and 5.4b) that ITZ powder showed characteristic diffraction peaks

of crystalline ITZ at  $2\theta$  scattered angles  $14.5^\circ$ ,  $17.6^\circ$ ,  $20.4^\circ$ ,  $23.5^\circ$  and  $25.4^\circ$  as previously described [10]. The existence of sharp diffraction peaks indicates the crystalline nature of ITZ. While there were no diffraction peaks of ITZ in ITZ-NPs of either (PLA-PEG-PLA)<sub>n</sub> or PEG7%-g-PLA NPs (Figs. 5.4a and 5.4b, respectively), indicating that ITZ was at an amorphous state in the ITZ-NPs. Combined with DSC observations as shown in (Figs. 5.3a, and 5.3b), we can deduce that ITZ was dissolved into the NPs matrix in the form of solid solution.

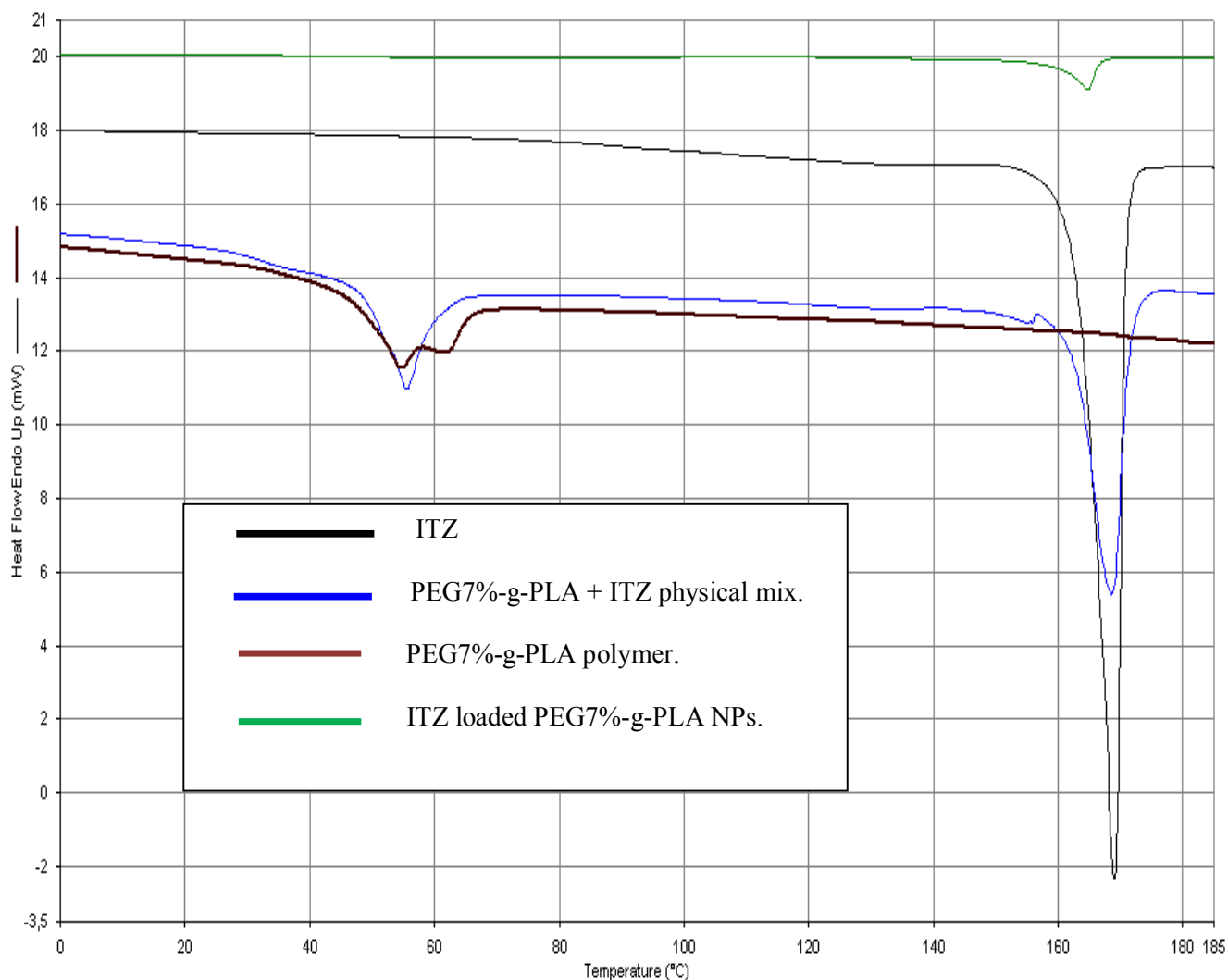


**Figure 5.3b.** DSC curves of ITZ, physical mixture of PEG7%-g-PLA with ITZ, PEG7%-g-PLA copolymer, and ITZ loaded PEG7%-g-PLA NPs.

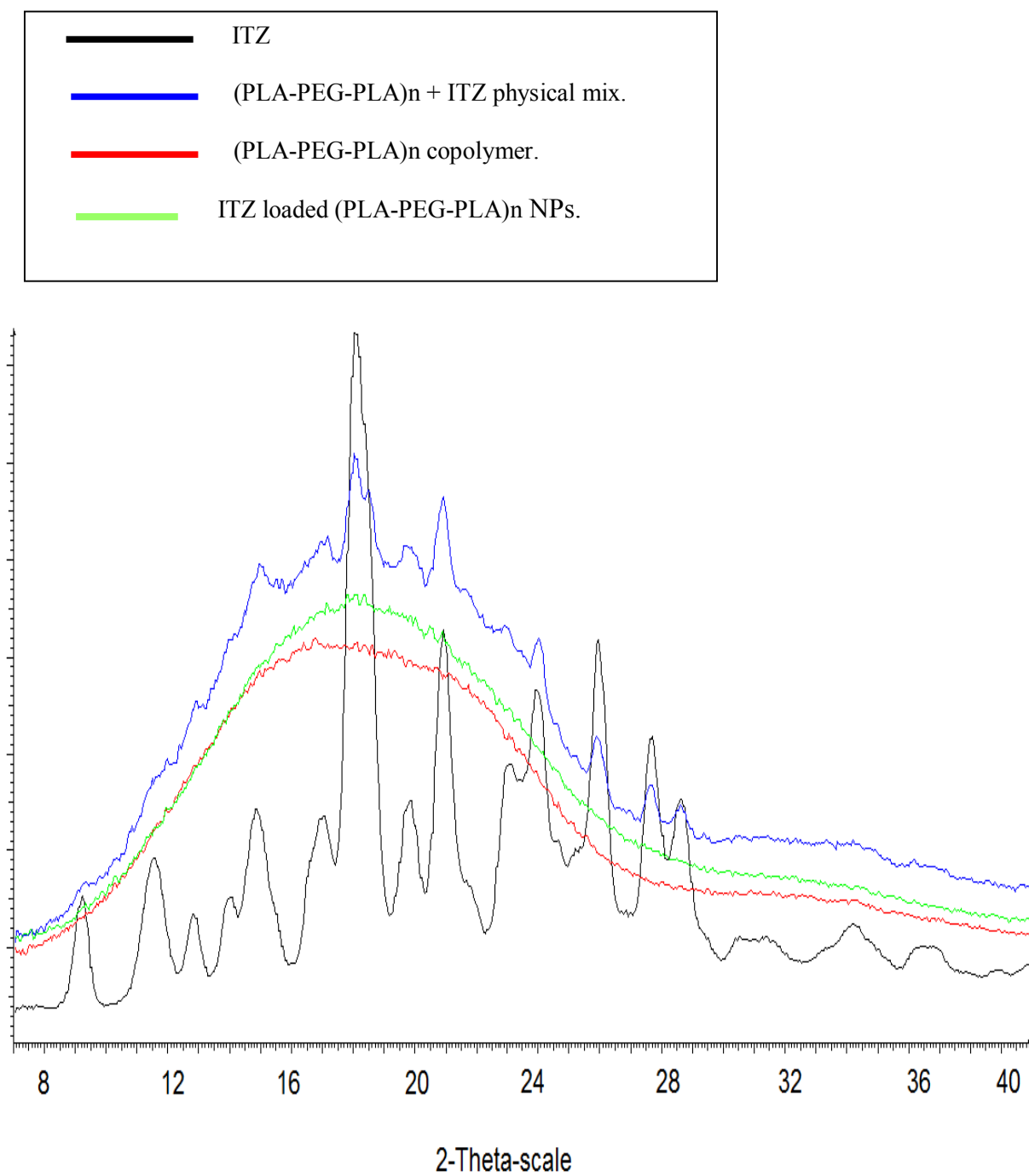


**Figure 5.4a.** XRD spectra of ITZ, physical mixture of (PLA-PEG-PLA)<sub>n</sub> with ITZ, (PLA-PEG-PLA)<sub>n</sub> copolymer, and ITZ loaded (PLA-PEG-PLA)<sub>n</sub> NPs.

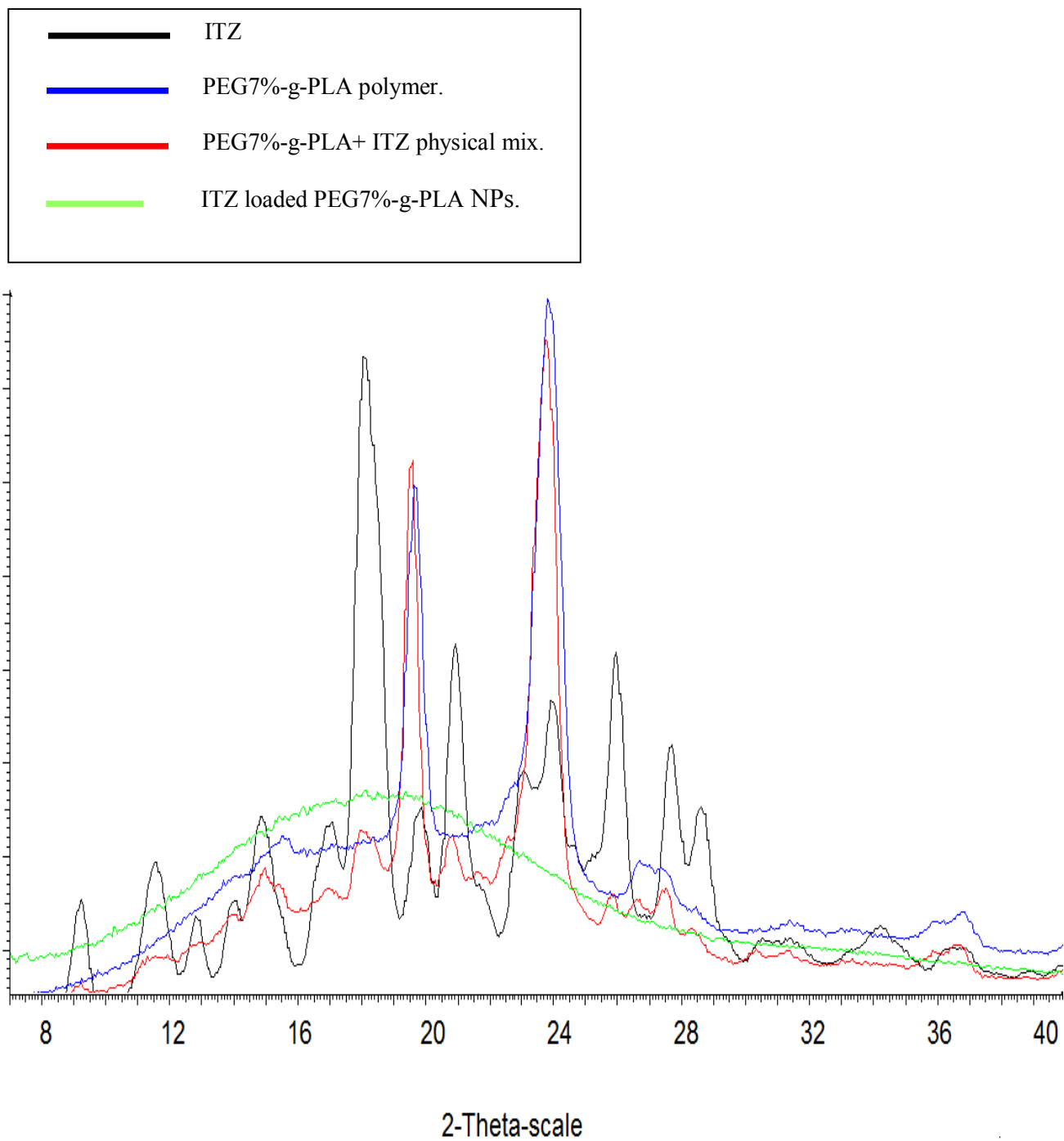


**Figure 5.4b.** XRD spectra of ITZ, physical mixture of PEG7%-g-PLA with ITZ, PEG7%-g-PLA copolymer, and ITZ loaded PEG7%-g-PLA NPs.

### 5.5.6. Fourier transform infrared spectroscopy (FT-IR) study

FT-IR analysis was done to investigate any possibility of chemical interactions between ITZ and each polymeric matrix. Specific FT-IR characteristic peaks of ITZ powder were seen at 800–3400  $\text{cm}^{-1}$  as shown in (Figs. 5.5a and 5.5b). The characteristic peaks of itraconazole at 1700, 1520 and 1380 $\text{cm}^{-1}$  were still noticed in the physical mixture of each polymer and itraconazole. For ITZ-NPs of either (PLA-PEG-PLA)<sub>n</sub> or PEG7%-g-PLA NPs, ITZ characteristic FT-IR peaks were significantly reduced in intensity or could not be seen in the obtained spectra (Figs. 5.5a and 5.5b, respectively). Similar findings were observed before with ITZ loaded albumin NPs [10]. This suggested that there were some interactions between ITZ and either polymer in the ITZ-NPs giving another evidence supporting the successful encapsulation of ITZ inside PEG/PLA NPs.

### 5.5.7. In Vitro Drug Release.

The in vitro drug release features of ITZ-NPs were evaluated by the dialysis bag method as shown in Fig. 5.6. Tween® 80 was added to the external release medium to maintain sink conditions for ITZ because it has limited solubility in PBS [39]. A biphasic release profile was observed for all investigated ITZ-NPs. A rapid initial ITZ release of about 20–45% of the drug content was observed after 10 h of the release experiment. This finding might be due to the desorption of the drug particles adsorbed at or close to the surface of NPs [40]. After the initial burst, sustained release of ITZ was seen in the following 100 h. Both processes of drug diffusion and NPs matrix erosion govern ITZ release from ITZ-NPs during the second sustained phase [41, 42]. In case of ITZ solution, ITZ was completely released after 18h (Fig. 5.6). This could be due to the rapid diffusion of ITZ out of the dialysis bag. While for ITZ-NPs, slow ITZ release was observed for all batches. Both PEG7%-g-PLA and (PLE-PEG-PLA)<sub>n</sub> NPs exhibited faster ITZ release compared to PLA NPs. This could be due to the role of PEG chains that favor more water uptake followed by rapid core wetting and hence faster ITZ diffusion or release from the NPs matrix. After 4.5 days, PEG7%-g-PLA, and (PLA-PEG-PLA)<sub>n</sub> released ~ 93% and 100% of their ITZ contents, respectively. ITZ release pattern was nearly similar for both PEG/PLA systems for the first 50 h. During the next 50h of the release experiment, (PLA-PEG-PLA)<sub>n</sub> NPs showed faster release pattern compared to PEG7%-g-PLA NPs.

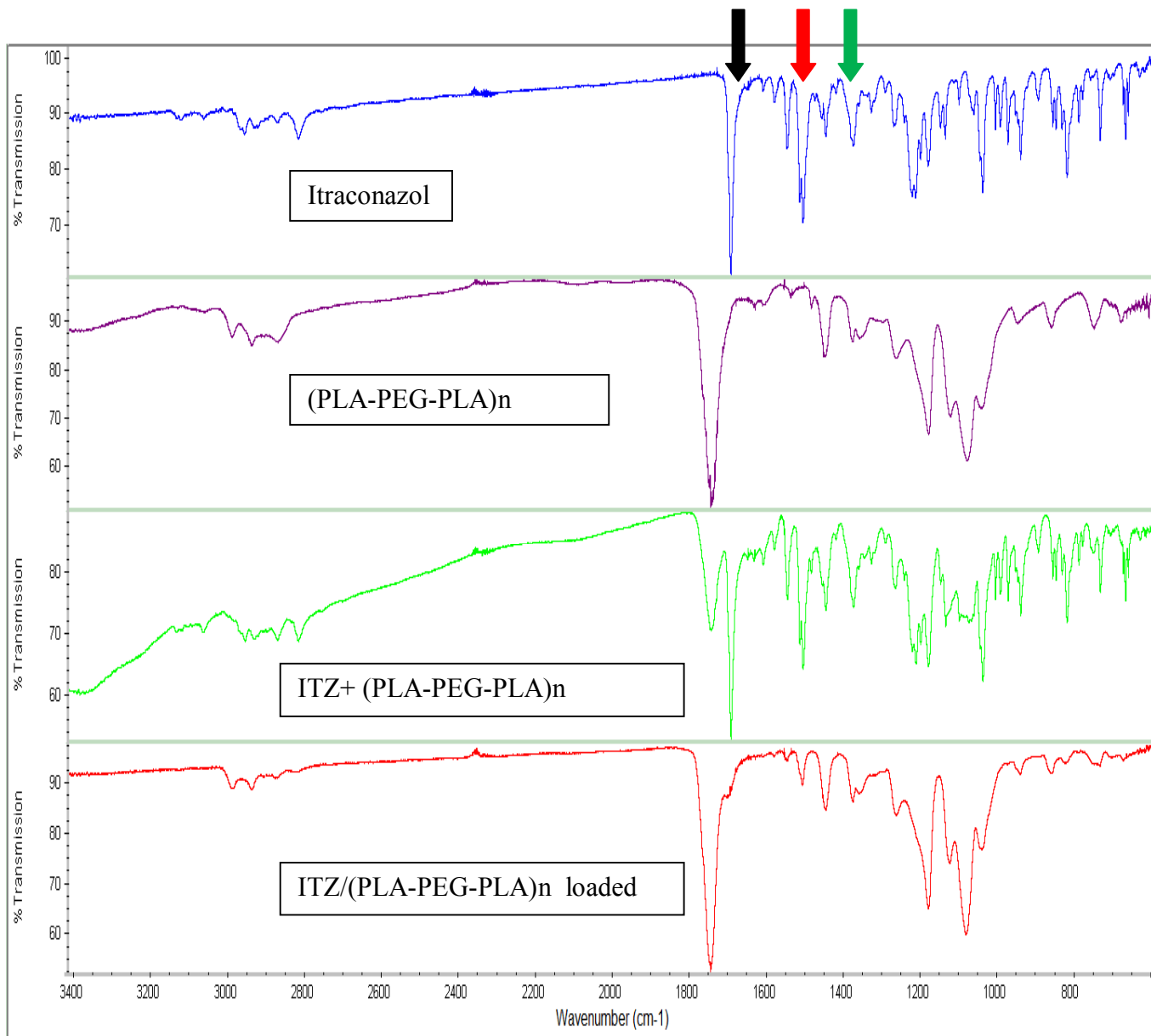


**Figure 5.5a.** FT-IR spectra of ITZ, physical mixture of (PLA-PEG-PLA)<sub>n</sub> with ITZ, (PLA-PEG-PLA)<sub>n</sub> copolymer, and ITZ loaded (PLA-PEG-PLA)<sub>n</sub> NPs [ITZ main characteristic peaks are marked with arrows].

The possible reason behind that is the peculiar polymer architecture of the multiblock copolymer, (PLA-PEG-PLA)<sub>n</sub> allows a major portion of PEG to be entrapped inside the core during NP formation as shown previously [27, 43]. This might lead to rapid wetting of the NPs core compared to PEG7%-g-PLA NPs, in which most PEG chains are located at NPs surface. Overall, the results show that ITZ is released from the ITZ-NPs at a

slower rate than from its solution and that the release patterns could be controlled by modulating the polymer architecture.

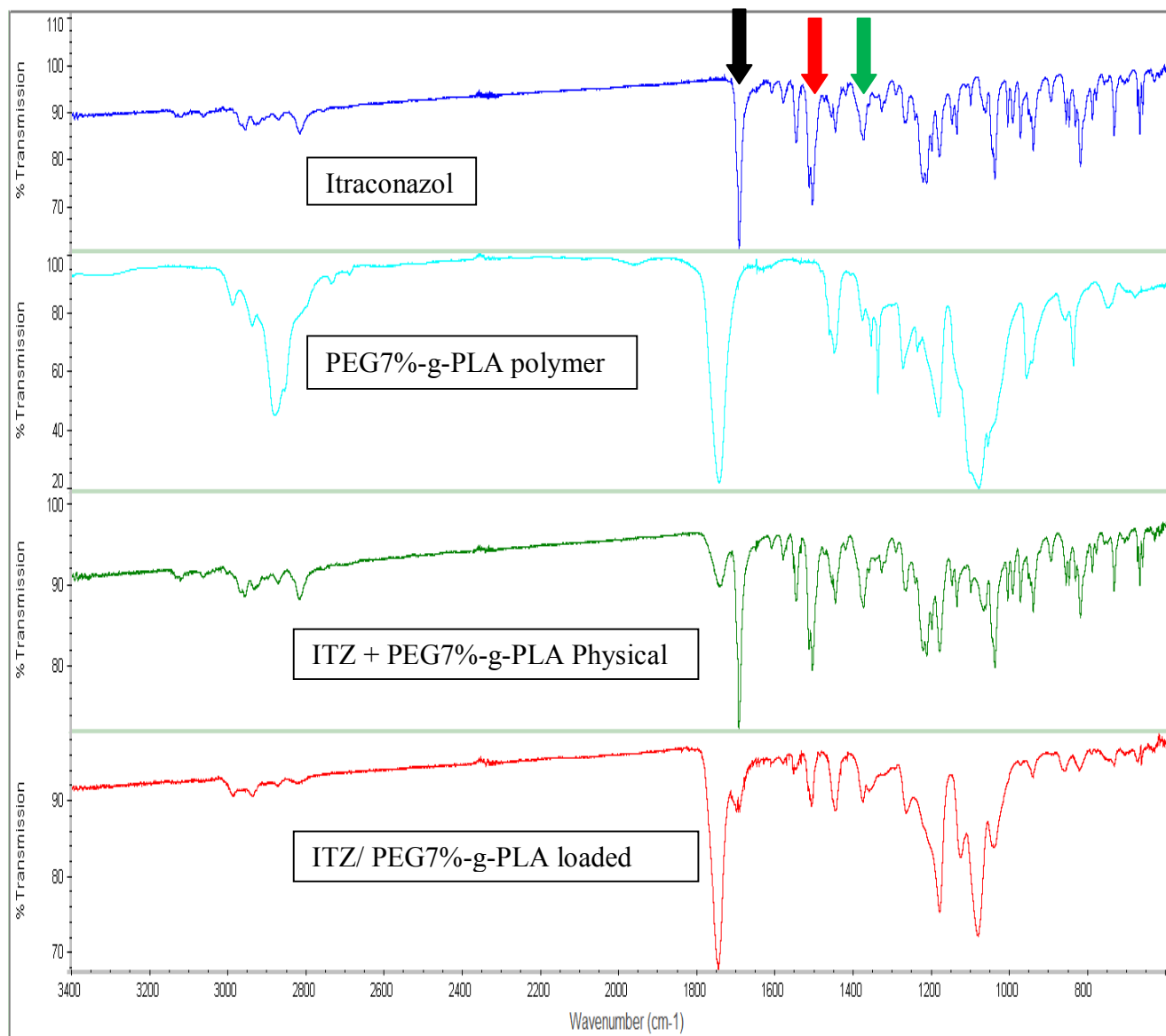


**Figure 5.5b.** FT-IR spectra of ITZ, physical mixture of PEG7%-g-PLA with ITZ, PEG7%-g-PLA copolymer, and ITZ loaded PEG7%-g-PLA NPs [ITZ main characteristic peaks are marked with arrows].

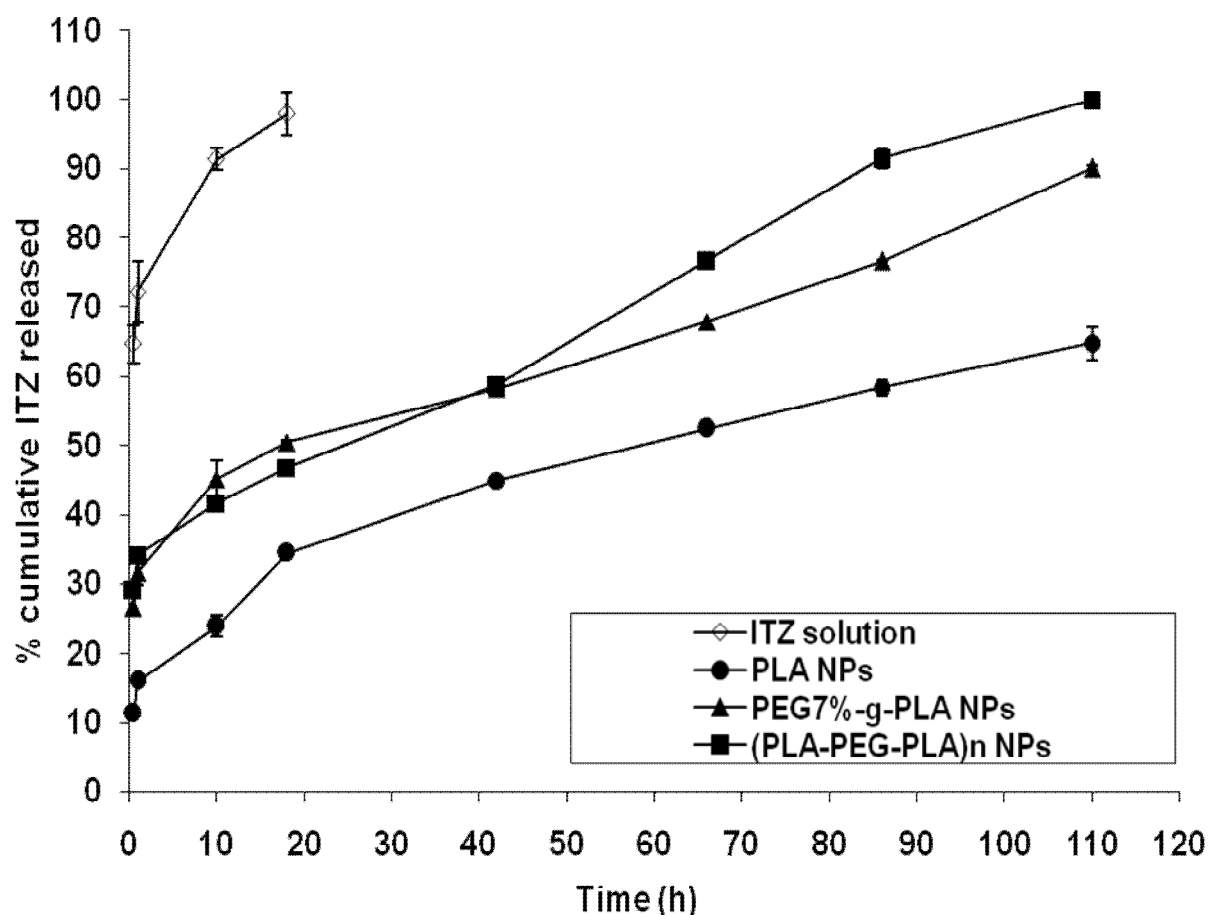


**Figure 5.6.** In vitro release behavior of ITZ from PEG/PLA NPs either from PEG7%-g-PLA or (PLA-PEG-PLA)<sub>n</sub> in comparison to PLA NPs and ITZ solution; values are represented as mean  $\pm$  S.D. of three independent experiments.

#### 5.5.8. Hemolysis analysis:

To ensure blood safety profile or hemocompatibility of the developed formulations, ITZ-NPs effect on RBCs hemolysis was investigated after incubating particles with rat blood. As shown in Fig. 5.7, all ITZ-NPs either PLA, PEG7%-g-PLA, or (PLA-PEG-PLA)<sub>n</sub> NPs exhibited less hemolytic potential below 40% over the concentrations range of ITZ (5-20  $\mu\text{g/mL}$ ). For example, the hemolysis tendency values of ITZ-PLA, PEG7%-g-PLA, (PLA-PEG-PLA)<sub>n</sub> NPs at ITZ conc. of 20  $\mu\text{g/mL}$  were 37.5, 33.7, and 33.5%, respectively. On the other hand, ITZ solution caused much more serious hemolysis. At the highest investigated concentration of ITZ, 20  $\mu\text{g/mL}$ , the hemolysis tendency was

95%. The results indicated that ITZ-NPs did not exhibit any marked effect on RBCs hemolysis or in another way it could be concluded that ITZ-NPs were more hemocompatible than free ITZ.

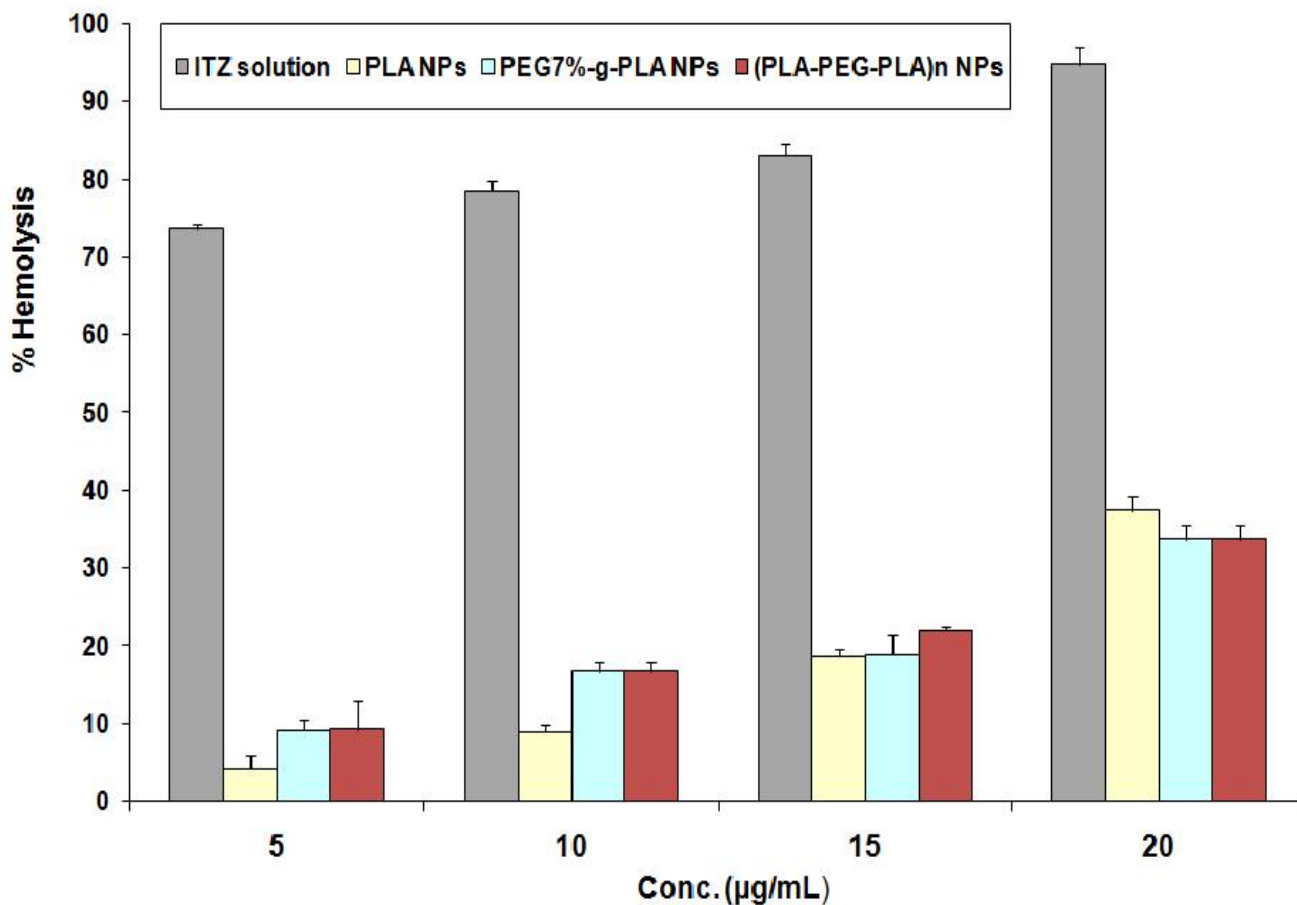


**Figure 5.7.** Erythrocyte lysis caused by ITZ loaded PEG/PLA NPs preparations compared to free ITZ and ITZ-PLA NPs. Values are expressed as mean of % lysis of three separate experiments  $\pm$ S.D

### 5.5.9. Fungal growth inhibition in Petri Plate Culture

Five treatments [ITZ-Water, ITZ-DMSO, ITZ/PLA NPs, ITZ/PEG7%-g-PLA NPs, and ITZ/(PLA-PEG-PLA)n NPs] were tested on two clinical strains of either *Candida albicans* or *Aspergillus fumigatus* (Figs. 5.8a and 5.8b, respectively). For *Candida* results, ITZ-DMSO solution showed the highest fungal inhibitory potency evidenced by

the largest diameter of the inhibitory zone surrounding ITZ-DMSO application (Figure 5.8a and Table 5.2). This might be explained by the complete solubility of ITZ in DMSO giving a better chance for ITZ to penetrate into the fungal cell membranes. Control experiment with DMSO alone did not show any observable antifungal activity. ITZ-Water did not exhibit any marked antifungal action over the incubation period of time (2 days). This could be due to the limited solubility of ITZ in water and hence limited diffusion into the agar medium. The poor solubility of ITZ could also affect its penetration potential into the fungal cell membrane. It is reported that itraconazole is an ergosterol synthesis inhibitor that exert its action by inhibiting the fungal CYP450 dependant enzyme, lanosterol 14- $\alpha$ -methylase in the fungal cell membrane [44, 45]. For ITZ, to exhibit its antifungal action, it must show a sufficient penetration level into the fungal cell membrane which could not be achieved by ITZ-Water formulation. All ITZ-NPs showed greater inhibition compared to ITZ-Water. This could be explained by the ability of NPs to enhance the aqueous solubility of ITZ, improve its bioavailability and hence its penetration ability into the fungal cells membrane. Moreover, it is important to take into consideration that nanoparticles mobility in solid media as agar is expected to be limited or hindered; hence inhibition of the fungal growth will be an indirect estimate for the ability of the particles to release ITZ into the medium in a finally dissolved form that is able to penetrate the fungal membrane. PEG/PLA NPs of either PEG7%-g-PLA and (PLA-PEG-PLA)<sub>n</sub> showed enhanced antifungal capability in comparison to ITZ-PLA NPs. This might be due to the faster release of ITZ from PEG/PLA NPs as seen before in the release section (Fig. 5.6). Over two days, ITZ was released from PEG7%-g-PLA and (PLA-PEG-PLA)<sub>n</sub> NPs at 58.5 % and 60 %, respectively compared to PLA NPs where only 45 % of ITZ was released. Similar results were obtained with the *A. fumigatus* strains (Fig. 5.8b), where PEG/PLA NPs exhibited greater antifungal action compared to either ITZ-Water or ITZ-PLA NPs. This indicated an enhanced antifungal capability of ITZ loaded PEG/PLA NPs in comparison to other formulations.

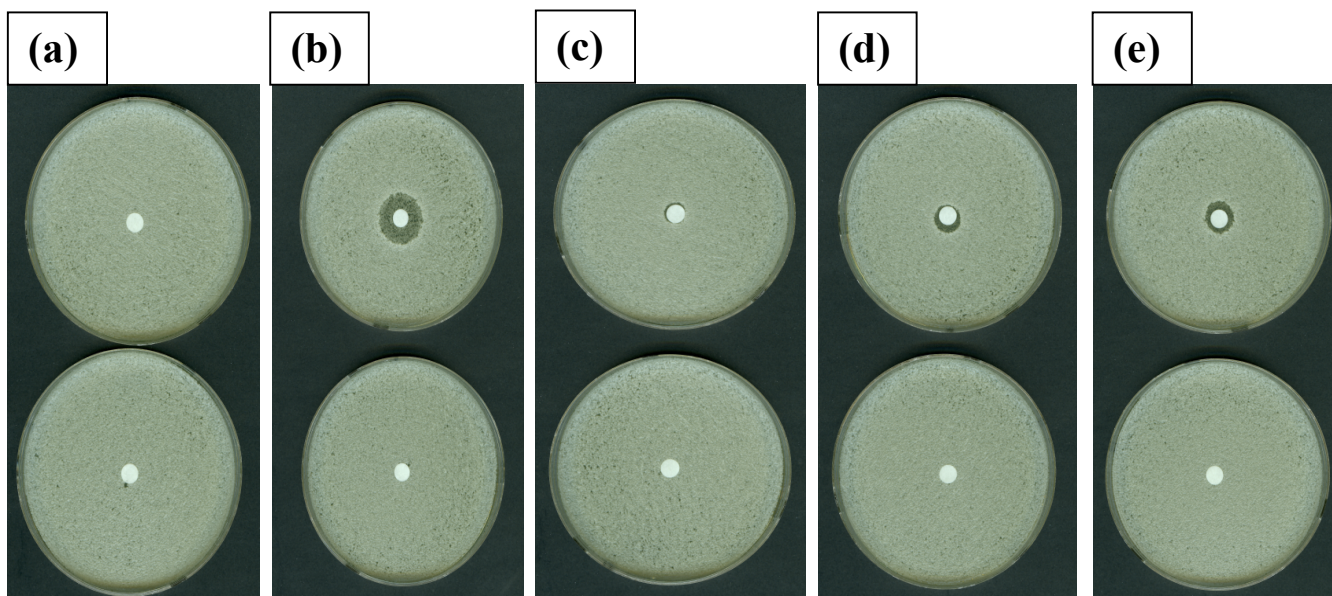


**Figure 5.8a.** Plates inoculated with *C. albicans* fungal cells and incubated at 30 °C, treated with 12.5  $\mu$ l of (a) ITZ-Water, (b) ITZ-DMSO, (c) ITZ-PLA NPs, (d) ITZ-PEG7%-g-PLA NPs, and (e) ITZ-(PLA-PEG-PLA)<sub>n</sub> NPs. Lower plates (a-e) represent control experiments corresponding to each upper plate either using only the solvent in case of ITZ-Water, and ITZ-DMSO or only blank NPs ( no ITZ) in case of NPs formulations.

**Table 5.2.** Diameter of growth inhibition zone measured with *c. albicans* fungal strains.

<i>Formulation</i>	<i>Test plate (cm)</i>	<i>Control plate (cm)</i>
ITZ-Water	0	0
ITZ-DMSO	1.9	0
PLA NPs	0.7	0
PEG7%-g-PLA NPs	1.1	0
(PLA-PEG-PLA) <sub>n</sub> NPs	1	0

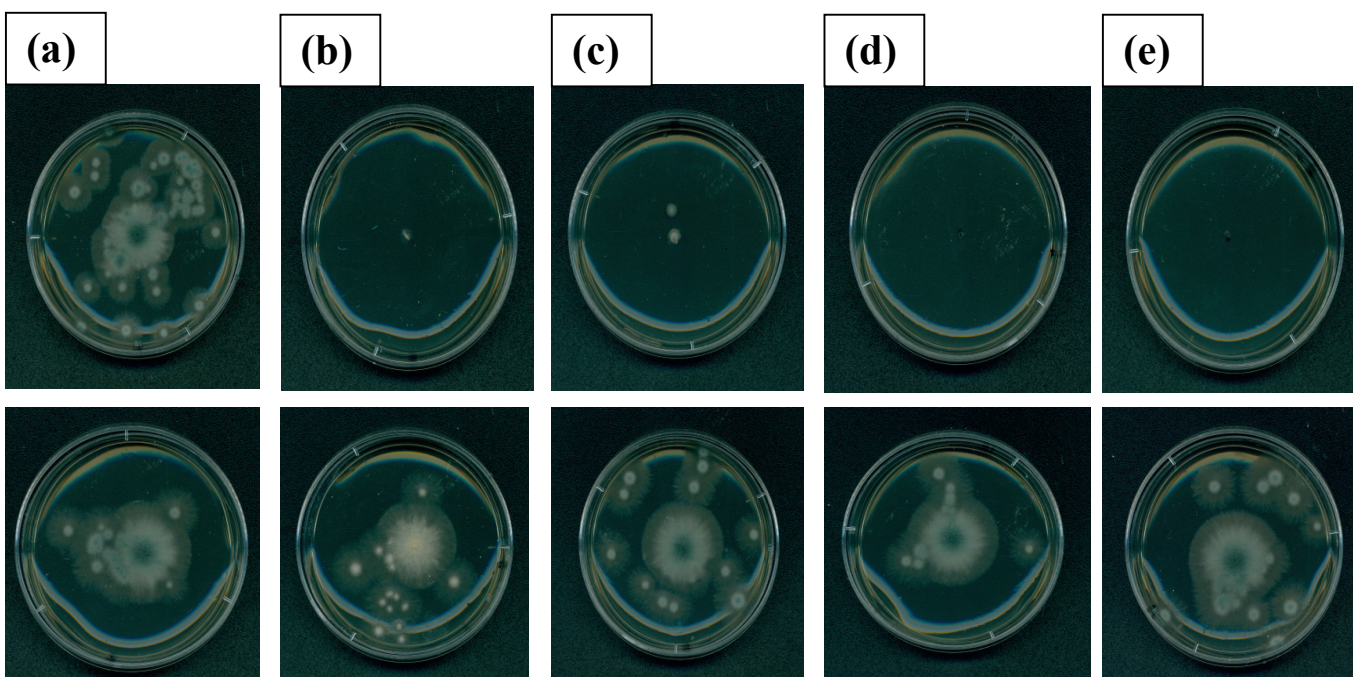


**Figure 5.8b.** Plates inoculated with *A. fumigatus* fungal cells and incubated at 30 °C, treated with (a) ITZ-Water, (b) ITZ-DMSO, (c) ITZ-PLA NPs, (d) ITZ-PEG7%-g-PLA NPs, and (e) ITZ-(PLA-PEG-PLA)<sub>n</sub> NPs. Lower plates (a-e) represent control experiments corresponding to each upper plate either using only the solvent in case of ITZ-Water, and ITZ-DMSO or only blank NPs ( no ITZ) in case of NPs formulations.

## 5.6. Conclusions

In the present work, ITZ loaded PEG/PLA NPs were prepared from two PEGylated polymers, PEG7%-g-PLA, and multiblock copolymer of PLA and PEG, (PLA-PEG-PLA)<sub>n</sub> with nearly similar PEG insertion ratio and similar PEG chain length. These nanoparticles were formulated in order to enhance the aqueous dispersability or solubility of ITZ, control its release and hence improve its antifungal effect. Spherical particles with sizes in the range of 185–285 nm were prepared with high loading efficiency. In vitro release studies showed that ITZ was released from NPs in a controlled fashion. Hemolysis analysis revealed that all ITZ-NPs were more biocompatible than the free ITZ itself. ITZ loaded PEG/PLA NPs demonstrated an enhanced antifungal action in comparison to ITZ-Water. The obtained results suggest the possibility of use of

PEG/PLA NPs as an efficient carrier for the delivery of ITZ. This may result in reduced frequency of ITZ administration, reduced accumulation inside the body and hence better clinical outcome. However, despite the promising *ex vivo* data, an actual *in vivo* data is needed to explore that indeed ITZ loaded PEG/PLA NPs could exhibit an improved antifungal effect than ITZ itself.

### **5.7. Acknowledgment**

The work was supported in part by a grant of Fond Quebecois de la Recherche en Nature et Technologie (FQRNT). Sherief Essa thanks the Ministry of Higher Education, Egypt for granting him a scholarship during his Ph.D.

## 5.8. References

1. Walsh, T.J., Pizzo, A., 1988. Treatment of systemic fungal infections: recent progress and current problems. *Eur J Clin Microbiol Infect Dis* 7, 460-75.
2. Horn, R., Wong, B., Kiehn, T.E., Armstrong, D., 1985. Fungemia in a cancer hospital: changing frequency, earlier onset, and results of therapy. *Rev Infect Dis* 7, 646-55.
3. Yu, B.G., Okano, T., Kataoka, K., Sardari, S., Kwon, G.S., 1998. In vitro dissociation of antifungal efficacy and toxicity for amphotericin B-loaded poly(ethylene oxide)-block-poly([beta]-benzyl--aspartate) micelles. *Journal of Controlled Release* 56, 285-291.
4. Zhao, Q., Zhou, H., Pesco-Koplowitz, L., 2001. Pharmacokinetics of intravenous itraconazole followed by itraconazole oral solution in patients with human immunodeficiency virus infection. *The Journal of Clinical Pharmacology* 41, 1319-1328.
5. Boogaerts, M., Maertens, J., 2001. Clinical Experience with Itraconazole in Systemic Fungal Infections. *Drugs* 61, 39-47.
6. Cohen, B.E., 1998. Amphotericin B toxicity and lethality: a tale of two channels. *International Journal of Pharmaceutics* 162, 95-106.
7. Walsh, T.J., Tepler, H., Donowitz, G.R., Maertens, J.A., Baden, L.R., Dmoszynska, A., Cornely, O.A., Bourque, M.R., Lupinacci, R.J., Sable, C.A., dePauw, B.E., 2004. Caspofungin versus Liposomal Amphotericin B for Empirical Antifungal Therapy in Patients with Persistent Fever and Neutropenia. *New England Journal of Medicine* 351, 1391-1402.
8. Willems, L., Van Der Geest, R., De Beule, K., 2001. Itraconazole oral solution and intravenous formulations: a review of pharmacokinetics and pharmacodynamics. *Journal of Clinical Pharmacy and Therapeutics* 26, 159-169.
9. Peeters, J., Neeskens, P., Tollenaere, J.P., Van Remoortere, P., Brewster, M.E., 2002. Characterization of the interaction of 2-hydroxypropyl- $\beta$ -cyclodextrin with itraconazole at pH 2, 4, and 7. *Journal of Pharmaceutical Sciences* 91, 1414-1422.

10. Chen, W., Gu, B., Wang, H., Pan, J., Lu, W., Hou, H., 2008. Development and evaluation of novel itraconazole-loaded intravenous nanoparticles. *International Journal of Pharmaceutics* 362, 133-140.
11. Akkar, A., Müller, R.H., 2003. Intravenous itraconazole emulsions produced by SolEmuls technology. *European Journal of Pharmaceutics and Biopharmaceutics* 56, 29-36.
12. Yi, Y., Yoon, H.J., Kim, B.O., Shim, M., Kim, S.-O., Hwang, S.-J., Seo, M.H., 2007. A mixed polymeric micellar formulation of itraconazole: Characteristics, toxicity and pharmacokinetics. *Journal of Controlled Release* 117, 59-67.
13. PDR, T., Physician's Desk Reference. 59th ed. 2005, Montvale, NJ.
14. Rabinow, B., Kipp, J., Papadopoulos, P., Wong, J., Glosson, J., Gass, J., Sun, C.-S., Wielgos, T., White, R., Cook, C., Barker, K., Wood, K., 2007. Itraconazole IV nanosuspension enhances efficacy through altered pharmacokinetics in the rat. *International Journal of Pharmaceutics* 339, 251-260.
15. Panyam, J., Labhasetwar, V., 2003. Biodegradable nanoparticles for drug and gene delivery to cells and tissue. *Advanced Drug Delivery Reviews* 55, 329-347.
16. Soppimath, K.S., Aminabhavi, T.M., Kulkarni, A.R., Rudzinski, W.E., 2001. Biodegradable polymeric nanoparticles as drug delivery devices. *Journal of Controlled Release* 70, 1-20.
17. Pandey, R., Ahmad, Z., Sharma, S., Khuller, G.K., 2005. Nano-encapsulation of azole antifungals: Potential applications to improve oral drug delivery. *International Journal of Pharmaceutics* 301, 268-276.
18. Italia, J., Yahya, M., Singh, D., Ravi Kumar, M., 2009. Biodegradable Nanoparticles Improve Oral Bioavailability of Amphotericin B and Show Reduced Nephrotoxicity Compared to Intravenous Fungizone®. *Pharmaceutical Research* 26, 1324-1331.
19. Peng, H.-s., Liu, X.-j., Lv, G.-x., Sun, B., Kong, Q.-f., Zhai, D.-x., Wang, Q., Zhao, W., Wang, G.-y., Wang, D.-d., Li, H.-l., Jin, L.-h., Kostulas, N., 2008. Voriconazole into PLGA nanoparticles: Improving agglomeration and antifungal efficacy. *International Journal of Pharmaceutics* 352, 29-35.

20. Brewer, E., Coleman, J., Lowman, A., 2011. Emerging Technologies of Polymeric Nanoparticles in Cancer Drug Delivery. *Journal of Nanomaterials*
21. Zhang, L., Pornpattananankul, D., Hu, C.M.J., Huang, C.M., 2010. Development of Nanoparticles for Antimicrobial Drug Delivery. *Current Medicinal Chemistry* 17, 585-594.
22. Gref, R., Lück, M., Quellec, P., Marchand, M., Dellacherie, E., Harnisch, S., Blunk, T., Müller, R.H., 2000. 'Stealth' corona-core nanoparticles surface modified by polyethylene glycol (PEG): influences of the corona (PEG chain length and surface density) and of the core composition on phagocytic uptake and plasma protein adsorption. *Colloids and Surfaces B: Biointerfaces* 18, 301-313.
23. Peracchia, M.T., Gref, R., Minamitake, Y., Domb, A., Lotan, N., Langer, R., 1997. PEG-coated nanospheres from amphiphilic diblock and multiblock copolymers: Investigation of their drug encapsulation and release characteristics. *Journal of Controlled Release* 46, 223-231.
24. Chen, J., Tian, B., Yin, X., Zhang, Y., Hu, D., Hu, Z., Liu, M., Pan, Y., Zhao, J., Li, H., Hou, C., Wang, J., Zhang, Y., 2007. Preparation, characterization and transfection efficiency of cationic PEGylated PLA nanoparticles as gene delivery systems. *Journal of Biotechnology* 130, 107-113.
25. Yang, A., Yang, L., Liu, W., Li, Z., Xu, H., Yang, X., 2007. Tumor necrosis factor alpha blocking peptide loaded PEG-PLGA nanoparticles: Preparation and in vitro evaluation. *International Journal of Pharmaceutics* 331, 123-132.
26. Dong, Y., Feng, S.-S., 2004. Methoxy poly(ethylene glycol)-poly(lactide) (MPEG-PLA) nanoparticles for controlled delivery of anticancer drugs. *Biomaterials* 25, 2843-2849.
27. Essa, S., Rabanel, J.M., Hildgen, P., 2010. Effect of polyethylene glycol (PEG) chain organization on the physicochemical properties of poly(D,L-lactide) (PLA) based nanoparticles. *European Journal of Pharmaceutics and Biopharmaceutics* 75, 96-106.
28. Nadeau, V., Leclair, G., Sant, S., Rabanel, J.-M., Quesnel, R., Hildgen, P., 2005. Synthesis of new versatile functionalized polyesters for biomedical applications. *Polymer* 46, 11263-11272.

29. Essa, S., Rabanel, J.M., Hildgen, P., 2010. Effect of aqueous solubility of grafted moiety on the physicochemical properties of poly(D,L-lactide) (PLA) based nanoparticles. *International Journal of Pharmaceutics* 388, 263-273.
30. Quesnel, R., P., Hildgen, 2005. Synthesis of PLA-b-PEG multiblock copolymers for stealth drug carrier preparation. *Molecules* 10, 98-104.
31. Li, J., Xiao, H., Li, J., Zhong, Y., 2004. Drug carrier systems based on water-soluble cationic [ $\beta$ ]-cyclodextrin polymers. *International Journal of Pharmaceutics* 278, 329-342.
32. Muranaka, M., Hirota, K., Ono, T., 2010. PEG-PLA nanoparticles prepared by emulsion solvent diffusion using oil-soluble and water-soluble PEG-PLA. *Materials Letters* 64, 969-971.
33. Bouillot, P., Babak, V., Dellacherie, E., 1999. Novel Bioresorbable and Bioeliminable Surfactants for Microsphere Preparation. *Pharmaceutical Research* 16, 148-154.
34. Zambaux, M.F., Bonneaux, F., Gref, R., Maincent, P., Dellacherie, E., Alonso, M.J., Labrude, P., Vigneron, C., 1998. Influence of experimental parameters on the characteristics of poly(lactic acid) nanoparticles prepared by a double emulsion method. *Journal of Controlled Release* 50, 31-40.
35. Beletsi, A., Panagi, Z., Avgoustakis, K., 2005. Biodistribution properties of nanoparticles based on mixtures of PLGA with PLGA-PEG diblock copolymers. *International Journal of Pharmaceutics* 298, 233-241.
36. Zhang, L., Hu, Y., Jiang, X., Yang, C., Lu, W., Yang, Y.H., 2004. Camptothecin derivative-loaded poly(caprolactone-co-lactide)-b-PEG-b-poly(caprolactone-co-lactide) nanoparticles and their biodistribution in mice. *Journal of Controlled Release* 96, 135-148.
37. Liu, M., Dong, J., Yang, Y., Yang, X., Xu, H., 2005. Characterization and release of triptolide-loaded poly (D,L-lactic acid) nanoparticles. *European Polymer Journal* 41, 375-382.
38. Panyam, J., Williams, D., Dash, A., Leslie-Pelecky, D., Labhasetwar, V., 2004. Solid-state solubility influences encapsulation and release of hydrophobic drugs

- from PLGA/PLA nanoparticles. *Journal of Pharmaceutical Sciences* 93, 1804-1814.
39. Cha, E.-J., Kim, J.E., Ahn, C.-H., 2009. Stabilized polymeric micelles by electrostatic interactions for drug delivery system. *European Journal of Pharmaceutical Sciences* 38, 341-346.
  40. Magenheim, B., Levy, M.Y., Benita, S., 1993. A new in-vitro technique for the evaluation of drug-release profile from colloidal carriers - ultrafiltration technique at low-pressure. *International Journal of Pharmaceutics* 94, 115-123.
  41. Panyam, J., Dali, M.M., Sahoo, S.K., Ma, W., Chakravarthi, S.S., Amidon, G.L., Levy, R.J., Labhasetwar, V., 2003. Polymer degradation and in vitro release of a model protein from poly(D,L-lactide-co-glycolide) nano- and microparticles. *Journal of Controlled Release* 92, 173-187.
  42. Mittal, G., Sahana, D.K., Bhardwaj, V., Ravi Kumar, M.N.V., 2007. Estradiol loaded PLGA nanoparticles for oral administration: Effect of polymer molecular weight and copolymer composition on release behavior in vitro and in vivo. *Journal of Controlled Release* 119, 77-85.
  43. Sant, S., Thommes, M., Hildgen, P., 2008. Microporous Structure and Drug Release Kinetics of Polymeric Nanoparticles. *Langmuir* 24, 280-287.
  44. Isoherranen, N., Kunze, K.L., Allen, K.E., Nelson, W.L., Thummel, K.E., 2004. Role of itraconazole metabolites in CYP3A4 inhibition. *Drug Metabolism and Disposition* 32, 1121-1131.
  45. De Beule, K., 1996. Itraconazole: pharmacology, clinical experience and future development. *International Journal of Antimicrobial Agents* 6, 175-181.

## **CHAPTER SIX**

---

### **GENERAL DISCUSSION**

Nanoparticles are a particular class of submicron colloidal carriers with special characteristics such as their unique combination of high drug loading and the possibility of high stability and controlled release. This study was constituted mainly with the following objectives in mind; firstly, to develop polymeric nanoparticles (NPs) based on functionalized PLA polymers. Secondly, to understand in depth the influence of copolymer chemical structure and copolymer architecture on the physicochemical properties of the obtained particles. Polymer architecture was early defined as the arrangement of a single polymer molecule, which has a role in determining the physicochemical parameters of the whole polymer [1]. Thirdly, to develop nanoparticle formulations with optimal drug delivery characteristics like small size, neutral surface charge, sufficient drug loading, and controlled release profile. The developed particles were investigated as a carrier for an antifungal drug, itraconazole (ITZ). In this study we are also trying to understand the effect of polymer architecture on drug loading and release pattern from NPs matrix.

Conventional polymers such as PLA, PGA and their copolymers (PLGA) have been widely investigated for nanoparticle preparation [2-5]. NPs made from those polymers might suffer many drawbacks as their rapid uptake by the reticuloendothelial system after intravascular administration, low drug loading efficiency particularly for hydrophilic drugs, and in many cases inability to release their payload completely [6-8]. Moreover, the physicochemical properties of the developed particles are not easy to be tuned as required for each application. Hence, functionalization of polymer blocks has been attempted to develop copolymers with enhanced drug delivery properties, mainly high drug loading and controlled release behavior. Functionalized poly(D,L-lactide) (PLA) nanoparticles development mainly depend on introducing a flexible moiety onto PLA hydrophobic cores in attempt to improve the drug delivery properties of the obtained NPs. A variety of pendant substituents could be grafted onto PLA to generate polymers of different physicochemical properties and hence different drug incorporation behavior than PLA itself. PLA homopolymer structure was modified by attaching different

functional groups to the polymer backbone and the influence of such modification or functionalization on the nanoparticles properties was investigated.

### **6.1. Synthesis and characterization of functionalized poly(D,L)- lactide (PLA) polymers**

Novel functionalized poly(D,L)- lactide (PLA) copolymers were successfully developed using a synthetic protocol, previously published by our group [9]. This protocol was developed to synthesize branched polyesters having reactive groups. Allyl glycidyl ether (AGE) was added to dilactide to obtain a PLA backbone with pendant allyl functions (PLA-allyl). The major advantage of using allyl molecule is its ability to be easily attached to the PLA backbone after ring opening polymerization of dilactide. PLA-allyl itself is an intermediate used to obtain various chemical functions because the allyl function can be easily modified. For example, by hydroboration, a primary alcohol is obtained and by oxidation of alcohol with Jones mixture, the corresponding acid could be also obtained.

We have used this synthetic protocol to synthesize functionalized PLA copolymers that have some potential as drug delivery systems. Various functionalized PLA copolymers were successfully synthesized with different grafting moieties (palmitate versus PEG), different PEG grafting densities (2.5%, 7%, or 20% mol/mol of lactic acid), or different architectures (block versus grafted copolymer). Most of the developed polymers were solid enough at room temperature, showing their potential to self assemble into solid nanoparticles as confirmed later by DLS and AFM tools. The synthesized copolymers present the basic nucleus for designing a comparative physico-chemical study of nanoparticles developed from those copolymers. A detailed investigation of the developed particles was done to get a deeper understanding of the effect of PLA functionalization on drug delivery behavior from PLA particles. Furthermore the chain organization behavior of nanoparticles developed from functionalized PLA copolymers was also investigated using phase imaging AFM, <sup>1</sup>HNMR and XPS.

Following this protocol, palmitic acid was grafted onto PLA backbone at 2.5 mol % of lactic acid monomer, referred as palmitic acid 2.5%-g-PLA. Also, methoxy PEG was grafted onto PLA backbone at different densities; 2.5, 7, and 20 mole % of lactic acid monomer, referred as PEG2.5%-g-PLA, PEG7%-g-PLA, and PEG20%-g-PLA, respectively [9]. Multiblock copolymer, (PLA-PEG-PLA)<sub>n</sub> was also synthesized as previously reported by our group [10] using PEG with  $M_n$  of 1500 and succinic acid was used as condensing agent to link the already synthesized triblock copolymers.

Gel permeation chromatography (GPC) was used to characterize the synthesized polymers (Tables 2.1, 3.1, and 4.1). Synthesized polymers exhibited uniform molecular weight distribution as revealed by the narrow polydispersity index values from GPC data. <sup>1</sup>H NMR spectra and chemical structures of synthesized copolymers are shown in Figs. 2.1, 3.1, and 4.1. Typical spectra were obtained for the synthesized copolymers with the characteristic peaks corresponding to the major protons constituting each polymer, were observed. A detailed description of the <sup>1</sup>H NMR spectra with identification of the major characteristic peaks can be found in chapters 2, 3, and 4.

Thermal properties of functionalized PLA copolymers and, namely, their glass transition temperatures ( $T_g$ 's) were investigated using differential scanning calorimetry, DSC (Tables 2.1, 3.1). As seen from DSC data, the molecular structure of each polymer affects significantly the glass transition ( $T_g$ ) of PLA. For example, grafting PEG chains onto the PLA backbone resulted in an increased  $T_g$  value compared to PLA homopolymer due to enhanced chain rigidity (Tables 2.1, 3.1). Another possible factor affecting  $T_g$ , is the nature of pendant functional group.  $T_g$  of palmitic acid2.5%-g-PLA was shifted to a lower value (19 °C) compared to either PLA homopolymer (46.4 °C) or PEG2.5%-g-PLA (50°C) [Table 2.1]. The significant lowering of  $T_g$  indicates that the nature of the pendant group onto PLA backbone affects remarkably the PLA backbone rigidity. Fatty acid esters were found to have a remarkable plasticizing action on PLA chains [11].

Another important factor affecting  $T_g$  of functionalized PEG/PLA copolymers, is the PEG chain organization behavior (i.e. the way PEG and PLA chains are connecting

together). The organization mode of PEG chains onto PLA chains results into either separation or mixing between both phases in the obtained copolymer. Thus, copolymer thermal properties, mainly the glass transition ( $T_g$ ), could be affected. Phase mixing between PEG and PLA chains would augment the entrapment of PEG chains into PLA chains. This might enhance the mobility of PLA chains or what is called plasticization effect, resulting in a lower  $T_g$ , as reported earlier [12, 13]. During the phase separation, PEG chains branched over PLA backbone might enhance the chain rigidity of PLA resulting in higher  $T_g$  value. The physicochemical properties of the nanoparticles are affected by the phase organization behavior of the polymer chains. Multiblock copolymer, (PLA-PEG-PLA) $_n$  showed lower  $T_g$  value at 39 °C, compared to grafted PEG-g-PLA copolymers, 53 °C (Table 3.1). Thus, the effect of branching (phase separation) was predominant for PEG-g-PLA copolymer, whereas the effect of PEG chains entrapment (phase mixing) inside PLA domains might lead to a predominant plasticizing effect in case of (PLA-PEG-PLA) $_n$  copolymer.

It can be concluded from DSC data that molecular structure, polymer architecture, nature of the pendant functional group and, PEG/PLA chain organization behavior affected remarkably the thermal characteristics of functionalized PLA copolymers.

## **6.2. Preparation and physicochemical characterization of NPs**

NPs were successfully prepared from functionalized PLA copolymers using an O/W emulsion solvent evaporation method by co-dissolving the polymer (with or without the drug) in DCM followed by precipitating the polymer droplets into nanoparticles in an aqueous phase having 0.5 % PVA as a stabilizer after organic solvent evaporation. High pressure homogenization technique was used efficiently to control the size of the emulsion droplet that will be solidified later into nanoparticles. The first task was the assessment of the major physicochemical properties of the obtained particles e.g. size, zeta-potential, drug-polymer interactions, and drug loading. Monodispersed and nearly spherical particles with smooth surfaces were obtained by this technique (Figs. 2.2, 3.2, 4.2, and 5.1). NPs formulations showed particle size in the range of 150–300 nm (Tables 2.2, 3.2, 4.2, and 5.1). Blank NPs formulations (no drug) showed nearly similar particle

size to that of loaded ones for all NPs types (Tables 2.2, 3.2). Thus, drug loading level had no apparent effect on particle size, suggesting that the size was largely controlled by controlling the homogenization parameters (mainly pressure and time of homogenization). The architecture of PEG/PLA copolymers (i.e. arrangement of building blocks) affected the size of the obtained particles (Table 3.2). In PEG-g-PLA NPs, PEG chains are expected to be more mobile creating a steric barrier around PLA core preventing particle aggregation. In case of (PLA-PEG-PLA)<sub>n</sub> NPs, the polymer architecture allows some PEG chains to be embedded inside PLA core leaving some uncovered areas at the surface that might showed some aggregating tendency due to PLA hydrophobic interactions.

The zeta potential was calculated to assess whether the presence of PEG in PEG/PLA NPs affects the particle surface charge or not. The zeta potential values of all NPs were almost neutral (close to zero value) as shown in Tables 2.2, 3.2, 4.3, and 5.1. The greater reduction in zeta potential values of all NPs irrespective of the type of polymer used, could be explained by the existence of a fraction of PVA at the surface of NPs (Table 2.2, 3.2) which might have a significant role in masking the actual surface charge of PLA NPs. This is a major drawback of using PVA as an emulsifier that it is easily adsorbed onto the NPs surface, hence affecting both physicochemical and biological behavior of NPs.

Phase image analysis using TM-AFM was done on NP samples to detect PEG chains at the surface of pegylated NPs. In case of PEG-g-PLA, highly intense dark coat surrounds the surface of brighter core could be seen indicating the existence of hydrophilic PEG chains around hydrophobic PLA chains that represent the core [Fig. 3.2(b); right panel, P]. In the case of (PLA-PEG-PLA)<sub>n</sub> multiblock copolymer NPs, fewer dark regions are found at the surface of NPs compared to PEG-g-PLA NPs [Fig. 3.2(c); right panel, P]. The main differences in the AFM phase imaging could be explained by the peculiar architecture of each polymer. In case of (PLA-PEG-PLA)<sub>n</sub> multiblock copolymer, PEG chains are covalently linked with two PLA chains. This might affect the mobility of PEG chains towards the aqueous phase of the O/W emulsion

during NPs formation. PEG chains could find difficulty migrating towards the surface of NPs in contrast to PEG-g-PLA NPs.

PEG-g-PLA NPs showed better encapsulation efficiency (% EE) than multiblock copolymers either for ibuprofen (Table 3.2) or itraconazole (Table 5.1). The last finding could be attributed to the enhanced steric hindrance of the more mobile PEG chains at NPs surface in case of grafted copolymers, thus reducing premature diffusion of drug into the external aqueous phase during solidification of the NPs. DSC was used for detecting the final state of the encapsulated drug inside the NPs matrix as well as investigating any possible interaction between the drug and the polymeric matrix.

Thermal analysis of NPs showed that drug molecules might be molecularly dispersed (solid solution) into the polymer matrix as found with itraconazole, ITZ (Figs. 5.3, 5.4) or in other cases, drug crystals are dispersed in the polymer matrix (solid dispersion) as shown with ibuprofen (Figs 2.3, 3.3). The final state of the drug inside nanoparticles detected by the interaction between the drug and the polymer using DSC and PXRD analysis.

(PLA-PEG-PLA)<sub>n</sub> NPs showed faster degradation rate ~ 44% compared to PEG7%-g-PLA (30%) after 25 days emphasizing the rapid core (PLA) wetting in the multiblock copolymer NPs (Fig. 3.5). This might be due to entrapment of most of PEG chains into the NPs core while in case of grafted PEG-g-PLA polymer, most of PEG was found to be at the surface of NPs.

The last findings confirm the following assumptions. First, high pressure homogenization technique is an efficient one for obtaining small sized particles, suitable for drug delivery applications, irrespective of the type of polymer used initially to prepare the particles. Second, PVA remains attached to the NPs surface, whatever the number of washing steps done to remove it. This affects the real contribution of PEG chains in masking the surface charge of PLA particles. Third, PEG chain organization behavior had a major impact on the size of the particles, drug loading efficiency, and surface

characteristics of the obtained particles. Fourth, drug could be encapsulated onto NPs either in the form of crystalline or molecular dispersion depending mainly on the forces of interactions involved between drug and polymer. Those findings also suggest that the physicochemical properties of PLA- based NPs can be tuned by judicious selection of both polymer composition and polymer architecture.

### 6.3. $^1\text{H-NMR}$ and XPS analysis of NPs

XPS was used to gain information on the surface chemistry of nano-scaled carriers developed from functionalized PLA copolymers. Another benefit of XPS is to provide a method for differentiating the existence of PVA, PEG, and drug (ibuprofen) at the NPs surface. A comparison was made between PEG-g-PLA, and (PLA-PEG-PLA)<sub>n</sub> NPs of similar PEG insertion ratio. The results are listed in Table 3.4. An increase in C–C–O peak area at 286.5 eV representing the PEG chains and a decrease in C–C peak area at 285 eV representing the PLA chains can be observed at PEG-g-PLA NPs surface, indicating an increase of PEG content on the particles surface. When PEG was covalently attached to the PLA backbone as in case of (PLA-PEG-PLA)<sub>n</sub> NPs, the concentration of the repeating glycol unit C–C–O at 286.5 eV (PEG chains) was decreased correspondingly to the increase in C–C at 285 eV (PLA chains). Simply, these results showed that (PLA-PEG-PLA)<sub>n</sub> NPs displayed less existence of PEG chains at the surface compared to PEG-g-PLA NPs of nearly similar PEG content (Table 3.4). PEG-g-PLA NPs exhibited an enhanced immiscibility of both PEG and PLA chains resulting in enhanced phase separation of both components during NPs formation and hence, easy migration of PEG chains towards the surface of NPs while the cores will be predominantly hydrophobic. The architecture of (PLA-PEG-PLA)<sub>n</sub> NPs allowed the interpenetration of a major portion of PEG chains into the NPs core that is consisting mainly of hydrophobic PLA chains. PVA was found adsorbed onto the surface of NPs irrespective of the multiple washing steps performed to remove it [14, 15]. XPS showed the possibility of chemical interaction between PLA-COOH and PVA-OH end groups in case of PLA and PEG-g-PLA NPs. This reaction was diminished in case of multiblock copolymer. To sum up, even with the same PEG chain length and grafted degree, the percentage of PEG migrated to the surfaces were greatly influenced by the polymer architecture either grafted or block copolymer of PEG/PLA.

$^1\text{H-NMR}$  measurements resolved the NPs core-corona structure.  $^1\text{H-NMR}$  spectra of all pegylated NPs in  $\text{D}_2\text{O}$  showed the presence of methylene protons of PEG chains at 3.6 ppm (Figs. 2.4, 3.4). Signals from PLA methyl or methylene protons were absent or diminished in intensity. The results from  $^1\text{H NMR}$  experiments suggest the formation of micelle like NPs with some ordered configuration, presumably a core-corona system, where PEG segments form a highly hydrated corona surrounding a core composed of solid PLA.

Based on all results (AFM, DSC,  $^1\text{H-NMR}$ , erosion, and XPS), a schematic representation of different chain organization of NPs (depending on the polymer composition and architecture), is shown in Figs. 2.5, and 3.7. The difference in chain organization behavior was found to have an effect on the physicochemical properties of the obtained NPs.

#### **6.4. In vitro release**

One of the main purposes of this study was to investigate the effect of the starting polymer architecture and copolymer composition on drug release profiles from PLA NPs. In the first part of the study, different NPs formulations made from different functionalized PLA polymers were compared for their in vitro release of ibuprofen as a model drug (Figs. 2.7, 3.6). Generally speaking, drug solubility, drug diffusion and biodegradation of the nanoparticle matrix control the release process. In the case of nanoparticles, where the drug is molecularly dispersed, the release occurs by diffusion or erosion of the matrix under sink conditions. In case of nanoparticles entrapping the drug in a crystalline form, the release process will be controlled mainly by the drug dissolution process which is the slowest step. DSC and PXRD indicated that ibuprofen exists in a crystalline state inside all NPs irrespective of their polymer structure. Thus, the main rate limiting step controlling drug release will be the dissolution of drug crystals into the polymeric matrix followed by their diffusion out of the matrix into the release media. The polymer that favors more water uptake and hence rapid core wetting would facilitate drug dissolution and hence faster drug release. PEG/PLA NPs either made from PEG-g-PLA NPs or (PLA-PEG-PLA)<sub>n</sub> showed faster drug release compared to PLA NPs and this

could be attributed to the role of PEG chains in enhancing nanoparticle core wetting resulting in faster drug dissolution followed by its rapid diffusion. The higher release rates exhibited by multiblock copolymers compared to PEG-g-PLA could be also related to the differences in polymer architecture that allows different chain organization behavior when the NPs are suspended into the release medium. In case of PEG-g-PLA, a major fraction of PEG chains was located at the surface as confirmed by XPS and AFM while the cores will be predominantly hydrophobic. For (PLA-PEG-PLA)<sub>n</sub>, a major portion of PEG was entrapped inside the PLA chains, enhancing the process of core wetting and hence faster drug dissolution. This difference in chain organization was found to have a major effect on the release kinetics of the encapsulated drug from NPs.

PEG/PLA NPs either made from PEG-g-PLA or (PLE-PEG-PLA)<sub>n</sub> were investigated as a drug carrier for itraconazole, ITZ. The in vitro drug release features of ITZ-NPs are shown in Fig.5.6. The results show that ITZ is released from the ITZ-NPs at a slower rate than its diffusion from solution through the dialysis membrane. PEG/PLA NPs prepared either from PEG-g-PLA or (PLE-PEG-PLA)<sub>n</sub> copolymers exhibited faster ITZ release compared to PLA NPs. This could be explained by the same fact as before with ibuprofen except that PEG chains would favor more water uptake enhancing faster ITZ diffusion not dissolution as with ibuprofen. ITZ was found molecularly dispersed into NPs matrix as confirmed by DSC and PXRD (Figs. 5.3a, 5.3b, 5.4a, and 5.4b).

## 6.5. Plasma protein adsorption

Differences in the protein adsorption behavior could help predict the in vivo fate of different NPs types, and hence, design optimal drug carriers suitable for intravenous drug targeting. DLS was used to reveal the possibility of plasma protein (PP) adsorption onto NPs surface and whether there is any difference between PEG-g-PLA NPs of different PEG grafting densities in their ability to adsorb PP (Figs. 4.4, 4.S1). This was simply done by monitoring the size distribution changes of NPs after incubation for a period of time with plasma proteins solution. PEG7%-g-PLA or PEG20%-g-PLA NPs did not adsorb significant quantities of plasma proteins compared to either PLA or PEG1%-g-PLA NPs. In fact, PEGylated NPs tend to adsorb less proteins than PLA NPs [16, 17]. It was important for us to perform this test to confirm the ability of PEG chains on the

surface of PEG-g-PLA NPs to repel plasma proteins *in vitro*. These observations confirm that either PEG7%-g-PLA or PEG20%-g-PLA NPs could withstand the serum environment and that protein adsorption onto their surface occurs to a limited extent, if at all [18].

Based on the *in vitro* data, plasma protein adsorption on the surface of PEG-g-PLA nanospheres strongly depends on PEG chain density at the surface of the particles, which played a major role in repelling the plasma proteins *in vitro*. Moreover, the optimum PEG grafting density expected to induce stealthiness *in vivo* varies from 4-7%.

## 6.6. Cellular toxicity and uptake studies

NPs made from PEG-g-PLA polymers of different PEG densities were well tolerated and exhibited no adverse effects on the cell viability as shown by cell proliferation assays (Fig. 4.5).

The interaction of RHO encapsulated nanoparticles with macrophage-like cells (RAW 264.7 cells) was investigated by fluorescence microscopy (qualitative) and fluorimetry analysis (quantitative) [Figs. 4.6, 4.7]. It could be seen from microscopy results (Fig. 4.6) that nanoparticles made from PEG-g-PLA copolymers showed less internalization by macrophage cells than PLA nanoparticles. Moreover, to achieve sufficient masking of NPs hydrophobic core, PEG grafting density higher than 1% is usually required to obtain lower internalization by macrophage cells.

For estimation of the actual amount of NPs internalized after incubating RAW 264.7 cells for 24 h at 37 °C with different concentrations of RHO loaded NPs, fluorescence analysis was used (Fig.4.7). Similar findings to microscopy results were obtained. PEG-g-PLA NPs of different PEG densities resulted in lower degree of internalization compared to PLA NPs in macrophages cell lines. It also could be seen that the higher the PEG grafting density, the lower the uptake of NPs by macrophage cells. This may be ascribed to surface hydrophilicity and neutral surface charge of PEG-g-PLA NPs. However, increasing the grafting density from 7% to 20 % didn't show significant differences in their uptake ability indicating that the steric effect of PEG is concentration dependent [19].

### 6.7. Hemolysis analysis of ITZ-NPs

To demonstrate the ability of PEG/PLA copolymers as an effective carrier for ITZ, we investigated drug loading efficiency, release pattern, and ITZ dispersion state into either PEG-g-PLA or (PLA-PEG-PLA)<sub>n</sub> NPs. Preliminary in vitro characterization data suggested that ITZ was entrapped into NPs with good loading efficiency, slow release pattern, and that ITZ was molecularly dispersed into NPs. However, the safety potential of ITZ loaded NPs should be tested to confirm the ability of NPs to efficiently entrap ITZ, slowly release it, and reduce its localized concentration in contact with tissues or cells. To achieve that, hemolysis test was investigated after incubating particles with rat blood. As shown in Fig. 5.7, all ITZ-NPs either PLA, PEG7%-g-PLA, or (PLA-PEG-PLA)<sub>n</sub> NPs exhibited less hemolytic potential than ITZ solution over the concentrations range of ITZ (5-20 µg/mL). On the other hand, ITZ solution caused much more serious hemolysis. The results indicated that ITZ-NPs did not exhibit any marked effect on RBCs hemolysis or in another way it could be concluded that ITZ-NPs were more hemocompatible than free ITZ.

### 6.8. Fungal growth inhibition in Petri Plate Culture

It was crucial to confirm the pharmacological activity of ITZ loaded NPs to warrant the ability of NPs to improve the therapeutic potential of ITZ as hypothesized. This was done by investigating the antifungal ability of ITZ-NPs compared to ITZ itself. Two clinical strains of either *Candida albicans* or *Aspergillus fumigates* were used in this study (Figs. 5.8a and 5.8b, respectively). Those two strains were selected due to their high susceptibility to ITZ action. ITZ-NPs showed greater inhibition of both fungal strains compared to ITZ-Water. This could be explained by the ability of NPs to enhance the aqueous solubility of ITZ, improve its bioavailability and hence its penetration ability into the fungal cells membrane. PEG/PLA NPs of either PEG7%-g-PLA and (PLA-PEG-PLA)<sub>n</sub> showed enhanced antifungal capability in comparison to ITZ-PLA NPs. This could be due to the faster release of ITZ from PEG/PLA NPs as seen before in the release section (Fig. 5.6). Similar results were obtained with *A. fumigatus* strains (Fig. 5.8b), where PEG/PLA NPs exhibited greater antifungal action compared to either ITZ-Water

or ITZ-PLA NPs. This indicated an enhanced antifungal capability of ITZ loaded PEG/PLA NPs in comparison to other formulations. The enhanced activity of ITZ loaded PEG/PLA NPs could be explained by the smaller size of the particles and the existence of PEG chains onto PLA particles surface. Those two factors were responsible for not only enhancing the aqueous solubility of ITZ but also keeping it dispersed for a period of time sufficient to enhance its contact and penetration potential into the fungal cell membranes.

Two mechanisms can be hypothesized for the delivery of ITZ from NPs into the fungal cells: first by releasing ITZ near the cell surface resulting in a faster internalization of free ITZ, and second by cellular uptake of nanoparticles followed by release of ITZ in the cytosol. However the solid nature of agar hindering the mobility of NPs, suggests that the former mechanism is the more likely to occur. In combination to these mechanisms, the sustained release of ITZ explains the larger inhibition zones observed over time with the PEG/PLA NPs compared to ITZ-water and ITZ-DMSO (Figs 5.8 a, b).

PEG/PLA NPs ability to enhance the antifungal activity of ITZ is associated with two aspects. The first one is the ability of small sized, water soluble PEG/PLA nanoparticles to enhance the dispersability of ITZ in water. The second one is the ability of NPs to enhance ITZ contact with the fungal spores on the plate surface leading to faster drug internalization [20, 21], penetration into the spores and hence, improved antifungal action.

## 6.9. References

1. Qiu, L.Y., Bae, Y.H., 2006. Polymer architecture and drug delivery. *Pharm Res* 23, 1-30.
2. Kumari, A., Yadav, S.K., Yadav, S.C., 2010. Biodegradable polymeric nanoparticles based drug delivery systems. *Colloids and Surfaces B: Biointerfaces* 75, 1-18.
3. Musumeci, T., Ventura, C.A., Giannone, I., Ruozi, B., Montenegro, L., Pignatello, R., Puglisi, G., 2006. PLA/PLGA nanoparticles for sustained release of docetaxel. *International Journal of Pharmaceutics* 325, 172-179.
4. Kolachala, V.L., Henriquez, O.A., Shams, S., Golub, J.S., Kim, Y.-t., Laroui, H., Torres-Gonzalez, E., Brigham, K.L., Rojas, M., Bellamkonda, R.V., Johns, M.M., 2010. Slow-release nanoparticle-encapsulated delivery system for laryngeal injection. *The Laryngoscope* 120, 988-994.
5. Soppimath, K.S., Aminabhavi, T.M., Kulkarni, A.R., Rudzinski, W.E., 2001. Biodegradable polymeric nanoparticles as drug delivery devices. *Journal of Controlled Release* 70, 1-20.
6. Delie, F., Berton, M., Allémann, E., Gurny, R., 2001. Comparison of two methods of encapsulation of an oligonucleotide into poly(D,L-lactic acid) particles. *International Journal of Pharmaceutics* 214, 25-30.
7. Govender, T., Stolnik, S., Garnett, M.C., Illum, L., Davis, S.S., 1999. PLGA nanoparticles prepared by nanoprecipitation: drug loading and release studies of a water soluble drug. *Journal of Controlled Release* 57, 171-185.
8. Leo, E., Brina, B., Forni, F., Vandelli, M.A., 2004. In vitro evaluation of PLA nanoparticles containing a lipophilic drug in water-soluble or insoluble form. *International Journal of Pharmaceutics* 278, 133-141.
9. Nadeau, V., Leclair, G., Sant, S., Rabanel, J.-M., Quesnel, R., Hildgen, P., 2005. Synthesis of new versatile functionalized polyesters for biomedical applications. *Polymer* 46, 11263-11272.
10. Quesnel, R., P., Hildgen, 2005. Synthesis of PLA-b-PEG multiblock copolymers for stealth drug carrier preparation. *Molecules* 10, 98-104.

11. Jacobsen, S., Fritz, H.G., 1999. Plasticizing polylactide - The effect of different plasticizers on the mechanical properties. *Polymer Engineering and Science* 39, 1303-1310.
12. Kulinski, Z., Piorkowska, E., Gadzinowska, K., Stasiak, M., 2006. Plasticization of poly(L-lactide) with poly(propylene glycol). *Biomacromolecules* 7, 2128-2135.
13. Piorkowska, E., Kulinski, Z., Galeski, A., Masirek, R., 2006. Plasticization of semicrystalline poly(L-lactide) with poly(propylene glycol). *Polymer* 47, 7178-7188.
14. Sahoo, S.K., Panyam, J., Prabha, S., Labhasetwar, V., 2002. Residual polyvinyl alcohol associated with poly (D,L-lactide-co-glycolide) nanoparticles affects their physical properties and cellular uptake. *Journal of Controlled Release* 82, 105-114.
15. Scholes, P.D., Coombes, A.G.A., Illum, L., Davis, S.S., Watts, J.F., Ustariz, C., Vert, M., Davies, M.C., 1999. Detection and determination of surface levels of poloxamer and PVA surfactant on biodegradable nanospheres using SSIMS and XPS. *Journal of Controlled Release* 59, 261-278.
16. Tobío, M., Gref, R., Sánchez, A., Langer, R., Alonso, M.J., 1998. Stealth PLA-PEG Nanoparticles as Protein Carriers for Nasal Administration. *Pharmaceutical Research* 15, 270-275.
17. Gref, R., Domb, A., Quellec, P., Blunk, T., Müller, R.H., Verbavatz, J.M., Langer, R., 1995. The controlled intravenous delivery of drugs using PEG-coated sterically stabilized nanospheres. *Advanced Drug Delivery Reviews* 16, 215-233.
18. Liu, J., Zeng, F., Allen, C., 2005. Influence of serum protein on polycarbonate-based copolymer micelles as a delivery system for a hydrophobic anti-cancer agent. *Journal of Controlled Release* 103, 481-497.
19. Mainardes, R.M., Gremiao, M.P., Brunetti, I.L., da Fonseca, L.M., Khalil, N.M., 2009. Zidovudine-loaded PLA and PLA-PEG blend nanoparticles: influence of polymer type on phagocytic uptake by polymorphonuclear cells. *J Pharm Sci* 98, 257-67.
20. Amaral, A.C., Bocca, A.L., Ribeiro, A.M., Nunes, J., Peixoto, D.L.G., Simioni, A.R., Primo, F.L., Lacava, Z.G.M., Bentes, R., Titze-de-Almeida, R., Tedesco,

- A.C., Morais, P.C., Felipe, M.S.S., 2009. Amphotericin B in poly(lactic-co-glycolic acid) (PLGA) and dimercaptosuccinic acid (DMSA) nanoparticles against paracoccidioidomycosis. *Journal of Antimicrobial Chemotherapy* 63, 526-533.
21. Peng, H.-s., Liu, X.-j., Lv, G.-x., Sun, B., Kong, Q.-f., Zhai, D.-x., Wang, Q., Zhao, W., Wang, G.-y., Wang, D.-d., Li, H.-l., Jin, L.-h., Kostulas, N., 2008. Voriconazole into PLGA nanoparticles: Improving agglomeration and antifungal efficacy. *International Journal of Pharmaceutics* 352, 29-35.

## **CHAPTER SEVEN**

---

# **CONCLUSIONS AND PERSPECTIVES**

## 7.1. Conclusion

NPs were successfully fabricated using functionalized copolymers of PLA with different molecular architectures. Applying different characterization tools, notably DLS, AFM, XPS, and DSC, changes could be detected in the physicochemical characteristics of the nanoparticles prepared from different functionalized copolymers of PLA. Molecular architecture of the polymer is an important parameter controlling surface characteristics of NPs which in turn determine their physicochemical properties like encapsulation efficiency, % PVA adsorbed at the surface of NPs, zeta potential, thermal characteristic, NPs surface organization and drug release kinetics. Both AFM phase imaging and XPS studies showed that (PLA-PEG-PLA)<sub>n</sub> NPs displayed less amount of PEG on the surface due to the possibility of PEG chains interpenetration inside the PLA core of NPs. This resulted in lower  $T_g$ , rapid degradation of the polymeric matrix, and faster drug release from NPs compared to PEG-g-PLA NPs. While for PEG-g-PLA NPs, most PEG chains were located at the NPs surface. The architecture of PEG-g-PLA copolymer allowed enhanced immiscibility of both PEG and PLA blocks resulting in enhanced phase separation of both components during NPs formation and hence, easy migration of PEG chains towards the surface of NPs while the cores will be predominantly hydrophobic. NPs prepared from PEG-g-PLA copolymers were found to have more suitable drug delivery characteristics e.g. small size, good drug loading, lower adsorption of plasma proteins, lower uptake by macrophage cell lines, enhanced antifungal activity of encapsulated ITZ, and sustained release profile. For those features, PEG-g-PLA could be explored further as a promising nanoparticles delivery system for many drugs trying to optimize their biopharmaceutical performance in the body.

These results suggest that the physicochemical properties of PLA- based NPs can be tuned by judicious control over the following factors; polymer composition, nature of pendant functional group, % grafting density over the polymer backbone, and finally polymer architecture. Our results also favor the urgent search for another biocompatible emulsifier other than PVA for the preparation of NPs to avoid the unwanted effect of PVA on NPs properties e.g. NPs surface charge and cellular uptake pattern. This study has also shed the light on the use of nanospheres as a dispersing agents for slightly

insoluble drugs taking advantage of NPs small size, and the surfactant property of the used polymer i.e. PEG/PLA, to keep the drug dispersed into aqueous solution over a prolonged period of time. This action could enhance the pharmacological activity of many water insoluble drugs.

## **7.2. Future work**

The in vitro encouraging results obtained in this thesis justify in vivo evaluation of a number of PEG-g-PLA NPs formulations. Thus, ITZ loaded PEG-g-PLA NPs will be evaluated in vivo to determine their pharmacokinetics and biodistribution. Furthermore, antifungal activity of ITZ NPs will be evaluated in albino guinea pigs infected with either systemic *aspergillosis* or *candidosis*. When it comes to the usefulness of PEG-g-PLA copolymers as delivery systems, other drugs e.g. anticancer drugs may be tried to be encapsulated into those types of particles.